MIA LIIMATAINEN
THE EFFECT OF MICROSTRUCTURE ON BENDABILITY OF
ULTRA-HIGH STRENGTH STEELS

Master's Thesis Work

ABSTRACT

In recent years there has been an increasing interest to utilize ultra-high strength steels (UHSS) in various industries such as transportation, due to the possibility to produce structures with lighter weight without the need to make amends for performance level. Yet, a major challenge concerning the application of UHSS is their formability. Factors affecting bendability has been widely studied, yet there exists a lack of information concerning a fundamental comprehension of the effect of microstructure on bendability of UHSS. The aim of this work was to study the microstructural factors governing bendability of UHSS. In particularly the effects of surface hardness and homogeneity of surface microstructure, i.e. deviation of hardness, were studied.

The materials used in this work were direct quenched 8-12 mm thick UHSS microalloyed with niobium and comprising various carbon (C) and manganese (Mn) contents, rolled to different temperatures. In present work microstructural examination was performed by applying FESEM. The effects of finish rolling temperature (FRT), and C and Mn contents on the developing microstructure were studied. Bending tests were carried out for determining minimum bending radius and for comprehending failure in bending. Microhardness measurements were performed in order to comprehend the effects of hardness and homogeneity on bendability, and to relate microstructure with hardness.

The microstructures of the materials comprise principally a mixture of lath-like bainite and martensite, and a surface layer of granular bainite and/or ferrite reaching to various depths. It is found that microstructure is highly dependent on FRT, and C and Mn concentrations. The results suggest that strain localization, i.e. development of shear bands, is precursor for damage in bending in case of complex phase UHSS. Shear bands are observed to develop at the depth range of 0.1-0.5 mm from upper surface at maximum 45° shear stress directions. Hence it is suggested that the properties of the upper surface layers govern bendability. It is found that hardness of surface determines bendability due to its relation with several properties, which govern the onset of diffuse necking and strain localization. The soft layer is required to reach to 2.3-4.4 % relative to the total sheet thickness, and requirements concerning its hardness level are determined by the desired bending radius. The soft layer is achieved by low FRT and by adjusting the carbon and manganese concentrations. Furthermore it is found that a homogenous surface microstructure contributes to increased bendability. In an inhomogeneous microstructure resistance to dislocation movement varies locally. Therefore grains possessing softer orientations and phases possessing lower hardness levels are susceptible to strain localization.

TIIVISTELMÄ

Mia Liimatainen: Mikrorakenteen vaikutus ultralujien terästen särmättävyyteen
Tampereen teknillinen yliopisto
Diplomityö, 188 sivua, 10 liitesivua
Maaliskuu 2015
Materiaalitekniikan diplomi-insinöörin tutkinto-ohjelma
Pääaine: Metallimateriaalit
Tarkastaja: Apulaisprofessori Pasi Peura

Avainsanat: Ultralujat teräkset, särmättävyys, myötymän paikallistuminen, leikkausnauhat, homogeenisuusindeksi, pinnan kovuus

Mielenkiinto ultralujien terästen hyödyntämiseen eri teollisuuden aloilla on viime vuosien aikana kasvanut johtuen mahdollisuudesta valmistaa kevyempiä rakenteita ilman, että suorituskyvyssä tarvitsee tehdä myönnytyksiä. Ultralujien terästen käyttöä on kuitenkin tyypillisesti rajoittanut niiden rajalliset muovattavuusominaisuudet. Särmättävyyteen vaikuttavia tekijöitä on laajasti tutkittu, mutta perusteellinen ymmärrys mikrorakenteen vaikutuksesta ultralujien terästen särmättävyyteen puuttuu. Täten tämän työn tarkoituksena oli tutkia mikrorakenteen vaikutusta ultralujien terästen särmättävyyteen. Erityisesti yläpinnan kovuuden ja mikrorakenteen homogeenisuuden, eli kovuuden hajonnan, vaikutusta tarkasteltiin.

Työn materiaalit olivat kuumavalssattuja ja suorasammutettuja, niobiseostettuja 8-12 mm ultralujia teräksiä. Koemateriaalit valssattiin eri lämpötiloissa ja ne koostuivat eri hiili- ja mangaanipitoisuuksista. Mikrorakennetarkastelu suoritettiin FESEM:llä, jotta valssauksen lopetuslämpötilan (FRT) ja hiili- ja mangaanipitoisuuksien merkitys mikrorakenteeseen tunnistettaisiin. Työssä suoritettiin särmäyskokeet minimisärmäyssäteiden määritystä sekä leikkausnauhojen tutkimista varten. Mikrokovuusmittaukset suoritettiin yläpinnasta sekä keskilinjalta, jotta kovuuden ja homogeenisuuden vaikutus särmättävyyteen ymmärrettäisiin. Lisäksi mikrorakenteen ja kovuuden yhteys pyrittiin tunnistamaan.

Koemateriaalien mikrorakenteet koostuivat pääasiassa sälemäisestä bainiitista ja martensiitista, sekä pinnalle muodostuneesta kerroksesta granulaarista bainittia ja/tai ferriittiä, jonka paksuus riippui materiaalista. Työn perusteella mikrorakenne riippuu merkittävästi FRT:stä ja hiili- sekä mangaanikoostumuksista. Tulosten perusteella myötymän paikallistuminen, eli leikkausnauhojen muodostuminen, johtaa vaurioon kompleksifaasisten ultralujien terästen särmäyksessä. Leikkausnauhat muodostuivat 0.1-0.5 mm syvyydelle pinnasta noin 45° kulmaan, eli maksimileikkausjännitysten suuntaisesti. Täten ehdotetaan, että pinnan ominaisuudet kontrolloivat särmättävyyttä. Tulosten perusteella pinnan kovuus kontrolloi särmättävyyttä, johtuen kovuuden suhteesta ominaisuuksiin, jotka määrittävät diffuusiokuroutumisen ja myötymän paikallistumisen alkamisen. Pehmeän pintakerroksen on ulotuttava 2.3-4.4 % syvyyteen suhteessa koko levyn paksuuteen. Pinnan kovuusvaatimus sen sijaan riippuu halutusta särmäyssäteestä. Pehmeä pintakerros saadaan aikaiseksi matalalla FRT:llä sekä pienillä hiili- ja mangaanikoostumuksilla. Työn perusteella homogeeninen pinnan mikrorakenne johtaa parempaan särmättävyyteen, koska tällöin ei muodostu paikallisia venymän keskittymiä. Epähomogeenisessa mikrorakenteessa rakeet, jotka ovat orientoituneet edullisemmin muodonmuutokseen nähden sekä pehmeämmät faasit ovat alttiina myötymän paikallistumiselle.

ACKNOWLEDGMENTS

CONTENTS

ATTACHMENT 1: MECHANICAL PROPERTIES OF TEST MATERIALS

ATTACHMENT 2: FESEM IMAGES OF MICROSTRUCTURES AT THE MIDDLE SECTIONS OF SELECTED MATERIALS

ATTACHMENT 3: CORRELATION BETWEEN HARDNESS AT THE CENTRE LINE AND MINIMUM BENDING RADIUS TRANSVERSE TO ROLL-ING DIRECTION

ATTACHMENT 4: HOMOGENEITY INDEX OF EACH HEAT AT GIVEN DEPTHS

ATTACHMENT 5: STANDARD DEVIATION OF HARDNESS OF EACH HEAT AT GIVEN DEPTHS

ATTACHMENT 6: THE EFFECT OF AUSTENITE GRAIN SIZE ON HARNDESS

SYMBOLS AND ABBREVIATIONS

AHSS	advanced high strength steels
A_2O_3	aluminum oxide
A %	percent elongation
bcc	body-centered cubic
B_s	bainitic transformation start temperature
CaS	calcium sulfide
CL	centre line
CP	complex phase
Cr_2O_3	chronium oxide
DP	dual-phase
DQ	direct quenching
E	Young's modulus
EBSD	electron backscatter diffraction
et al.	lat. et alii or et alie, and others
FB	ferritic-bainitic
FeO	wustite
FeS	iron sulfide
FESEM	field electron scanning electron microscope
Fe_2O_3	hematite
Fe_3O_4	magnetite
Fe_3C	cementite
FRT	finish rolling temperature
GB	granular bainite
HI	homogeneity index
HSLA	high-strength low-alloyed
HT	hot-formed
HV	Vickers pyramid hardness
i.e.	lat. id est, that is, in other words
K-S	Kurdjumov-Sachs
LB	lower bainite
MgS	magnesium sulfide
MnO	manganese oxide
MnS	manganese sulfide
MP	multiphase
M_s	martensitic transformation start temperature
M/A	martensite-austenite
ND	normal to rolling direction
QT	quenched and tempered
R	bending radius
R-value	material anisotropy
RA	reduction in area
RD	rolling direction
RP 0.2	yield point set at 0.2 % strain
R^2	square of sample correlation coeffiecient
SEM	scanning electron
T	temperature
TD	transverse to rolling direction

TMCP	thermomechanical controlled process
TRIP	transformation induced plasticity
TS	tensile strength
TWIP	twinning-induced plasticity
UB	upper bainite
UHSS	ultra high strength steels
YS	yield strength
wt.%	weigth percent
A	unit area
a	side of unite cell
A_0	initial cross sectional area
A_f	cross sectional area at fracture
$\mathbf{b}$	burgers vector
C	empirically determined value (0.6-0.7)
d	average diameter of second phase
f	volume fraction of second phase
F	force
k	strength coefficient
k_S	springback coefficient
l_f	gauge length of fracture
l_0	initial gauge length
m	strain rate sensitivity
M_B	bending moment
M	Taylor factor
n	work hardening exponent
R_i	inner bending radius
R_m	mean radius
R_{min}	minimum bending radius
R_n	neutral radius
R_o	outer bending radius
S	soft portion
t	sheet thickness
v	dislocation velocity
y	distance from surface
w	width of sheet
α_1	bending angle before springback
α_2	bending angle before springback
$\dot{\gamma}$	shear strain rate
ε	strain
$\dot{\varepsilon}$	strain rate
ε_0	strain where strain hardening is dominant
ε_A	critical value, where bifurcation of uniform deformation initiates
ε_B	critical value, where strain localization initiates
ε_{BS}	bending strain
ε_t	true strain
$\dot{\varepsilon}_t$	true strain rate
θ	angle between the direction of the slip and the applied force
θ_B	bending angle
σ	stress

σ_A	critical value, where bifurcation of uniform deformation initiates
σ_B	critical value, where strain localization initiates
σ_f	flow stress
σ_{st}	standard deviation
σ_t	true stress
σ_u	applied stress in uniaxial tension
σ_0	stress where strain hardening is dominant
σ_{YS}	yield strength
τ_R	resolved shear stress
τ_s	shear stress
τ_{CRSS}	critical shear stress
ϕ	angle between normal to the slip plane and the applied force
ϵ_t	true stress

1. INTRODUCTION

In recent years there has been an increasing interest to utilize ultra-high strength steels (UHSS), i.e. steels with yield strength higher than 700 MPa, in various industries, such as transportation [1]. This is due to the possibility to produce structures with lighter weight and reduced material thickness without the need to make amends for performance level. Hence cost savings are achieved as a result of e.g. lower material requirements, lower transportation costs due to the light-weight design and certain processing costs. [1, 2] However, a major challenge concerning the application of UHSS is their formability, which is typically poor [3]. UHSS are mainly applied to components which are formed by bending and hence the bendability of UHSS has been widely studied [2].

Bending is highly common sheet metal forming process [4]. The behavior of material during bending differs compared to that during tensile testing [5]. Therefore it is suggested that mechanical properties attained from tensile testing do not provide reliably precise information regarding to bendability of UHSS [6]. During bending the outer layers are subjected to the greatest strains and hence the yield strength is exceeded first at these layers [7]. As deformation is further carried on until the point in which plastic strengthening cannot accommodate with the stress increase, uniform plastic deformation turns into non-uniform plastic deformation, i.e. diffuse necking onsets [8, 9]. Eventually deformation increasingly localizes into a narrow band, termed as shear band [10]. According to several studies, strain localization, i.e. formation of shear bands, is precursor for damage in bending. Therefore considerable scientific effort has been made to identify the factors contributing to the formation of shear bands. [3, 11] The formation of shear bands is commonly related to several mechanical properties of the material including e.g. work-hardening capability and strength, and moreover to texture, defects, homogeneity of phase structure and surface roughness [2, 12, 13].

It is generally accepted that bendability of UHSS is governed by local ductility instead of total elongation. It is suggested by Yamazaki et al. that the homogeneity of microstructure notably affects bendability, since in case of inhomogeneous microstructure local hotspots of stress and/or strain occurs in the microstructure. Yamazaki et al. have developed a homogeneity index, i.e. basically deviation of hardness measurements, which can be applied to evaluate homogeneity of microstructure. [2] In addition to homogeneity of microstructure, the beneficial effect of a soft surface layer on bendability has been widely recognized. The beneficial effect of the soft surface layer is due the increased deformation capability that it provides at the region, which is subjected to the greatest strains. [14]

However there exists a lack of information concerning a fundamental comprehension of the effect of microstructure on bendability of UHSS. Thus the aim of this study is to comprehend the microstructural factors contributing to the formation of shear bands in bending UHSS. In particularly, the effects of surface hardness and homogeneity are studied. In order to reach this goal, microhardness measurements of several UHSS were performed and the results were examined together with bendability results for studying the effects of both homogeneity index and surface hardness on bendability. Furthermore, interrupted bending tests, i.e. bending to various angles, were carried out so that the initiation site of shear bands is able to comprehend.

Chapters 2-6 constitute the literature survey of this work. First in Chapter 2 UHSS are introduced, including a presentation of several families and typical microstructural constituents of UHSS. Second, deformation of both single crystal and polycrystalline material are studied, in particularly plastic deformation is examined. In Chapter 4 the phenomenon of strain localization is described and additionally factors governing its formation are presented. In Chapter 5 bending process is described, including mechanics of bending and failure in bending. In Chapter 6 factors affecting bendability are studied. These factors comprise several mechanical properties, homogeneity of phase structure, texture, several defects and surface quality. In Chapter 7 the experimental procedures and materials applied in this work are presented. In Chapter 8 the results are presented followed by discussion in Chapter 9. Finally in Chapter 10 conclusions are presented and in Chapter 11 proposals for future are presented.

2. ULTRA-HIGH STRENGTH STEELS

Steels with extremely high strength levels are generally termed as ultrahigh-strength steels (UHSS). The designation ultra-high strength is not specific, since no universally accepted strength level for the term has been determined. Furthermore, as steels with increasingly great strength levels are developed, the strength range for which the term is used is progressively increasing. [15] Depending on the source, the minimum yield strength criterion to be classified as UHSS varies as much as in the range of 560-1380 MPa. However it appears that most typically steels with yield strength higher than 700 MPa are graded as UHSS. [16, 17, 18] Depending on the steel type, the desired strength level is attained due to different strengthening mechanisms, such as grain refinement, precipitation hardening and phase hardening [19]. The desired mechanical properties for UHSS can be achieved by judicious selection of alloying elements, microstructural control and optimizing processing parameters [20].

Ultra-high strength steels can be manufactured by three various manners. These methods include quenched and tempered (QT), thermomechanical controlled process (TMCP) and direct quenching (DQ). QT method is probably the most well-known heat treatment of steels. The aim of QT is to produce a microstructure consisting of martensite or mixture of bainite and martensite. This is achieved by cooling the material in a sufficiently rapid manner from the austenite phase, to avoid the formation of softer phases such as ferrite. After quenching the strength level of the material is higher than desired, yet it can be too brittle to be applied in most structural applications. Thus the material can be tempered in order to achieve desired ductility properties. [21]

Increasing requirements concerning reduction of manufacturing costs without affecting adversely on usability properties of UHSS have led to development of direct quenching (DQ) method. DQ is a special case of thermomechanical rolling comprising controlled hot rolling followed by direct quenching to room temperature. The time-temperature diagrams of conventional QT and DQ method are represented in Figures 1a and 1b. [22]

a)   b)
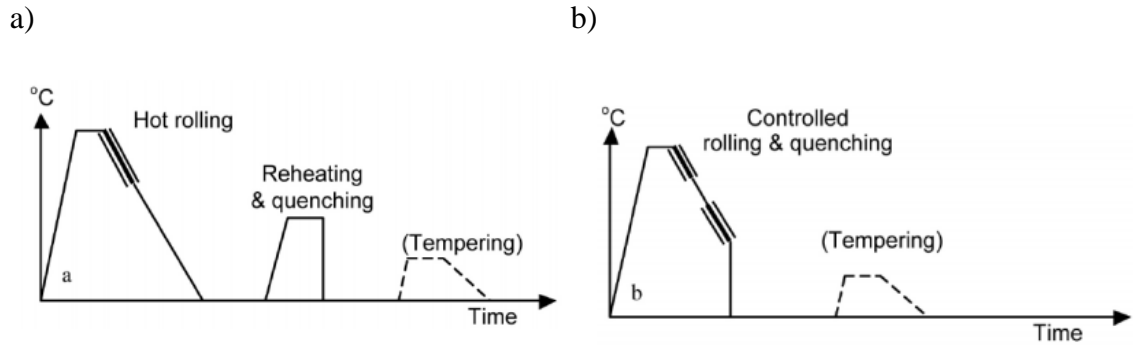
Figure 1: Time-temperature diagrams of a) conventional QT method and b) DQ method [22].

The difference in the process routes between conventional QT and DQ can be noticed from Figure 1a and 1b. In case of QT process, after hot rolling the plates are cooled and cut, and then reheated in order to form austenite followed by water quenching. In this case the austenite is always recrystallized prior to quenching. Instead, in case of DQ, material is water quenched immediately after hot rolling from a temperature approximately 900°C. When applying DQ method, the austenite can be recrystallized or non-recrystallized. This condition depends on the chemical composition and the rolling pass schedule. [23] Direct quenching compared to conventional QT method, enables a better microstructural control and to achieve higher strength levels for a given chemical composition [22]. Furthermore, as one stage of the process is eliminated, the process is more rapid and energy efficient [24].

Ultra-high strength steels are required for successful light-weight design. UHSS are exploited in various industries in several applications, such as cranes, commercial vehicles, containers, offshore platforms, and agricultural and forestry machinery. The utilization of UHSS enables a reduced material thickness at an equal performance level and to increase performance level without changing dimensions. A reduction in material thickness leads to a decrease in weight and volume, and consequently results in cost savings from procurement, manipulation and processing. Due to a reduction in volumes and weight, transportation costs are decreased and additionally low unit weights enable to utilize smaller transport units and lifting devices. Furthermore, reduced material thickness leads to lower welding and laser cutting costs due to shorter operating times and in case of welding less filler materials are needed. The potential savings depend on the particular application. [25]

2.1.1 Classification of Ultra-high strength steels

The classification of UHSS is not entirely unambiguous. This is because they can be classified in various ways, such as in terms of composition, microstructure or manufacturing methods. In this work designation is done in terms of strength level. Here, all steel types with yield strength greater than 700 MPa are classified as UHSS. Yet, this classification

system is not explicit, since many steel types can be developed to different steel grades. The ultra-high strength class is highly wide and includes several different steel families. [15]

Reche classifies UHSS into three main steel families, which are dual phase (DP), transformation induced plasticity (TRIP) and multiphase (MP) steels [26]. However this proposition is rather inadequate. Typically steels belonging to the advanced high strength steels (AHSS) family can have yield strength in excess of 700 MPa. AHSS are complex multiphase steels, which consist of various volume fractions of ferrite, bainite, retained austenite and martensite. Carefully selected chemical compositions and precisely controlled heating and cooling processes lead to multiphase microstructures that provide desired properties in AHSS. [18] Generally DP, TRIP, complex phase (CP) and martensitic steels are graded as AHSS steels [27]. Figure 2 presents various steel families and their strength and elongation properties.
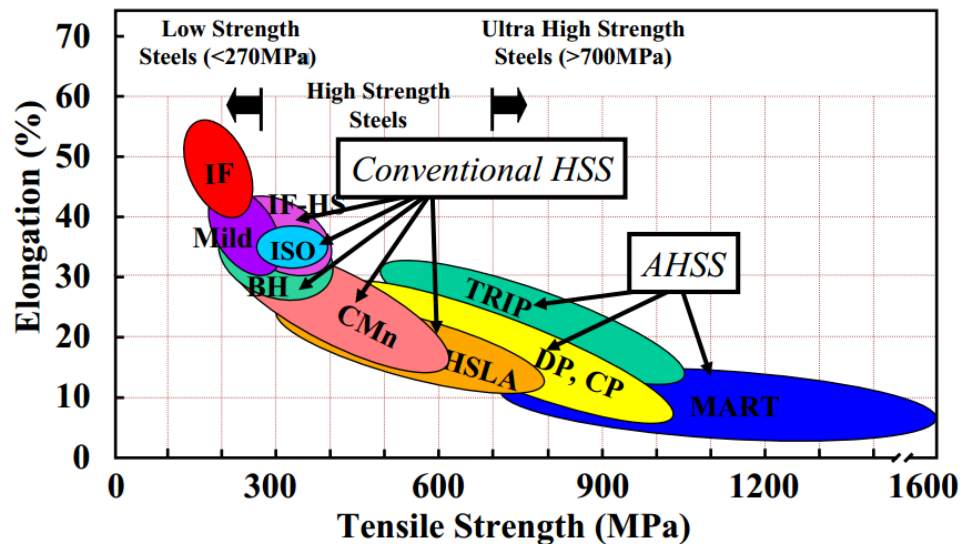
Figure 2: Various steel families, and their strength and elongation properties [28, p. 9].

In some cases, high-strength low alloy (HSLA) steels can also be graded as ultra-high strength steels due their strength properties (Figure 2). In this work ultra-high strength steels belonging to AHSS family and additionally HSLA steels are briefly discussed.

There appears not to be a universally accepted definition for CP or MP steels and occasionally the definitions of these two families overlap. MP steels, in the simplest way, can be classified as steel types that are not single-phase materials. [29] According to Reche, MP steel stands for a microstructure consisting of ferrite/bainite or precipitation-hardened bainite or mixture of bainite and martensite. [26] Yet, in this work MP steel refers to steel containing more than one phase and thus encompasses nearly all UHSS. In this work term CP steels refers to steels that are composed of a highly fine microstructure consisting of

several various microstructural constituents. Typically the microstructure is composed of different amounts of bainite, martensite, ferrite and M/A constituents. Mechanical properties of multiphase steels, and hence CP steels, depend highly on the morphology, volume fractions and distribution of the constituents [30].

DP steels consist of a ferritic matrix containing hard second phases in the form of islands. Second phase can be martensite or martensite / bainite. [26] DP steels are formed by controlled cooling from austenite phase or from ferrite plus austenite phase to ferrite followed by rapid cooling that transforms the remaining austenite to martensite. Due the production process, a small volume fraction of bainite or retained austenite can be present. [31] DP steels provide a combination of high strength and total elongation, in particularly uniform elongation. In addition due its high work hardening capability it provides good fatigue and energy absorption properties. [26]

TRIP steels consist of a ferritic matrix containing islands of retained austenite. In addition to retained austenite, hard phases, such as bainite and martensite, are present in various amounts. [32] Due to the transformation of austenite into martensite during deformation, significant strain hardening occurs and hence the initiation of necking is delayed, providing high uniform elongation [26].

HSLA steels can be defined as low-carbon steels that contain small amounts of alloying elements in order that desired strength levels are attained. Yet, generally the strength level of HSLA steels does not exceed 700 MPa. Characteristics of HSLA steels are described in ASTM specifications. [33]

2.1.2 Typical microstructural constituents and phases of UHSS

As discussed previously, UHSS can consist of several different phases and microconstituents. Here the most typical phases and microconstituents are discussed briefly. These include ferrite and cementite phases, and selected morphologies of bainite, martensite and M/A constituents.

Ferrite is the other allotropic modification of iron. The crystal structure of ferrite in temperatures lower than 910 ° is body-centered cubic (bcc). Here polygonal and quasipolygonal ferrites are shortly introduced. Polygonal ferrite forms at the highest austenite phase transformation temperatures and with the slowest cooling rates. Ferrite grains nucleate at grain boundaries of austenite and grow away from grain boundaries forming equi-axed grains. The strength of polygonal ferrite is proposed to depend mainly on its grain size and dissolved elements. For example by adding micro-alloying elements, such as niobium or titanium, the grain size of polygonal ferrite can be affected. Quasipolygonal ferrite forms as a consequence of more rapid cooling compared to polygonal ferrite. The transformation mechanism is reconstructive, indicating that diffusion of all atoms takes place. During the transformation, the composition does not change, only the crystal structure

changes from face-centered cubic (fcc) to bcc. This is achieved by a rapid, short distance transition of atoms across the austenite-ferrite interfaces. The grains of quasipolygonal ferrite are coarse and they are able to cross the grain boundaries of austenite. In addition its grain boundaries are irregular, which is in contrary to the case of polygonal ferrite. [34]

Cementite is a phase consisting of carbon and iron (Fe_3C). It is the most stable carbide of iron [35]. Cementite can be present in several different forms, e.g. as a precipitate in ferrite or as a constituent of for example bainite. Cementite is hard and brittle; the hardness of cementite basically varies in the range of 1000-1500 Vickers [36]. Therefore in higher volume fractions, its presence typically degrades ductility and formability [37].

Martensite refers to a metastable microconstituent that is achieved by cooling the material in a sufficiently rapid manner, so that diffusion is prevented. Martensite stands for ferrite that is supersaturated with carbon. The formation of martensite is diffusionless shear transformation. Martensite can be classified as lath or plate martensite according its morphology. [38] The developing morphology is dependent on the carbon content. Lath martensite forms in alloys with a carbon content (wt. %) less than 0.06, plate martensite forms with a carbon content (wt. %) greater than 1 and a mixed structure in contents between. [39] Due to low carbon contents in materials used in this work, only lath martensite is considered.

Due to coordinated movement of atoms during the formation of martensite, the austenite and martensite lattices are closely connected [40]. Lath-martensite is known to nearly satisfy Kurdjumov-Sachs (K-S) orientation relationship with respect to austenite. The microstructure of lath martensite is hierarchical consisting of packets, blocks, sub-blocks and laths. The grain of parent austenite is divided into packets, which consist of blocks. Blocks are composed of sub-blocks, which still consists of parallel laths. The laths in the same block have the same variant of the K-S orientation relationship. [41] In case of K-S orientation relationship, 24 crystallographic variants of martensite are able to develop from a single crystal of austenite [42]. The hierarchical microstructure is illustrated in Figure 3.
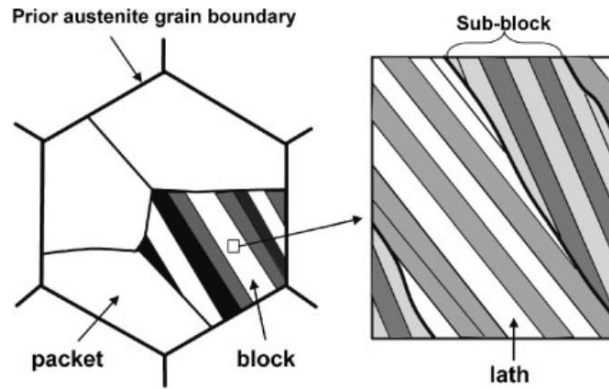
Figure 3: Schematic illustration of lath martensite [43].

The length of the laths highly affects strength and hardness properties. It has been discovered that boundaries of the sub-blocks act as obstacles for dislocation movements and thus increase its strength. [43, 44]

Martensite-austenite (M/A) island is a microstructural constituent that forms when the cooling rate is not sufficiently rapid in order to get full martensite nor slow to deposit carbide. The carbon-containing austenite maintains in a blocky and/or flaky island pattern and partially transforms to martensite. The composition of M/A islands depends on the alloying and the cooling rate. The properties of M/A islands are highly governed by the amount of retained austenite, which is principally determined by the alloying elements. [45]

Bainite refers to a microstructure that develops as austenite decomposes into ferrite and cementite. The presence of carbides in the microstructure is however not essential, since their formation is secondary reaction, as seen later. [46] Bainite is composed of aggregates of plates or laths of ferrite, which are separated by a second phase, such as untransformed austenite, martensite or cementite. These aggregates are referred as sheaves, and the laths and plates are termed as sub-units. [36] In literature, there is a controversy regarding to the formation of bainite. Yet, generally it is proposed, that bainite forms by a displacive, diffusionless transformation. According to this theory, a subunit nucleates with carbon partitioning and grows displacively until due the plastic relaxation in the neighbouring austenite the growth is stopped. After this, carbon leaves the supersaturated ferrite by diffusion and precipitation into the austenite. The formation, i.e. nucleation and growth, of new subunits occur on the tips of the old ones. Carbon can also precipitate within the subunit, in which case lower bainite (LB) is formed. [47] In LB, cementite precipitates can develop from the carbon-enriched austenite or supersaturated ferrite. In case of cementite precipitation from supersaturated ferrite, there is orientation relationship termed as Bagaryatski orientation relationship. [48]

Bainitic microstructures can be classified in several manners; however in this work a classification system proposed by Zajac et al. is applied. This is based on the morphology

of ferrite and the type of the second phase. Zajac et al. classifies bainitic microstructures into five various classes, yet here only granular bainite, lower bainite and upper bainite are discussed (Figure 4). Granular bainite (GB) consists of a highly dislocated irregular type of ferrite with second phases of a granular morphology. [49] The ferritic matrix comprises bunches of bainite, where thin austenite regions are present between the subgrains [36].The second phase constituents, which can be bainite, mixture of "incomplete" transformation products, M/A, martensite, degenerated pearlite or debris of cementite, are distributed between the ferrite grains. The structure of GB does not contain carbides. The mechanical properties of granular bainite are remarkably affected by the M/A islands. [49] A higher bainite start temperature (B_S) promotes the formation of GB [50]. Additionally it is proposed that its formation is furthered by a low boron content and a high strengthening level of austenite [51, 52]

LB comprises regions of lath like ferrite with cementite precipitated inside the ferrite laths. The cementite particles typically precipitate merely in one variant of the orientation relationship. Such that they are parallel arrays inclined at approximately 60° to ferrite laths. Most of the cementite particles are in contact with ferrite laths, yet it is possible that smaller particles are enclosed inside ferrite laths. [48, 49]

Upper bainite (UB) consists of regions of lath like ferrite and cementite particles that are located between these regions. The second phase is always cementite, which has precipitated from austenite. Ferrite laths grow in groups which are termed as bainite bunches. The laths in the same bunch are parallel and they possess an identical crystal orientation. [53] In case of UB, the ferrite laths have a K-S type of orientation relationship with the austenite in which it forms [46]. In UB, there is additionally an orientation relationship between cementite particles and the austenite from which they precipitate. This relationship is termed as Pitsch orientation relationship. [53] In case the steel is alloyed with micro-elements, the laths can consist of precipitation hardened carbides [54]. The cementite particles in upper bainite are rather coarse, and hence they can act as nucleation sites for cracks [53]. Figure 4a presents schematically the structure of granular bainite, 4b lower bainite and 4c upper bainite.
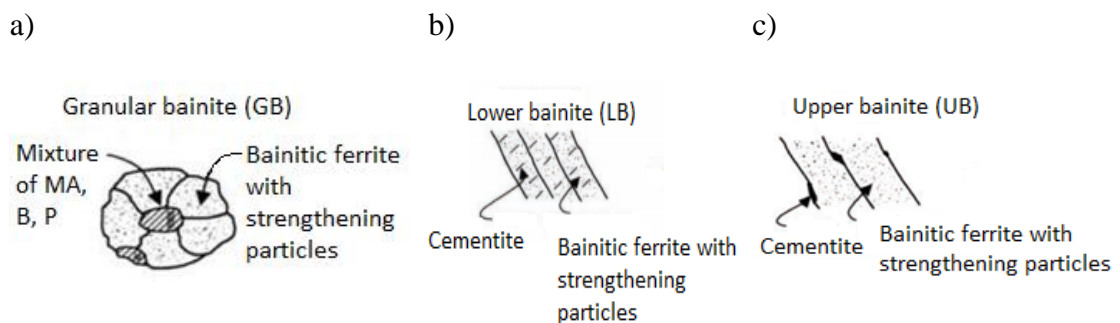
Figure 4: a) Schematic illustration of granular bainite, b) lower bainite and c) upper bainite [49].

Between these three classes, GB tends to form at highest temperatures, followed by UB and finally LB at the lowest temperatures [55].

3. DEFORMATION OF MATERIAL

When a solid material is subjected to a sufficient force, it results in deformation of the material. Deformation can be either temporary or permanent. Temporary deformation is termed elastic deformation and it disappears when the applied forces are removed. Permanent deformation, which is referred to as plastic deformation, is irreversible and thus it stays after the applied forces are removed. The type of material along with several other factors determines the extents of elastic and plastic deformation. [56]

A comprehension of the terms stress and strain are essential for analyzing the deformation of a material. Stress can be determined as the intensity of force *F* at a unit area *A*. [57] The most significant types of stresses are tensile, compressive and shear stresses. Tensile stress stands for a stress induced to a specimen, when subjected to two equal and opposite forces pulling, while in a compressive stress the forces are pushing. Shear stress refers to a stress induced in a specimen, when subjected to two opposite forces of equal in value that are operating tangentially across the resisting section. [58] Strain refers to the amount of deformation in the body that occurs as external forces are applied to the material [57].

Elastic deformations are due to an increase in the inter-atomic distances. When atoms move away from their equilibrium positions, forces that try to return atoms to their equilibrium positions, start to affect. The deformation of material is reversible up to a certain limit of the applied stress. Plastic deformation occurs as atoms are displaced for several hundreds or thousands of lattice constants as the material is subjected to external forces. Due the large displacement, the atoms are not able to return to their initial locations as the external forces are removed. Thus residual deformation remains after removing the external forces. Plastic deformation can occur by several mechanisms, but the most characteristic and common is so-called slip mechanism. This is realized by the motion of dislocations. [59]

The calculated shear strength of a perfect metals crystal is 1000 to 10,000 times greater than observed shear strengths. This is due to crystalline imperfections, i.e. dislocations, which are present in real crystalline lattice. Dislocations are one of the most significant microstructural characteristics controlling the mechanical properties of crystalline materials. [60] Dislocations are created when metal solidifies and as metal crystalline is deformed even more dislocations are created. Thus the density of dislocations can vary from 10^6 cm/cm^3 to 10^{12} cm/cm^3. [61] Dislocations are line defects, which extend over several hundreds or even thousands of lattice parameters whereas in the other two directions they extend to a significantly smaller number of lattice distances. Dislocations can be classified into edge dislocations and screw dislocations. [59] Edge dislocation is defined as an extra half-plane of atoms above (or below) the dislocation line. It generates a field of

elastic deformation around the dislocation. The lattice above the dislocation is in a state of compression whereas below the dislocation there is a state of tension. In Figure 5 the concept of edge dislocation is illustrated. [62]

a)   b)
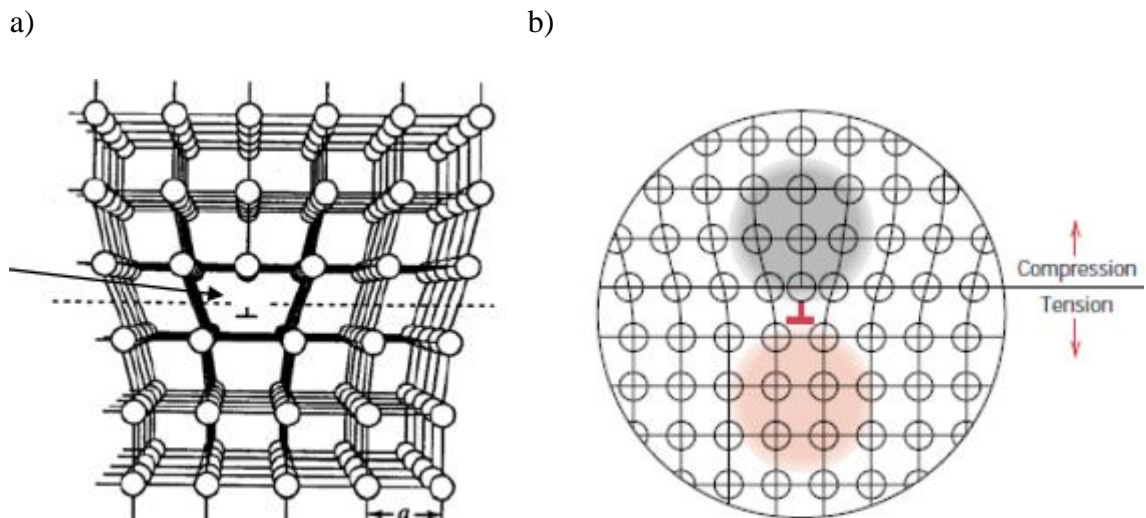
Figure 5: a) Schematic representation of an edge dislocation and b): illustration of compression and tension states [62].

In Figure 5a the arrow indicates the edge dislocation line. Below this line the atoms are pulled apart while above this line they are pressed together. In Figure 5b the idea of compression and tension states are illustrated. In case of an edge dislocation, the Burgers vector is perpendicular to the dislocation line. [62] Screw dislocation is more difficult to visualize in a crystal, it is illustrated schematically in Figure 6.
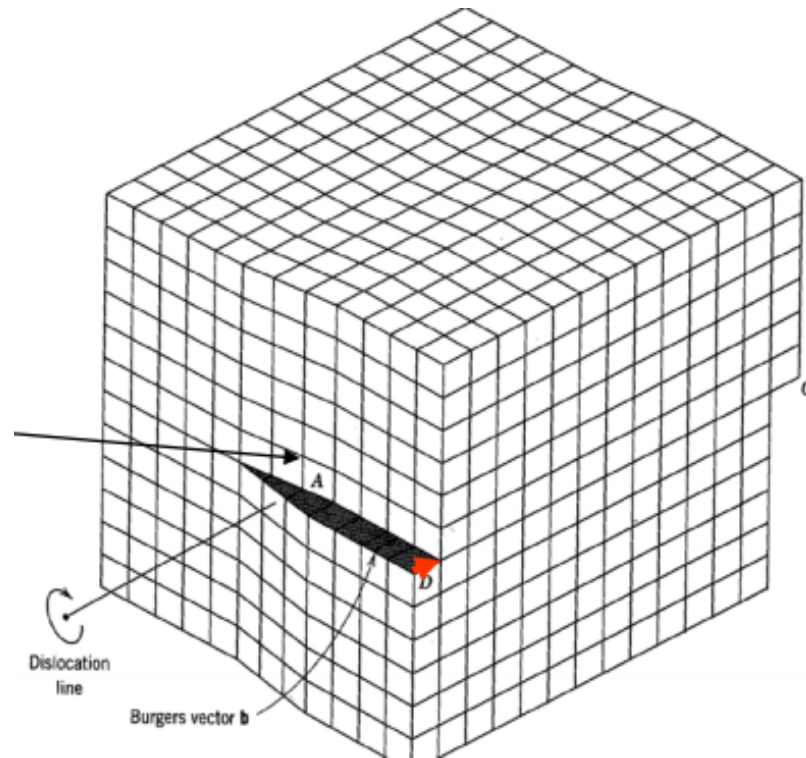
Figure 6: Schematic representation of a screw dislocation [62].

In a screw dislocation the Burgers vector is parallel to the dislocation line, thus it can glide in any plane. In case of a screw dislocation, the atomic planes generate a spiral surface around the screw dislocation line. Moreover various combinations of these two types, which are called mixed dislocations, can be produced. [63]

Deformation of a polycrystalline material is more complex that in the case of single crystal. Thus in this chapter the deformation of a single crystal is first discussed, followed by the observation of deformation of polycrystalline material. In particularly plastic deformation of both single crystal and polycrystalline are discussed profoundly.

3.1   Deformation of single crystal

The term single crystal stands for a crystalline material that consists of one crystal in the whole material mass [59]. The arrangement of atoms in a single crystal is perfect, repeated and periodic, and it reaches throughout the whole sample without any disturbance. Furthermore a single crystal does not have grain boundaries. [61] As elastic deformation of single crystals occurs, the atoms are not displaced permanently with respect to each other. The elastic deformation of single crystal follows Hooke's law:

$$\sigma = E\varepsilon \tag{1}$$

Where σ equals to the stress applied to the material, E is the modulus of elasticity and ε is strain. According to Hooke's law (1) stress is directly proportional to strain and the occurring displacement is via mild warping of crystal lattice without atoms changing their relative positions or losing neighbour atoms. Since the displacement is not permanent, as the deforming forces are removed, the lattice returns to its original shape and size. [61]

Plastic deformation is produced by dislocation movement. The mechanism and rules of dislocation movement can be studied by observing the deformation of single crystals. [64] Plastic deformation in single crystals takes place either by slip or twinning. Both of these occur due to pure shear stresses. Deformation by slip occurs as one part of the crystal either moves or glides over another part along particular planes. [61] Slip occurs step-by-step by the movement of dislocations [65]. Slip mechanism takes place by the slipping of crystal planes complying with specific rules of crystallography. According to these rules of crystallography, plastic deformation takes place most probably in the densest crystalline planes, i.e. slip planes and within these planes in the densest directions, i.e. slip directions. Slip planes together with slip directions form slip systems, and the preferred slip system depends on the material. [59] The concepts of slip plane and slip direction are represented in Figure 7.
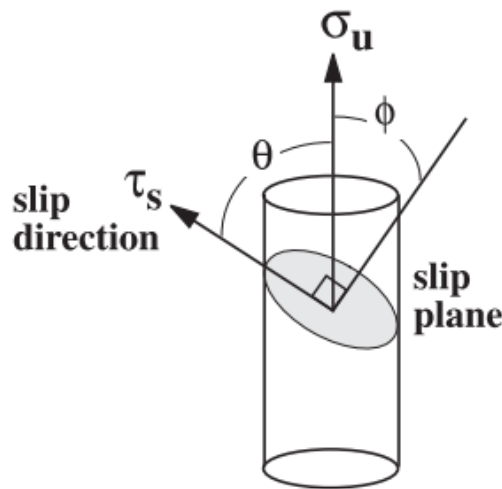
Figure 7: A schematic presentation of slip plane and slip direction [66, p. 351].

In Figure 7 σ_u is the applied stress in uniaxial tension, ϕ is the angle between normal to the slip plane and the applied force and τ_s is the shear stress, θ is the angle between the direction of the slip and the applied force.

The capability of material to experience plastic deformation is highly dependent on the amount of independent slip systems that are able to operate during deformation. [67] In case of a polycrystalline material, slip occurs simultaneously on several slip systems and due to the interplay between dislocations the process is fairly complex. Thus a simple

case of single crystal deformation with dislocation glide on a single slip system is informative to explore. In this simplification, the single crystal can be considered as a deck of cards, in which each card acts as a slip plane on which deformation will take place. In figure 8a a single crystal tensile bar is represented. The lines across the bar illustrate the slip system that will become active.

(a)   (b)   (c)
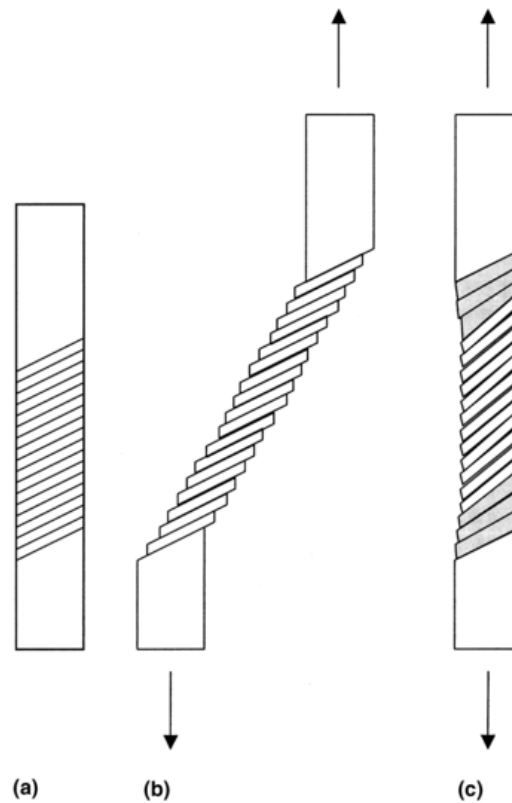
Figure 8: Illustration of slipping, a) Single tensile bar prior to slipping, b) Displacement of the top of the sample versus bottom of the sample due to restriction of slipping to occur only in certain slip planes and c) The reorientation of the lattice [68].

Since slip is limited to occur at the slip planes, deformation causes a displacement of the top of the sample in comparison to the bottom of the sample, as illustrated in Figure 8b. However, as deformation occurs the slip planes rotate, leading to a development of the lattice orientation during deformation as shown in Figure 8c. In Figure 8c the tilted slip planes stand for regions where strain accommodation bending takes place, while in the untilted regions pure lattice rotation occurs. [68] As slipping occurs, the crystal lattice rotates in such way, that under uniaxial tension the active slip direction or in case of uniaxial compression the active slip-plane normal proceeds towards alignment with the direction of the applied stress. As a result, the orientation of the crystal alters during deformation and this consequently leads to a change of the Schmid factor, which will be discussed later. [69]

To understand the plastic properties of crystal structures, it is essential to comprehend their slip systems. During slip atoms move from an equilibrium position to an adjacent

equilibrium position through the shortest distance. The crystal structure of ferrite is bcc; the unit cell is shown in Figure 9a. In this kind of crystals, slip always occurs along $< 111 >$ direction and the shortest atom to atom translation vector is $\frac{1}{2}a_0 < 111 >$. The slips systems of a bcc crystal structure are $[(110)[\bar{1}11], (112)[11\bar{1}]$ and $(321)[\bar{1}11]$. The crystal structure of austenite is fcc; the unit cell is presented in Figure 9b. In fcc metals the slip system is$(111)[1\bar{1}0]$ and the closest atom to atom distance is $a/\sqrt{2}$. [70]

a)   b)
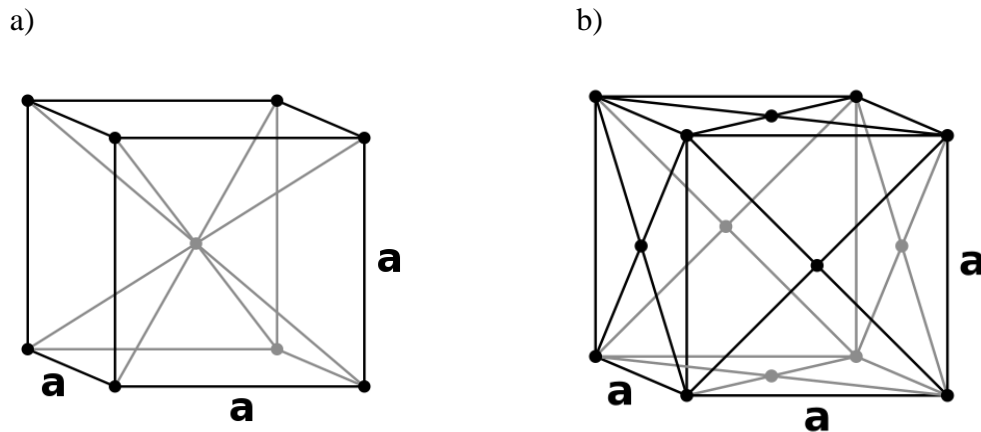
Figure 9: a) Unit cell of bcc and b) Unit cell of fcc [71].

In Figure 9, a stands for the side of a unit cell.

The amount of stress that is needed to trigger slip is a function of the orientation of the slip system, and consequently the lattice, to the imposed deformation [68]. For single crystals this relationship is determined by the Schmid law. The resolved shear stress operating in a certain slip plane along a certain slip direction lying in the slip plane can be defined as:

$$\tau_R = \sigma \cos \phi \cos \theta \qquad (2)$$

where σ is the applied stress in uniaxial tension, ϕ is the angle between normal to the slip plane and the applied force and θ is the angle between the direction of the slip and the applied force. All these factors are illustrated in Figure 7. Slip occurs once resolved shear stress τ_R is greater than the critical resolved shear stress τ_{crss}. It is possible that in a particular crystal, there are several available slip systems. As the tensile load is increased, the resolved shear stress on every slip system increases and finally on one system the critical resolved shear stress is reached. On this slip system, termed as the primary slip system, the crystal first starts to deform. As the load is further increased, the critical resolved shear stress can be reached also in other slip systems and consequently they also start to operate. The primary slip system is the one with the greatest Schmid factor $\cos \phi \cos \theta$. [70]

3.2   Deformation of polycrystalline material

Nearly all engineering alloys are polycrystalline, which refers to a material that is an aggregate of several crystals or grains [61]. The total deformation of a polycrystalline material is due to crystallographic slip resulting from movement of dislocation on the active slip system, and elastic lattice distortion [72] Deformation and slip in polycrystalline materials are more complex compared to single crystals. Due to several reasons crystals of polycrystalline aggregate do not deform like single crystals. Firstly since each crystal or grain is surrounded by other grains, it cannot deform freely. [61] Secondly, as grain boundaries affect the deformation, they prevent easy propagation of slip from grain to another [70]. Surrounding grains resist deformation and thus larger stress is needed to deform a polycrystalline material compared to single crystal. Furthermore, as the orientation of each grain or crystal is different. [61] Hence some crystals are oriented more favorably to the loading force from the point of view of plastic deformation [59].

At low and intermediate temperatures, there are two principal processes by which deformation occurs. These processes are twinning, which occurs on certain planes, and dislocation movement, which occurs along particular slip systems. Slip systems are specified by a slip plane and a direction of dislocation glide, which commonly are the most atomically close-packed planes and directions in the lattice, as discussed previously. [68]

When a metal crystal is under tension, the sliding blocks turn towards the direction of pulling force. In consequence, the slip planes orient themselves with the direction of deformation. This similar phenomenon takes place when a polycrystalline material is under stress. Slip starts first in the grains in which the slip system is most favorably oriented in relation to the applied stress. [73] In the most favorably oriented crystallites slip planes form 45° angle with the external loading force [61]. As the deformation continues, also the less favorably oriented grains rotate and orient themselves into a new position so that they can deform. After a particular degree of deformation, the majority of grains have a certain plane in the direction of deformation. This is referred to as preferred orientation. [73]

Plastic deformation in polycrystalline material is never entirely homogenous [61]. The deformation is highly affected by the difference in behavior between various grains and grain boundaries [74]. In general, grain size, grain orientation, orientation of adjacent grains and the appearance of grain boundaries all have an effect on the local material response resulting in heterogeneous stress and strain fields at the microstructural scale. Therefore several theories have been proposed to explain the non-uniformity of deformation between adjacent grains and in the neighbouring area of grain boundaries. [75]

3.2.1 Lüders bands

A stress-strain curve attained by pulling a polycrystalline bcc metal contains both an upper and a lower yield point. At the lower yield point, plastic deformation occurs through travelling of a type of plastic wave termed as Lüders band. [76, p. 1296] Yield point phenomenon is consequence of locking and unlocking dislocations. The motion of dislocations is hindered by solute atoms, i.e. Cottrell atmosphere appears. Hence yield strength increases until the Cottrell atmosphere is broken and therefore the dislocation are unlocked from solutes. [77] It is proposed that in case the initial dislocation density is notably high, like in case of martensite, this phenomenon does not occur. Instead of a lower initial dislocation density, like in case of ferrite, this phenomenon occurs and therefore Lüders bands form. Lüders band refers to localized region of plastic deformation that appears in polycrystalline bcc metals. [78] In other words, Lüders band can be regarded as locally deformed plastic phase, while outside the band still only elastic deformation occurs [79]. According to Shaw and Kyriakides, Lüders bands are considered as macroscopic slip bands [80]. Lüders bands appear on the surface of the sample and they are oriented at approximately 50° to the loading direction [81, p. 151]. These bands are considered as material instabilities, which result in a macroscopic nonuniform plastic deformation in the range of 1-4 %. The development of these bands is a dislocation impelled phenomenon. In steels Lüders bands form once the yield point has been exceeded at the initial part of the plastic regime of the material. [82] The growth of these bands occurs at a nearly constant stress level. In consequence, in the stress-strain curve, there is no work hardening apparent before the band has expanded completely across the sample. [78] In Figure 10 is represented a stress-elongation response of a steel manifesting Lüders band, i.e. Lüders strain.
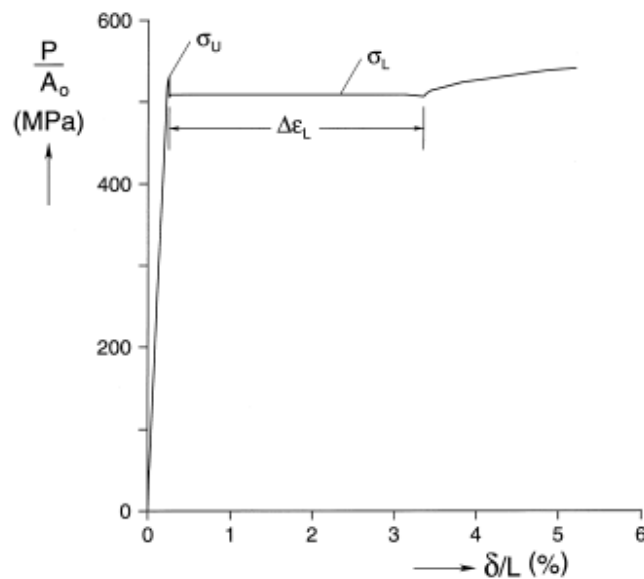
Figure 10: A stress-elongation response of a steel exhibiting Lüders band [80, p. 843].

After the entire sample is consumed by Lüders deformation, the deformation becomes uniform once again [82].

4. STRAIN LOCALIZATION

It is generally known that plastic deformation of materials is not uniform [83]. Even though homogeneous stress is applied to the material, the deformation centers in a narrow strip zone as the deformation increases. That kind of concentration of deformation is termed as strain localization and the strip zone is referred to as the shear band. [10] Yet, the formation of shear bands, i.e. strain localization, does not occur immediately once bifurcation of uniform deformation takes place. The initiation of non-uniform deformation is termed as diffuse necking. This is consequently followed by localization of strain into a narrow band, i.e. shear band. Figure 11 illustrates the schematically the difference between these two phenomenon.

diffuse neck   localized neck
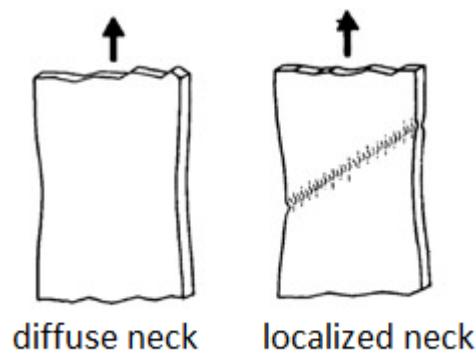
Figure 11: Schematic illustration of the difference between diffuse and localized neck [57].

In this work mainly factors effecting localized necking, i.e. formation of shear bands, are discussed. Yet, since the formation of shear bands follows the occurrences of uniform plastic deformation and diffuse necking, it can be proposed that by delaying these phenomenona additionally strain localization is delayed. In this work the term localization is always relates to the phenomenon of localized necking, indicating that shear bands are formed. A true stress-strain curve in Figure 12 illustrates the initiation points of diffuse and localized necking as the strain increases.
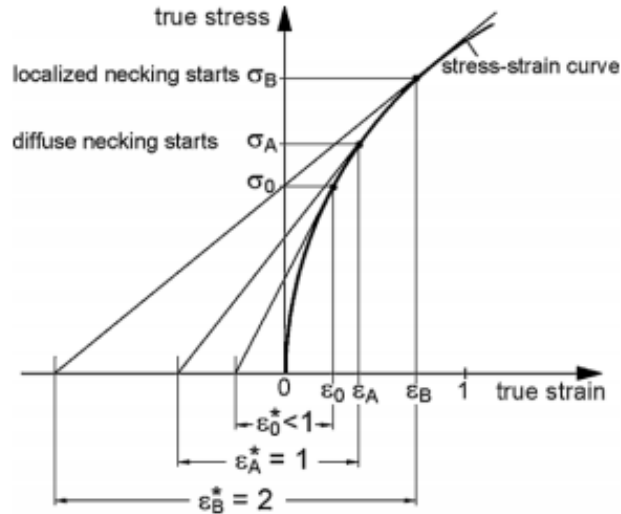
Figure 12: True stress strain curve presenting the initiation of diffuse and localized necking in terms of true strain [84, p. 2047].

In Figure 12 ε_0 and σ_0 stand for strains and stresses where strain hardening is dominant, ε_A and σ_A equal to critical values, where bifurcation of uniform deformation initiates, i.e. diffuse necking, and ε_B and σ_B represent critical values where strain localization initiates [84].

Strain localization is considered to be a precursor to material failure during deformation. Materials' failure by strain localization occurs commonly in various events such as in forming, punching, high speed deformation and ballistic impact. Therefore it is significant to understand and predict this phenomenon, in order to develop high formability materials. Strain localization occurs in several materials such as in plastics and metals. Due to its frequency and significance the mechanism of the strain localization has been widely studied. [3]

In this chapter first the phenomenon of strain localization is discussed, including a profound review on the bands of localized straining, i.e. shear bands. Next the effect of work hardening capability on strain localization is observed. Following this, the influence of microstructure homogeneity on strain localization is studied. In the case of microstructure homogeneity texture, defects and homogeneity of phase structure are considered. Finally, the relationship between strain localization and surface roughness is examined.

4.1 Description of strain localization

Strain localization is a highly complex phenomenon, in which an initially uniform deformation localizes into a narrow region, which is termed as shear band [85, p. 201]. It occurs in various materials, such as metals, rocks and organic compounds, and in various loading conditions. It has been found that there is a critical strain at which strain localization takes place. Before the critical strain is reached, the deformation occurs homogeneously in a

macroscale. [3] The amount of plastic deformation, which induces the initiation of strain localization, depends on the material; it varies from 0,01 to higher [83]. Inhomogeneous deformation of metals is highly undesirable as it leads to localized tearing and produces a rough appearance. Therefore the occurrence of strain localization often affects materials mechanical properties determinatively and thus limits the usage of material for a destined structural application. There is a variety of mechanisms that strain localization may occur and its length scale can vary from nanoscale to macro scale. [86, 9-20]

Already in the late 19th century, it was observed by Considere that loss of uniform deformation is the precursor to material failure [87]. Today it is known that the initiation of non-uniform deformation in simple tension of plastic materials is related to the achievement of maximum nominal stress and that the consequential strain localization results into failure. [88, p. 1889] Thus the initiation point of strain localization is generally used as the criteria to establish the forming limit diagram of materials [89].

One example of plastic deformation localization is necking that occurs during uniaxial tension. Localization of deformation results from the competition of two various processes, which are geometric softening and work hardening. [90] Geometric softening refers to a phenomenon wherein the force required to induce a slip is lower once the crystal has been deformed. It is highly dependent on the orientation of the tensile axis within the crystal. [91] As far as the hardening of sample is predominant, the sample deforms uniformly and new regions that are unhardened participate in deformation. Once the deformation increases to a certain level, the stability of plastic flow disappears and necking initiates. [90] In other words, in generalized sense strain localization occurs once local softening begins. The localization of plastic deformation into a shear band can be due to several reasons. When local softening occurs, for example due to the presence of an inclusion, the material at that region will reach the peak stress while elsewhere in the material the peak stress is not yet reached. At that region of the material runaway deformation occurs since increasing deformations can be maintained at decreasing stress. [85, p. 202]

4.1.1 Introduction to shear bands

Shear bands are considered as non-crystallographic band-like regions, where plastic flow is concentrated at [92]. Shear bands can either persist in which case the deformation proceeds in a non-uniform manner, or alternatively local deformation can lead to a direct ductile fracture [13]. It is characteristic for shear bands that massive collective dislocation activity occurs in narrow local deformation region, whereas in the abutting matrix comparably uniform flow occurs. Inhibiting homogeneous slip contributes to the formation of shear bands. [92] The initiation of a shear band occurs with a crystallographic slip within a single grain and therefore the initial orientation affects its formation. However after the initiation it extends over the entire cross-section of the sample along the shear

direction without a crystallographic feature. [3] This means that shear bands pass through the slip planes and are capable of crossing existing grain boundaries into other orientations. These band-like regions have clearly defined boundaries, in metals their width is several microns. [10, 83] In Figure 13 a microstructure consisting of a shear band is represented.
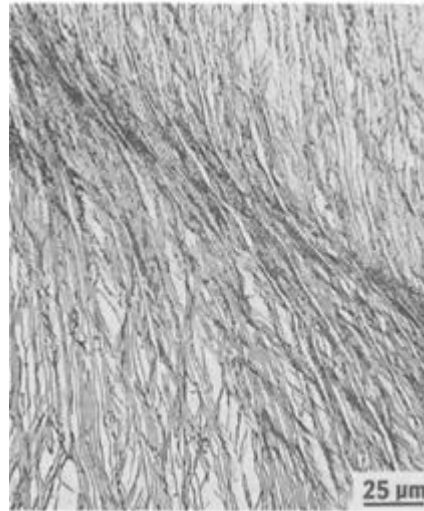
Figure 13: Illustration of a shear band [93, p. 47].

The direction of the bands depends on the direction of the acting force. On the deformed surface of the material the traces of formed bands are perpendicular to the direction of acting force. On the side surfaces of the material, the traces go at an angle of 15-55°. [83] Furthermore, Lopes found a relationship between the formed shear bands and the slip planes; shear bands are found to be parallel to the slip planes [94]. The strains inside and outside the shear band differ. Whereas the state of stress is nearly identical in these regions and therefore it is practically identical to the macroscopic stress that is calculated from the external load and outer appearance of material. [10]

4.2 The Effect of work-hardening capability on strain localization

Work hardening has a significant role in the onset and development of localized deformation. [12]. Work hardening, additionally known as strain hardening, is a significant strengthening process for steels, which refers to a phenomenon, wherein during deformation of metals the yield strength increases as the strain increases [95, p. 29]. The work hardening of a material can be described by Hollomon Equation: [96]

$$\sigma_t = k\varepsilon_t{}^n \tag{3}$$

where σ_t refers to true stress, k is strength coefficient, ε_t is true strain and n is the work hardening exponent. The strength coefficient is equal to the true stress when true strain is

1 [97, p. 269]. This indicates that in case of steels with greater strength, the magnitude of k is additionally greater. Additionally, it is noteworthy to clarify, that the magnitude of n changes with deformation.

Strain hardening results from the appearance of dislocations within a material and the resistance they offer to the propagation of other dislocations [95, p. 29]. Dislocations are stored due to two different reasons: either they accumulate by trapping one another in a random manner, or they are needed for the compatible deformation of various constituents [98]. Several properties, such as strength, ductility and deformability, are related to strain hardening characteristics. [99] Furthermore strain hardening has an effect on the fracture resistance of the material. It has been noticed that as the strain hardening rate increases, the materials resistance to fracture increases. [100]

Plastic deformation is realized fundamentally by the movement of dislocations [59]. This is heterogeneous inherently, which is represented by the existence of a dislocation line. Additionally the fact that dislocations require sources for their development is another evidence for heterogeneity. [101, p. 319] During the movement of dislocations, they react with each other and during this new dislocations are created. Therefore the dislocation density increases as the material is being deformed. Due to the high elastic stress field around the dislocations, the energy level of crystals increases as the amount of dislocations increase. Moreover the elastic stress field that is around the dislocations hinders their movement. Due to the surrounding elastic stress field, the dislocations are not able to approach each other within a particular limit. Consequently, dislocations pile-up behind each other at a particular distance. [59]

The strain hardening properties of materials can be indicated by the strain hardening exponent, i.e. n-value [99]. Strain hardening exponent determines how fast strength and hardness of material increase [102]. A higher strain hardening exponent indicates that a material work hardens at a higher rate due to plastic deformation. It has been found that n-value equals the true strain at the ultimate tensile strength that is the limiting amount of strain for homogeneous deformation. [103] A high n-value indicates that the material can work harden sufficiently in critical regions, so that the strain is transferred to neighboring regions. Therefore materials, that have high work hardening capability, are capable of increasingly delay plastic instability and consequently prevent strain localization. [104, pp. 15-16] For processes that comprise plastic deformation, it is preferred that the applied material has a high strain hardening exponent [103].

The work hardening exponent is highly dependent on the microstructure of the material [99]. The crystal structure delineates the nature of dislocations and has an effect on the barrier structure, which develops during deformation [105, pp. 6-7]. The interaction between dislocations of the same slip system with the same slip plane and same Burgers vector is rather weak. Therefore in such case the resulting work hardening is also weak. [101, p. 319] In case of bcc metals, the strain hardening is principally dependent on the

formation of athermal barrier structures, such as dislocation pile-ups at grain boundaries [105, pp. 6-7]. Work-hardening capability is highly dependent on the dislocation density. A high initial dislocation density indicates that the material's capacity to produce new dislocations is low, and hence it possesses low work-hardening capacity. Therefore work-hardening capability is notably dependent on the microstructure of the material. High temperature transformation products provide greater work-hardening capability compared to low transformation products. This is due to the lower initial dislocation density, which high temperature transformation products possess. [99, 103] Strain hardening exponent is affected by the strain ratios [99]. The effect is dependent on the microstructure. It can be proposed that in case of high temperature transformation products possessing a low initial dislocation density, n-value first increases and then slowly decreases. Instead, in case of low temperature transformation products possessing a high initial dislocation density, it can be assumed that the n-value decreases from immediately from the beginning.

The effect of work hardening capability on the width of the region in which deformation localizes has been studied. However, there is no mutual understanding that how work-hardening capability affects the width of a shear band. According to Xu et al., a high work-hardening capability results in a wider band [99]. On the contrary Shawki and Hartley found that smaller work-hardening capacity leads to a wider band [3].

Negative work-hardening rates precede plastic instabilities [94]. It has been found that strain softening, even in small amounts, promotes strain localization [106]. Lopes et al. suggest that localization of deformation is primary due to thermal, textural (geometrical) or structural softening and the development of shear bands is related to softening. Structural softening refers to the decrease of the strength of the obstacles to the propagation of dislocations. Geometrical softening is related to crystallographic rotations which are capable of optimizing the orientation of slip systems in the most grains. It is rather easy to define if thermal softening is the source for flow localization. However, it is difficult to distinguish whether structural or textural softening is the origin of localization. According to Lopes et al. in case of steels the origin for softening is structural. [94]

4.2.1 Work-hardening of multiphase steels

The work hardening of MP, in particularly DP steels, has been widely studied. Alloys consisting of two or more phases typically work-harden much faster compared to those consisting of a single phase. This is due to the fact that various phases are not equally easy to deform and thus the amount of plastic deformation varies between the phases. This means that gradients of deformation form with a wavelength identical to the distance between the phases. Once such alloys are deformed, dislocations are stored in them to accommodate the gradients of deformation and consequently enable the various phases to deform in a consistent manner. [98]

When a material consisting of phases possessing different hardness's is being deformed, the strain is concentrated in the softest phase. Plastic deformation occurs in the harder phases only after soft phases have sufficiently been strain-hardened. [107, p. 159] The softer phases are generally ferrite or austenite. When ferrite is subjected to tensile stress, it elongates through the sliding of the crystal plane, which is due to the stacking of dislocations under shear stress. Dislocation pinning occurs as a consequence of the increasing amount of sliding lattices. Therefore, the strain hardening impact is realized and the strength of the material is increased. [99] Ghassemi-Armaki et al. investigated the deformation response of ferrite and martensite in dual phase steel. They suggest that the hardness and strength in a single ferrite grain are not spatially uniform. They found that the strength and hardness values in the interior of the grain are smaller compared to values at the interfaces between the ferrite and the martensite phases. Furthermore it is found that in the subsequent tensile deformation the interior region of the individual ferrite grain work hardens whereas at the interface softening occurs. [108, p. 201]

Dual phase steels are capable of work harden at high rates, which results in the attainment of high maximum uniform elongation values. Consequently they are highly able to resist diffuse necking. The work-hardening rates of dual phase steels can be increased either by increasing the volume fraction of second phase or by decreasing their size. The work-hardening rate of dual phase steels can be defined as:

$$work-hardening\ rate = {f}/{d} \tag{4}$$

Where f equals to the volume fraction of the second phase and d is the average diameter of the second phases. However, an increase in the volume fraction of the second phase results to a greater tensile strength. This leads to an increase in uniform elongation and therefore the net result of concurrently increasing the tensile strength and the work hardening rate is to decrease the maximum uniform elongation. [109, pp. 95-106] However a study by Calcagnotto et al. suggests that, in case of DP steels, grain refinement which leads to an enhancement in strength, does not affect significantly on uniform elongation [110]. Reducing the size of the second phase islands at constant volume fraction does not have a considerable effect on the tensile strength. Thus Balliger and Gladman implicit that by reducing their size for a given value of volume fraction a maximum uniform elongation will be achieved without changing the tensile strength level. [109, p. 106] Taylor et al. studied the relationship between hardness and mechanical properties of dual phase steels. Taylor et al. suggest that as the hardness of the ferrite phase increases, the yield strength of the material linearly increases and therefore its work hardening capability respectively decreases. This indicates that constituents with lower strength govern the onset of yielding. [111, pp. 436-437]

4.3 The effect of microstructure homogeneity on strain localization

The appearance of strain localization is highly dependent on the initial microstructure [112, p. 4207]. The microstructure of a material is specified by the type, structure, amount, shape and topological arrangement of phases and lattice defects. It results from the structural phase transformations and/or mutual reaction processes between structural defects. [76, p. 682-844]

It is proposed that strain localization is due to inhomogeneity of material properties [13]. An inhomogeneous microstructure refers to a structure where are several local sites, where strain localization can occur and thus microcracks can nucleate [16, p. 20]. It is suggested that microstructure must be inhomogeneous in some degree in order that strain inhomogeneity can occur [86, p. 26]. While, according to Hu et al. the strains required to cause localization are significantly smaller for an inhomogeneous matrix than for a homogeneous matrix [113, p. 908].

Non-uniform deformation can be a consequence of several microstructural factors. Firstly due to the various combinations of crystal orientations, the materials are intrinsically inhomogeneous leading to non-uniform deformation. [114, pp. 14-15] Secondly, a microstructure consisting of different phases with various hardness's leads to an inhomogeneous deformation due to the incompatibility of plastic deformation between the harder and the softer phases [2]. Furthermore, the appearance of various imperfections results in non-uniform deformation [13]. The effects of all these factors on strain localization are discussed in this chapter.

4.3.1 Texture

It is generally known that microstructure highly affects properties of materials. Microstructure of polycrystalline materials can be classified as the combination of orientation and morphology of the components. Morphology refers to the shape of the components whereas orientation is connected with its crystallography. [115, p. 1] The crystallographic orientation of polycrystalline materials is typically non-random, i.e. there is typically a pattern in the appearing orientations [116, p. xi]. Crystallographic orientation indicates how the atomic planes in a volume of crystal are situated in relation to a fixed orientation [117]. Non-random orientation distributions are termed as preferred orientations or texture [116, p. xi]. Thus texture is a constituent character of microstructure [115, p. 1]. In case the material is textured, the properties will vary according to the test direction, since several properties of single crystals vary with the crystallographic direction or plane. The crystallographic orientation of grains affects materials physical, mechanical and chemical properties. [118] Texture affects significantly properties, such as Young's Modulus,

strength, ductility and Poisson's ratio. According to Bunge, the effect of texture on material properties is in several instances 20-50 % of the property values. [117, p. 3]

Texture develops or changes at several processes, such as solidification, annealing and phase transformation [115, pp. 153-163]. During controlled rolling of steel, texture develops and changes as a consequence of three type of processes, which are deformation, recrystallization and transformation. The texture that the material inherits is directly linked to the texture of the parent austenite phase. [119, p. 3024] It is feasible to tailor texture in materials to improve a certain property. There are several techniques used to study texture in materials. X-ray and neutron diffraction have been traditionally used, however recently other techniques have been developed for complete characterization of texture in materials. In the case of rolled sheet steel, the texture is generally represented as being of the type of {hkl}[uvw]. This implies that the orientations of the grains in the sheet are such that {hkl} planes are located parallel to the sheet plane, while their [uvw] direction point parallel to the rolling direction (RD). [115, pp. 153-163] Xie and Nakamachi studied the formability of bcc steels sheets. They suggest that in bcc steels the more {111} orientations and γ-fiber texture the more strain localization is hindered. [120, p. 67] Fiber textures are the paths along which grains rotate during deformation to the stable orientations [68]. Instead, {001} orientations were found to promote strain localization [120, p. 67].

An inhomogeneous matrix consists of grains of various Taylor factors corresponding to various crystallographic orientations [85, p. 202]. Taylor factor refers to an average orientation factor, i.e. Schmid factor, which is dependent on the texture and on the crystallographic characteristics of the expected slip systems. Taylor factor M is typically used to relate the yield strength (σ_{ys}) measured in a polycrystal in terms of the critical resolved shear stress (τ_{crss}), in the individual crystals: [121, p. 465]

$$\sigma_{ys} = M\tau_{CRSS} \tag{5}$$

It is worthwhile to notice the similarity to Schmid's law (2). Taylor factor is generally regarded as the slip resistance or the sum of shears needed to obtain a particular deformation. This implies that a higher Taylor factor signifies greater plasticity and therefore a greater dislocation density inside the given grain. [122, pp. 3047-3055] Therefore grains with a lower Taylor factor will deform first, and consequently their dislocation density increases. Eventually grains with a higher Taylor factor will additionally deform, but the amount of deformation is smaller compared to the ones with a smaller Taylor factor. [123]

It is suggested that the orientation and slip geometry differences between the neighbouring grains result in the localization of deformation [12]. As a material is being deformed, the orientation of each grain affects its deformation mechanisms and the specific selection of activated slip systems for that grain [124, p. 629]. Therefore the orientation of individual grains and the local Taylor factor affect the amount of deformation occurring within

every grain, i.e. the crystallographic orientation affects the ease of dislocations to move. [125]. As discussed previously strain localization is generally due to local softening. When a material is being deformed, some grains reorient themselves for easy slip. [85, p. 202] Orientations with greater Taylor factor are commonly the orientations that are more inclined to rotate to softer orientations. Therefore these orientations are expected to present textural softening. [126]

In a polycrystalline material every grain has its own dislocations on its preferred slip planes that have varying orientations compared to the adjacent grains. Therefore, during plastic deformation, dislocations that move on a specific slip plane cannot continue their movement from one grain another in a straight line. [73] As the misorientations between neighbouring grains increase, the effectiveness of the grain boundary to act as an obstacle to slipping highly increases. Consequently the slip in one grain cannot easily propagate through grain boundary into adjacent grains to form shear bands. [127, p. 583] The grains in which slip conditions are favorable due to their orientation, the deformation occurs by primary slip in the inner area. Whereas, grains in which slip conditions are less favorable, the deformation typically localizes in grain boundary regions. This is due to the additional shear displacements that are necessary to cause grain rotation and maintain grain-to-grain adjacency. [125] In a polycrystalline material the compatibility of strain components at the boundaries between grains limits the amount of possible slip systems [67, p. 208].

The effect of texture on strain localization has been mainly studied in the case of aluminum alloys. Texture is considered to be one of the most significant factors influencing the formation of shear bands in the case of aluminum sheet materials [12]. This is confirmed by Kuroda and Tvergaard, who found that texture affects shear band formation considerably. According to their research, relating to the bendability of aluminum alloy sheet, the texture that gives greatest tensile stress exhibits earlier shear band formation. [114] Moreover, in case of aluminum alloys, it has been observed that crystallographic textures that include high amount of rolling texture components can have an increasing effect on the roughness of the surface. Beaudoin et al. discovered that in aluminum sheets grains with similar orientations, i.e. clusters, can act corporately to form thinning in localized areas. Thinning is a type of surface roughening. [12] Surface roughness has been found to promote strain localization; this is further discussed in Subchapter 4.4.

4.3.2 Defects

Real crystals are never perfect; they always contain a significant amount of various defects. These defects have an influence on materials' physical, chemical, mechanical and electronic properties. However it must be noticed, that the effect of defects is not necessarily detrimental; they play a significant role in several processes such as deformation. [63] In this chapter the effect of three-dimensional defects on non-uniform deformation and thus strain localization are discussed. Volume defects in crystals can be defined as

clusters of vacancies or atoms. These defects are commonly divided into four classes based on a combination of the size and influence of the particle; however in this chapter only voids and inclusions are discussed. Voids are regions in the solid where are no atoms; in other words they are holes. Voids can be formed by the clustering of vacancies or by trapped gases. Inclusions are foreign particles that entered the system as dirt or large precipitate particles that are formed by precipitation. [128, pp. 106-107] In addition to such three-dimensional defects, the influence of grain boundaries is observed. Grain boundaries are defined as two-dimensional planar defects.

It has been experimentally discovered that defects in material have a significant effect on the initiation and growth of localized shear zones [129]. Imperfections in material result in localization at such strain that would not cause localization in a material that does not include imperfections. [13] In polycrystalline aggregates shear bands often commence to emerge at those regions were material imperfections occur. [129] According to Glema and Lodygowski the initial imperfections have a crucial effect on the shear band characteristics [130, p. 6].

First non-metallic inclusions are concerned. Nonmetallic inclusions can have an influence on various mechanical properties of steels [131]. The effect depends on their size, distribution and composition [132]. Manganese sulfides, silicates and alumina, and combinations of oxides are typical inclusions. The appearance of particular inclusions depend on the steelmaking route. [133, pp. 3-4] The presence of nonmetallic inclusions lead to an inhomogeneous deformation, due to the hardness difference between the hard inclusions and the soft matrix [134, p. 7]. Glema and Lodygowski investigated the influence of material inclusion on strain localization. According to their research, inclusions affect plastic deformation, and localization pattern and position. [130, p. 6] Furthermore, Xu et al. discovered that microcracks can nucleate at the interfaces between inclusions and the matrix [3]. Nonmetallic inclusions are additionally nucleation sites for voids, which will be discussed next [133, p. 4].

It has been discovered in several studies that microscopic voids in ductile metal promote significantly the localization of plastic flow in narrow shear bands. It is suggested that as the deformation continues, the density of voids increases and damage localizes within the shear band. This consequently results in the formation of a shear crack, which proceeds through void sheeting across the material. [135, p. 262] This is schematically represented in Figure 14.
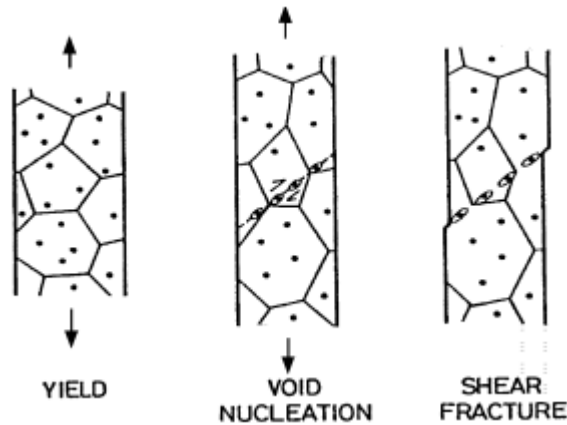
Figure 14: Schematic presentation of the shear fracture produced by void sheeting mechanism [135, p. 262].

However, according to Lievers et al. if the most of the voids nucleate early in the deformation process, when the strain hardening rate is still high, the appearance of strain localization is not promoted. [136]

In structural alloys voids primarily initiate at second phase particles by means of matrix particle decohesion and particle cracking [137]. Moreover microvoids can nucleate and grow from several other sources. According to Tan et al. this can take place at triple junctions between grains of similar phases. Greenfield and Margolin suggest that microvoids nucleate at interfaces between dissimilar phases. Moreover as reported by Gysler et al. slipband intersections are nucleation locations for voids and according to Gardner et al. dislocation cell boundaries can act as nucleation sites for voids. [138, 139, 140] Avramovic-Cingara et al. studied nucleation of voids in dual-phase steels. They found that nucleation can occur by four various mechanisms. First, voids can nucleate on cracked martensite particles. This mechanism occurs commonly on coarse martensite particles or on particles that are interconnected through fiber-like distribution of martensite phase. This occurs on small strain levels. Second, the nucleation of voids can occur between two martensite particles along the grain boundary. This takes place commonly at larger slightly larger strains the above mentioned. Third, Voids can nucleate at interface between the ferrite and martensite matrix. In this mechanism void nucleation primarily occurs on the interface perpendicular to the tensile axis. This mechanism was observed to occur most commonly. Fourth, voids can nucleate at inclusions, as mentioned previously. These last two mentioned mechanisms can occur in all strain levels. [141]

Next the effect of grain boundaries on strain localization is discussed. Grain boundaries have been found have a significant effect on inhomogeneous deformation [75]. In a polycrystalline material grain boundary is an area where two grains that have dissimilar orientations meet. Additionally in this area the arrangement of atoms highly differ from that occurring in single perfect crystal. Grain boundaries act as barriers to dislocation movement, since they exert repulsive force on dislocations that are coming down the slip plane.

[61] Therefore the presence of grain boundaries leads to the development of pile-ups and stress concentration sites [75]. Dislocation pile-up refers to an array of parallel dislocations that are forced against some obstacle [70]. Dislocation pile-up against a grain boundary is illustrated in Figure 15.
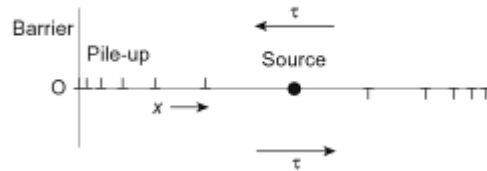
Figure 15: Illustration of dislocation pile-up at a grain boundary [142, p. 203].

Moreover it has been observed that the interaction between slip and grain boundaries introduces heterogeneities [75].

Furthermore the adjacent grains impose limitations on the amount of deformation that occurs within every grain [125]. Assuming that the less favorably oriented crystallites surround the favorably oriented crystallites, the unfavorably oriented crystallites hinder the deformation of favorably ones. Thus high local strains can be generated which instigate plastic deformation in the less favorably oriented crystallites. Consequently almost all the crystallites participate in the process of plastic deformation. However the degree of deformation varies between the crystallites. [59]

4.3.3 Homogeneity of phase structure

A microstructure is considered to be inhomogeneous if there are hard particles or phases, which consequently leads to a non-uniform deformation [98]. The homogeneity of the microstructure can be evaluated by defining the hardness differences between the phases. The effect of the homogeneity of phase structure on strain localization has been discussed is several studies. In particularly localization of deformation in case of dual phase steels, consisting of regions with significant hardness differences, have been widely studied. Many studies suggest, that the hardness differences between the neighbouring phases play a significant role in strain localization and thus in the initiation of fracture.

It has been observed in several studies that in case of an inhomogeneous phase structure, strain localization results from the incompatibility of plastic deformation between the harder and the softer phases [2, 143, 144, 145]. In case of inhomogeneity local hot-spots of stress and/or strain occurs in the microstructure. These hot-spots occur particularly at phase boundaries that act as nucleation sites for voids [146]. In an inhomogeneous structure, the region that has lower hardness becomes first deformed as the material is subjected to stress. Moreover the softer region will deform more. [143] According to Bergström, in case of a DP steel, plastic deformation does not occur in the martensite phase

for strains below necking [144, p. 1]. Therefore there occurs a difference in the deformation between the harder and the softer regions, as the deformation is localized in the softer phase [143]. Moreover, an inhomogeneous phase structure leads to strain hardening inhomogeneity, which consequently promotes strain localization [147, p. 2]. However, as proposed earlier, work hardening capability improves with an inhomogeneous phase structure, which consequently delays the onset of non-uniform elongation.

Ghadbeigi et al. evaluated the local plastic deformation in a dual-phase steel. They discovered that localization of deformation firstly occurred either inside large ferrite islands or close to the interphase between ferrite and martensite. It was found that shear bands form at areas of highest strain values. The maximum strain values in the martensite-rich regions were 30 % whereas in the ferrite-rich regions the values were continuously over 70 %. The formation of the band starts inside the ferrite, but after the crack has initiated it propagates almost perpendicular to the interphase through the martensite phase. After this the propagation can expand to the adjacent ferrite phase. The developed bands are oriented at about 45° with respect to the loading direction. [145] Hu et al. found similar results in their studies. They suggest that in an inhomogeneous material strain localization is nucleated in soft grains, particularly near the boundary between the soft and the hard phase. [113, p. 908] However, according to Li in aluminum sheet alloys shear bands may initiate from second-phase particles. These second-phase particles can be located far under the free surface where the material undergoes the most macroscopic deformation. [12]

The deformation behavior of ferrite-martensite dual phase steels has been studied by Akbarpou and Ekrami. They observed that at the beginning martensite deforms elastically, followed by partly plastically and partly elastically deformation and eventually it deforms plastically, whereas ferrite deforms always plastically. [96] The deformation of the second phase is dependent on the strength difference between two phases. A greater difference in the strength properties corresponds to elastic deformation of the hard phase, whereas a lower difference corresponds to plastic deformation of hard phase. The yield strength of the second phase increases with the carbon content, which depends on the volume fraction of the second phase. As the volume fraction of the second phase increase its strength respectively decreases. Therefore by increasing the volume fraction of the second phase, the strength difference between the two phases decreases. This is desirable in terms of homogeneity, whereas undesirable concerning the work hardening behavior of the material. [103]

4.4   The effect of surface roughness on strain localization

Due to various industrial processes, specific features can be produced at the surface of the material, such as local hardening, roughness, recrystallization and residual stresses [148]. The relationship between surface roughness and strain localization has been widely studied. In case of polycrystalline material, an initially flat surface is roughened after

plastic deformation. [149, p. 1] According to certain simulations surface waviness is the cause of strain localization, whereas some studies claim that the surface waviness results from strain localization. [150, p. 815] However it is generally accepted that both of them essentially result from non-uniform deformation at the scale of the crystalline grains [151]. In Figure 16 deformed surface is schematically illustrated:
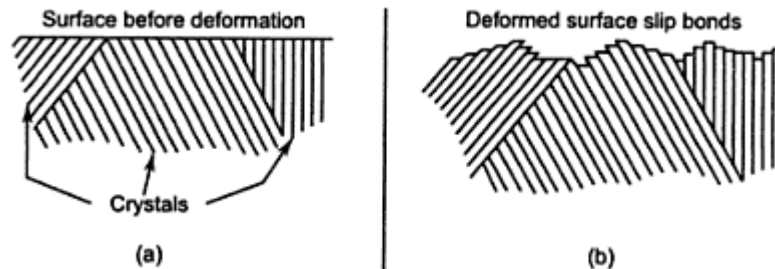
Figure 16: Surface (a) prior to deformation and (b) after deformation [61, p. 144].

It can be noticed that after plastic deformation on the surface of crystal there appears step marking, i.e. slip band, which is produced by slip or shear deformation of metals along slip planes [61]. Slip bands are clusters of slip lines that are formed due to slipping along crystallographic planes, i.e. slip bands follows crystallographic directions. Slip bands are localized banded structures, which from within a crystal when strained. [152, p. 1321] Slip bands appear at the surface of the specimen, where dislocations that proceeded across one slip plane have left the crystal [76, p. 1262]. The formation of slip bands occurs with a dislocation changing from one slip plane to another, i.e. cross slipping [152, p. 1333]. It is important not to confuse slip bands with shear bands.

It can be concluded that both surface roughening and strain localization are due to orientation and slip geometry inequalities between neighboring grains [153, p. 405]. Therefore crystal structure influences surface roughness. Sheets that consist of crystals with a small amount of available slip systems generally experience greater surface roughness. This is because few available slip systems are available to adapt local deformation and the incompatibilities that exist between two grains are large. Furthermore it is suggested, that surface roughness develops linearly with strain and it is linearly dependent on grain size. [154]

Surface roughening during sheet forming can provide nucleation sites for strain localization [151]. The thinner the sheet is, the more severe the surface imperfections become. [155, p. 191] Guilhem et al. investigated the effect of surface roughness on strain localization in polycrystalline aggregates. They found that once surface roughness is great enough, localizations driven by the local roughness topology replaces the localization bands driven by grain orientation. However this influence is found to occur only at the surface of the material. [148]

5. BENDING ULTRA HIGH STRENGTH STEELS

UHSS are required to attain equal forming properties to conventional high-strength steels, in order to apply them in various applications. The utilization of UHSS for example in automotive industry has increasingly grown. This is due to the demand to limit energy consumption and air pollution, which can be achieved by reducing the weight of the car body. Furthermore, increasingly demanding requirements on safety levels must be fulfilled. UHSS sheets are typically applied to components that are formed by bending. [2] Some bending is always involved in sheet metal forming [57]. Thus in order to satisfy market needs, UHSS with ever increasing formability properties must be developed.

Bending is a common metalworking operation in sheet metal forming, in which a force is applied to the material resulting it to bend at an angle. Bending along a straight line is a highly general sheet forming process, which can be performed in several various methods. The capability to bend a sheet metal without failure to a certain radius depends on several factors. Bending severity is typically defined as the proportion of bending radius R to the original sheet thickness t. [4] With successful bending it is possible to substitute for welding. This is beneficial, since bending is typically more risk-free, inexpensive and efficient compared to welding [156, p. 25]. Figure 17 illustrates the principle of air bending.
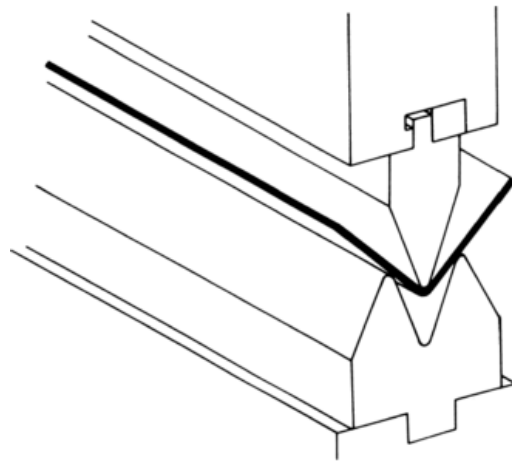
Figure 17: Principle of air bending [157, p. 212-220].

Forming a sheet includes always both elastic and plastic deformation. In bending only the bend region is subjected to plastic deformation, whereas the material away from the bend does not deform plastically [4]. The behavior of metals during tensile testing and during bending differ. When a material is subjected to uniaxial tension, it shows necking as the stress reaches its maximum value. Necking refers to a phenomenon in which the width and thickness of the specimen reduce substantially at a localized cross section before tensile failure. Necking occurs since the material is no longer capable to harden sufficiently

fast to maintain uniform deformation. In bending, the same amount of strain hardening will have occurred on the outer surface of the specimen. However below the upper surface, where the strain is smaller, necking is prevented. [5] It is crucial for sheet metal forming industry to understand and characterize the strain behavior of sheet metals, since large strains are involved in these forming processes due to stretching, drawing and bending [72].

In this chapter the mechanics of bending are discussed. First the variables used in examining bending mechanics are represented. Next the bending process is described in terms of the forming strains and stresses, followed by a representation of springback. Eventually failure in bending is discussed.

5.1   Mechanics of bending

During a bending process the specimen does not deform homogeneously at any point. The outer fiber of the specimen is subjected to tensile stresses as against the inner fiber is exposed to compression. The maximum strains occur at the surfaces of the specimen, but the signs of the strain component are opposite at these two various surfaces. [7] A simulation of stress and strain fields at the end of a bending procedure are demonstrated in Figure 18.
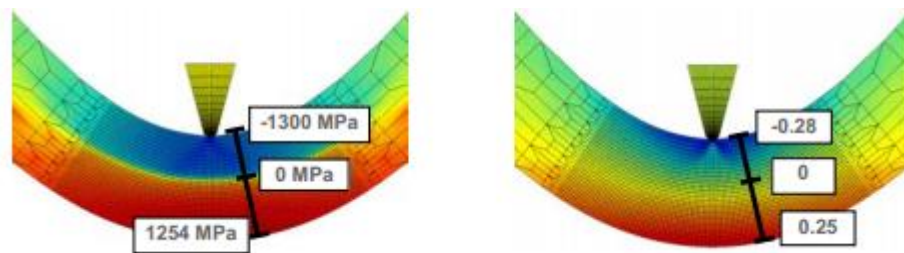
Figure 18: A simulation of stress and strain fields at the end of a bending test [7, p. 7].

Fracture starts at the outer fiber, where the maximum tensile stress and strain occur [158]. In the cross section, there is a plane, i.e. neutral axis, which segregates the zones exposed to tension and compression. Neutral axis refers to the line of zero stress and strain in a bend and thus its length remains the same, on contrary to the both outside and inside surfaces of the sheet. In the beginning of bending, the neutral axis is close to the middle section of the sheet thickness. However, as the bending is carried on, the neutral axis transfers towards the compression side, i.e. inner surface, of the bend. [159] This shift is due to the various deformations occurring at the compressive and tensile sides. Furthermore, the thickness of the sheet is reduced at the bend region [160]. Figure 19 the variables employed in the examination of bending mechanics are illustrated.
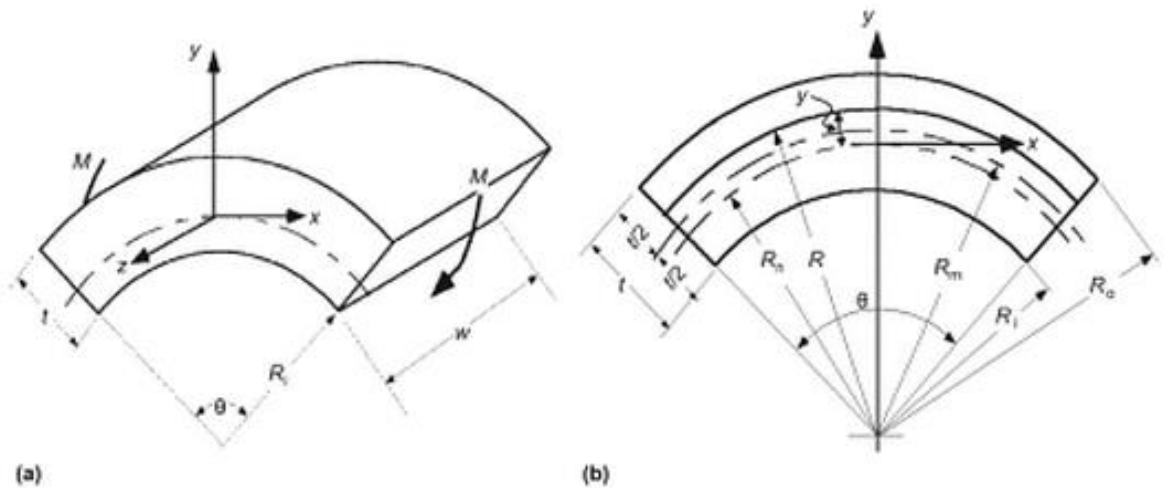
Figure 9: Variables employed in examining sheet bending [159].

In Figures 19a and 19b, M is the constant bending moment, t is the sheet thickness, θ is the bending angle, R_i is the inner bending radius, R_o is the outer bending radius, w is the width of the sheet, R_n is the neutral radius, R is the radius of an arbitrary layer and R_m is the mean bending radius, which is defined as $R_i + {}^t/_2$. [159]

The bending process can be divided into three stages in terms of the forming strains and stresses. In the beginning of the bending the stress values are below the yield strength and the strains remain elastic. Therefore, as the external bending force is removed, the sheet returns to its original shape. At the second stage, as the bending is carried on, the yield strength is first exceeded at the outer surface layers of the material, which consequently deform plastically. As the bending radius decreases, the yield point is also exceeded in the inner parts and the material deforms plastically towards the middle section. However somewhere in the middle section, there is a region that remains in the elastic stage. This region drives to return the sheet straight. At the third stage, once the bending radius is of the same order as the thickness of the sheet, the elastically deformed region nearly disappears and the deformation of the sheet in the cross section is almost completely plastic. [161, pp. 4-5] The stress and strain distributions in bending in these three various stages are illustrated in Figure 20.
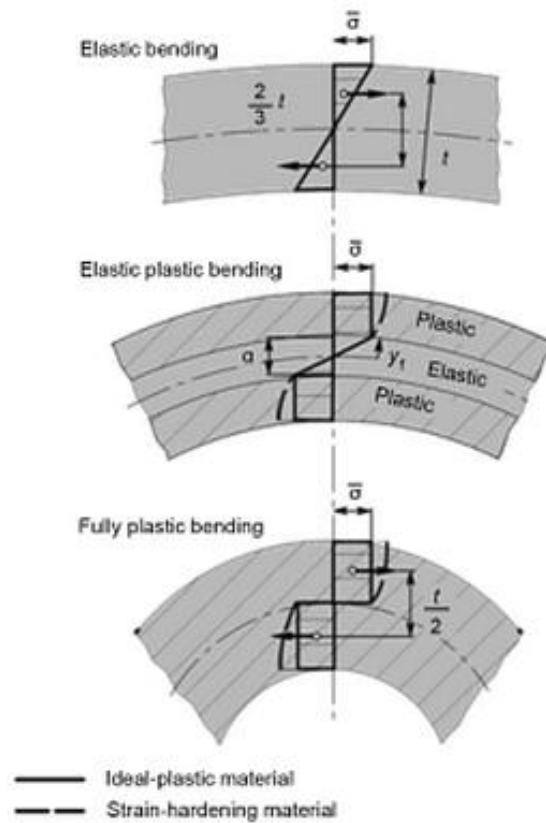
Figure 20: Stress and strain distributions in the three stages of bending [162, p. 21].

There are several types of equations that define the bending strain. The bending strain ε_{bs} at the outer surface at a distance *y* from neutral axis can be expressed approximately: [162, pp. 20-21]

$$\varepsilon_{bs} = 1 \pm \ln \frac{y}{R_m} \tag{6}$$

where R_m is the mean bending radius (Figure 19). Different kind of equations have been presented for example by Zhang et al. and Wu et al. [163, 164]

Next a phenomenon called springback will be discussed, which occurs after a sheet metal forming process. Due to this phenomenon the dimensions of the bent part change; this is represented in Figure 21.
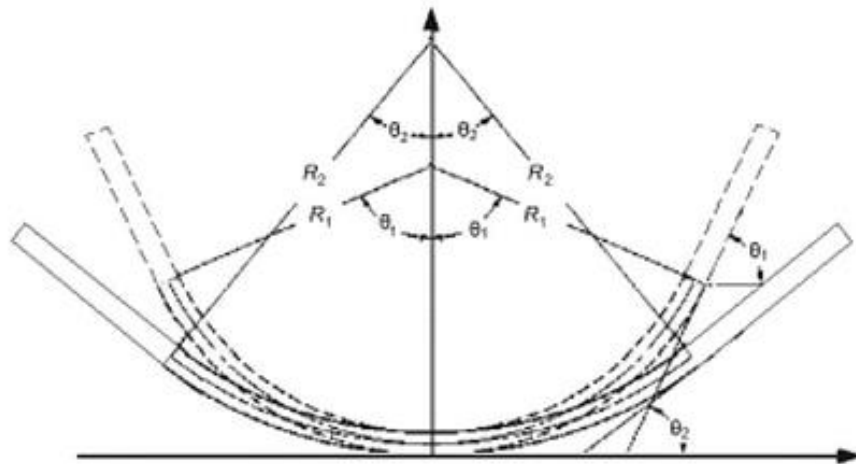
Figure 21: Representation of the phenomenon of springback in air bending [162, p. 22].

Springback is one of the primary formability concerns when forming high-strength steels. It is due to the variations in bending stresses and it is a highly complex phenomenon since its extent depends on several factors [95, p. 16]. The greatest tensile stress occurs at the outer surface of the bend specimen, the stress decreases towards the middle section and eventually becomes zero at the neutral axis. The material most adjacent to the neutral axis has been stressed to values below the elastic limit and consequently this material generates an elastic band around the neutral axis. The material further from the neutral axis has been stressed above the yield strength and therefore has been plastically deformed. When the die opens, the recovery of the elastic band to its original condition is restricted by plastically deformed zones. [159] In other words, after forming, residual stress stays in the final product as result of plastic deformation. Due to residual stress, occurs elastic recovery of the formed part. This elastic recovery is called springback and it produces an error in the shape of the final product. [165] Figure 22 illustrates the springback forces.
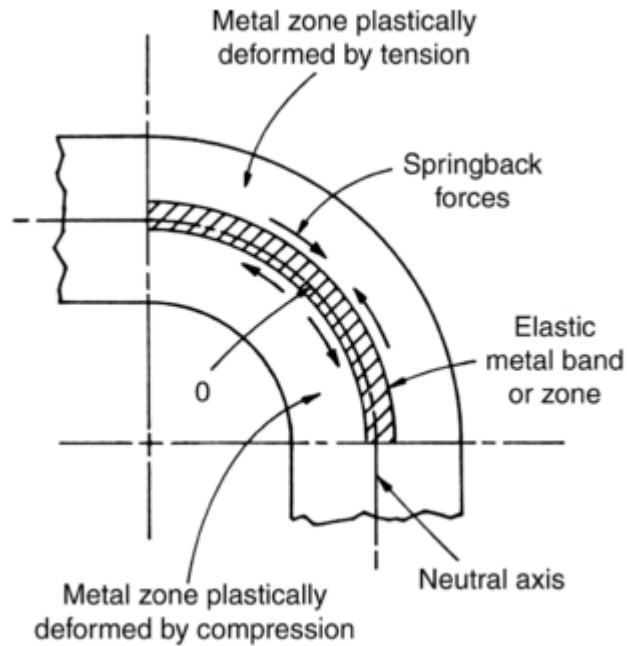
Figure 22: Representation of springback forces [159].

Springback is affected by the material properties. The most significant material parameter relating to springback is Young's modulus. Young's modulus depends on the inter-atomic bonding forces and in rolled materials it varies depending on the testing direction. [166, pp. 221-222] Springback is nearly proportional to the normal anisotropic value R, which refers to the proportion of the plastic width strain to the longitudinal strain. Furthermore springback is affected by the strain hardening exponent; it decreases as the strain hardening exponent decreases. [167] Chemical composition and heat treatment can have also an influence on the value. Moreover several process parameters, such as tools, press machines and friction conditions, affect springback. [166, pp. 221-222] The amount of springback is typically expressed in terms of the springback coefficient k_S, which is defined as:

$$k_S = \frac{\alpha_2}{\alpha_1} \tag{7}$$

where α_1 is the bending angle before springback and α_2 is the bending angle after springback. [160, p. 14]

5.2 Failure in bending

Two various failure modes are possible to occur in bending sheet metals. Either tensile failure can occur on the outside of the bend or buckling on the inside of the bend. [57] However according to several studies, failure occurs principally on the outside of the bend, where the maximum tensile stress and strain occur [158]. Cracking occurs at the point where tensile strains at the upper layers of the bend are sufficiently great [57]. A

study by Reche et al, it was found that in V-bending the cracks initiated either from the outer surface or just below the outer surface of the specimen. These can be assumed to be due to the detrimental combination of locally high tensile stress and strain levels with lower local damage resistance. [7] The limit to the bendability is typically determined so that once there is a visible increase in roughness at the outer surface of the bending zone, the limit is exceeded [168, p. 1].

The fracture is highly dependent on the microstructure, voids, inclusions and micro-cracks in the material [88, p. 1889]. According to Mattiasson et al. metal sheets typically fail by ductile fracture, which can occur either by ductile normal fracture or ductile shear fracture. The former mode results from void nucleation, growth and coalescence, while latter mode is due to the localization of shear band. [169] Furthermore, it is suggested, that voids and strain localization can collaborate in promoting ductile fracture to occur at the outer free surface of a bent specimen [136]. According to Kaupper and Merklein, in the case of dual phase steels, microscopic damage occurs prior to the initiation of strain localization, due to the high work hardening capability of DP steels. Instead, in the case of more homogeneous complex phase high-strength steels, the development of shear bands occurs first, followed by the development of microscopic damage within the local-ization region. [170, p. 248]

5.2.1 Failure in bending due to the formation of shear bands

First the role of shear bands in failure in bending is discussed. Several studies suggest that failure in bending occurs as consequence of strain localization. This is confirmed by Steninger and Melander, who observed that in bending low carbon steel, the deformation at the outer fiber of the bend specimen is homogeneous during the first stages of bending. Eventually, as the bending angle is sufficiently increased, deformation localized into shear bands. Shear cracks nucleate at the surface of the specimen after a specific amount of deformation. These cracks propagate along the shear bands and finally the specimen fractures. [158] It is possible for the crack to change its direction due to its interaction with conjugate shear bands. This is shown in Figure 23.
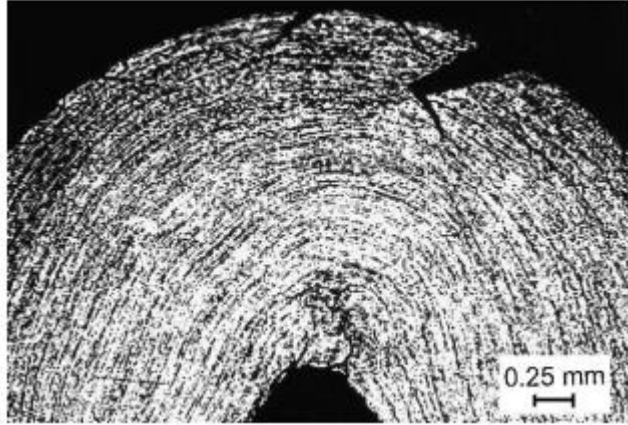
Figure 23: Longitudinal cross-section of a bent aluminum alloy specimen [135, p. 263].

In Figure 23 the critical role of shear bands in crack propagation is illustrated.

Additionally, Mattei et al. studied the mechanisms leading to the formation of surface cracks in case of aluminum alloys by in-site bend test. They found that the deformation of grains occurs by slip on certain crystallographic systems and that shear generally accompanies stretching. In the majority of grains merely one set of coarse bands was found to be visible at the free surface. Whereas, near the outer surface grains with couple of visible sets of coarse bands were noticed. Strain localization was found to cause necking of these surface grains, which led to an intergranular crack to propagate and eventually resulted into a final failure. Therefore it can be concluded that strain localization is the motor of damage development. [150, pp. 816-818]

In a study by Davidkova et al. concerning bending of Al-Mg alloys, it was also found that failure typically includes localization of the plastic flow into narrow and intense transgranular shear bands, which propagate through the microstructure. According to their study, cracks initiate by simple shearing of the matrix and then grow by development of voids at second phase particles that are situated in the sheared zone. Subsequently, these voids grow and combine, which enables the crack to advance. In other words, it is suggested in their study that cracks propagate by traditional ductile mechanism of fracture, which includes nucleation of voids at second phase particles, followed by growth of voids and eventually their coalescence. Moreover they found that cracks propagate along shear bands. [153] In Figure 24 various stages of matrix shearing and crack development during bending are presented.
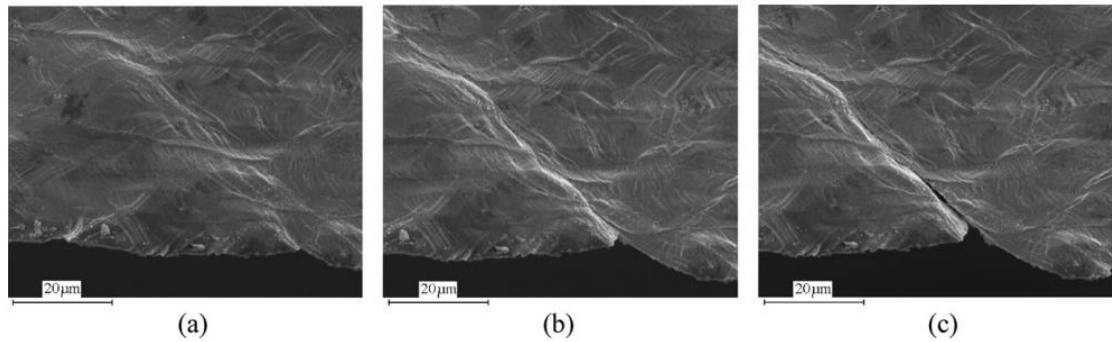
Figure 24: Illustration of cracks development in a bent specimen with an increasing bending angle. Bending angle is a) 110°, b) 135° and c) 145° [153].

In Figure 24a strain localization is presented, as the applied bending angle is 110°. In Figure 24b the bending angle is 135° and the formation of shear band can be observed. Finally in Figure 24c, the bending angle is 145° and crack propagation can be noticed. It can be seen from Figure 24, that shear bands initiate and grow from low points of the outer surface of the specimen and cracks are developed along these bands. Davidkova et al. suggest that the fracture is transgranular, since the cracks propagate through the grains by shearing. [153]

It can be concluded that according to several studies the formation of shear bands due to strain localization is the cause for failure in bending. It is stated that the appearance of shear bands causes voids and hence cracks to form "inside" the shear bands. Furthermore shear bands are suggested to govern the growth of cracks.

5.2.2 Failure in bending due to the formation of voids

Next the case that the nucleation of voids occurs prior to strain localization is considered. In sheet metal forming processes unforeseen fractures is associated with the formation of microvoids [134]. Nagataki et al. suggest that fracture in bending occurs as a consequence of void nucleation by shear mode crack propagation [171]. Voids typically generate at a low strain by either internal cracking of particles or by particle-matrix decohesion. Due to the fact that the particles are nearly non-deformable at room temperature, voids grow with increasing strain. The rate of void growth is dependent on the stress and strain states in the material and on the shapes of particles. Voids keep on growing until their volume in the material is so large that deformation becomes unstable. As the deformation becomes unstable, the strain localizes to a thin sheet of material. In this region occurs rapid void growth and final fracture. [139, 140, 141]

In Subchapter 4.3.2 the formation of voids as a precursor of strain localization is discussed. It can be concluded that voids can nucleate from several sites, e.g. interfaces between dissimilar phases and cracked martensite particles. Yet, when concerning the nucleation of voids prior the formation of shear bands, it is noteworthy to recognize that the

role of inhomogeneous hardness distribution is highly emphasized. This is in consistent with the suggestion of Kaupper and Merklein that the formation of voids prior to the appearance of shear bands occurs typically in DP steels [170].

6. FACTORS AFFECTING BENDABILITY OF UL-TRA-HIGH STRENGTH STEELS

Considerable scientific effort has been made to find convenient criteria to predict bendability of metal sheets [172]. The bendability of metal sheets is typically understood as the limit strain or stress states up to which the forming process is performed without failure. The bending limit can be specified as the amount of strain that triggers a visible increase in roughness at the outer surface of the bending zone. The minimum bending radius is concluded from this. [168, p. 1] Typically bendability is defined by the ratio of minimum bending radius (R_{min}) achieved without damage to the sheet thickness (t). Therefore the smaller this ratio is the greater the bendability of the material is [135, p. 258]. The bending limit is inevitably user-dependent, since bending damage is evaluated visually, and thus subjectively and intuitively [170].

The bending process is limited by the appearance of shear bands, thickness inhomogeneities, microcracks and finally failure on the outer surface of the bent specimen. These defects are fundamentally dependent on the width to thickness ratio, cold working, hardening, anisotropy and the condition of edges, which all have an influence on the ductility of the bent material. Several of these factors are related to the microstructural properties of the material, such as the appearance of inclusions and voids. [173, p. 102]

Typically, at a particular stage of bending, stable bending is suspended by the formation of shear bands. As a sufficiently large deformation is induced, the deformation becomes heterogeneous accompanying with the formation of shear bands. [10] Kaupper and Merklein observed that in multiphase steels, pores and shear cracks first occur in the macroscopic shear bands within the localization phase [170]. That is, the formation of shear bands governs the bendability of metal sheets. [114, p. 2] According to Pavlov the following factors induce deformation nonuniformity, and thus the formation of shear bands, in bending:

- the friction between the tool and the material,
- the shape of the tool and the specimen that is to be deformed,
- residual stresses in a deformed specimen,
- the character of the deforming forces,
- the nonuniformity of the material properties and
- combination of all of these factors. [90]

These all factors lead to nonuniform stress. In case the state of stress in a deformed component is nonuniform, it results in a nonuniform deformed state and nonuniformity of deformation. Therefore it is concluded that the bendability of steel sheets is governed

with several factors. [90] However in this study it is concentrated in discussing the effect of material properties on the bendability. It is significant to recognize, that the factors discussed above concerning strain localization hence fundamentally affect bendability. Therefore in this chapter few equal factors are discussed, but in this present chapter only concerning bendability.

6.1 Mechanical properties

There is no consensus in literature concerning the effects of several mechanical properties on bendability. These properties include tensile and yield strengths, ductility and work-hardening capability. Typically these values can be tentatively used to predict the bendability of UHSS sheets. However, generally these values do not provide reliably precise information regarding to bendability of ultra-high strength steels. [26, p. 16] Yet, it is generally accepted that local ductility, i.e. local elongation, governs bendability instead of total elongation [2]. In this chapter the effect of strength, ductility, work hardening capability and surface hardness of material on bendability are discussed.

6.1.1 Strength

Yamazaki et al. suggest that the tensile strength of ultra-high strength steels does not affect their bendability. They claim that even a microstructure consisting of martensite can have good bending properties if its microstructure is homogeneous. [2, p. 39] This is consistent with the proposal by Chen et al. According to a study by Chen et al., in case of steels with a tensile strength greater than 700 MPa there is no relationship between tensile strength and hole expansion ratio, which is basically governed with similar factors as bendability. Instead, in case of steels with a tensile strength lower than this given value, there is a significant inverse correlation. [174, p. 722] On the other hand, many studies suggest that the bendability is generally decreased as the strength increases. For example, Tsoupis et al. observed in their study concerning bendability of sheared edges, that high strength steels with greater strengths are more sensitive to cracking than the steels with lower strength levels [175, p. 5]. However, bendability is governed by the formation of shear bands and according to few studies there is relationship between strength and strain localization. This indicates that a relationship between strength and bendability would exist, on contrary to some proposals presented above. Xu et al. discovered that the strength of the steel affects highly on the occurrence of shear localization. They suggest that the higher the strength of the steels, the more prone they are to shear localization. [3] Furthermore, Masuda and Tozawa and Tozawa discovered that the ratio of shear yield strength to tensile yield strength can be utilized in estimating the bendability. They suggest that a greater shear yield strength compared to tensile yield strength leads to superior bendability. [11]

Furthermore tensile strength strongly affects maximum uniform elongation of the material, which has an effect on the formation of shear bands and consequently on bendability [109, pp. 105-106]. It has been found experimentally, that the strain at the bending limit is larger than the strain at the uniform elongation and smaller compared to strain at fracture in the tensile test [167]. Yet, according to a study by Nagataki concerning bendability of fully martensitic high strength steels, it is not possible to evaluate bendability by the uniform elongation obtained by a tensile testing [6].

The relationship between yield strength and bendability in case of aluminum alloys has been widely studied; however consensus on this affair does not exist. In several studies it has been found that the bendability of aluminum alloys decreases as the yield strength increases, while in some studies no correlation between these factors have been found. However, it is noteworthy to recognize that the strength levels of aluminum alloys are notably smaller and hence the effect of strength can be different in their case compared to UHSS. [176, p. 559]

6.1.2 Ductility

Ductility refers to a measure of an amount that a material is able to deform before failure occurs. In general, ductility is quantified with two various parameters: % elongation and % reduction of area. Parameter % elongation is defined as:

$$\% \, elongation = 100 \times \frac{(l_f - l_0)}{l_0} \tag{8}$$

where l_0 is the initial gauge length and l_f is the gauge length at fracture. Parameter % reduction of area is determined as:

$$\% \, reduction \, of \, area = 100 \times \frac{(A_0 - A_f)}{A_0} \tag{9}$$

where A_0 is the initial cross sectional area and A_f is the cross sectional area at fracture. [57]

It has been found in several studies that bendability of high strength steels does not correlate with total elongation. This has been proved in studies by Lämsä et al. concerning the correlation between bendability and tensile properties of high-strength steels, by Yamazaki et al. concerning the effect of microstructure homogeneity on bendability and by Oka and Takechi concerning the influence of metallurgical factors on the formability of steels [2,143, 177]. In Figure 25, the effect of total elongation on minimum bending radius is shown in case of high strength steels with yield strength in a range of 600-1150 MPa.
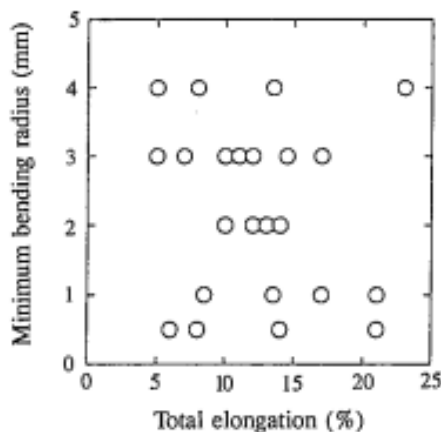
Figure 25: The correlation between total elongation and minimum bending radius [2].

In Figure 25, it is illustrated that in case of high strength steels, there is no correlation between total elongation and bendability. The UHSS utilized in the study by Yamazaki et al. are cold rolled low carbon steels comprising different microstructures. The microstructures were primary consisting of martensite and bainite, second phase islands in ferrite matrix and fully martensitic microstructures. [2]

According to Nonaka et al. in the case of UHSS, if total elongation increases, the properties governed by local elongation, such as bendability, will be degenerated. This implies that there is an incompatibility between total elongation and local elongation. Total elongation is improved by a structure containing ferrite and a hard phase, so that ferrite phase provides high elongation whereas hard particles provide high strength. On the other hand in case of local elongation it has been noticed that microstructure homogeneity is significant in order to avoid strains to concentrate locally. [178]

The amount of uniform elongation and thus bendability is affected by the phase structure. In study by Motovilina et al. it was found that bainite with granular morphology provides higher uniform elongation compared to lath-like bainite. [179, p. 680] This can indicate that in case of lath-bainite, the hardness difference between the carbides and the matrix is greater, which promotes strain to localize at their interface. Additionally, due to the fact that granular bainite forms at higher temperatures its hardness is lower compared to lath-like bainite. A lower hardness can be assumed to contribute to increased uniform elongation due to the greater work-hardening capability. Moreover, the amount of retained austenite has an effect on the uniform elongation but not on the total elongation. [180, pp. 50-51] Yet, according to Sandvik and Nevalainen an increase in the amount of retained austenite improves uniform elongation only if it is uniformly distributed between bainite laths [181, p. 213].

Empirically a correlation between bendability and reduction in area at fracture in a tensile test (RA) has been found. Yet, it is noteworthy to consider that this study was performed

to aluminum alloys. It is presumed that the fracture strain in the outer surface of the material being bent is identical to the one in tensile test specimens. It is suggest that: [135]

$$\frac{R_{min}}{t} = \frac{C}{RA} - 1 \tag{10}$$

where C empirically determined to equal 0,6-0,7. According to this equation, the greater the reduction in area is, the smaller the minimum bending radius is. Lloyd et al. found a correlation between reduction in thickness and bendability in the case of aluminum alloys with various ductility properties. This is represented in Figure 26.
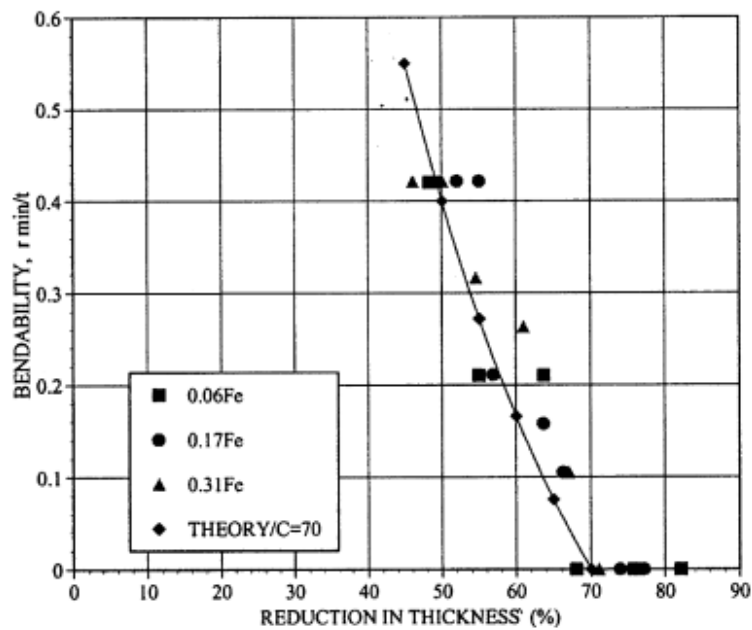
Figure 26: Correlation between reduction in thickness and bendability in the case of aluminum alloys [182].

It can be observed from Figure 26, that the greater the reduction in thickness is, the superior is the bendability of the material. However it must be taken into account, that this correlation is found in the case of materials with significantly smaller strength properties compared to high-strength steels.

Strain rate highly affects sheet formability. Strain-rate sensitivity is a significant parameter in the elongation and ductility of materials. Both the total elongation and the local elongation during post uniform elongation increase as the strain-rate sensitivity increase. [183] Strain rate sensitivity factor can be expressed as: [105]

$$m = \frac{d\sigma_f}{d\log(\dot{\varepsilon})} \tag{11}$$

where σ_f is the flow stress defined at constant strain and temperature and $\dot{\varepsilon}$ is the strain rate. Since the post-uniform elongation increases with strain-rate sensitivity, the tendency of strain localization is decreased. The crystal structure of the steel is one of the most significant factors affecting strain rate sensitivity. As the character of dislocations and primary short-range dislocation obstacles between bcc and fcc metals are dissimilar, the rate sensitivity differs. Bcc metals are more strain rate sensitive compared to fcc metals. [166, pp. 8-9] Furthermore grain size affects strain rate sensitivity. In case of bcc metals a larger grain size leads to increasing strain rate sensitivity. [105, pp. 6-7]

6.1.3 Work-hardening capability

A material must be able of straining uniformly, in order to obtain better bendability. The strain hardening co-efficient reflects the capability of the material to distribute strain all over the sheet and therefore the ability to delay localized deformation. A greater strain-hardening coefficient indicates that the material will harden more as it is being deformed and hence its resistance to localized deformation will respectively be greater. [184]

In literature there is disagreement over the effect of the strain hardening exponent on the bendability of sheets. According to Leu et al. bendability improves as the strain hardening exponent "n" increases [167]. Lämsä et al. also found a correlation between the coefficient of work hardening and minimum bending radius in case of structural steels (YS>700 MPa) [177]. Furthermore according to Takanaka et al., the strain hardening exponent affects bendability [167]. On the other hand, Yamazaki et al., Bettaieb et al. and Hudgins et al. claim that there is no correlation between the minimum bending radius and the strain hardening exponent [2, 185,186].

Leu et al. have developed a formula that can be utilized in approximating the minimum bending radius on the inner surface of bent part. This formula takes account of sheet thickness, material anisotropy and strain hardening. According to Leu et al. minimum bending radius on the inner surface of bent part is obtained as: [167]

$$R_{ic} = \frac{t}{2}(\frac{1}{\exp\left(\frac{n(1 + \mathrm{R} - \mathrm{value})}{2\sqrt{1 + 2\mathrm{R} - \mathrm{value}}}\right) - 1} - 1) \tag{12}$$

Where t is sheet thickness, n is strain hardening exponent and $R - value$ in material anisotropy. According to equation (12), a higher strain hardening leads to a smaller minimum bending radius, i.e. increased bendability.

6.1.4 Surface hardness

Hardness is a complex material property that is dependent on the strength and plasticity of the metal being tested, and moreover on the utilized test method. It is a mechanical

property that represents an influence of complex elastic and plastic stress fields formed in the tested material. It refers to the capability of a material to resist permanent indentation or deformation when in contact with a specific indenter under a certain load. Typically the hardness of a material is quantified by pressing an indenter of known geometry and mechanical properties into the material being tested. The size of the consequential indentation, i.e. the amount of plastic deformation that the material experiences during the test, indicates to the hardness of the material. [187] Hardness can be defined as: [188]

$$H = \frac{F}{A} \tag{13}$$

where F is the applied force and A is the unit area of the indentation. The geometry of the indenter can be spherical (Brinell test), pyramidal (Vickers and Knoop tests) or conical (Rockwell test) [187].

It has been experimentally observed that there is a relationship between hardness properties with several mechanical properties. Both hardness and modulus of elasticity are dependent on material structure and the corresponding molecular interactions and therefore these parameters have a connection. [189] A linear correlation has been found between both strain hardening coefficient and strength coefficient with hardness. The strain hardening coefficient is found to decrease as the hardness increases, whereas the strength coefficient increases with the hardness [190]. Furthermore generally a higher hardness indicates lower ductility [191].

As discussed previously, the maximum tensile strains occur at the outer surface of the specimen. The materials capability to prevent failure in bending is according to Ragab and Salef related to the ductility of the outer surface of the specimen. [173, p. 102] A soft layer on the surface of the material reduces the susceptibility to surface cracking when bending the sheet [192]. Due its lower hardness, the soft surface layer has enhanced ductility properties [193]. Kawamura and Seto have invented formulas which define the hardness of the soft portion in the surface of steel sheet and its thickness to achieve increased bendability. These formulas have been specified for ultra-high strength cold rolled steel sheet having a tensile strength of not less than 1270 MPa. According to Kawamura and Seto the thickness of the soft portion must satisfy:

$$Hv(S)/Hv(CL) \leq 0.8, \tag{14}$$

Where $Hv(S)$ stands for the hardness of the soft portion and $Hv(CL)$ stands for the Vickers hardness in the center line. The thickness of this soft portion must satisfy:

$$0.10 \leq t(S)/t \leq 0.30, \tag{15}$$

Where $t(S)$ is thickness of the soft portion and t is the sheet thickness. This signifies that in a 8 mm sheet, the thickness of the soft layer must be in the range of 0.24-0.8 mm. [14]

Instead, according to a patent application by JFE Steel Corporation, in the case of high-strength steels with a tensile strength higher than 780 MPa, the softer surface region should preferably extend to a depth of 1.5 to 3.0% relative to the total sheet thickness. This means that in case of a 8 mm sheet, the soft layer should be in the range of 0.12-0.24 mm, which differs from the suggestion made by Kawamura and Seto. It is suggested that in case the soft surface layer appears to an higher extent than 3,0 % relative to the total sheet thickness, the strength requirements will not be satisfied. Furthermore it is proposed that the volume fraction of bainite in the surface region should be less than 80 % and the volume fraction of ferrite should be at least 10 %. In addition to the minimum volume fraction of ferrite, its grain diameter should be in the range of 2-15 μm. In case the grain diameter exceeds this limit, cracking at ferrite grain boundaries is promoted. On the other hand, if the grain diameter of ferrite grains is less than 2 μm, adequate workability will not be obtained. [194]

Taylor et al. studied the relationship between hardness properties and hole expansion tests, which are like bending tests, governed by local properties. They found that in the case of a dual phase steel, an increase in hardness in as-received condition of matrix or second phase leads to reduced hole expansion ratio. In particularly a good correlation is found between the hardness values in as-received of martensite and hole expansion value. However after shearing, due to the plastic deformation in the region adjacent to the hole edge, the hardness values of these constituents will change. It is expected that ferrite will work harden to a higher degree compared to martensite. Consequently it is proposed by Taylor et al. that the hole expansion ratio values are not significantly dependent on the hardness of ferrite in as-received condition. [111] However, this suggestion can be questioned due to the previous discussion concerning the effect of initial dislocation density on work-hardening capability and hence strain localization.

6.1.5 The effect of chemical composition on mechanical properties

In this chapter the effect of the typical alloying elements on microstructure and thus mechanical properties affecting bendability are discussed. Principally the effect of various alloying elements on strength and hardness are considered. The considered alloying elements are mainly carbon and manganese however additionally other elements are briefly discussed in Table 1.

Carbon is an essential element for strengthening steel. The hardness of bainitic and martensitic microstructures increases rather linearly with the carbon content. It is an austenite stabilizer by decreasing martensite and bainite start and finish temperatures. Adding carbon refines the bainitic and martensitic microstructures. The hardness of such microstructures increases rather linearly with the carbon content. It is suggested that the hardness of

a completely bainitic microstructure increases approximately 190 Vickers as the percentage by weight of carbon increases by one unit. [36, p. 293] According to patent by JFE Steel Corporation concerning bendability of hot rolled steels sheet having a yield strength greater than 780 MPa, in order to obtain good bendability, the carbon content should be not less than 0.05 in order that a sufficiently fine microstructure is achieved. [194] However the amount of carbon must not exceed a certain level, since bendability tends to deteriorate as result from hardening caused by increase in the hard phase [195]. Furthermore, this is confirmed by Lee et al. They suggest that the bendability decreases as the carbon content increases, since higher carbon content leads to a reduction in the lath size of martensite and to a larger amount of dislocations. [196] Therefore it can be concluded that there is an optimum amount of carbon, in order to achieve desired bendability. Generally it is suggested that the carbon content should be in the range of 0.04 to 0.15% in case of UHSS [194].

Manganese is a solid solution strengthening element. Manganese stabilizes austenite by decreasing transformation temperatures. Adding manganese promotes the formation of retained austenite and refines the ferritic structure. [168] An excessive amount of manganese can produce manganese segregation, which leads to inhomogeneous properties and thus decreased bendability. Generally it is proposed that the manganese content is preferred to be in the range of 0.5 to 2.5%. Manganese can combine with sulfur and form MnS inclusions, which especially deteriorate local ductility and thus affect detrimentally on the bendability of UHSS. [14] The amount of sulfur should be 0.0050% or less, since it has a degrading effect on the bendability. Furthermore the segregation of manganese is found be detrimental concerning bendability. [194] Figure 27 presents the effect of the location of a hard segregation band on bendability.
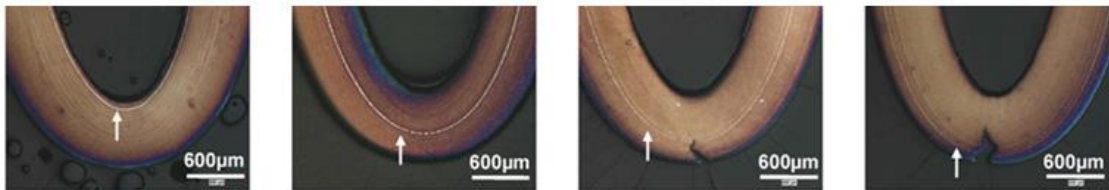

Figure 27: The effect of the location of a hard segregation band on bendability [168].

It can be observed from Figure 27, that the presence of a hard segregation band is particularly detrimental in case the segregation band is located close to the straining surface. The material used in the experimental by Reche et al. is a low alloy TRIP-aided steel. Further information concerning the effect of such bands can be found in this given study by Reche et al. [168]

The Chemical composition, in particularly carbon and manganese contents, affects the martensite (M_S) and bainite (B_S) start temperatures. Bainite start temperature in terms of chemical composition can be defined as: [50]

$$Bs(°C) = 830 - 270(\%C) - 90(\%Mn) - 37(\%Ni) - 70(\%Cr) \qquad (16)$$
$$- 83(\%Mo)$$

As the bainite start temperature is shifted to lower temperatures, the forming bainite and martensite will be formed consequently at lower temperatures. As bainite and martensite are formed in lower temperatures, the forming microstructure is finer. This is illustrated in Figure 28a. A finer microstructure, i.e. smaller packet and lath size, results in a greater hardness. This is represented in Figure 28b.

a)   b)
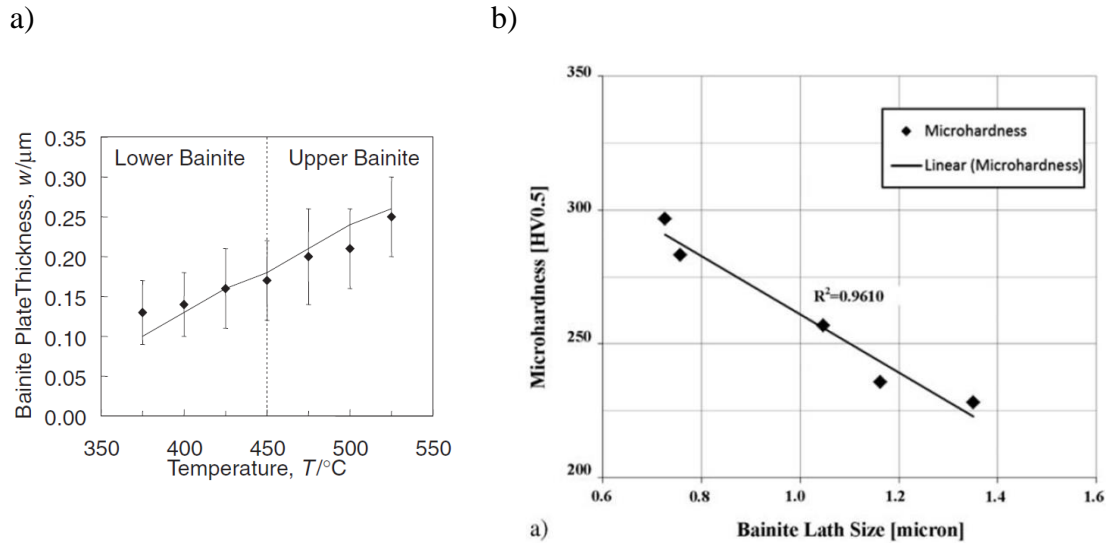
Figure 28: a) The effect of temperature on sub-unit size and [197] b): the effect of sub-unit size on hardness [198].

According to Bhadeshia, as the width of the bainite laths decrease from 1µm to 0,2µm, the hardness increases approximately 80 kg mm^{-2} [36].

The (B_S) and (M_S) temperatures also affect dislocation density. As the dislocation density increases, the movement of the dislocations is hindered, and thus the hardness respectively increases. As the (B_S) temperature is lower, the carbon content of the forming bainite is higher, since the carbon is being trapped in the bainitic ferrite. A correlation between the carbon content and dislocation density has been found, which indicates that carbon is trapped in the dislocations present in bainitic ferrite [199]. Moreover the dislocation density increases with decreasing phase transformation temperatures, since the strains following the transformation are greater with lower temperatures [200]. Furthermore it is proposed that low carbon equivalent is preferential in relation to bendability with high tensile strength, which indicates that the carbon and manganese contents needs to be limited [171].

In Table 1 the effects of certain alloying elements on microstructure and thus bendability are presented.

Table 1: Effect of certain alloying elements on bendability

Alloying Element	Effect	Suggested amount
Aluminum	• Strongly stabilizes ferrite. • Inhibits the formation of Fe_3C. • Acts as a deoxidizer. [201] • Increases the cleanliness of steel sheets [168]. • An excessive amount increases size of inclusions [194]. • In case, added in excess of a certain limit, has a deteriorate effect on the bendability and in a greater amount of surface defects [14].	0.005 to 0.10% [193, 194, 202, 14]
Chrome	• Increases hardenability. • Segregation of chrome can affect detrimentally bendability similarly as discussed in case of manganese. [7]	0.6 to 1.20 % [202]
Silicon	• Stabilizes austenite. • Contributes to solid solution hardening. • Improves ductility of the material. [14] • Typically connected with the formation of red scale [203]. • Tends to segregate and thus result in heterogeneous properties [168].	0.2 to 1.2% [193, 194, 202, 14]
Molybdenum	• Strengthens ferrite and hence decreases the hardness difference between the matrix and the second phase. • Delays the formation of pearlite, which content should be limited, since lamellar cementite leads to a reduced local deformation ability. [194] • Increases hardenability and the volume fraction of retained austenite [168].	0.01 to 0.50% [193, 194, 202, 14]
Boron	• Adding a particular amount contributes to obtaining an ideal amount of the hard phase. Thus certain boron content can improve bendability [193, 194].	0.0001 to 0.0030% [193, 194, 202, 14]

Calcium	• Can improve ductility through shape control of a sulfide such as MnS [194].	0.0001 to 0.0050% [193, 194, 202, 14]
Nitrogen	• Precipitates as nitrides. • At high temperatures can combine with titanium and form coarse precipitates. Cracks can initiate at these points during bending. [193, 194]	<0.005% [193, 194, 202, 14]
Titanium and niobium	• Reduces grain size of austenite and thus refines micro-structure, which consequently improves bendability. If the average grain size is more than a given size, cracking can origin at the grain boundary [14]. • Play an important role in retarding recrystallization during finish rolling, which leads to a pancake-like micro-structure promoting grain refinement during the austen-ite-ferrite transformation (Figure 29) [204]. • An excessive amount can lead to the formation of coarse precipitates and hence decrease bendability. • Niobium increases the strength of the ferrite phase and hence decreases the hardness difference between the matrix and the second phase. [193, 194]	Ti: 0.03 to 0.13%, Nb: 0.005 to 0.10% [193, 194, 202, 14]
Phosphorus	• Increases strength by solid solution. • Can segregate in grain boundaries and hence decrease bendability. [193, 194]	<0.04% [193, 194, 202, 14]

All the alloying elements contributing to increased hardenability lead to the formation of bainite at lower temperatures. This results in a bainitic microstructure possessing greater hardness, and as discussed in Subchapter 6.1.4 bendability decreases with increasing surface hardness.

As mentioned in Table 1, adding niobium and titanium leads to pancaked austenite. Pancaked austenite is preferred in terms of bendability. This is illustrated in Figure 29.
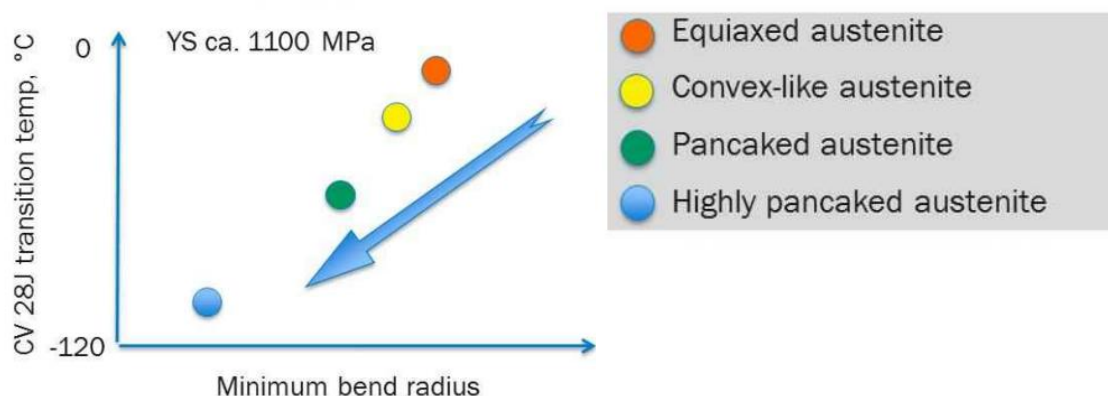
Figure 29: The effect of austenite morphology on bendability [205].

Pancaked austenite affects transformation kinetics so that bainite is formed at higher temperatures, which signifies that bainite possessing lower hardness is formed. On the other hand, it is suggested by Kaijalainen that extremely highly pancaked austenite contributes to the formation of horizontal carbides, which have been found to have a degrading effect on bendability on transverse to rolling direction. [206]

6.2   Homogeneity of phase structure

A homogeneous phase structure refers to a structure, in which no local "hot-spots" of stress and/or strain occur due to hardness differences between adjacent phases. The significance of homogeneous phase structure on bendability of high strength steels has been widely verified. It is well known, that a microstructure comprising phases of notably different hardness values deteriorates bendability. [146] It has been discovered that, the interfaces between various phases can act as nucleation sites for voids [207, p. 1610]. According to Oka and Takechi, the type of metallurgical structure has nearly no effect on the bendability, instead it is governed by the homogeneity of structure [143].

The effect of inhomogeneous phase structure on damage development in bending is particularly studied in the case of dual phase steels. In a study by Mohrbacher it is suggested, that when forming dual phase steels, under localized straining, intense dislocation pile-ups occur in single ferrite grains. This can result in delamination at the interface between the ferrite and martensite phases or in cracking of the martensite islands. [208] In Figure 30 characteristics and mechanisms of damage initiation and propagation in DP steel is represented.
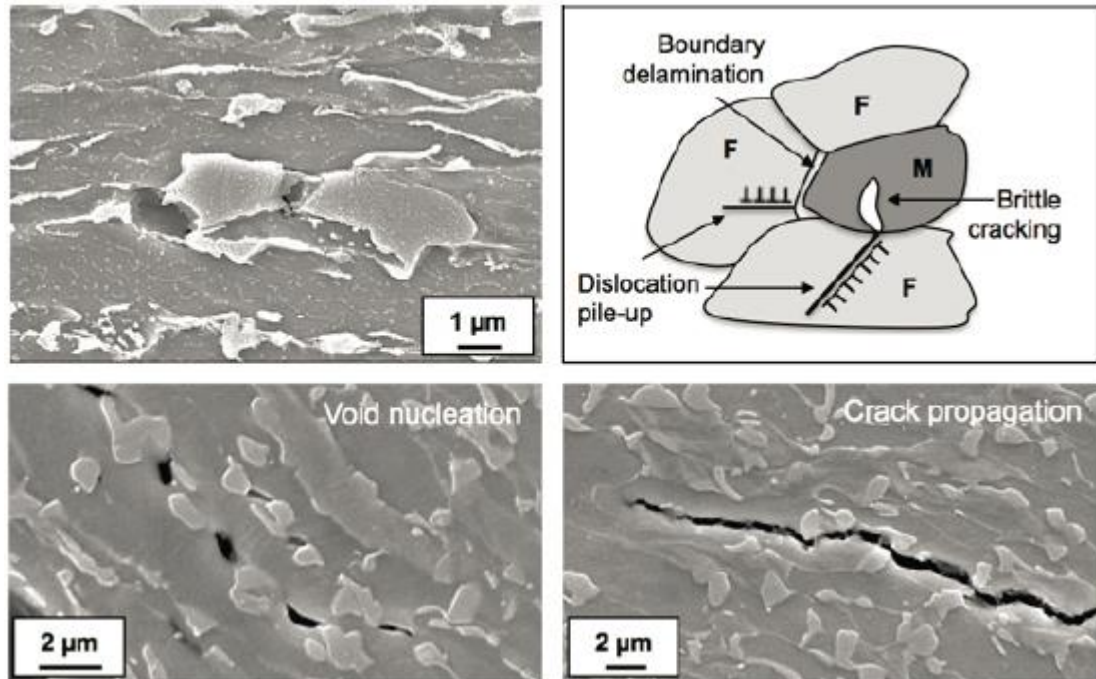
Figure 30: Mechanisms of damage initiation and propagation in dual phase steel [208].

In Figure 30 it is illustrated that a void can grow into a propagating crack. The critical stress needed for crack propagation depends on the size of the initial damage site. It is peculiar for the crack to propagate along ferrite-martensite phase boundary.

Yamazaki et al. investigated the relationship between microstructure and bendability of UHSS with a tensile strength of 1000 MPa. In this research UHSS with various microstructures were produced by varying the production conditions. It was discovered that microstructural homogeneity highly affects bendability of UHSS. According to the research good bendability can be achieved if the microstructure of the material is highly homogeneous. [2] In Figure 31 the correlation between microstructure homogeneity and minimum bending radius is presented.
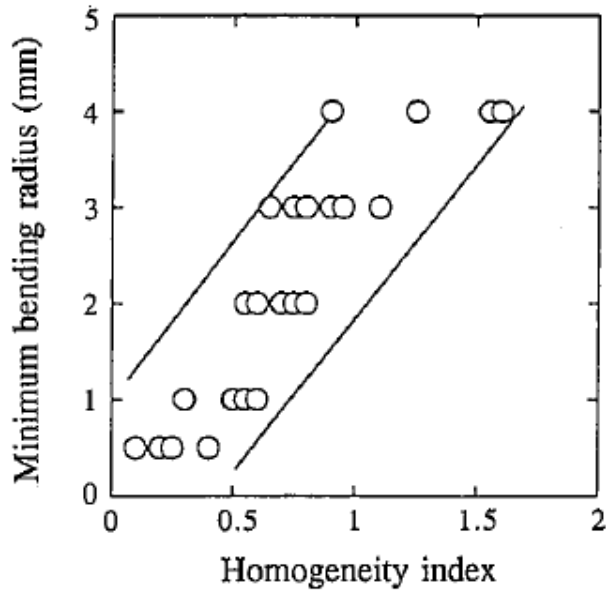
Figure 31: Correlation between homogeneity index and minimum bending radius [2].

According to Yamazaki et al. homogeneity index refers to the standard deviation of hardness measurements measured at intervals of 50 μm. Yamazaki et al. examined the homogeneity of the surface of the sample and therefore their research suggests that the homogeneity of the surface is critical concerning bendability. [2] Furthermore, homogeneity index can be defined as

$$HI = 100 \times \frac{standard\ deviation\ of\ hardness}{average\ hardness} \tag{17}$$

From now on, in this work term Homogeneity index refers to the definition described in equation (17) to distinguish it from the standard deviation of hardness measurements. A patent by Masashi et al. proposes that the standard deviation of the Rockwell hardness in the surface of a steel sheet must be less than 0.4 in order to attain good bendability. This is proposed for cold-rolled UHSS with a tensile strength exceeding 900 MPa. [209]

Yamazaki et al. studied the strain distribution of the bent surface to examine elaborately the relationship between microstructural homogeneity and bendability. It was observed that when bending a heterogeneous microstructure, local high strain and local low strain portions were produced. High strain portions mainly consist of ferrite whereas low strain portions primary consist of martensite. [2] This is in consistent with the proposals presented in Subchapter 4.3.3 concerning the localization of deformation in case of inhomogeneous phase structure. The strain values in a heterogeneous microstructure varied more abruptly compared to a homogeneous microstructure. This phenomenon can be noticed in Figure 32.
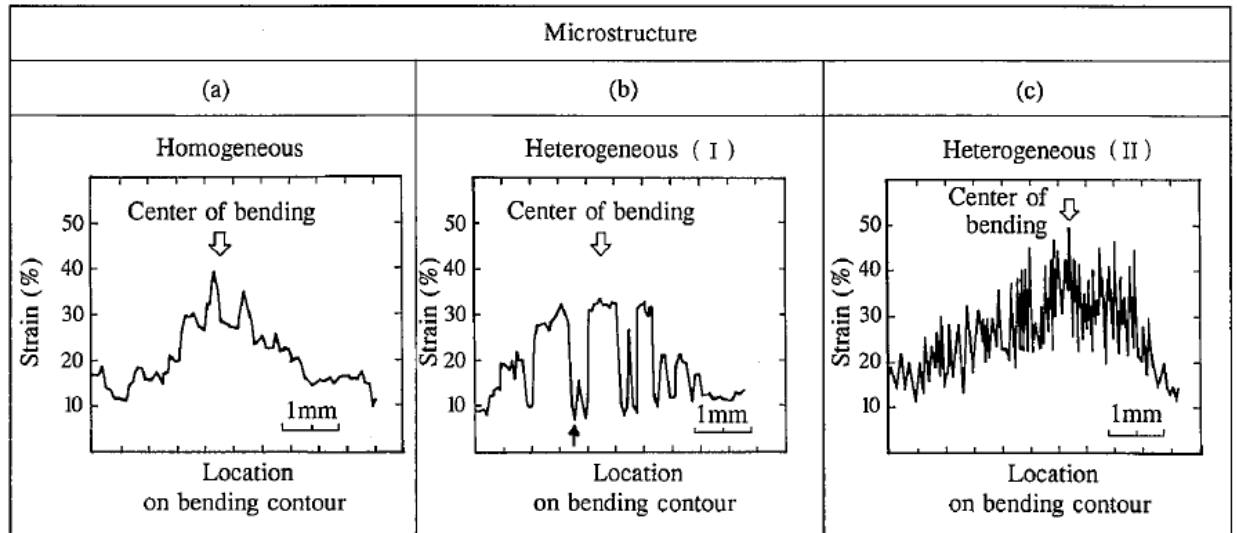
Figure 32: Illustration of strain values in homogenous and heterogeneous bent specimens [2].

In Figure 32b the microstructure of the bent specimen is heterogeneous lamellar, wherein portions of low strain are present at long intervals. Whereas, in figure 32c the microstructure is heterogeneous insular, wherein portions of low strains are present at short intervals. It was discovered that bending-induced cracking initiates at the interphase between the low strain and high strain portions, i.e. between the hard and soft phases. [2]

Mohrbacher has found similar results as Yamazaki et al. Mohrbacher suggests that multiphase steels are susceptible to local damage upon forming, because of the hardness differences between phases. [2, 208] Figure 33 demonstrates that how the hardness difference between ferrite and martensite in a dual phase steel affects the formability of the material.
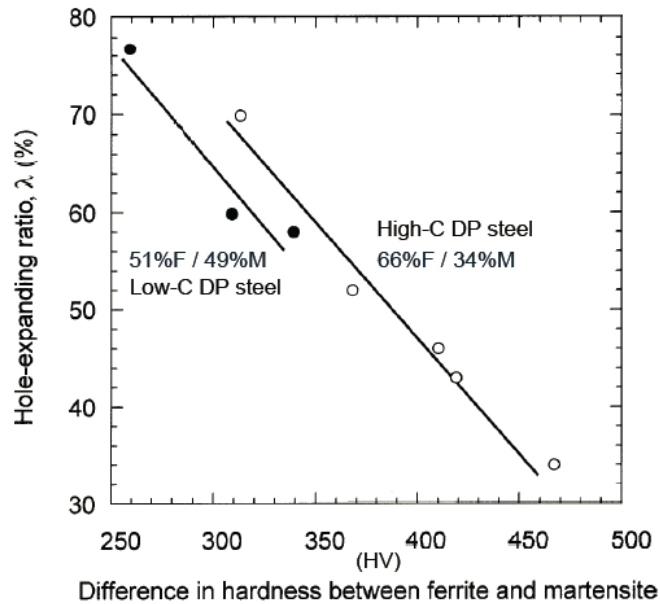
Figure 33: The effect of the hardness difference between ferrite and martensite on hole-expanding ratio [208].

It can be observed from Figure 33, that as hardness difference between various phases increase, formability deteriorates. Furthermore, in a research by Caballero et al. it was found that hardness difference between the bainitic matrix and martensite band play a role in premature crack nucleation [180, pp. 50-51]. In addition to Caballero et al. and Mohrbacher, Taylor et al. studied the effect of the hardness difference of the softer and harder phases on hole-expanding ratio [180, 208]. They also found that as the ratio between the hardness values of martensite and ferrite increases, the hole expansion ratio respectively decreases. A greater difference in the hardness values implies a greater strength disparity between these two constituents, which can result in a higher degree of strain localization at the interfaces. This consequently causes a higher degree of void formation during deformation. A greater hardness difference denotes a higher degree of strain portioning to the softer phase, which can produce more damage to the matrix. [111]

It is suggested that the size of the second phase, consisting of ferrite, martensite, pearlite, retained austenite, cementite and the like, should not exceed 3 μm. Since this promotes cracking at the interface between the main phase and the second phase, which consequently leads to a decrease in bendability. [194] It is found that the presence of second-phase particles affects bendability additionally in case of other materials than steels. Davidkova et al. suggest that the presence of second-phase particles tends to deteriorate the bendability of Al-Mg alloy sheets. [153, pp. 405-406]

6.2.1 Hardness of individual phases

The hardness of individual phases is not possible to be determined by microhardness measurement. Instead, with nanoindentation measurements this is possible. However several factors affect the reliability of the results obtained from nanoindentation measurements, thus the values presented in literature for certain phases significantly vary. Furthermore, the chemical composition and process parameters naturally affect the attained hardness values. Figure 34 illustrates nanoindentation of individual phases. [26, p. 44]
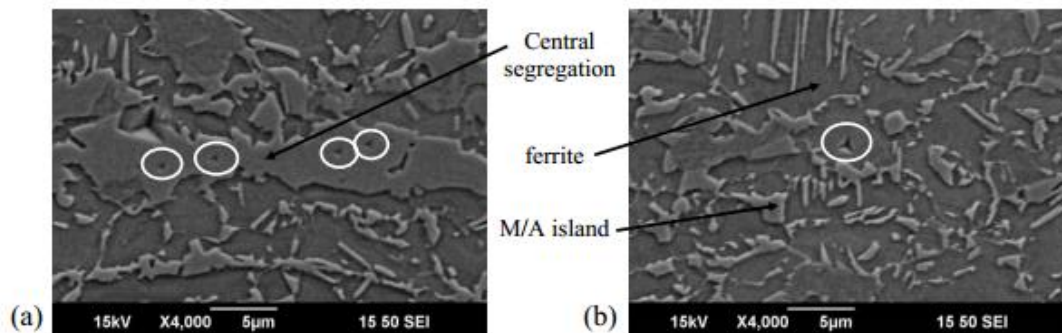
Figure 34: SEM observations after nanoindentation a) on the central segregation band, b) in the ferritic matrix [26, p. 44].

For ferrite phase the nanohardness values obtained in studies vary typically in the range of 2.9-3.7 GPa [210, 211]. For granular bainite the values are generally in the range of 4-5 GPa, however few significantly lower values have been also attained, and for lath-like bainite approximately 5 GPa [211, 212]. In the case of martensite, the values highly vary; they are in the range of 7-16 GPa [213]. The hardness of martensite is highly dependent on the carbon content; this is illustrated in Figure 35.
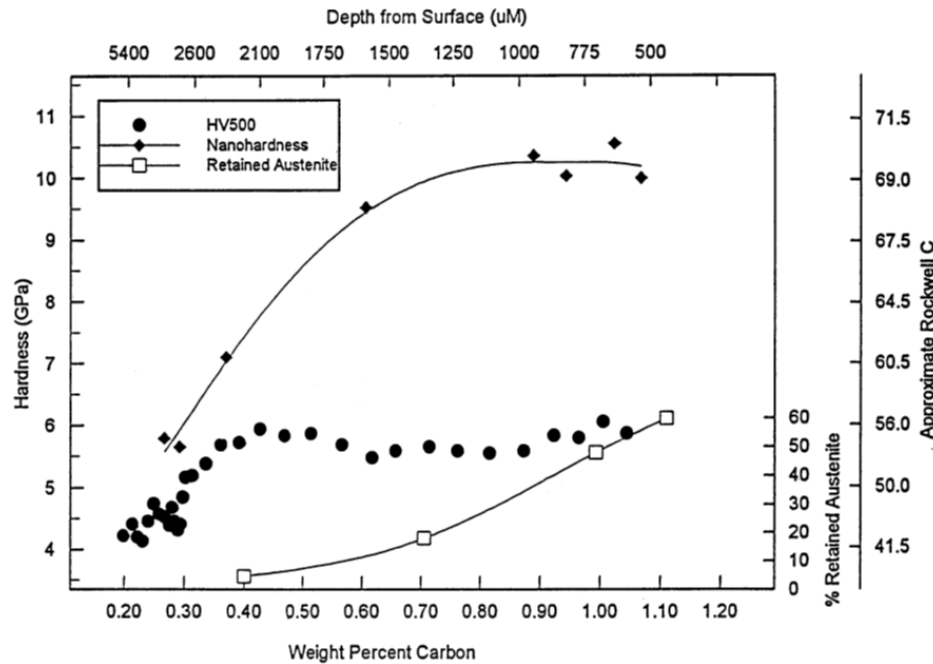
Figure 35: The effect of carbon content on the hardness of martensite and retained austenite [213].

The nanohardness values obtained for M/A constituents also highly vary; they are in the range of 11-20 GPa. The hardness of M/A constituents is highly dependent on their carbon content; as the carbon content increases their hardness respectively increase. Once the cooling rate increases, the carbon content of M/A constituents reduces and consequently their hardness decreases. [212] This is shown in Figure 36.
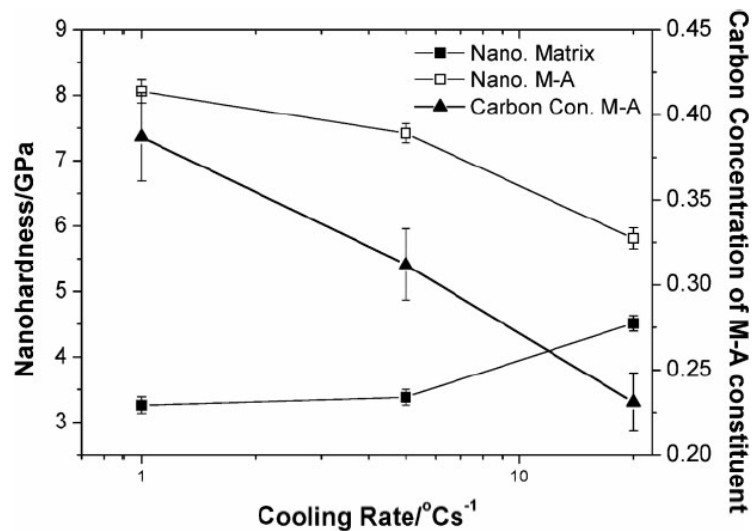
Figure 36: The influence of cooling rate on hardness of matrix and M/A constituents [212].

Figure 36 presents that as the cooling rate decreases, the hardness difference between matrix and M/A constituents increases. This phenomenon concerning the hardness difference is not dependent on the type of the matrix. Furthermore the size and morphology of

M/A constituents are dependent on cooling rate. With an increasing cooling rate, the size of M/A constituents is greater and their shape is irregular. Moreover, in case of higher cooling rate, their volume fraction increases. With smaller cooling rates their size is smaller and they are rod-like. [212]

In relation to complex phase steels, there are several possibilities to reduce the hardness difference between the matrix phases. Firstly the hardness differences can be reduced by replacing martensite with tempered martensite or bainite, as their hardness is lower than the hardness of martensite. Second option is to increase the hardness of the matrix by some strengthening mechanism, such as grain size reduction or precipitation hardening. Moreover an option is to reduce the amount of soft ferrite. [146]

6.3 Inclusions

The effect of the appearance of inclusions, in particularly MnS inclusions, on bendability has been widely discussed. Other typical non-metallic inclusions are various oxides, e.g. FeO, MnO, Al_2O_3 and Cr_2O, and sulfides, e.g. FeS, MgS and CaS. Inclusions have an effect on anisotropy as they are commonly connected with the initial solidification process and chemical segregation that is induced by solidification. Hot deformation process affects the shape of inclusions so that inclusions orient along the main plastic-strain directions. In hot deforming some inclusions deform along with the steel and thus become elongated. For example manganese sulfide inclusions are plastic at elevated temperatures and during hot rolling their morphology turns into highly elongated and oriented to the rolling direction. [133, pp. 3-4] Other deformable inclusions include for example FeO and MnO, i.e. these inclusions lose plasticity at temperatures above 400°C [214].Thus inclusions can result in different kinds of anisotropies with respect to bend properties as well as other mechanical properties [133, pp. 3-4]. In other words inclusions can cause heterogeneous behavior of the material. To minimize the anisotropy, the particle distribution should be homogeneous and the shape of the particles globular. [158] It is possible to reduce the anisotropy by lowering rolling reductions, as this leads to smaller ratio between inclusion length and thickness [133, p. 4].

As the fracture occurs by a ductile fracture process, there is a correlation between the volume fraction of inclusions and the total strain at fracture. As discussed previously, the initial stage of ductile fracture is the nucleation of voids and they readily nucleate at inclusions. [158] It has been observed by Pickerins, that inclusions that are near the surface and in a heavily elongated form eminently deteriorate the cold formability of steels. By stress concentration, this kind of inclusions can cause splits of differing intensity. These splits can result in a complete fracture or affect negatively the quality of the surface finish. [215] It is proposed that especially inclusions with aspect ratio 2.0 or more lead to strain concentration in the neighboring area of the inclusion and hence to cracking [216].

The influence of manganese sulfide inclusions on bendability is widely known. It has been generally recognized that the elongated MnS inclusions affect detrimentally bendability. [131] This is because cracks can initiate at this type of inclusions. It has been observed that voids nucleate specially in inclusions that are large and elongated. MnS inclusions have particularly an effect on bendability to transverse direction as they favor crack development along transverse direction. [26] The hardness of the steel matrix is greater compared to the hardness of MnS inclusions, on contrary to many other inclusions. In consequence, due to the local stresses, plastic slip can occur in the inclusions. Once plastic slipping occurs in an inclusion, slip bands within the inclusion are stopped at the inclusion-matrix interface which leads to a stress concentration across the boundary. [217] Hiam has observed that the loss of ductility increases as the amount of inclusions increase. The amount of sulphide inclusions increases with sulfur content, therefore according to Pradhan sulfur content should not be above 0,004 %. [218]

6.4   Precipitates

Precipitates are three-dimensional crystal defects. Here merely coherent precipitates are concerned. Coherent precipitates stand for precipitates, possessing crystal structure and atomic arrangement that have a continuous relation with the matrix. [219, p. 418] They are small particles; their size is a fraction of a micron. Precipitates are produced into the matrix by solid state reactions. Typically precipitates are used to increase the strength of the alloy by acting as barriers to dislocation motion. Their capability to hinder movement of dislocations depends on their size, internal properties and distribution. [128, pp. 106-107]

Nagataki et al. found that cementite precipitation has a considerable influence on bendability. Ohromi et al. have observed that cementite particles precipitate on {110} habit planes and grow in <111> directions in tempered martensite lath. Therefore in case of a bcc material, cementites precipitate on the slip planes and grow along the slip directions. Nagataki et al. discovered that in a low carbon ultra-high strength steel with a thickness of 1.4 mm bent with inside radius of 2 mm ($R/t = 0.7$), crack initiates at the boundary surface of cementite particles and matrix. Moreover it was observed that crack initiates principally on the habit plane on which cementite precipitates and propagates along the same direction as the cementite grows. This indicates that cementite precipitation leads to deterioration in the resistance of crack propagation. Cementite precipitation can be suppressed by tempering at a sufficiently low temperature. [171] At the lowest tempering temperatures, metastable epsilon carbides develop, and at higher temperature they are replaced with cementite, which was discussed above. It can be proposed that the presence of epsilon carbides affects bendability slightly detrimentally due the increase in hardness. [220, p. 101]

In a study by Castany et al. concerning bendability of aluminum alloys, it is suggested that grain boundary precipitates have an effect on the crack propagation, but not on the crack initiation. It is concluded that grain boundary precipitates contributes to crack propagation by promoting void coalescence. The nature and shape of grain boundary precipitates are significant parameters in governing crack propagation. According Castany et al. the appearance of non-spherical precipitates that are formed along grain boundaries are crucial in promoting crack propagation. [176, p. 564]

6.5 Texture

It is proposed that texture has an effect on formability of UHSS especially in case that {110}<011> and {100}<011> elements are present [221, p. 1]. As discussed above, the final microstructure inherits the texture that is directly connected to the texture of the parent austenite (γ). The recrystallization texture of austenite {100}<001> gives rise to the undesired {100}<011> upon transformation to ferrite. Hence in order to avoid the formation of {100}<011>, during the initial processing the recrystallization of austenite (γ) needs to prevented. It is proposed that the presence of {332}<113> element compensates the harmful effect of the undesirable {110}<011> component [119, p. 3024]. The main components of deformation texture of austenite, i.e. {110}<112> and {112}<111>, transform into {332}<113> and {113}<110> orientations in the ferrite. [222]

The initial and plastic deformation induced anisotropies have a significant effect on the bendability of steel sheets. These anisotropies can be characterized by the crystallographic texture. [120] It is characteristic for high-strength steels to possess strong anisotropy. Plastic anisotropy results from the interaction between macroscale boundary conditions and microscale activity. [223] The plastic strain ratio, which is known as the R-value, is used to determine the mechanical anisotropy of sheet metals [224]. This value refers to the proportion of the plastic width strain to the longitudinal strain and it is used to represent the formability of sheet metals. [184, 223] A greater R-value implies an increasing resistance to thinning and thus superior formability [134]. Leu et al. found that the normal anisotropic value R has an effect on ratio between the circumferential stress and the mean effective stress ($\sigma_\theta / \bar{\sigma}_e$) on the outer fiber. It was discovered that the stress ratio increases nearly linearly with the R-value. Therefore it was inferred that greater R-value implies improved bendability. [167] The effect or R-value on bendability in the case of aluminum alloys sheets is illustrated in Figure 37.
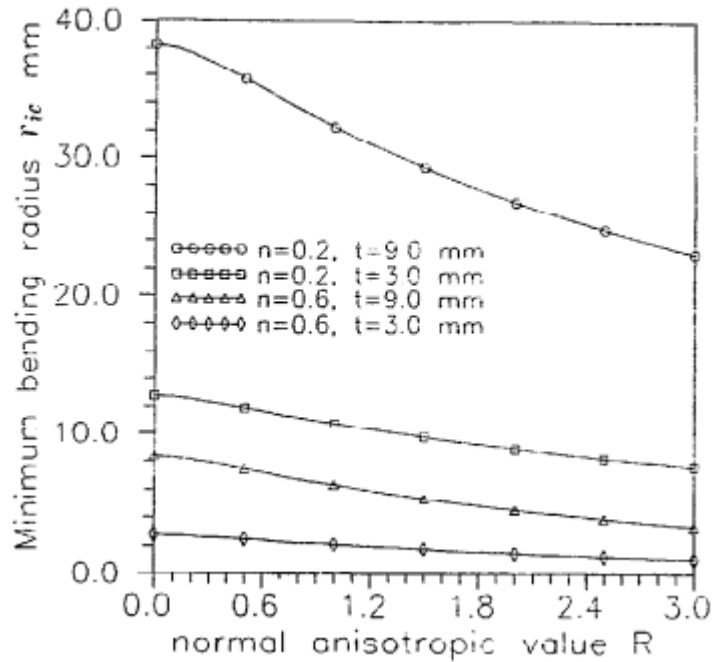
Figure 37: The effect of R-value on bendability in the case of aluminum alloys [167, p. 15].

It can be noticed from Figure 37, that the effect of R-value on bendability is rather small. It has been observed that a higher amount of γ texture components leads to a larger R-value and therefore to better formability of bcc steels. [223]

6.6 Surface quality

Plastic deformation in a polycrystalline material is highly complex and the developed surface is a consequence of several factors, as discussed in Subchapter 4.4. The significance of surface quality, in particularly surface roughness, on bendability has been noticed in several studies. In this chapter the effect of surface roughness on bendability is discussed. Including an observation of red scale, which is a surface defect commonly present in hot-rolled steels and affecting surface roughness.

The role of surface roughness on bendability has been particularly studied in case of aluminum alloys. The proposals of several such studies are rather uniform. It is suggested that damage during bending is due to the development of surface roughening and strain localization. It is found that the valleys, i.e. low points, of the outer surface are especially crucial, since it has been found that strain localizes to the bottom regions. [150] Lie and Dao studied the significance of surface roughness on bendability aluminum alloys, in a study concerning the micromechanisms of fracture initiation in bending of aluminum sheet alloys. Lie and Dao found that in aluminum sheet alloys crack initiates from the surface roughness owing to plastic deformations. Valleys of surface roughening can act as initiation sites for shear bands, which eventually lead to failure. [12] Furthermore,

Mattei et al. studied the influence of surface roughening in bending aluminum alloys. They also observed that initial surface roughness promotes the development of strain localization. Strain localization results locally in considerable alterations in grain shape and orientation, which at outer surface lead to surface waviness. Thus it is inferred that strain localization controls damage development and results in the generation of surface cracks. Lloyd studied the significance of surface roughness on bendability of aluminum alloys. He found that polishing of the surface topography increased bendability. [150, p. 815]

The presence of red scale on the surface of steel increases its roughness [225, p. 4]. Scale defects are typical surface defects observed in hot-rolled steels. Due to oxidation of steel, a three-layer scale develops, which consists of wustite (FeO), magnetite (Fe_3O_4) and hematite (Fe_2O_3). [226] This is presented in Figure 38.
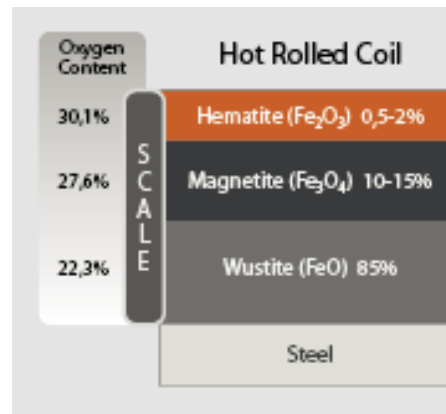

Figure 38: Illustration of scale [227].

Various types of scales can be present, including black or rolled-in scale that develops due to the rolling of harder oxides into the surface, and red scale, which formation is generally connected with high Si-content. [226] Yet, additionally in cases in which Si content has been extremely low, red scale has occurred. In this work only red scale is concerned.

It is proposed that red scale is powdered-αFe_2O_3 and it is highly difficult to remove. The development of red-scale has been studied in several researches, yet the mechanism of red scale formation has not been entirely understood. Various studies propose different reasons for the development of red scales. These include for example the influences of temperature and time, rolling forces and reduction, chemical composition (in particularly Si-content), reheating temperature and gas atmosphere. [226]

A study by Fukagawa et al. proposes that the formation of red scale is due to incomplete descaling of FeO before hot rolling. If remnants of FeO are fractured by hot rolling, the region beneath is exposed to air and thus to too much of oxygen together with iron ions. Then the reaction from FeO to Fe_3O_4 and Fe_2O_3 is highly accelerated. This process is

illustrated schematically in Figure 39, in which the upper image presents scale structure before rolling and the lower image after rolling. [228]
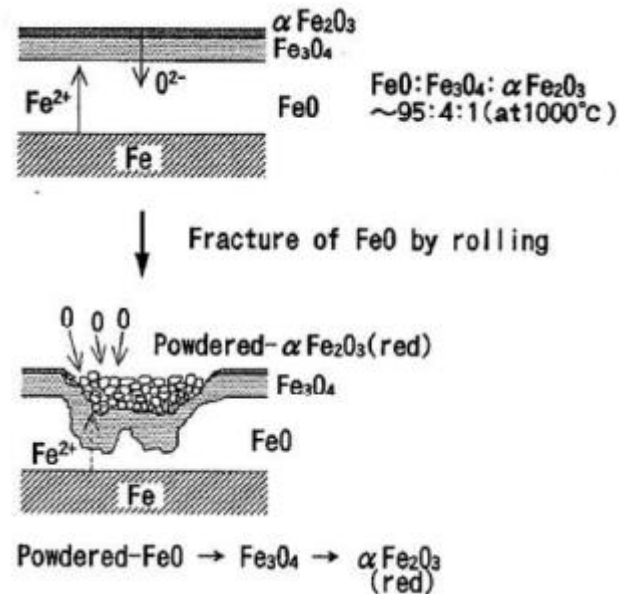
Figure 39: The mechanism of red scale formation as a consequence of the fracture of FeO layer [228].

Next, the effect of silicon content on the formation of red scale is discussed. Silicon is added in order to increase strength properties of steels through solid solution hardening without, at least in small additions, affecting the ductility. However, in hot-rolled sheets containing silicon, defects of heterogeneous red scale are commonly formed. Okada et al. suggest that as the amount of silicon exceeds 0.5 %, red scale is highly probable to occur. [228] When alloying silicon, Fe_2SiO_4 is developed at the interface between scale and steel. The melting point of Fe_2SiO_4 is approximately at a temperature of 1173°C and thus once this temperature is reached during reheating, it starts to melt. The melted phase then penetrates into grain boundaries of FeO. [229] According to Taniguchi et al., higher Si-content leads to a deeper penetration [230]. Once cooling after solidification, the eutectic compound FeO/Fe_2SiO_4 anchors the oxide, which leads to a difficulty to descale the steel [229]. Fukagawa et al. propose that in case of a steel containing silicon, the mechanism of the formation of red scale similar as discussed previously [228]. This is illustrated in schematically in Figure 40.
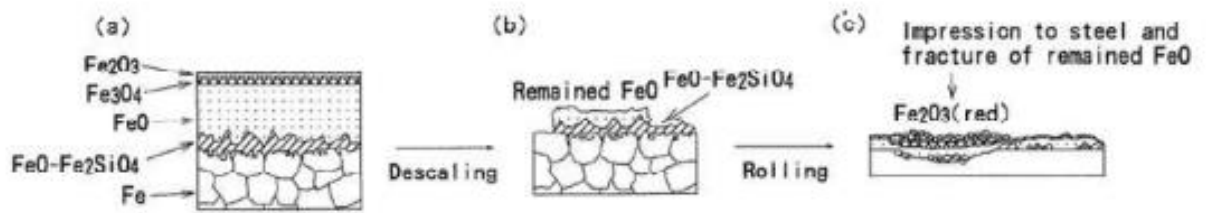
Figure 40: Illustration of formation of red scale in a material containing silicon [228].

In Figure 40a, development of primary scale presented, Figure 40b illustrates the remains of the scale after descaling and Figure 40c presents the formation of red scale.

In conclusion, whether the material contains silicon or not, red scale is formed due to the remaining FeO prior to hot rolling (Figures 39 and 40). Yet, as the Si-content increases, descaling becomes more difficult due to the FeO/Fe_2SiO_4 present in the interface between the steel and the FeO scale. This consequently leads to pronounced amount of red scale. It is found that by removing nickel the descaling ability is improved. Adding nickel leads to an increase in roughness at interface between the scale and the steel surface, and hence it hinders descaling. Adding phosphorus is found to improve descaling, due to its lowering effect on the eutectic temperature of FeO and Fe_2SiO_4. Therefore solidification is suppressed, which indicates that liquid compound is present at the interface between the scale and steel resulting in improved descaling capability. [204, 228]

7. EXPERIMENTAL PROCEDURES

The aim of this study was to comprehend the microstructural factors governing bendability of UHSS. In particularly the effects of surface hardness and homogeneity of surface are aimed to understand.

The main goal of the experimental procedures was to define the effect of microstructure homogeneity and surface hardness on bendability of UHSS. The variation of hardness measurements was applied as an indicator of the microstructural homogeneity, as described in Subchapter 6.2. Then the correlation between the homogeneity index and bendability was examined. Furthermore, it was strived to determine the required extent of the soft surface layer in terms of its proportion compared to the total sheet thickness, in order to assure desired bendability. In addition to the extent, the required hardness of this layer, in terms of desired minimum bending radius, was endeavoured to define.

First studied materials are represented. After this the applied test methods are illustrated. This includes, firstly, a microstructural investigation that was carried out by applying FESEM, in order to define the microstructure of upper surface and middle section. Bending tests were carried out so that the bending capability, i.e. minimum bending radius, of given materials could be quantified. Microhardness measurements were performed in order to both determine the hardness of the upper surface and middle section, and to evaluate microstructure homogeneity at upper surface. Eventually interrupted bending tests, i.e. bending selected samples to various angles, were carried out so that the initiation point of shear band formation could be identified. This was conducted by using FESEM, by examining microstructures of cross sections of bent regions.

7.1 Materials

The studied materials used in this work are direct-quenched UHSS. The yield strength of these materials is in the range of 700-1200 MPa. All of the materials were manufactured using hot strip rolling and direct quenching followed by leveling. Tempering was not performed, apart from the case of two steels. The thickness of used materials is mainly 8 mm, yet a few materials with a thickness of 10 mm and 12 mm were included. An extensive group of materials were selected in order to minimize the sensitivity of the results and thus to achieve reliable results. Several materials with equal chemical composition, but with different processing parameters were selected in order to understand the effect of rolling temperature on the forming microstructure. In addition materials with various chemical compositions, especially carbon and manganese contents, were selected to attain a fundamental understand of their effect.

In Table 2 the chemical compositions of the studied materials are represented (wt.%). Carbon content is presented as a more accurate value compared to contents of other elements. The values present the true compositions of the given heat.

Table 2: Chemical compositions of the test materials.

Composition	C	Mn	Si	P	S	Al	Nb	V	Cu	Cr	Ni	N	Mo	Ti	B
1	0.069	1.31	0,2	0.01	0.001	0.03	0.04	0.01	0.02	1	0.07	0.004	0.02	0.02	0.001
2	0.079	1.84	0,2	0.01	0.001	0.04	0.04	0.02	0.02	1.01	0.05	0.004	0.09	0.02	0.002
3	0.063	1.36	0,2	0.01	0.001	0.03	0.04	0.01	0.02	1	0.07	0.004	0.02	0.02	0.001
4	0.088	1.09	0,2	0.01	0.001	0,03	0.04	0.01	0.02	1	0.07	0.004	0.02	0.02	0.001
5	0.103	1.09	0,26	0.09	0.001	0.027	-	0.01	0.02	1.14	0.41	0.0053	0.02	0.023	0.0018
6	0.097	1.11	0,27	0.09	0.009	0.03	-	0.012	0.02	1.21	0.4	0.0045	0.02	0.023	0.0018
7	0.097	1.1	0,25	0.09	0.004	0.034	-	0.011	0.02	1.1	0.4	0.0047	0.02	0.03	0.0019
8	0.058	2.02	0,2	0.07	0.0017	0.031	0.082	0.013	0.017	0.057	0.036	0.0068	0.008	0.107	0.0004
9	0.076	1.9	0,2	0.09	0.0007	0.03	0.053	0.054	0.02	0.052	0.045	0.0064	0.011	0.088	0.0027
10	0.074	1.89	0,19	0.08	0.003	0.04	0.053	0.05	0.029	0.053	0.042	0.0055	0.008	0.091	0.0021
11	0.12	1.2	0,25	0.02	0.01	0.03	-	0.012	0.02	1.21	0.4	0.0045	0.2	0.07	0.002

Roughing and finish rolling temperatures for each composition presented in Table 3. The selected temperatures were applied in order to comprehend the effect of the magnitude of FRT on the developing microstructure. The presented temperatures represent the true temperatures of a given section of the heat. This signifies that different FRT values are presented in case of same heat, due to the difference in the actual temperatures between different sections.

Table 3: Hot rolling parameters.

Composition	Roughing [°C]	Finish rolling temperature [°C]
1	1005	815
1	990	788
2	1080	920

2	1050	870
2	1000	815
3	1080	920
3	1050	875
3	1025	838
3	1015	825
4	1010	790
5	1045	880
5	1050	855
5	995	802
6	1155	893
7	1150	898
8	1005	820
9	1105	905
10	1025	825

One heat was tempered to two different temperatures. These are presented in Table 4.

Table 4: Presentation of the two tempered sample.

Composi-tion	Roughing [°C]	Finish rolling temperature [°C]	Tempering temperature [°C]
3	1015	825	350
3	1015	825	550

As can be noticed from Table 3, several heats with an equal composition are rolled to different temperatures. From now on the heats are named according to their carbon and manganese contents, and finish rolling temperature. Carbon and manganese contents are

rounded to one decimal. Furthermore the tempered heats are identified by a symbol "T" followed by the utilized tempering temperature.

The thickness of materials is 8 mm, except for the ones whose thickness values are presented in Table 5.

Table 5: Thickness of heats that are not 8 mm.

Heat	Thickness [mm]
0.1C-1.1Mn 855°C	10
0.1C-1.1Mn 802°C	10
0.08C-1.9Mn 905°C	10
0.07C-1.9Mn 825°C	10
0.06C-2.0Mn 820°C	12

Heats with various thicknesses were selected due to need of large amount of heats in order that valid correlations could be defined. And a sufficient amount of heats with 8 mm thickness, for which the minimum bending radius had been defined, were not available.

The tensile test results in longitudinal direction of materials used are presented in Attachment 1 in Table 20. Yet, only the test materials of the present project are concerned, i.e. compositions 1-4 presented in Table 2.

7.2 Microstructural examination

Microstructures of selected materials were studied by using field emission scanning electron microscopy (FESEM). Specimens were prepared in samples manufactured of electro conductive material. Additionally specimens were etched in 2% nital. The direction of the investigated cross sections was RD-ND (Figure 43). The microstructures were examined at the upper surface at intervals of 0.1 mm, to the depth of 0.5 mm and at the middle section of the materials. In Table 6 the selected materials are presented.

*Table 6: Selected materials for microstructural investigation.*

Heat
0.06C-1.4Mn 920°C

0.06C- 1.4Mn 875°C
0.08C-1.8Mn 920°C
0.08C- 1.8Mn 870°C
0.07C-1.3Mn 788°C
0.07C-1.3Mn 815°C

As it can be seen from Table 6, the selected materials have three different chemical compositions; the most significant difference is in the carbon and manganese contents. In addition materials with an equal chemical composition, but various rolling temperatures are included. The variations in these factors are in order that their effects on the forming microstructure could be comprehensively understood.

7.3 Bending tests

To study the bending ability of test materials, three-point air-bending tests were carried out. These tests were performed in Production Technology Laboratory at University of Oulu. The aim of the bending tests was to determine the minimum bending radius whereby the specimen sheet can be bent without failure. The criterion for failure used in present work can be seen from Figure 42. The minimum bending radius was determined for each specimen transverse to rolling direction (TD) and in most cases also to rolling direction (RD). In present work the aim was to study in particularly TD bending, and hence minimum bending radius to RD is lacking in some cases. Figure 41 shows the bend orientation with respect to the coil.
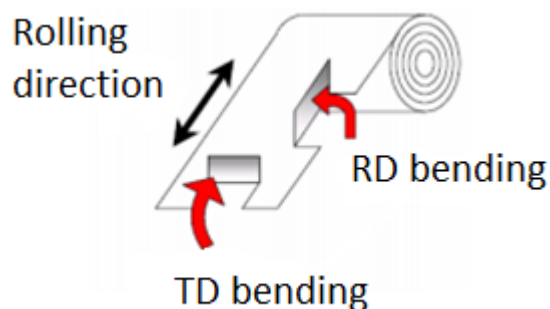
Figure 41: Illustration of bend orientations [Modified from 26].

It is noteworthy to mention that the directions described in Figure 41 do not correspond to the directions described in standards [231]. The applied bending angle was constantly 90° degrees. Whereas the radius was gradually decreased in order to define the minimum

bending radius. The quality of the bent was evaluated visually. The visual inspection procedure is explained in an article by Heikkala and Väisänen and can be seen in Figure 42.
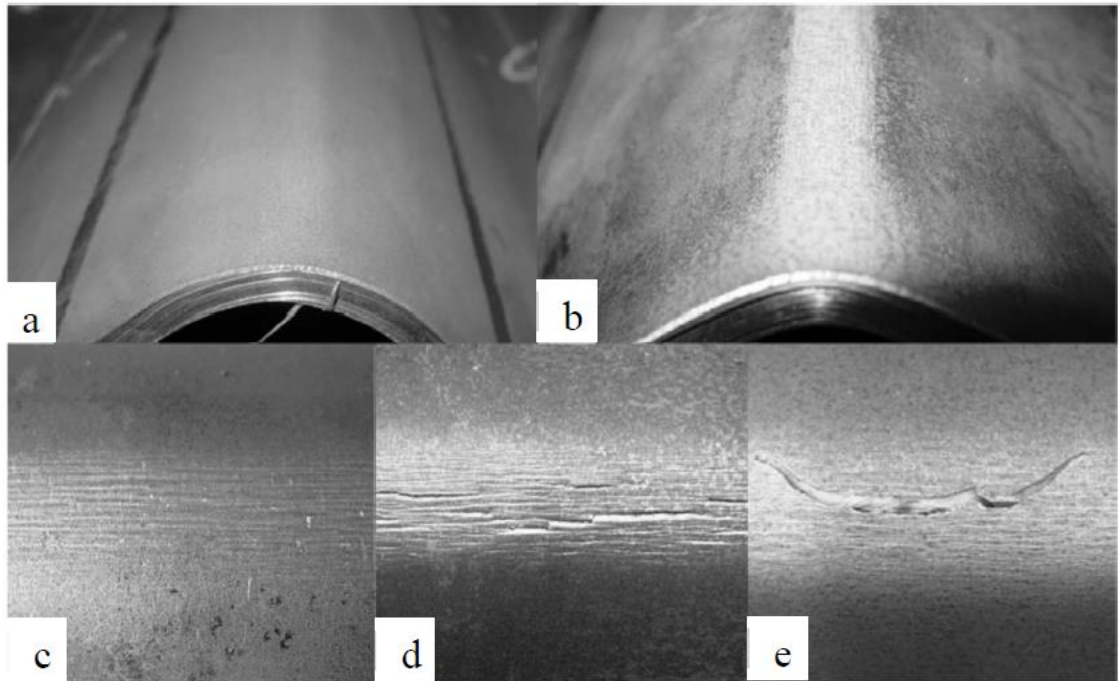
Figure 42: Visual inspection procedure. a) Flawless bend, b) nut-shape, c) surface waviness, d) surface cracks and e) cracks through sample [232].

In this work the surfaces presented in Figures 42a and 42b are accepted, instead the ones shown in Figures 42c-42e are regarded as failure.
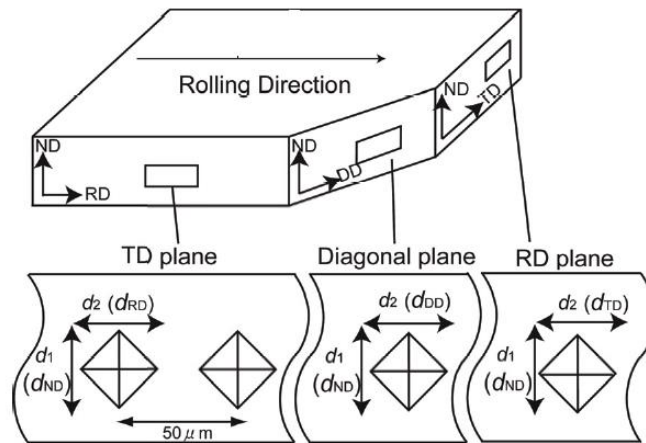
7.4 Microhardness measurements

Microhardness measurements were performed to each test material in the University of Oulu. The applied device in the material technology laboratory is termed as Micro-Indentation Tester. The specimens were prepared in samples of electro conductive material. Before the measurements the specimen were etched in 2% nital. The same samples were used in microstructural examination. All the microhardness measurements were performed by utilizing the Vickers indenter and the parameters presented in Table 7.

Table 7: Test parameters for microhardness measurements.

Load	1000 mN
Loading Speed	2000 mN/min
Unloading Speed	2000 mN/min
Pause	10 s

Fn Contact	25 mN
Approach Speed	15 µm/min
Acquisition Rate	10,0 Hz

The microhardness measurements were conducted in RD-ND –direction, i.e. in longitudinal direction. This direction is demonstrated in Figure 43.

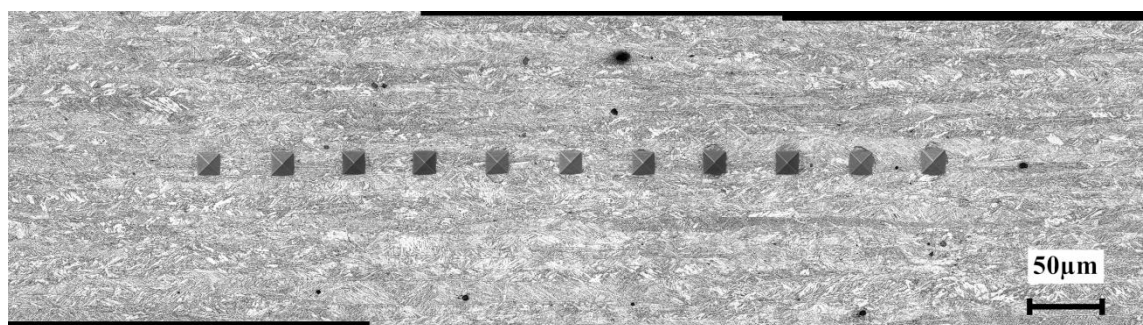*Figure 43: Illustration of the direction in which measurements were performed [233].*

The microhardness of each material was measured in every given depth ten times at intervals of 50 µm. The measurements were performed at the upper surface of the material from the depth of 50 µm to the depth of 500 µm at intervals of 50 µm, i.e. a total of 10x10 measurements were performed. In Figure 44 the measurements are illustrated to the depth of 300 µm.
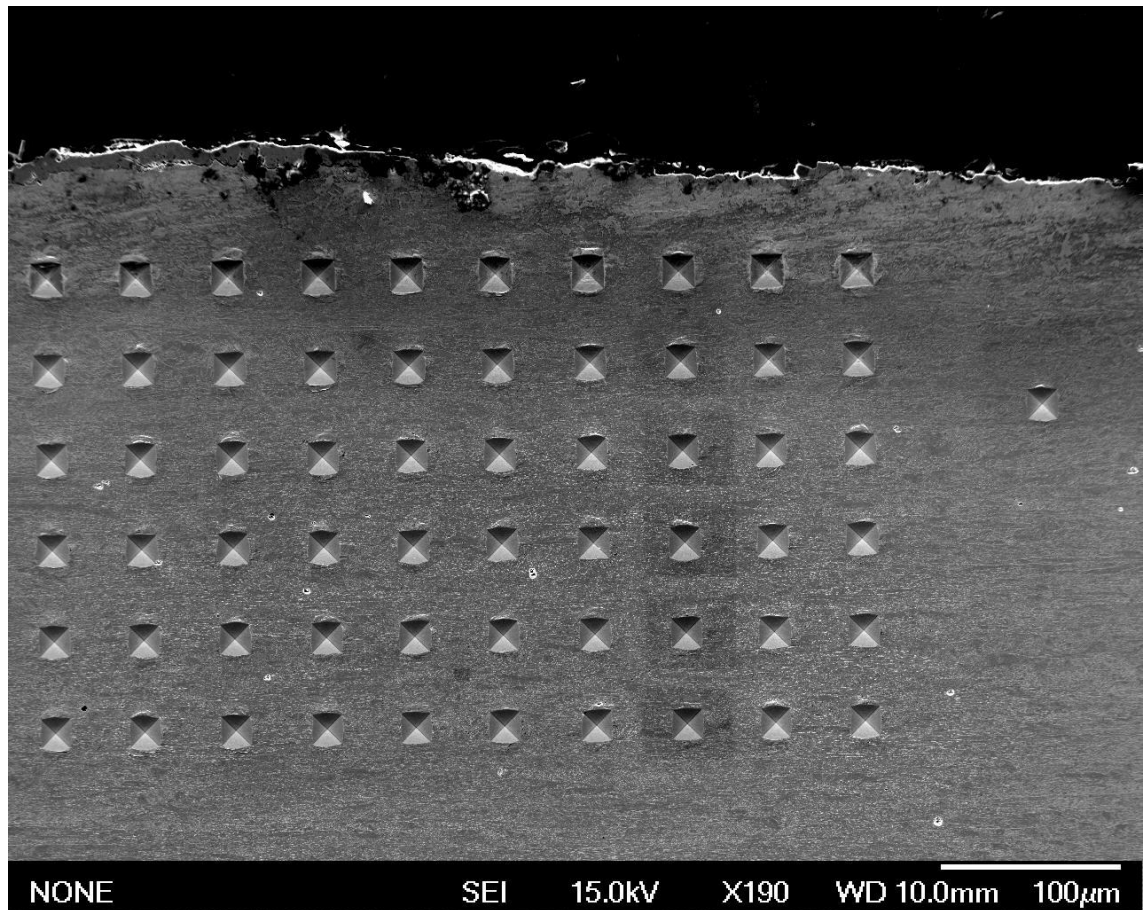
Figure 44: Illustration of the microhardness measurements from the upper surface.

Before starting to measure, it is important to verify that the surface of the sample is adjusted to the device so that the upper surface is straight. Otherwise the measured depths are not equal to the actual depths. It can be noticed from Figure 44 that the surface is not entirely smooth, which leads to distorted depth values. According to the Figure 44, the depth values may distort approximately 10 µm in a given depth.

In addition to the surface hardness, the hardness of the middle section was determined ten times at intervals of 50 µm. This is illustrated in Figure 45.

Figure 45: Illustration of the microhardness measurements of the middle section.

In Figure 45 the measurement point at the very right is the reference point.

7.5   Interrupted bending tests

Interrupted bending tests were carried out for two test materials, for the purpose to determine where shear bands first initiate at. The interrupted bending tests were only performed to transverse to rolling direction (TD). The interrupted bending tests were carried out at University Oulu, using the same equipment as described in Subchapter 7.3. The selected test materials are presented in Table 8. It is noteworthy to state that these tests were conducted after the results further presented in Subchapters 8.4 and 8.5 had been attained.

Table 8: Test materials for interrupted bending tests.

Heat	Thickness	Homogeneity Index at the depth of 200 µm ($HI = \frac{standard\ deviation\ of\ hardness}{average\ hardness}$)	Hardness at the depth of 200 µm [HV]	R_{min}(transverse)/t
0.07C-1.3Mn 815°C	8mm	3	360	2
0.08C-1.8Mn 870°C	8mm	3	445	6,25

These materials were selected in order to understand the effect of surface hardness on the formation of shear bands. The homogeneity index of these materials is equivalent, whereas the surface hardness is highly different.

The samples were bent to four various angles, but the radius was kept constant. The bending radius was determined so that it is slightly smaller than the minimum bending radius for the material. The applied bending radius was defined as $R_{min}/t - 0.5$. The bending angles and the radius for heat 0.07C-1.3Mn 815°C are presented in Table 9.

Table 9: Bending angles and radius for specimen 0.07C-1.3Mn 815°C.

Bending Radius	12, $((R_{min}/t) - 0.5 = 1.5)$
Bending Angles	42°, 56°, 85° and 95°

In Table 10 the bending angles and radius for specimen 0.08C- 1.8Mn 870°C are shown.

Table 10: Bending angles and radius for specimen 0.08C- 1.8Mn 870°C.

Bending Radius	45, $((R_{min}/t) - 0.5) = 5.625)$
Bending Angles	43°, 57°, 96° and 97°

8. RESULTS

In this chapter the results are presented. First, FESEM images of microstructures of the selected test materials are presented and the main microstructural constituents are characterized. Second, the surface hardness profiles to the depth of 500 μm and middle section hardness values of each sample are presented. Third, the bending test results, i.e. minimum bending radius for each sample, are shown. Next the relationship between surface hardness and bendability is presented, followed by the presentation of relationship between microstructure homogeneity and bendability. Finally, results of interrupted bending tests are demonstrated, including FESEM images of cross sections of bent regions.

8.1 Microstructures of selected materials

FESEM images of microstructures of selected materials are presented. The microstructures of the upper surface are observed and characterized immediately at the surface and additionally at the depths of 0.1 mm-0.5 mm at intervals of 0.1 mm. The applied magnification is in all cases x5000.

Basically, in case of all selected materials, the microstructure at middle section consists of a mixture of lath-like bainite and martensite. In heats comprising higher amounts of carbon and manganese and/or rolled at higher temperatures, the microstructure is finer and the volume fraction of martensite is greater. The microstructure at middle section of heat 0.07C-1.3Mn 788°C differs most significantly from others, since it comprises additionally M/A constituents in a bainitic ferrite matrix, i.e. granular bainite, and the volume fraction of martensite is rather negligible. Microstructures at the middle sections presented in Attachment 2.

8.1.1 Sample 0.06C-1.4Mn 920°C

Figures 46a-46f present the microstructure of the upper surface of sample 0.06C-1.4Mn 920°C.

a)

b)

c)

d)

e)

f)
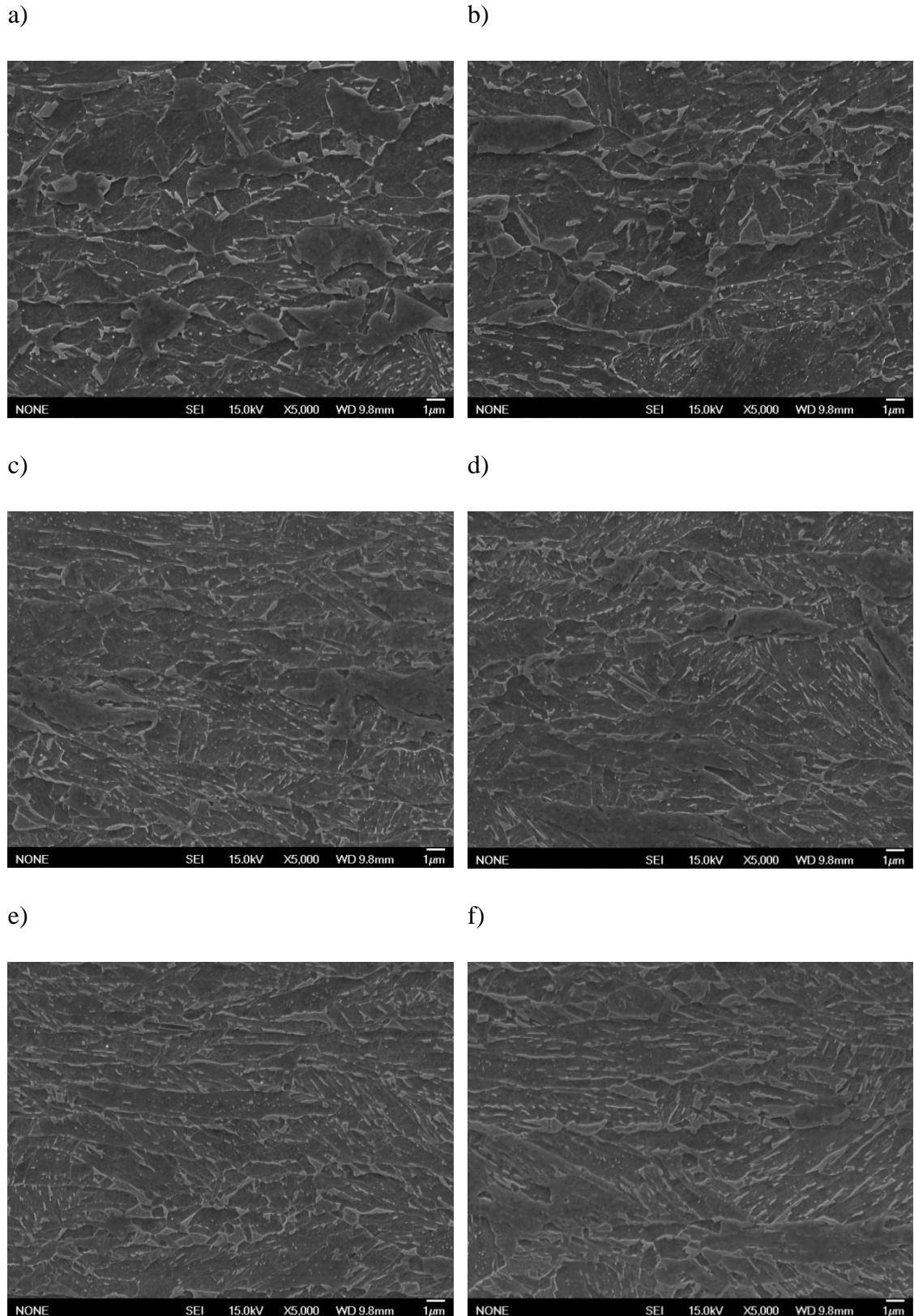
Figure 46: Microstructure of sample 0.06C-1.4Mn 920°C at the a) upper surface, b) 0.1 mm, c) 0.2 mm, d) 0.3 mm, e) 0.4 mm and f) 0.5 from upper surface.

It can be observed from Figure 46a that there is actually no ferrite layer at the surface. The structure of the surface consists mainly of M/A islands, lath-like bainite and regions

of carbides. Already at the depth of 0.2 mm (Figure 46c) the structure represents rather lath-like features. It is worth noticing that at the depth of 0.5 mm (Figure 46f), carbides that are horizontal are present.
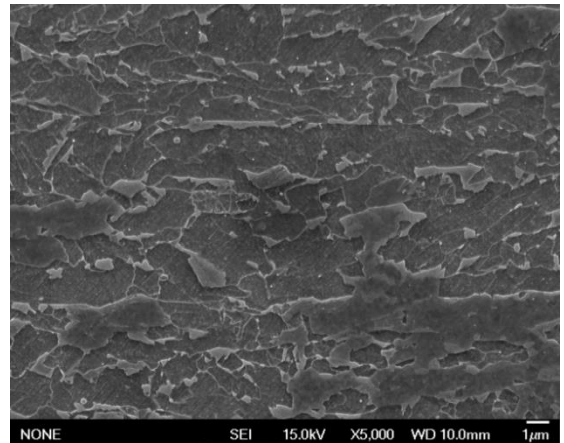
8.1.2 Sample 0.06C- 1.4Mn 875°C

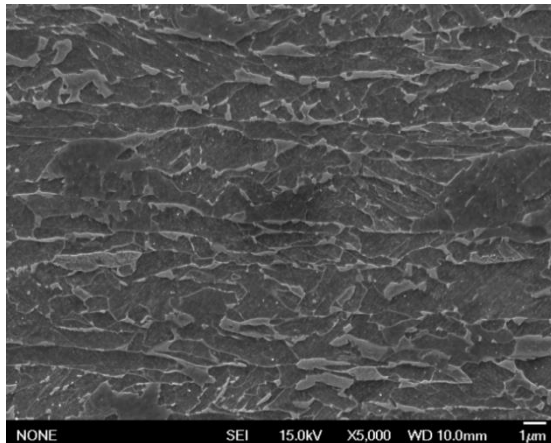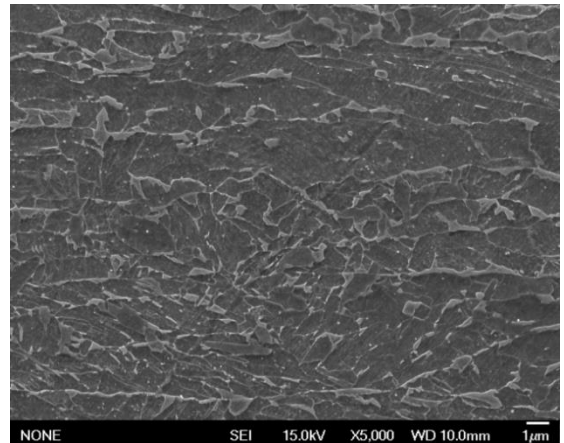Figures 47a-47f represents the microstructure of the upper surface of sample 0.06C-1.4Mn 875°C.

a)

b)

c)

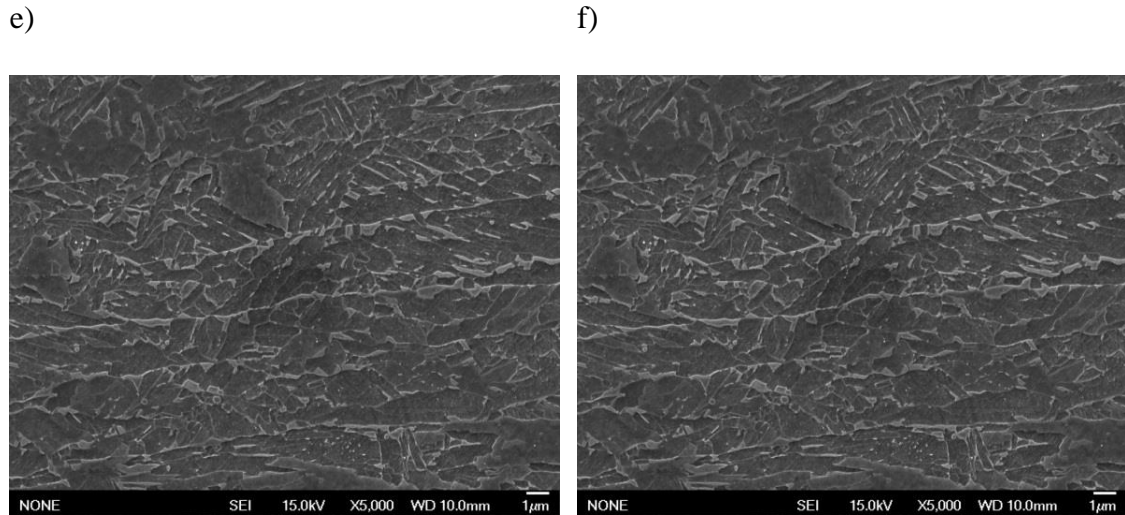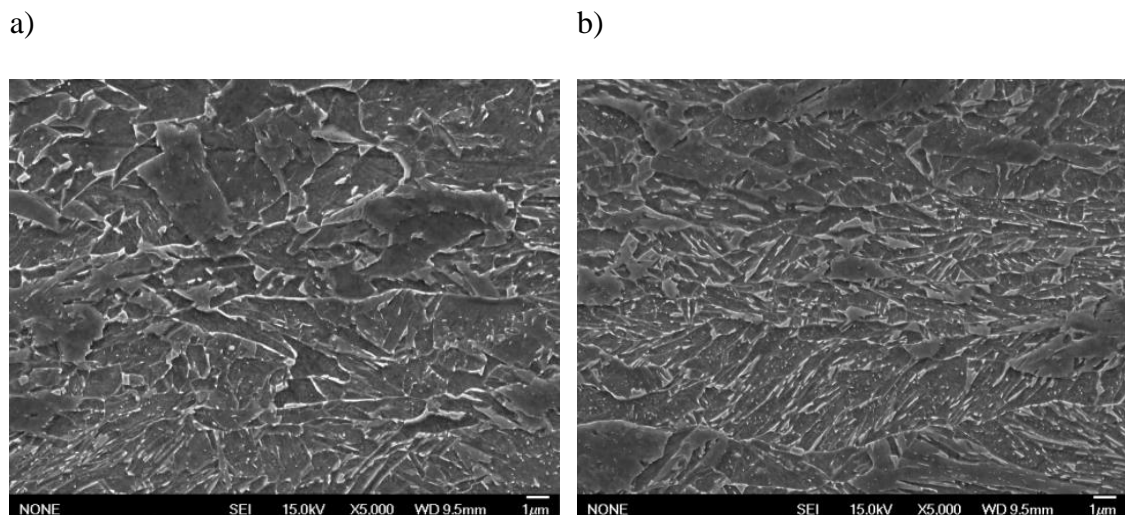d)

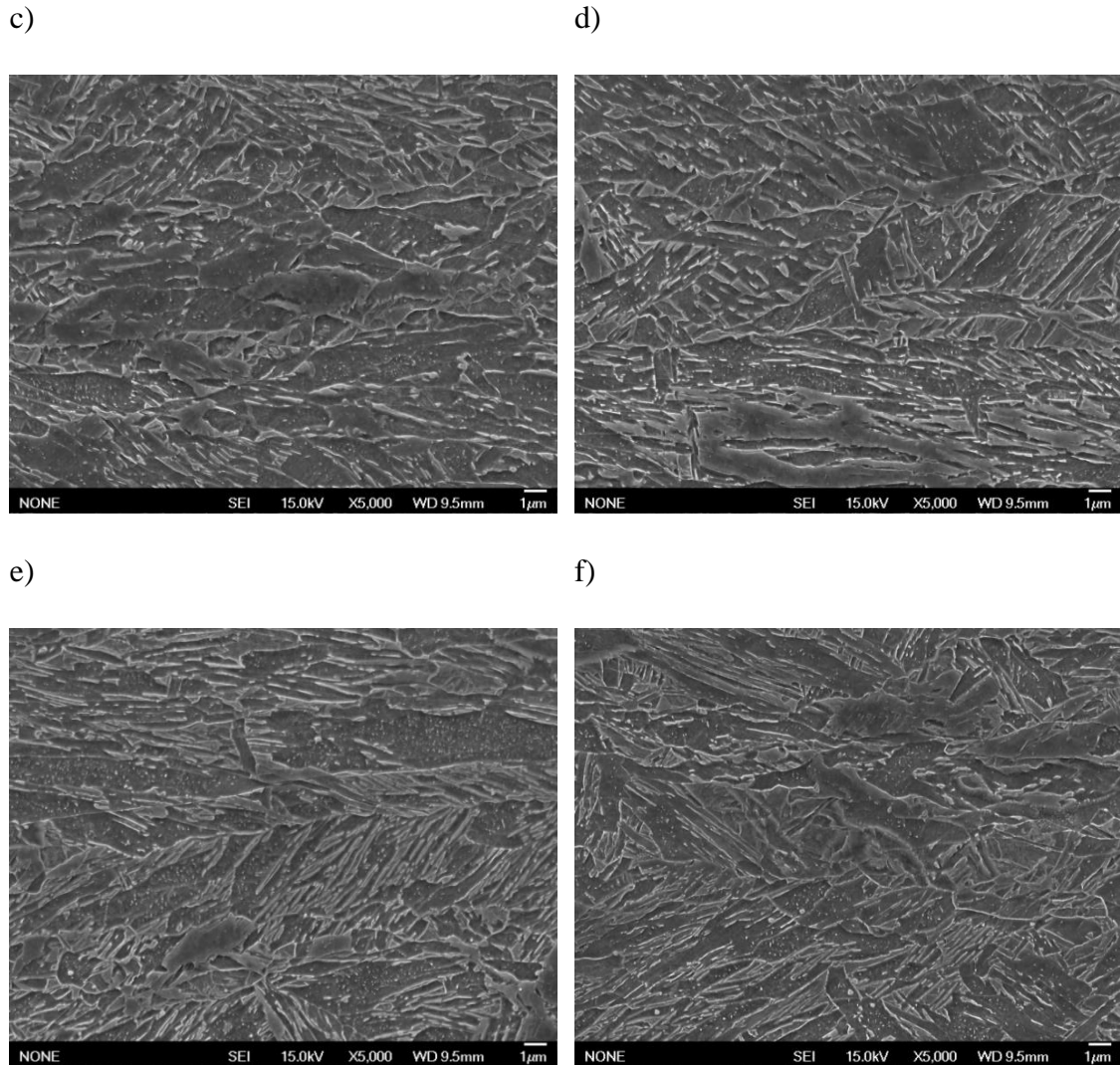e)   f)
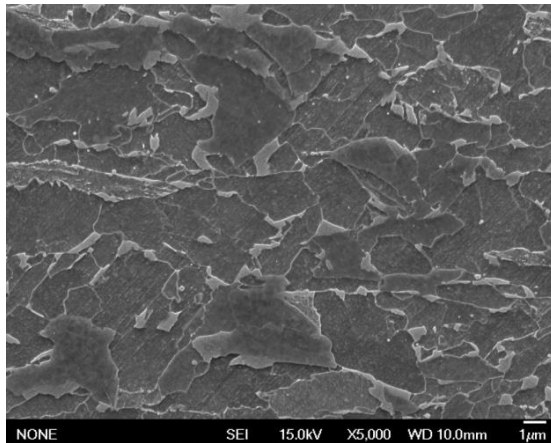
Figure 47: Microstructure of sample 0.06C- 1.4Mn 875°C at the a) upper surface, b) 0.1 mm, c) 0.2 mm, d) 0.3 mm, e) 0.4 mm and f) 0. 5mm from upper surface.

Figure 47a illustrates that there is an obvious layer consisting mainly of granular bainite at the surface of the material. Such layer expands approximately to the depth of 70 µm. According to Figures 47b-47f, below the layer of granular bainite, the microstructure consists principally of M/A islands of various sizes and morphologies, and lath-like bain-ite.

8.1.3 Sample 0.08 C-1.8Mn 920°C

Figures 48a-48f present microstructures of sample 0.08 C-1.8Mn 920°C at various depths from the upper surface.

a)   b)

c)   d)

e)   f)

Figure 48: Microstructure of sample 0.08 C-1.8Mn 920°C at the a) upper surface, b) 0.1 mm, c) 0.2mm, d) 0.3mm, e) 0.4 mm and f) 0.5 mm from upper surface.

There appears to be no layer of granular bainite at the surface. Instead the microstructure is immediately from the surface rather lath-like. Throughout the surface consists principally of lath-like bainite and from the depth of 0.3 mm additionally regions of martensite are present. Furthermore carbide-rich regions appear to present throughout the surface. From the depth of 0.4 mm (Figures 48e-48f) significant volume fractions of tempered martensite can be observed.

8.1.4 Sample 0.08C-1.8Mn 870°C

Figures 49a-49f represent the microstructure of the upper surface of sample 0.08C-1.8Mn 870°C.

a)

b)

c)

d)

e)

f)
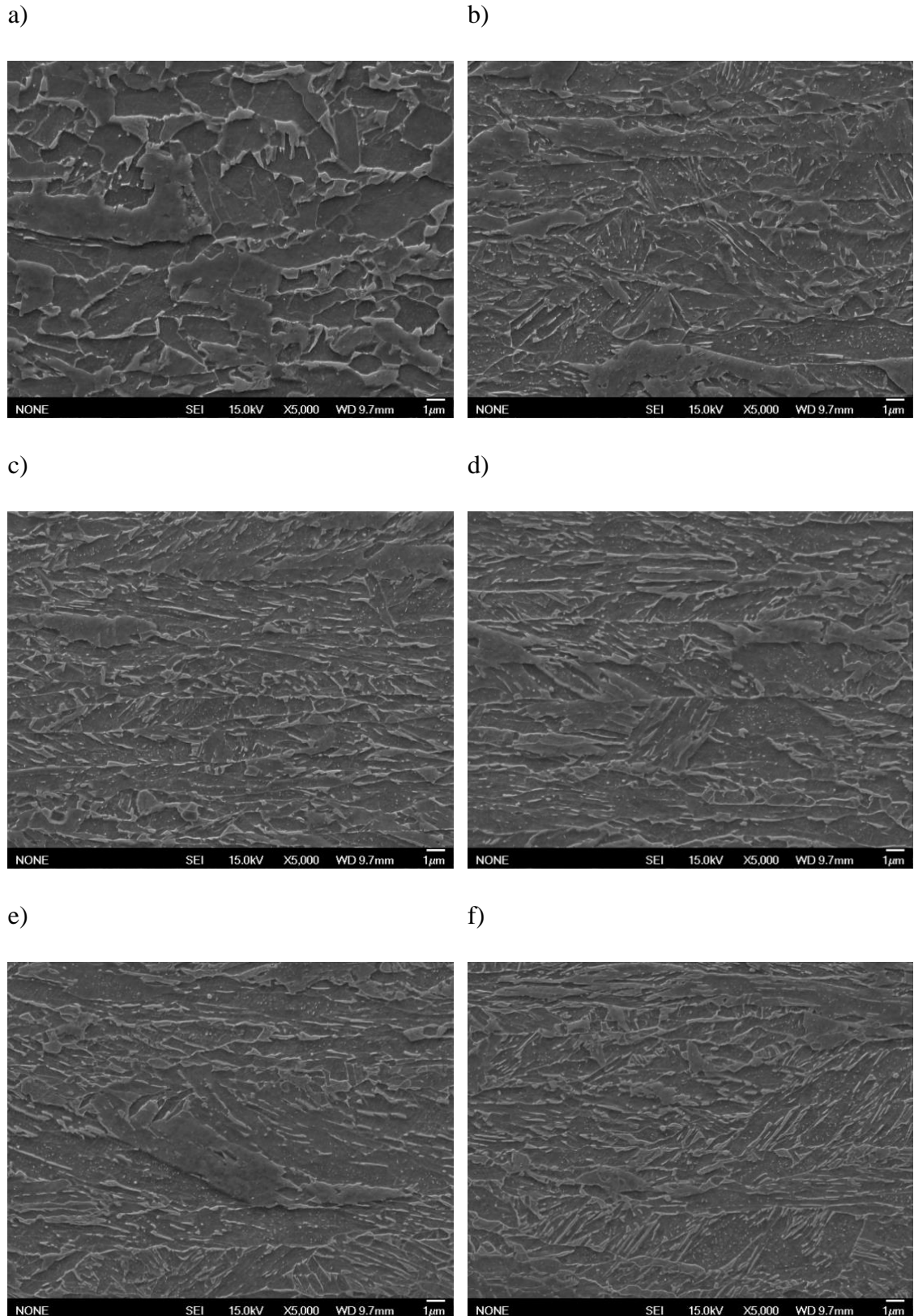
Figure 49: Microstructure of sample 0.08C-1.8Mn 870°C at the a) upper surface, b) 0.1 mm, c) 0.2 mm, d) 0.3mm, e) 0.4 mm and f) 0.5mm from upper surface.

Figure 49a shows that the microstructure at the surface is rather granular and no lath-like characteristics are present at this depth. Such granular layer reaches roughly to the depth
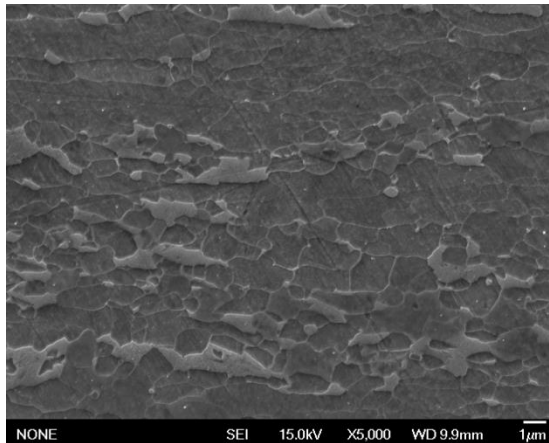
of 0.05 mm. As can be seen from Figure 49b, from the depth of 0.1 mm the microstructure is mainly lath-like, comprising principally lath-like bainite, M/A islands and carbide-rich regions.
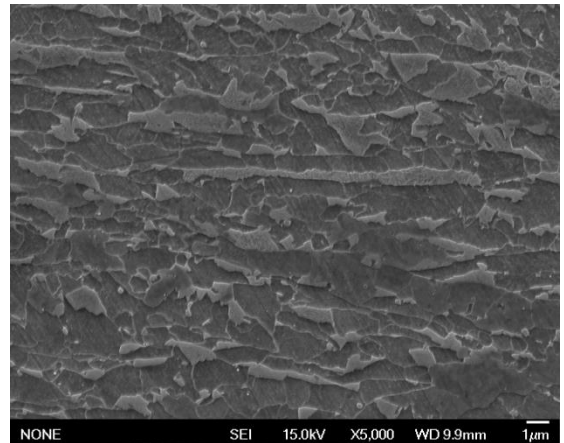
8.1.5 Sample 0.07C-1.3Mn 788°C

Figures 50a-50f present the microstructure of the upper surface of sample 0.07C-1.3Mn 788°C.

a)

b)

c)

d)

e)   f)

Figure 50: Microstructure of sample 0.07C-1.3Mn 788°C at the a) upper surface, b) 0.1 mm, c) 0.2 mm, d) 0.3mm, e) 0.4 mm and f) 0.5 mm from upper surface.

The microstructure throughout the surface is rather granular and no lath-like features are present. It appears to consist mainly of granular bainite.

A layer consisting of M/A islands in a matrix reaches to the depth of approximately 0.9 mm, as seen from Figure 51.

86.92µm

Figure 51: Illustration of the depth of the soft layer on the surface of sample 0.07C-1.3Mn 788°C.

The type of the matrix is assumed to be bainitic ferrite. Moreover, polygonal ferrite is present immediately at the surface. Still below the depth of 0.9 mm the microstructure consists mainly of granular bainite, but the volume fraction of M/A islands is significantly greater.

8.1.6   Sample 0.07C-1.3Mn 815°C

Figures 52a-52f present the microstructure of the upper surface of sample 0.07C-1.3Mn 815°C.
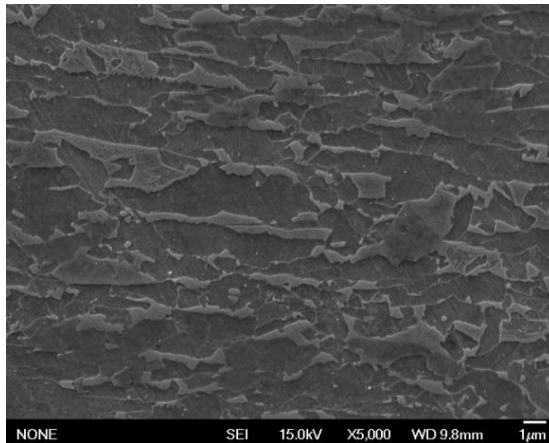
a)

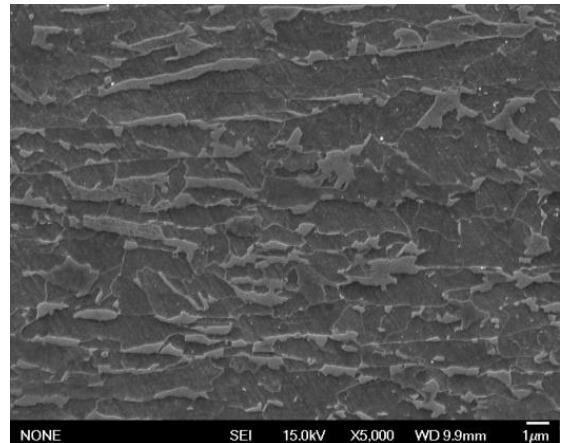b)
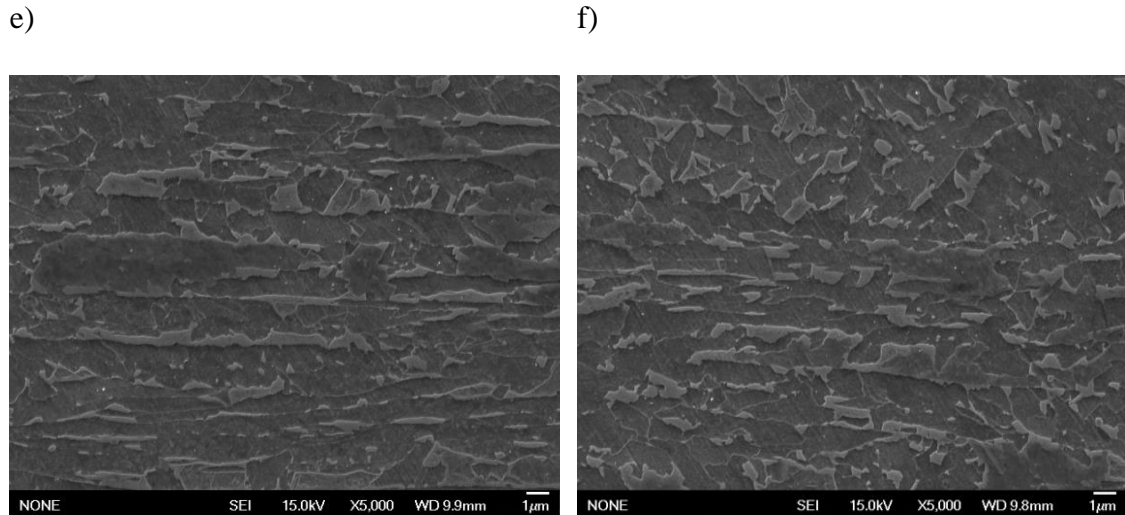

c)

d)

e)   f)
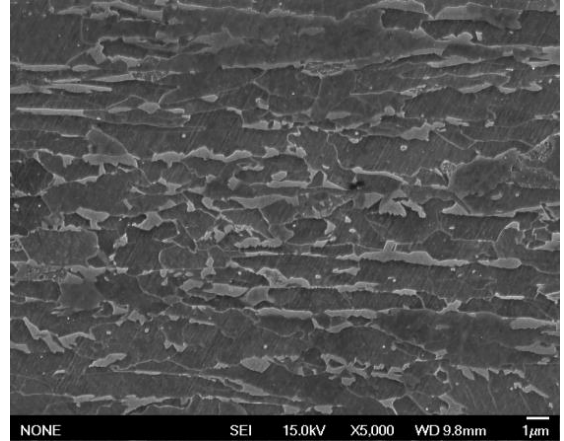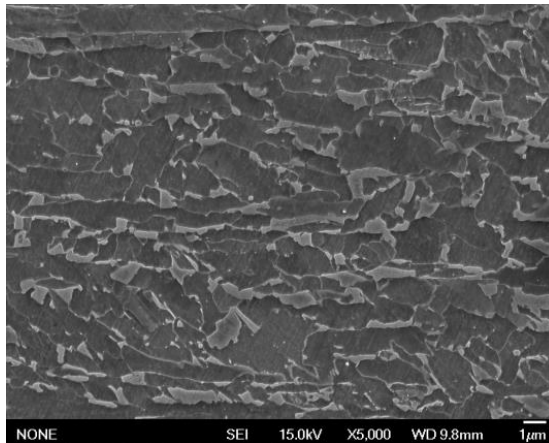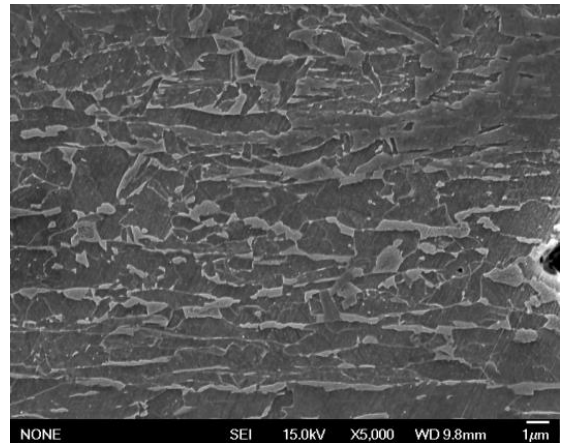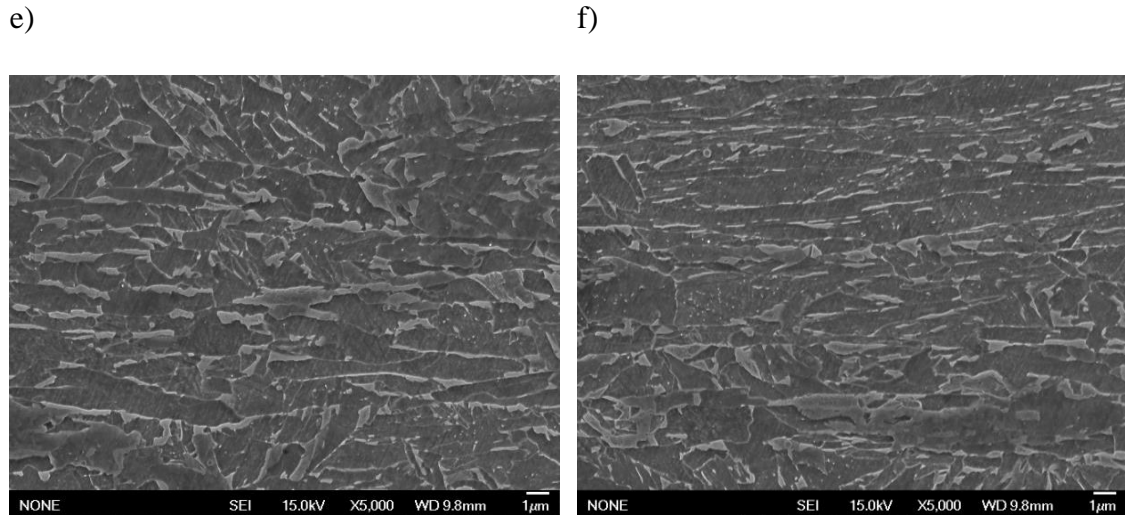
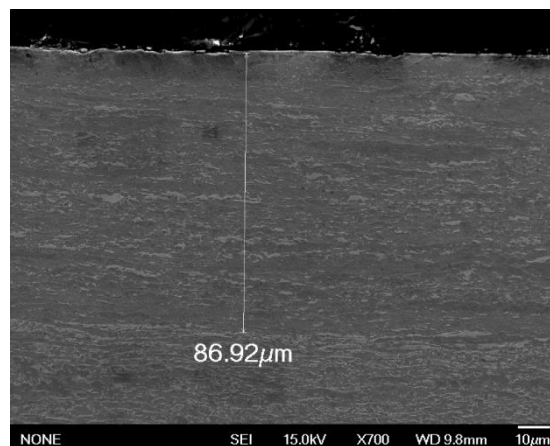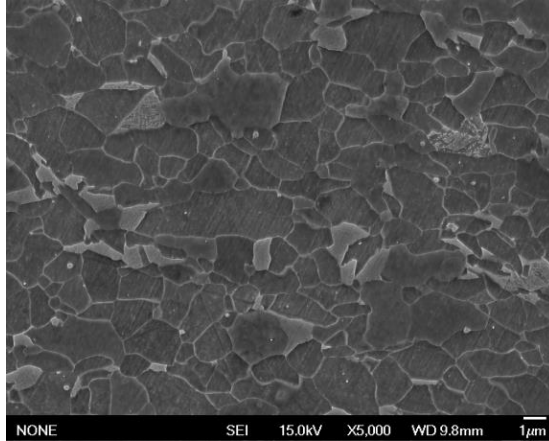

Figure 52: Microstructure of sample 0.07C-1.3Mn 815°C at the a) upper surface, b) 0.1 mm, c) 0.2 mm, d) 0.3mm, e) 0.4 mm and f) 0.5 mm from upper surface.

Figure 52a indicates that there is layer of mainly polygonal ferrite immediately at the surface of the sample. Below this layer to the depth of 0.4 mm (Figures 52b-52e) the microstructure is still rather granular and the volume fraction of lath-like features is nearly negligible. However at the depth of 0.5 mm more lath-like characteristic appear to be present. Yet, features of orientation are nearly negligible. Anyway, the microstructure throughout the surface consists mainly of M/A islands in a bainitic ferrite matrix.

8.2   Surface hardness profiles

In this chapter the surface hardness of the materials is presented to the depth of 0.5 mm and additionally at the middle thickness. First the influence of FRT is observed, by presenting materials with a rather equal chemical composition, but different FRT in same scatter. Secondly, the effects of carbon and manganese contents are shown, by presenting materials with various carbon and manganese contents with a given FRT in same scatter. In case of some heats, the hardness values are only defined to the depth of 0.3 mm

8.2.1   Effect of FRT

The surface hardness profiles of each material are presented in Figures 53-56. Here the effect of FRT of hardness is observed. Hence the materials presented in the same scatter have basically equal chemical composition, but their rolling temperatures differ. The yield strength level of heats presented in Figures 53-55 is at the range of 900-1200 MPa. While, the yield strength level of heats presented in Figure 56 is approximately 700 MPa.

Figure 53 presents the hardness of upper surface and centre line (CL) of heats containing 0.06-0.07 wt.% C and 1.3-1.4 wt.% Mn rolled in various temperatures. Furthermore two tempered heats are included.
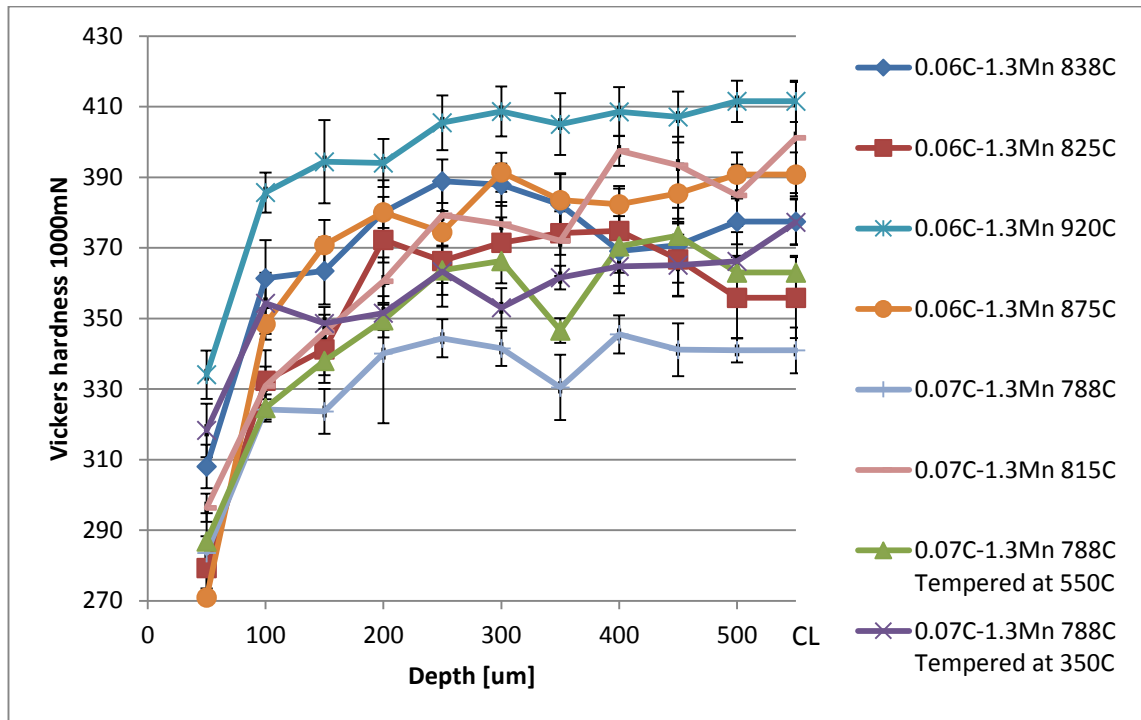
Figure 53: Hardness profiles of heats containing 0.06-0.07C and 1.3 Mn rolled in various temperatures.

It can be observed from Figure 53, that basically as the FRT increases the hardness throughout the surface and centre line increases. It can be noticed that the shape of the hardness profiles are nearly identical. This indicates that in case the hardness at the surface is low, the centre line hardness is respectively low. Moreover, in case of tempered materials, the one tempered at a lower temperature is harder.

Figure 54 presents the hardness of upper surface and centre line (CL) of heats containing 0.08 wt.% C and 1.8 wt.% Mn rolled in various temperatures.
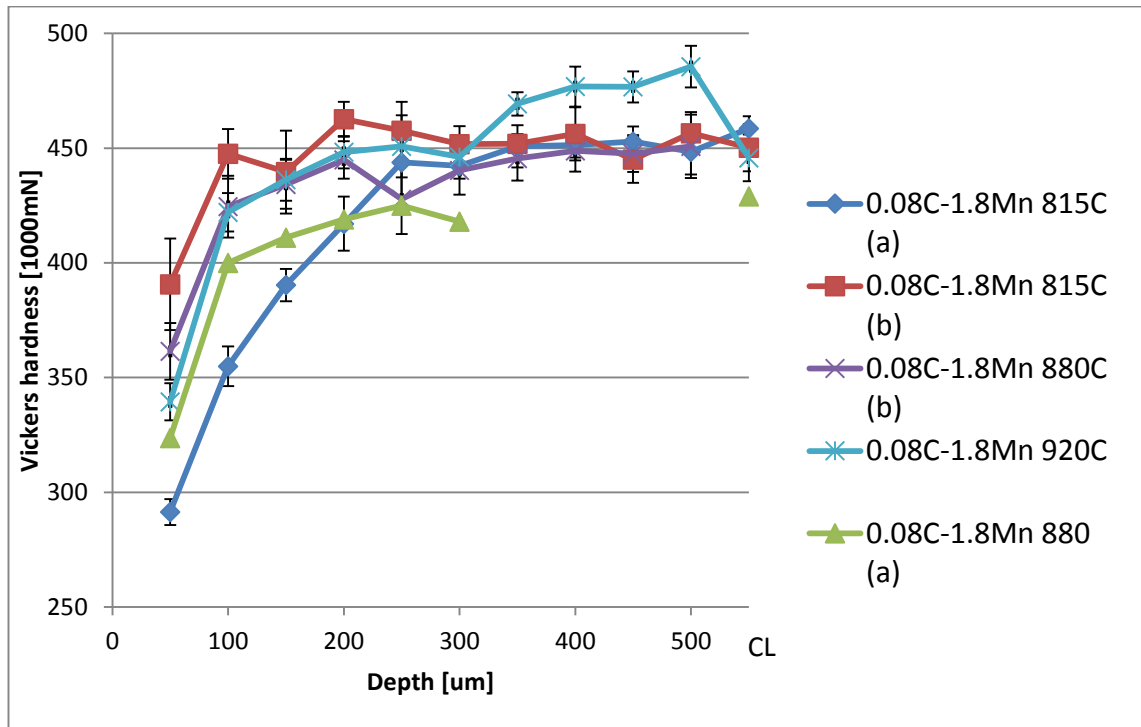
Figure 54: Hardness profiles of heats containing 0.08C and 1.8Mn rolled in various temperatures.

Identifiers (a) and (b) stand for nearly adjacent regions of same sample. It can be seen from Figure 54 that the average hardness values can rather highly vary within a given sample, even at the neighbouring regions. Here, the effect of FRT is not obvious. Yet, if regions (b) of samples rolled to temperatures of 880°C and 815°C are not included, it can be seen that hardness increases with an increasing FRT throughout the sample.

Figure 55 presents heats containing 0.1C and 1.1Mn rolled in various temperatures. It is noteworthy that these heats do not include niobium, whereas the heats presented in Figures 53 and 54 include 0.04 wt.% Nb.
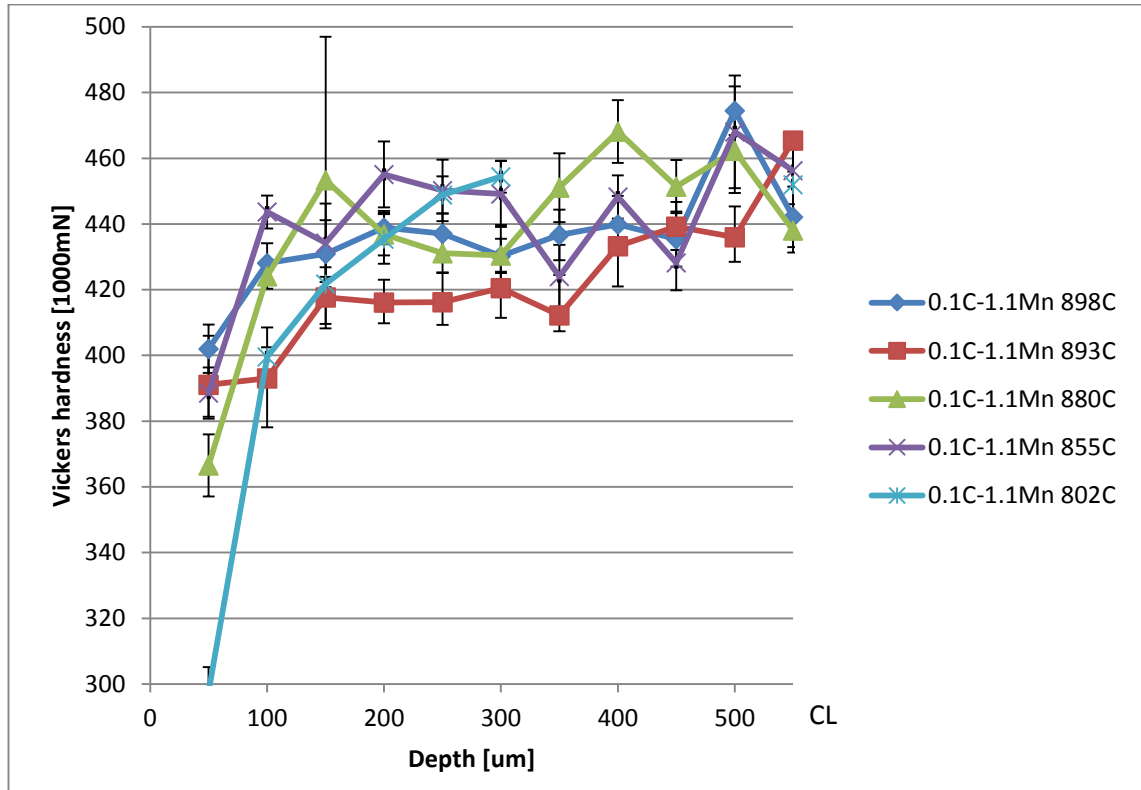
Figure 55: Hardness profiles of heats containing 0.1C and 1.1Mn rolled in various temperatures.

The hardness immediately at the surface (0.05 mm) is practically in accordance with FRT; it increases with an increasing FRT. Yet, the hardness values achieved at the centre line do not correspond precisely to FRT.

Figure 56 presents the surface hardness of heats with strength level of approximately 700 MPa.
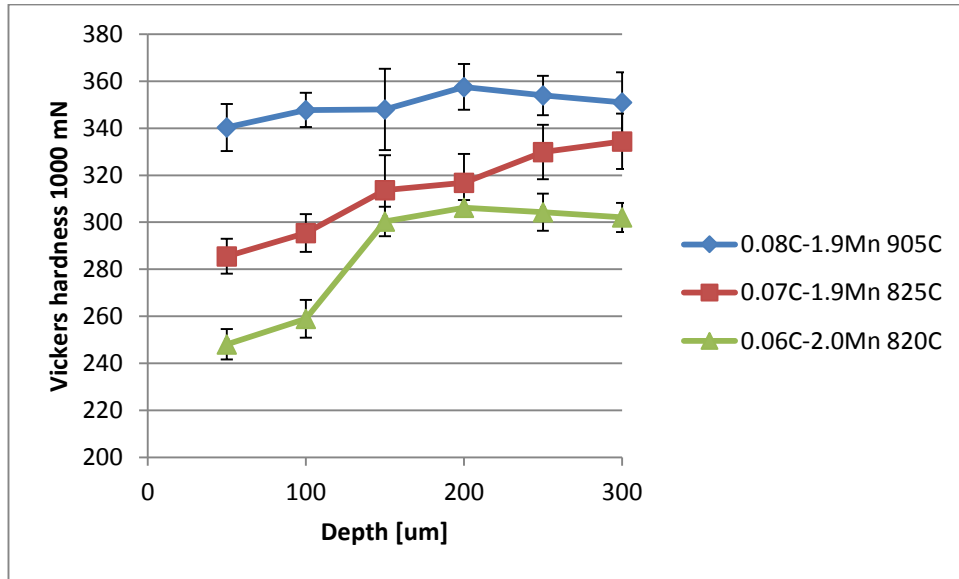
Figure 56: Hardness profiles of heats (YS~700 MPa) containing 0.06-0.08C and 1.9-2.0Mn rolled in various temperatures.

Figure 56 shows that hardness increases with FRT.

8.2.2 Effect of carbon and manganese contents

Here heats with different carbon and manganese contents rolled in rather equal temperatures are presented in the same scatter. Hence the effect of such contents can be identified. Basically, the materials possess three various compositions, these are presented in Table 11.

Table 11: Representation of three various compositions.

Heat	Carbon content	Manganese content	Niobium content
0.06C-1.3Mn	0.06-0.07	1.3	0.004
0.08C-1.8Mn	0.08	1.8	0.004
0.1C-1.1Mn	0.1	1.1	-

Figures 57 and 58 present hardness profiles of heats with different compositions rolled in a nearly equal temperature.
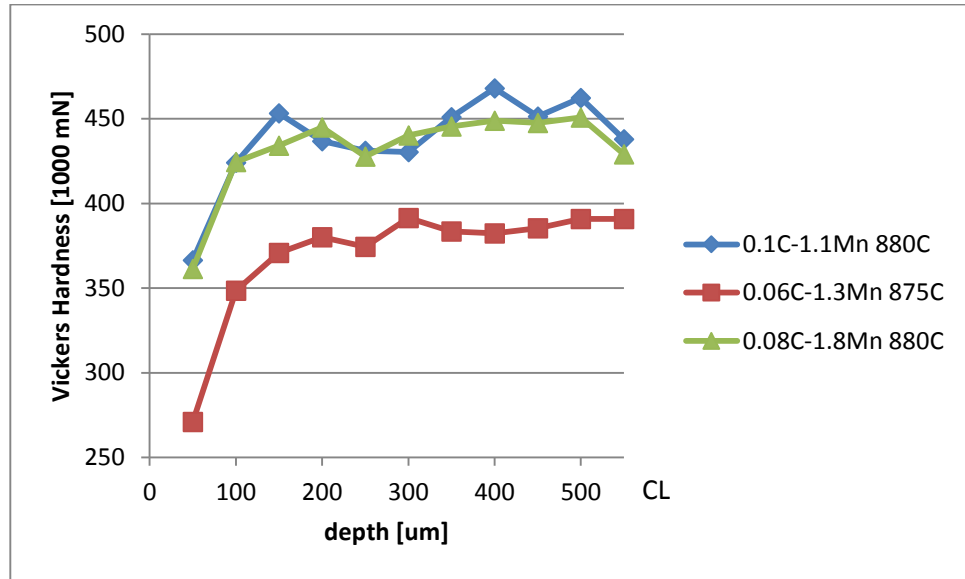
Figure 57: Hardness profiles of samples with various compositions rolled in 880°C.
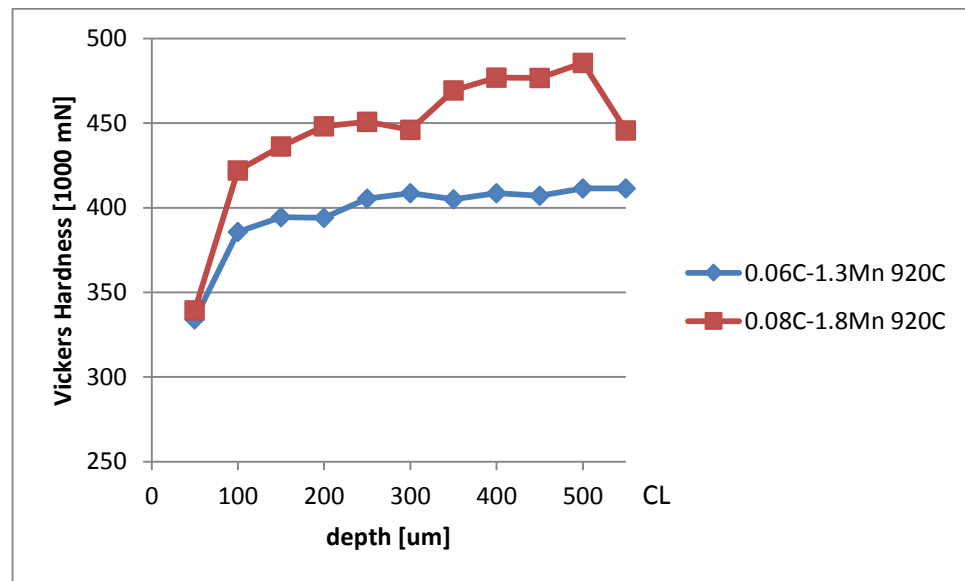
Figure 58: Hardness profiles of samples with various compositions rolled in 920°C.

It can be seen from Figures 57 and 58 that higher carbon and manganese contents lead to greater hardness values throughout the thickness.

8.3 Bending tests

In Table 12 the minimum bending radius (*R/t*) of each sample is illustrated in both to the longitudinal and transverse directions. Minimum bending radius to the longitudinal direction are lacking in case of some materials, because in this work only TD bending was studied.

Table 12: Minimum bending radius (R/t) of test materials.

Heat	R_{min} longitudinal/t	R_{min} transverse/t
0.1C-1.1Mn 802°C	3.5	Not qualified
0.1C-1.1Mn 898°C	3.5	3
0.1C-1.1Mn 893°C	3.5	2.5
0,06C-1,4Mn 920°C	4	3.5
0,06C-1,4Mn 875°C	3.5	2.5
0,06C-1,4Mn 838°C	-	1.75
0,06C-1,4Mn 825°C	-	1.5
0,08C-1,8Mn 920°C	5.625	4
0,08C-1,8Mn 870°C	5.625	6.25
0,08C-1,8Mn 815°C (a)	3.75	>8
0,08C-1,8Mn 815°C (b)	3.75	3 (estimation)
0.06C-2.0Mn 820°C	-	0.5
0.08C-1.9Mn 905°C	1.5	0.2
0.07C-1.9Mn 825°C	1	0.2
0.07C-1.3Mn 788°C T 350°C	-	1
0.07C-1.3Mn 788°C T 550°C	1.25	0.6
0.07C-1.3Mn 815°C	1.75	1
0.07C-1.3Mn 788°C	2	2
0.12C-1.2Mn 880°C	3.5	3.5
0.09C-1.1Mn 790°C	8	8

It is noteworthy to mention, that in this work the specimen were bended so that the upper surface was subjected to tension.

8.4 The Relationship between hardness and Minimum Bending Radius

The correlation between bendability and upper surface hardness on every given depth is defined. The average hardness of each depth is considered. Correlations between average hardness values of various depth ranges and bendability are defined. In addition to the surface hardness, the correlation between centre hardness and bendability is concerned. The case of sheets with thickness of 8 mm is considered separately from the sheets with thickness of 10 mm. Both the correlation coefficient and the R^2 value are presented.

8.4.1 Relationship between hardness and bendability in case of 8 mm samples

In Table 13 is presented the correlation between average hardness on given depth/depths from upper surface and bendability in the case of the 8 mm samples.

Table 13: The correlation between average surface hardness on given depth/depths and minimum bending radius in the case of 8 mm sheets.

Depth [um]	Correlation coefficient	R^2
50	0.542	0.293
100	0.797	0.635
150	0.829	0.687
200	0.852	0.726
250	0.764	0.584
300	0.828	0.686
350	0.824	0.679
400	0.786	0.618
450	0.783	0.614
500	0.775	0.600
50-200	0.784	0.615
100-200	0.840	0.705
100-300	0.839	0.704
150-300	0.833	0.695
150-200	0.846	0.716
150-350	0.835	0.697

According to Table 13, the most significant correlations are at the depth range of 100-350 μm. In case of an individual depth, the most significant correlation is at the depth of 200 μm. In Figure 59 the correlation between minimum bending radius and upper surface hardness at the depth of 200 μm is shown.
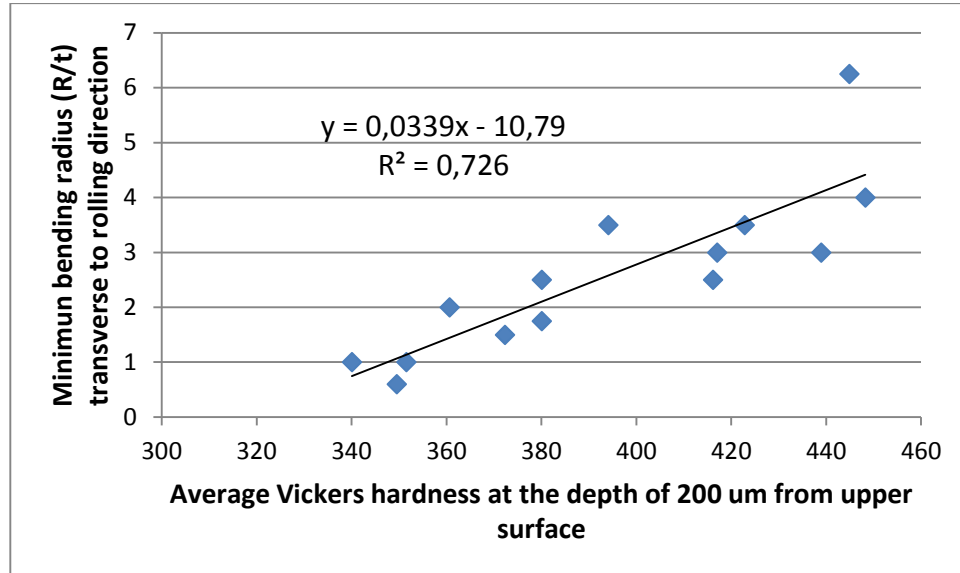
Figure 59: Correlation between minimum bending radius and upper surface hardness at the depth of 200 μm.

The point that most highly deviates from the trend line stands for sample 0.08C-1.3Mn 870°C. According to these results, the soft layer is required to extend at least to the depth of 200 μm from the upper surface in order to achieve good bendability, i.e. 3*t*. Yet, preferable the layer exceed to 350 μm. This is 2,25-4.38 % relative to the total sheet thickness. The magnitude of the hardness of the soft layer is dependent on the desired minimum bending radius. For example in case the desired R/t is 3, the hardness at the depth of 0.2 mm is required to be below approximately 400 HV.

It was found that the correlation between the hardness at centre line and bendability is not significant. The correlation coefficient is 0.4. In Attachment 3 the correlation is presented.

8.4.2 Relationship between hardness and bendability in case of 10 mm samples

In Table 14 is presented the correlation between average surface hardness at a given depth and bendability in the case of the 10 mm samples.

Table 14: The correlation between average surface hardness on given depth and minimum bending radius in the case of 10 mm sheets.

Depth [um]	Correlation coefficient	R^2

50	0.860	0.740
100	0.949	0.900
150	0.938	0.880
200	0.970	0.940
250	0.985	0.970
300	0.995	0.990
350	0.943	0.890
400	0.964	0.930
450	0.949	0.900
500	0.995	0.990

The correlations shown in Table 14 are all highly significant, apart from the correlation in depth 50 μm. However the amount of test materials is only four, which is significantly too small. Therefore these results are not reliable. In the case of a 10 mm sheet, the soft layer should extend to the depth of 2.25 % relative to the total sheet thickness, it means in micrometers that it must extend to the depth of 225 μm.

8.4.3 Effect of hardness on bendability; case 0.08C-1.8Mn 815°C (a) and (b)

In this chapter, sample 0.08C-1.8Mn 815°C is examined. Hardness measurements were carried out both at the region, where visually observable damage occurred, and where no damage occurred. These regions, indicated with signs "a" and "b", are presented in Figure 60.

Figure 60: Sample 0.08C-1.8Mn 815°C a) no visually observable damage and b) visually observable damage at the surface.

In Table 15, the measured hardness values on both of these regions are presented. It is noteworthy to mention that the hardness measurements were conducted prior to bending.

Table 15: Hardness values at region (a) without damage and (b) with damage, at depths in range of 0.05-0.5 mm from upper surface.

Heat	50 um	100 um	150 um	200 um	250 um	300 um	350 um	400 um	450 um	500 um	CL
0.08C-1.8Mn 815°C (a)	291	355	390	417	444	442	451	451	453	448	459
0.08C-1.8Mn 815°C (b)	391	448	440	463	458	452	452	456	445	457	450

It can be noticed from Table 15 that there is significant difference in the hardness values. The region where damage occurred, possesses a notably higher hardness thougout the surface compared to the neigboring region, where no damage occured.

8.5 The Relationship between microstructure homogeneity and minimum bending radius

Microstructure homogeneity is evaluated by the standard deviation of hardness measurements and by using the Equation (17). In this work the term homogeneity index refers to Equation (17). The sheets of 8 mm and 10 mm are considered together. Instead the two

tempered materials are not included, since their homogeneity values are highly different from the untempered samples.

The homogeneity of the microstructure is defined in terms of the deviation of the microhardness measurements. However the microstructures of the materials are rather complex and fine, whereupon the applied method does not define the hardness variations between neighbouring phases. Instead each measurement encompasses a various amount of several phases and presents the average hardness of these values. Moreover the effects of orientations of individual grains and defects on hardness values cannot be defined accurately with microhardness measurements. This is illustrated in Figure 61.
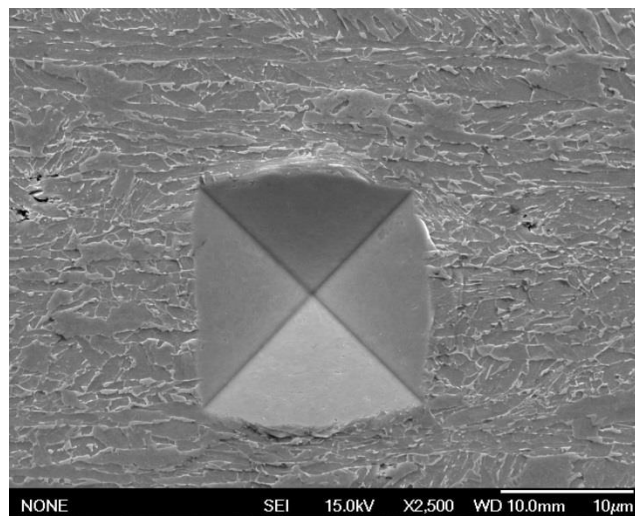
Figure 61: Illustration of a microhardness measurement.

8.5.1 Correlation between homogeneity index (HI) and minimum bending radius

The Homogeneity index (HI) is measured at every given depth in terms of Equation (17) and the utilized HI values are presented in Table 21 in Attachment 4. In Table 16 the correlation between homogeneity index at a given depth from upper surface and minimum bending radius transverse to rolling direction is shown. Both the correlation coefficient and the R-squared value are represented at each depth.

Table 16: Correlation between minimum bending radius on transverse to rolling direction and homogeneity index at a given depth

Depth [um]	Correlation coefficient	R^2
50	0.778	0.606
100	0.276	0.076
150	0.112	0.013

200	-0.244	0.059
250	0.611	0.373
300	0.163	0.027
350	-0.333	0.111
400	-0.266	0.071
450	-0.166	0.027
500	0.043	0.002

It can be observed from Table 16, that the most significant correlation is at the depth of 50 µm.

Figure 62 shows the correlation between homogeneity index at the depth of 50 µm and minimum bending radius transverse to rolling direction.
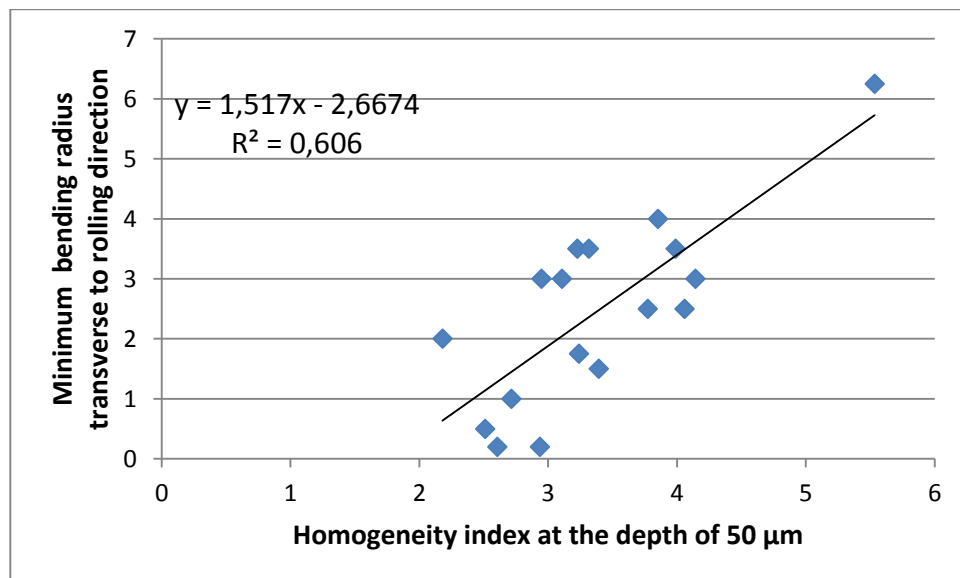
Figure 62: Correlation between homogeneity index at the depth of 50 um and minimum bending radius transverse to rolling direction.

8.5.2 Correlation between standard deviation of hardness measurements and minimum bending radius

In Table 17 the correlation between standard deviation at a given depth from upper surface and minimum bending radius transverse to rolling direction is shown. The used standard deviation values are presented in Table 22 Attachment 22. Both the correlation coefficient and the R-squared value are represented at each depth.

Table 17: Correlation between minimum bending radius on transverse to rolling direction and standard deviation of hardness measurements at a given depth

Depth [um]	Correlation coefficient	R^2
50	0.798	0.636
100	0.486	0.236
150	0.188	0.035
200	0.188	0.035
250	0.732	0.536
300	0.506	0.256
350	0.013	0.000
400	-0.168	0.028
450	0.192	0.037
500	0.323	0.105

It can be observed from Table 17, that the most significant correlation is at the depth of 50 µm. This is in consistent with the results attained above in Subchapter 8.5.1 concerning the correlation between homogeneity index and minimum bending radius. Figure 63 shows the correlation between standard deviation at the depth of 50 µm and minimum bending radius on transverse to rolling direction.
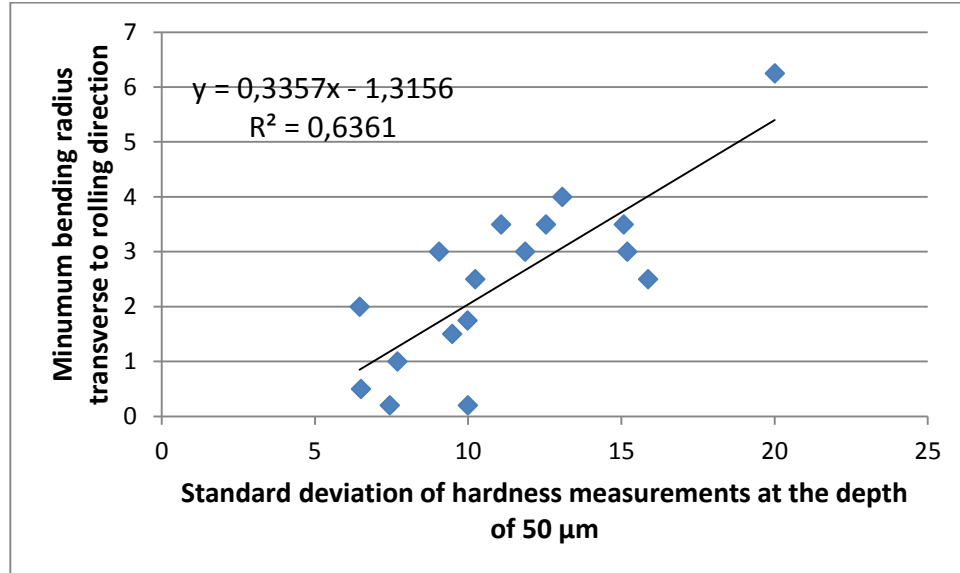
Figure 63: Correlation between standard deviation of hardness measurements at the depth of 50 um and minimum bending radius transverse to rolling direction

8.6   Interrupted bending tests

Interrupted bending tests were carried out to samples 0.08C- 1.8Mn 870°C and 0.07C-1.3Mn 815°C. Here microstructures of the cross sections of the two different samples

bent in various angles shown. The intention was to bend the samples in such severe matter, that visually observable damage occurs at the surface of the bend region. This was strived to ensure by selecting bending radius that are smaller than the ones defined earlier in case of bending to an angle of 90° (Table 12).

First the microstructures at the depth of 0.2 mm in case of unbent samples are presented, since the hardness values at this depth highly differed. Second, the effect of red scale on underlying microstructures of bent samples is shown. Next SEM images of sample 0.08C-1.8Mn 870°C bent in selected angles are represented. Eventually microstructures of cross sections in case of sample 0.07C-1.3Mn 815°C bent to different angles are shown.

8.6.1 Microstructures at the depth of 200 µm before bending

The hardness of these two test materials at the depth of 200 µm is significantly different; the hardness of sample 0.08C- 1.8Mn 870°C is 445 HV and 0.07C-1.3Mn 815°C is 360 HV (Figures 53 and 54). The microstructures at this depth are represented in Figures 64a-64d. These Figures describe the microstructures of straight samples, i.e. unbent samples. Figures 64a and 64b present sample 0.07C-1.3Mn 815°C and Figures 64c and 64d present sample 0.08C-1.8Mn 870°C.

a)

b)
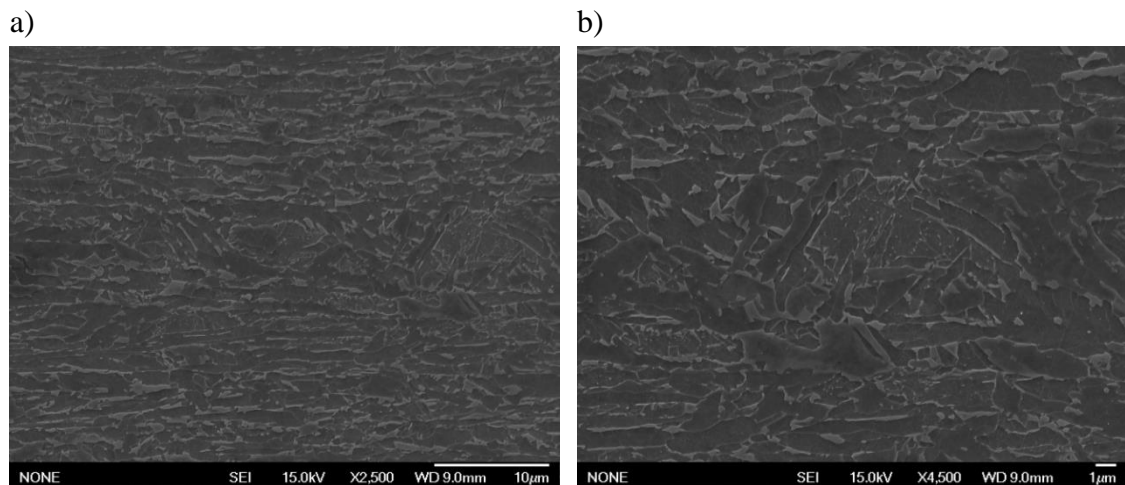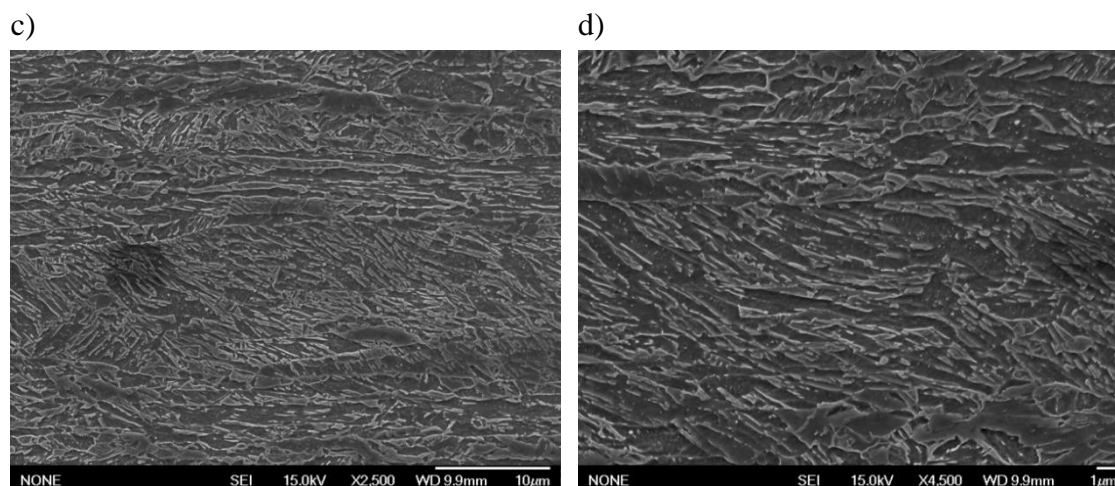
Figure 64: Microstructures of the unbent samples, a)-b) sample 0.07C-1.3Mn 815°C and c)-d) sample 0.08C-1.8Mn 870°C.

In Figures 64a and 64c the magnification is x2500, whereas in Figures 64b and 64d it is x4500. First the microstructure of sample 0.07C-1.3Mn 815°C at this given depth is considered. The microstructure consists mainly of M/A islands in a bainitic ferrite matrix. The morphology of the M/A constituents is chiefly equi-axed/spherical, but also elongated such constituents are present. The regions of rather equi-axed M/A islands in a bainitic ferrite matrix can be qualified as granular bainite. The diameter of the M/A constituents is approximately in the range of 0.5-1 μm.

Next, the microstructure of sample 0.08C- 1.8Mn 870°C at this particular depth is considered. The microstructure consists mainly of a mixture of lath-like bainite and martensite. Additionally regions of tempered martensite and M/A constituents are present; however the volume fraction of these constituents is rather small.

8.6.2 Effect of red scale

The materials were observed to contain stripes of red scale. This is illustrated in Figure 65.

Figure 65: Illustration of a sample containing stripes of red scale.

Therefore microstructures of adjacent regions of the same sample, one containing red scale and one without red scale are shown, in order to recognize whether red scale affects the underlying microstructure. This study was conducted for bent samples.

On the surface of the sample 0.08C-1.8Mn 870°C stripes of red scale were observed. Here microstructures of sample bent to an angle of 94° are shown both in case where red scale is present at the surface and in case no red scale appears. The microstructures immediately beneath the upper surface differs in case of the sample containing red scale compared to the sample without red scale. These cases are presented next to each other, in order to compare the microstructures. The microstructure of the upper surface of the sample containing red scale is presented in Figure 66a and the one without red scale is presented in Figure 66b. These represent the microstructures of a sample bent to an angle of 94°.

a)   b)
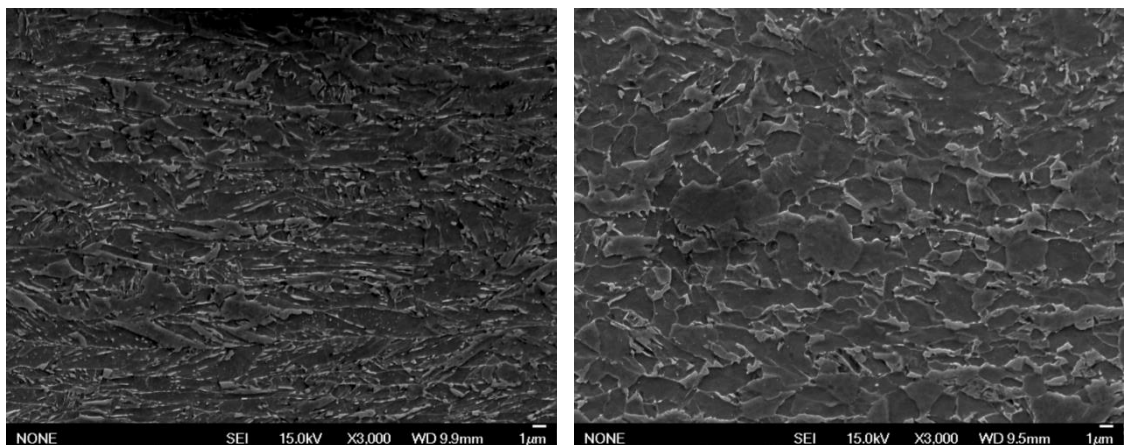
Figure 66: Microstructures of upper surface of sample 0.08C-1.8Mn 870• C at adjacent regions in case of a sample a) containing red scale and b) without red scale.

It can be observed from Figures 66a and 66b, that the microstructure immediately beneath the upper surface highly differs depending whether the sample contains red scale or not. In this case the amount of red scale in this particular region seemed to be extremely high by visual inspection. The microstructure of the sample containing red scale consists of a mixture of lath-like bainite and martensite immediately from the beginning of the upper surface. Instead, in case of the sample without red scale, there appears to be a layer containing granular bainite at the surface. This indicates that in case red scale is present the underlying microstructure consists of bainite formed at lower temperatures compared to the one without red scale. However at the depth of 0.2 mm the difference in the microstructure is not apparent. Figure 67 represents the microstructure of the sample at the depth of 0.2 mm a) containing red scale and b) not containing red scale.

a)   b)
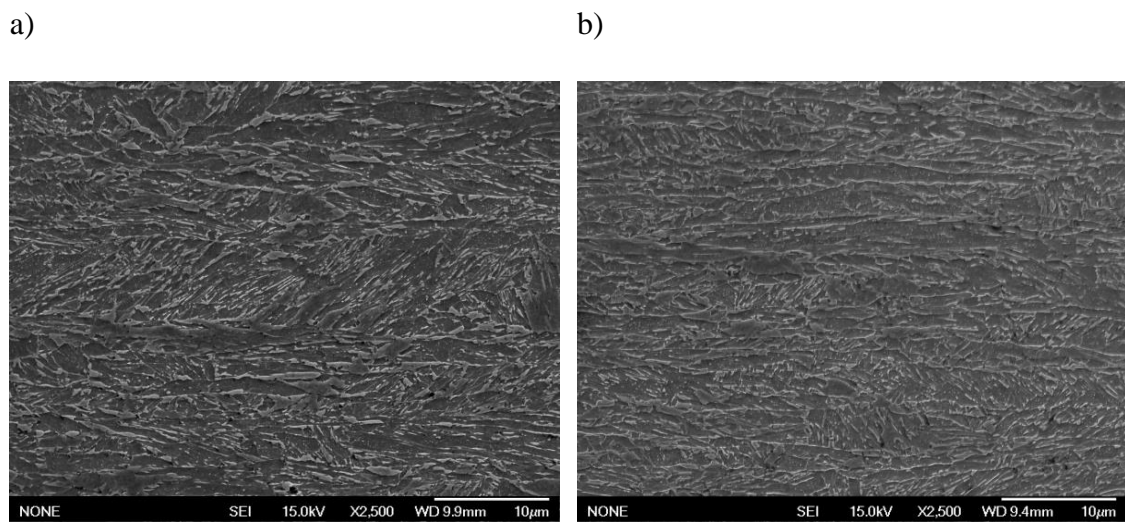
Figure 67: Microstructures of upper surface at the depth of 0.2 mm of the same material at adjacent region a) containing red scale and b) without red scale

Both of the microstructures at this depth consist of lath-like bainite and M/A constituents of various sizes and morphologies.

Furthermore, in case of sample 0.07C-1.3Mn 815°C bent to an angle of 85° stripes of red scale were observed. Figures 68a, 68c, and 68e present microstructures of region containing red scale and Figures 68b, 68d and 68f present microstructures of regions were red scale was not present.

a)   b)
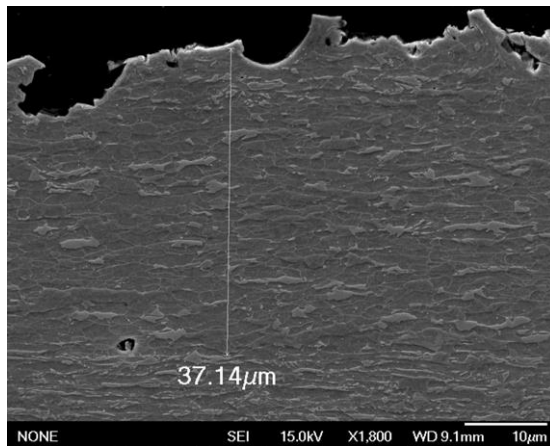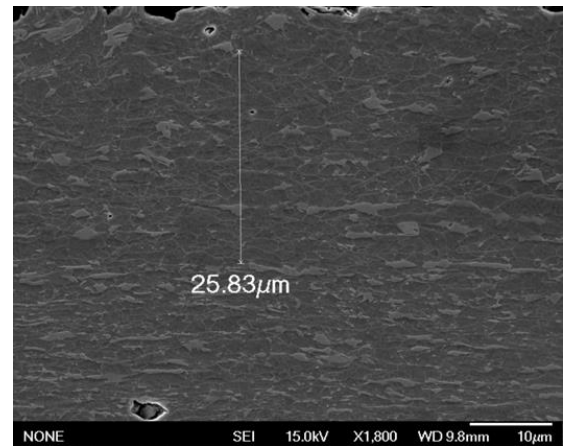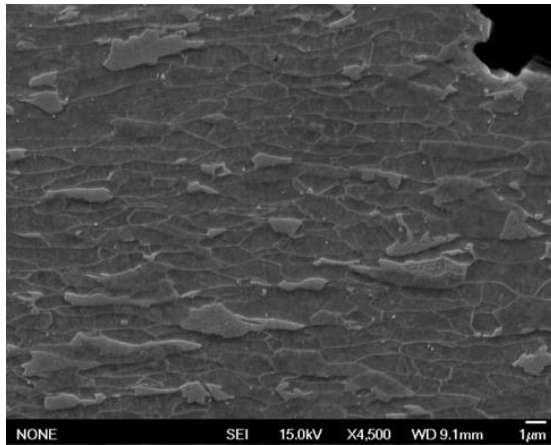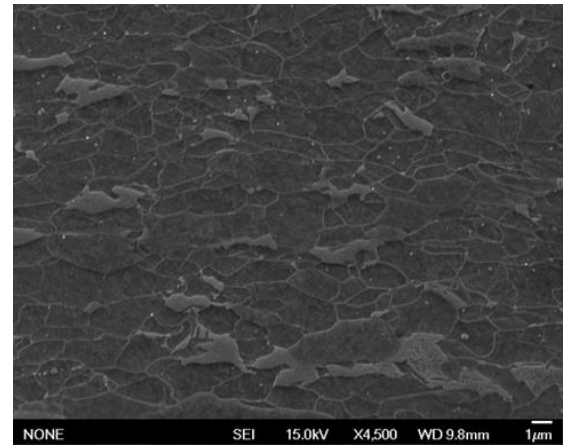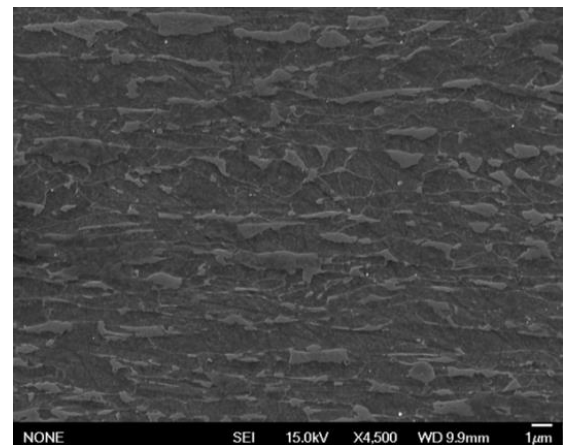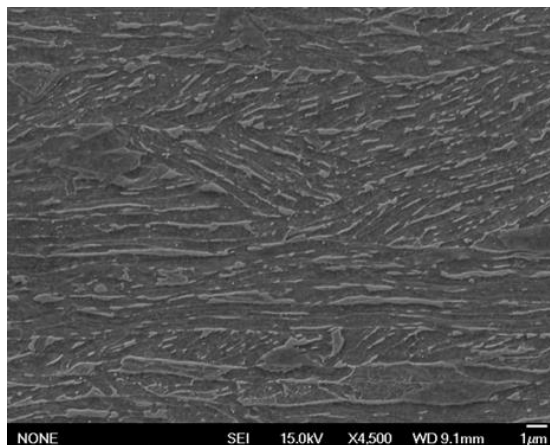
Figure 68: Sample 0.07C-1.3Mn 815°C bent to an angle of 85°. Figures a), c), and e) present microstructures of region containing red scale and Figures b), d) and f) present microstructures of regions were red scale was not present. Figures a)-d) present surface and Figures e) and f) present the depth of 0.2 mm.

It is worthwhile to notice that in case of sample containing red scale horizontal carbides were rather highly present. This is presented in Figure 69.
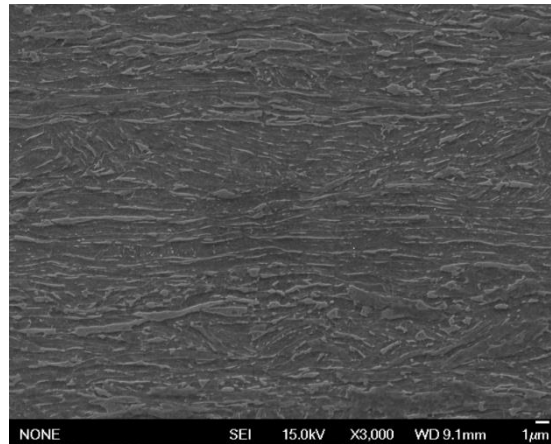
Figure 69: Microstructure of sample 0.07C-1.3Mn 815°C of a region containing red scale, at the depth of 0.15 mm containing horizontal carbides.

8.6.3 Sample 0.08C-1.8Mn 870°C bent to an angle of 57°

Here sample 0.08C-1.8Mn 870°C bent to an angle of 57° is presented in Figures 70a-70d.

a)
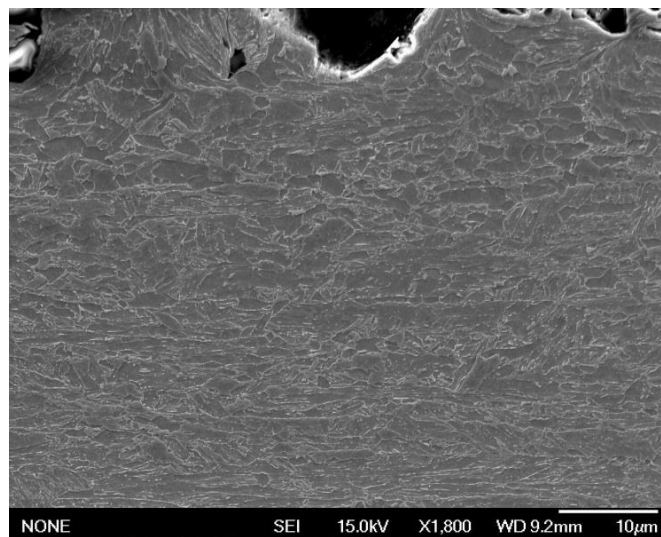
b)
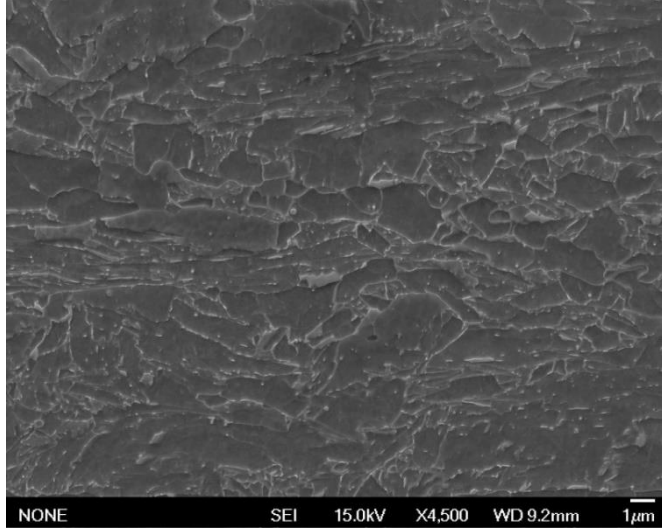
c)
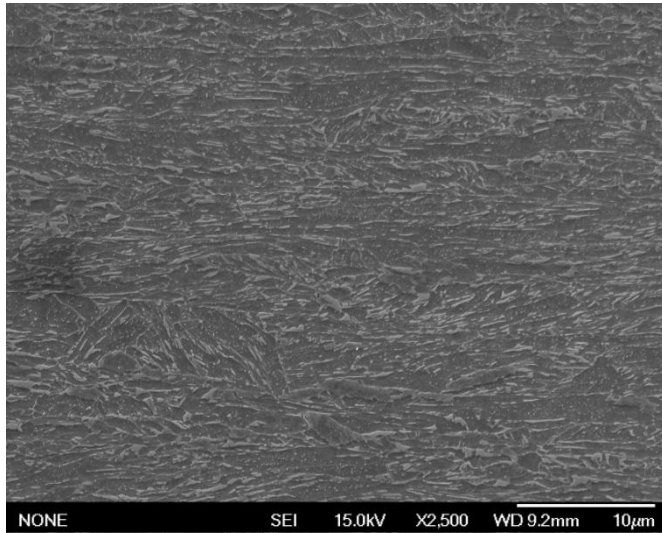
d)
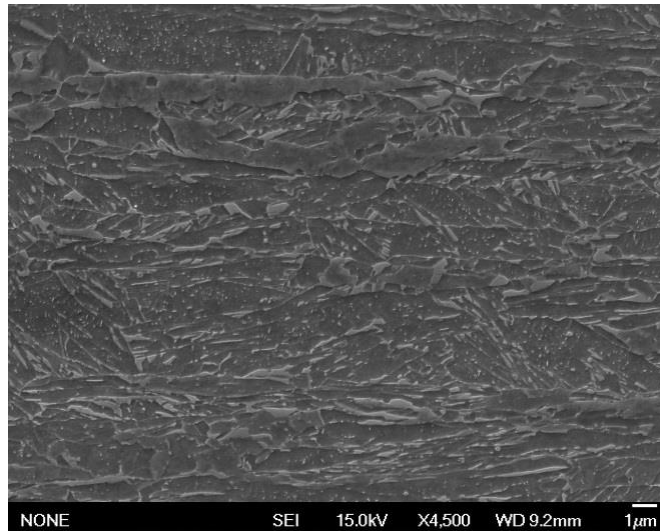
Figure 70: Microstructures of cross section of sample 0.08C- 1.8Mn 870°C bent to an angle of 57°. Figures a) and b) Microstructure of upper surface, and c) and d) micro-structure at the depth of 0.2 mm

It can be noticed from Figure 70a, that the surface has deformed a little. Yet, no signs of the appearance of shear bands are observed.

8.6.4 Sample 0.08C- 1.8Mn 870°C bent to an angle of 96°

Here sample bent to an angle of 96° is presented in Figures 71a-71d. On the surface of this sample red scale occurred. Yet, by visually observing, the red scale appeared not to be highly dense and its color was rather light.

a)
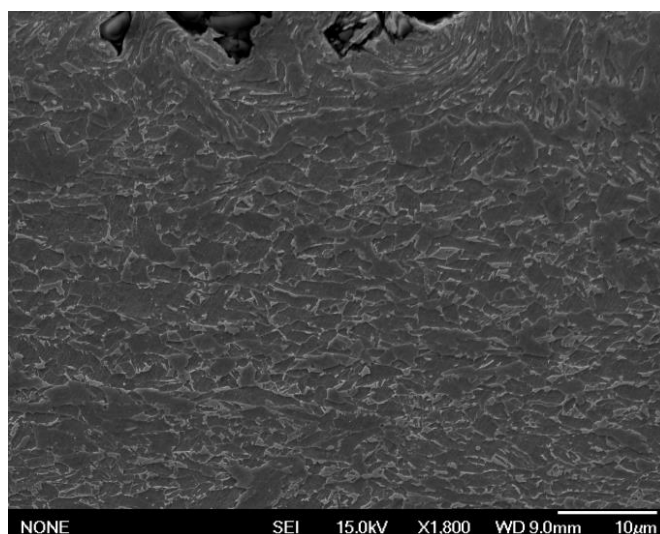
b)
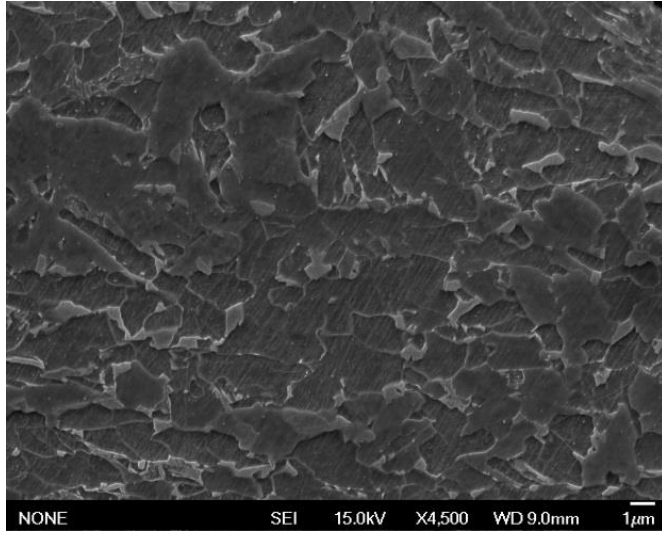
c)
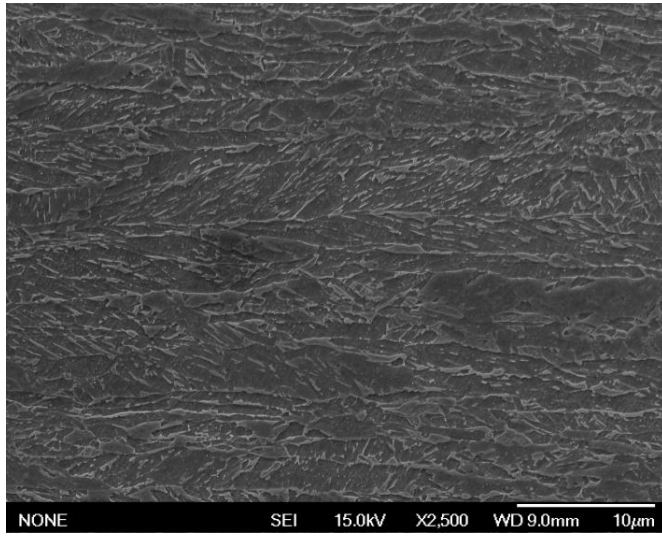
d)
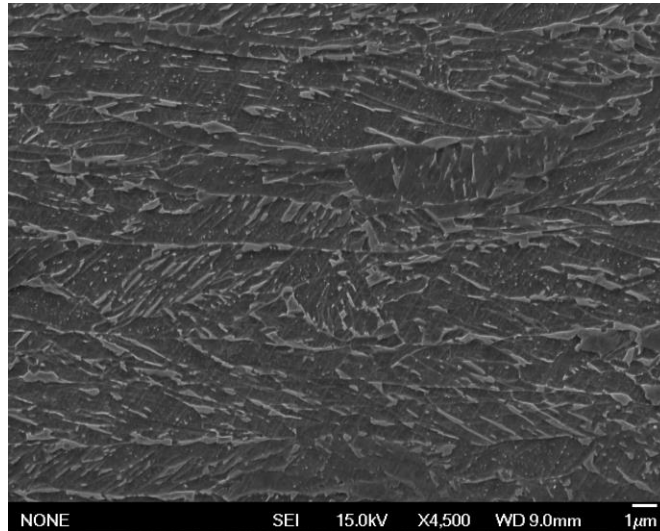
Figure 71: Microstructures of cross section of sample 0.08C- 1.8Mn 870°C bent to an angle of 96°. Figures a) and b) present microstructure of upper surface, and c) and d) microstructure at the depth of 0.2 mm.

On contrary to the presumption, in case of this sample, with visual examination no damage was noticed to occur at the surface and neither shear bands were found. This was highly unexpected, since the applied bending radius was smaller than the earlier defined minimum bending radius in bending to 90°, and additionally the material was bent to angles greater than 90°.

8.6.5 Sample 0.07C-1.3Mn 815°C bent to an angle of 42°

Here sample 0.07C-1.3Mn 815° bent to an angle of 42° is presented in Figures 72a-72d.

a)
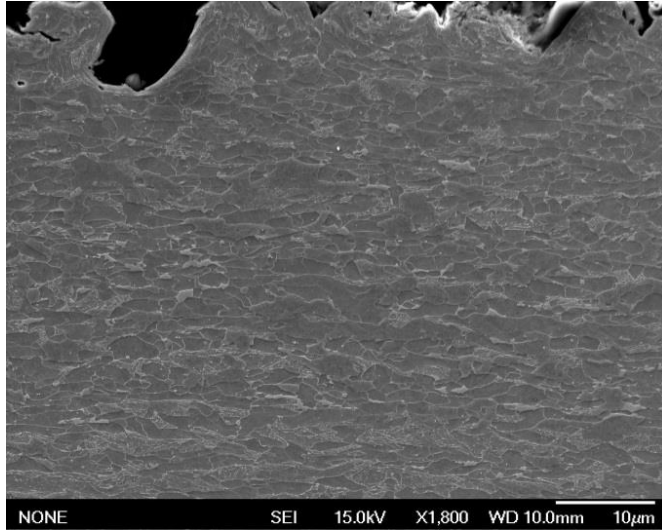
b)
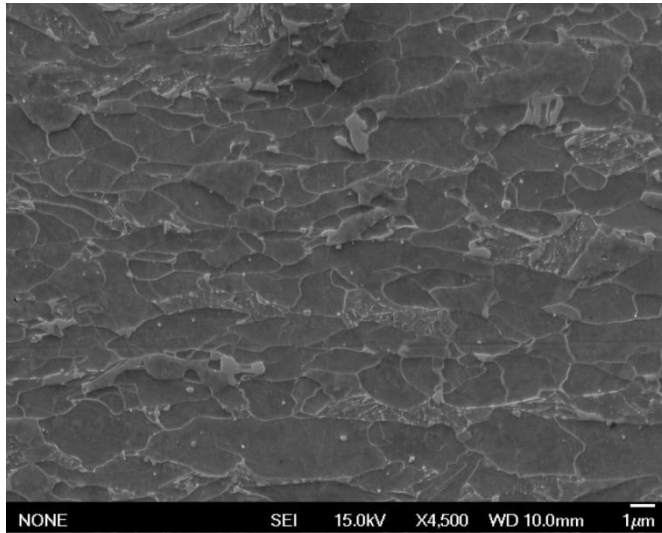
c)

d)

Figure 72: Microstructures of cross section of sample 0.07C-1.3Mn 815°C bent to an angle of 42°. Figures a) and b) present microstructure of upper surface, and c) and d) microstructure at the depth of 0.2 mm.

Shear bands are not found, which was highly expected to due to the notably small bending angle. Furthermore, due to the small bending angle, the material does not appear to be highly deformed.

8.6.6 Sample 0.07C-1.3Mn 815°C bent to an angle of 56°

Here sample 0.07C-1.3Mn 815° bent to an angle of 56° is presented.

a)

b)
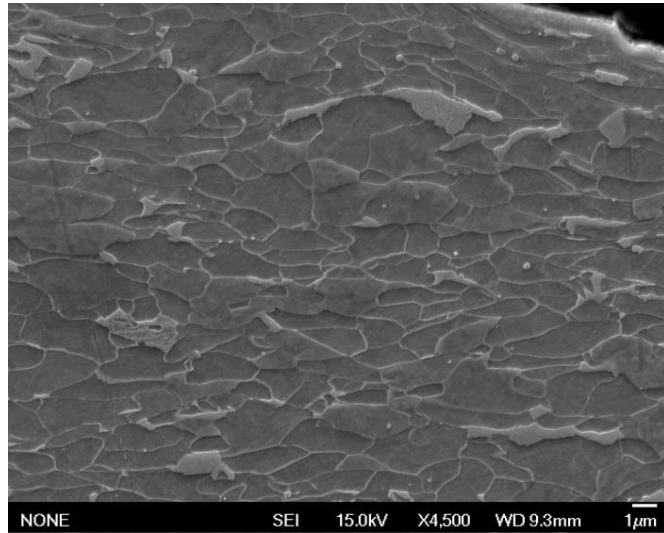
c)

d)
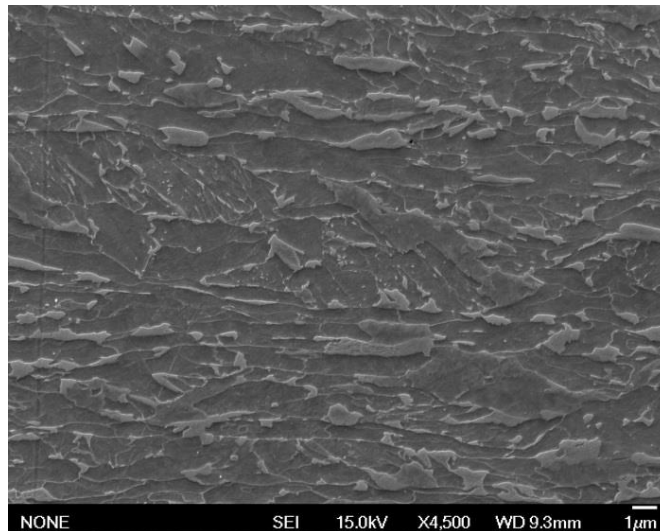
Figure 73: Microstructures of cross section of sample 0.07C-1.3Mn 815°C bent to an angle of 56°. Figures a) and b) present microstructure of upper surface, and c) and (d) microstructure at the depth of 0.2 mm.

In case of this sample horizontal carbides were observed at the depth of approximately 0.2 mm. This is shown in Figure 74.
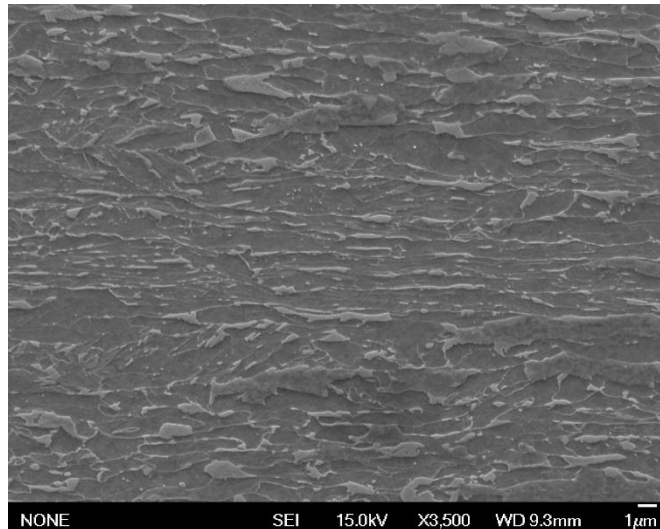
Figure 74: Presentation of horizontal carbides at the depth of 0.2 mm.

Few voids were additionally observed at the depth of 0.2 mm. An example is presented in Figure 75.
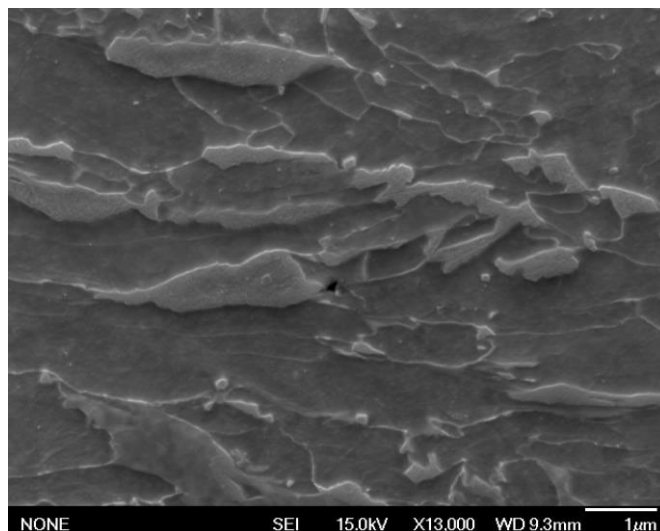
Figure 75: Presentation of void at the depth of 0.2 mm.

It is noteworthy to recognize that the void is located at the interface between a M/A island and the matrix.

8.6.7 Sample 0.07C-1.3Mn 815°C bent to an angle of 85°

In case of sample 0.07C-1.3Mn 815°C bent to an angle of 85° damage was observed to occur at the surface of the sample. More preciously the damage appeared at the regions of red scale. This is shown in Figure 76.

Figure 76: Damage occurring at the surface of the bent sample in regions containing red scale.

The microstructures are presented in case where damage occurred at the surface, i.e. red scale is present. In Subchapter 8.6.2 the microstructures of this sample of regions containing and not containing red scale were compared.

Figures 77a-77d present microstructures of sample 0.07C-1.3Mn 815°C bent to an angle of 85° at the surface and at the depth of 0.2 mm from upper surface.

a)
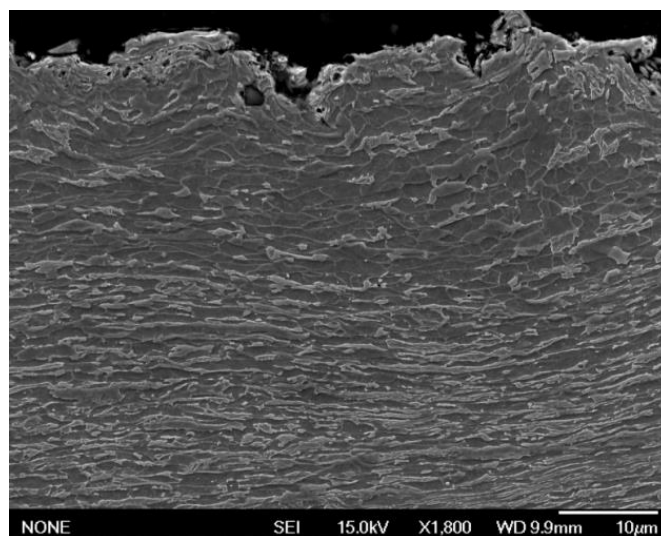
b)
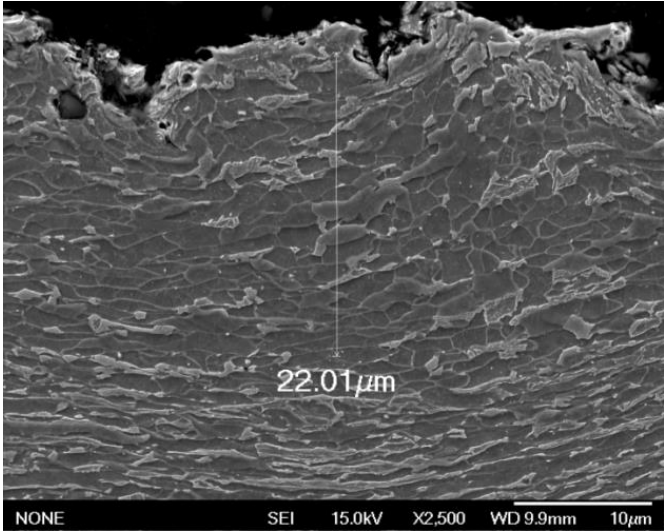
c)
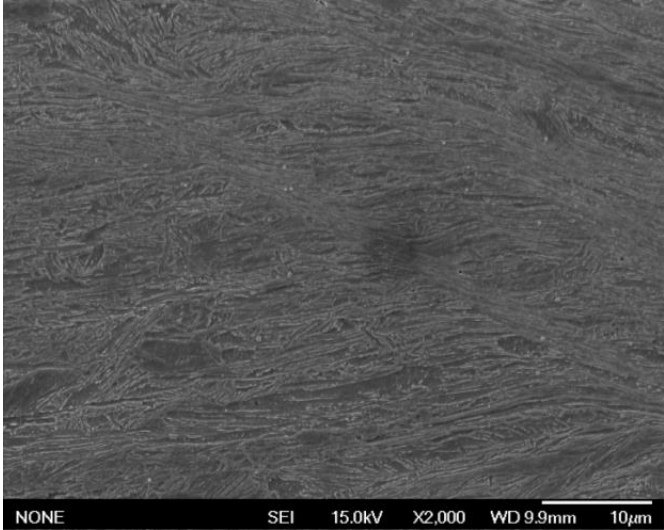
d)
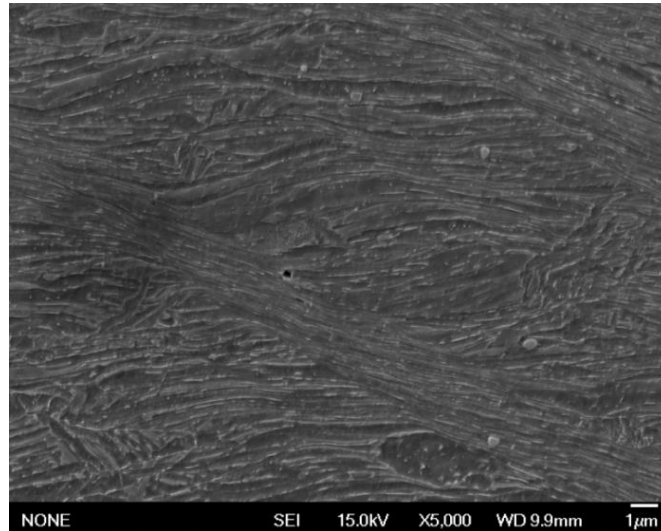
Figure 77: Microstructures of cross section of sample 0.07C-1.3Mn 815•C of a region containing red scale and a visually observed damage at the surface. Figures a) and b) Microstructure of upper surface, and c) and d) microstructure at the depth of 0.2 mm.

According to Figure 77b, the softer layer at the surface reaches approximately at the depth of 0.02 mm. From Figures 77c-77d, shear bands can be observed. In addition, horizontal carbides seem to present at the depth of 0.2 mm.

Figure 78 presents a fracture observed below the upper surface. The fracture occurs approximately at the middle of the bent region, i.e. at the region where the greatest strains occur. The fracture expands from approximately 120 µm (Figure 78a) to the depth of 400 µm from upper surface and as can be seen from Figure 78b it is oriented at an angle of 45° with respect to the surface.

a)
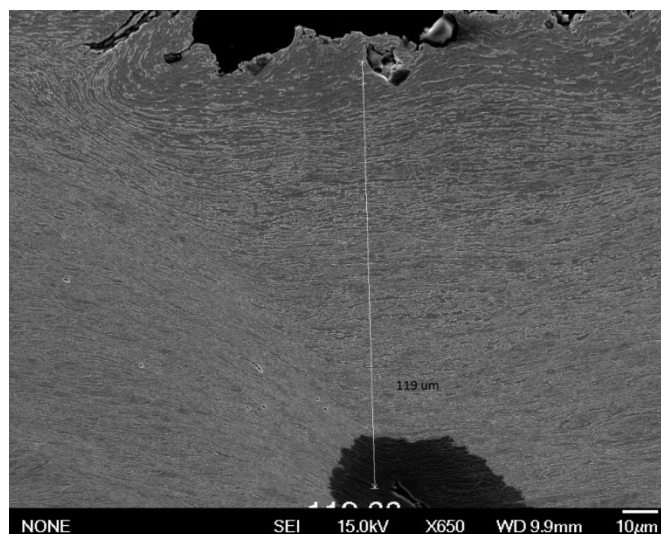
b)
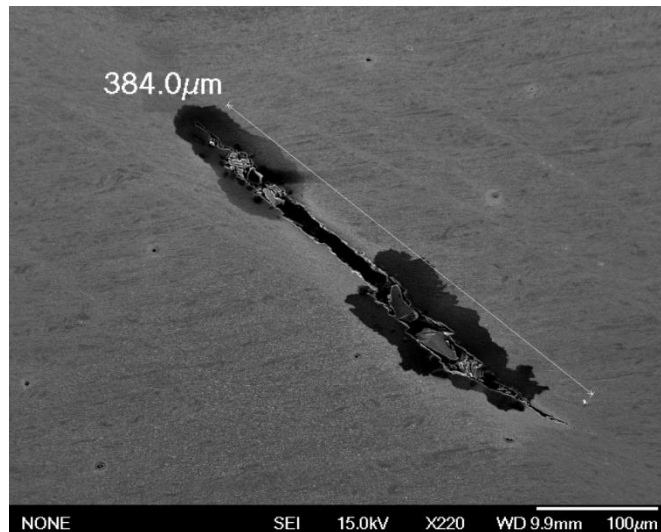
Figure 78: a) Representation of the top part of the fracture and its depth, and b) representation of the fracture and its length.

Moreover, as can be noticed from Figure 78b, several parallel shear bands can be noticed at both sides of the fracture. The role of shear bands in the initiation of fracture can be noticed from Figure 79.

Figure 79: The lower part of the fracture at the depth of 0.4 and shear bands.

It can be observed from Figure 79, that the volume fraction of shear bands is significantly high near the fracture. Additionally, near the fracture regions of horizontal carbides appear to be present in high volume fractions. This is presented in Figure 80.
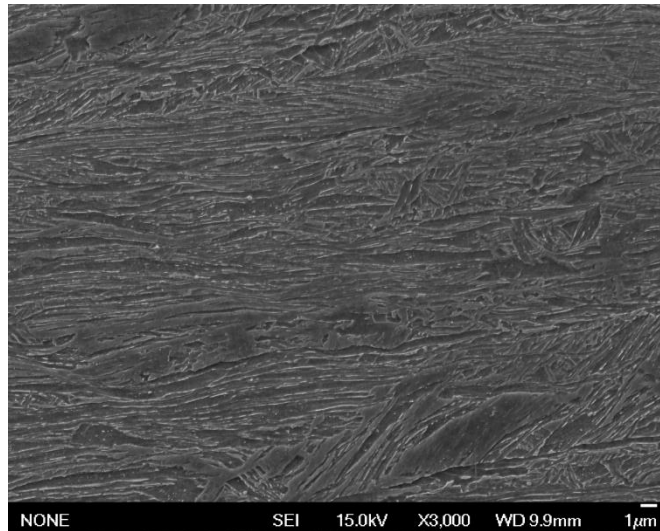
Figure 80: Microstructure consisting of horizontal carbides at the depth of 0.2 mm located near the fracture.

Such horizontal carbides were observed to present in rather high volume fractions from the depth of 0.05 mm to at least 0.5 mm.

Figures 81 and 82 presents a closer examination of shear bands.
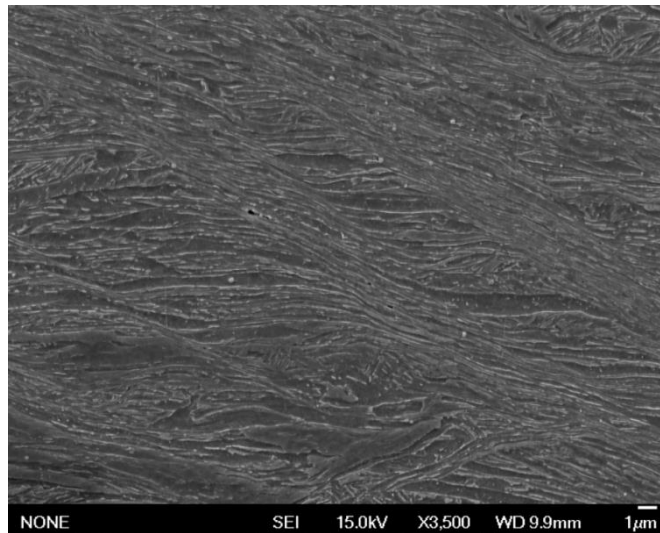
Figure 81: Parallel shear bands at the depth of 0.15 mm.
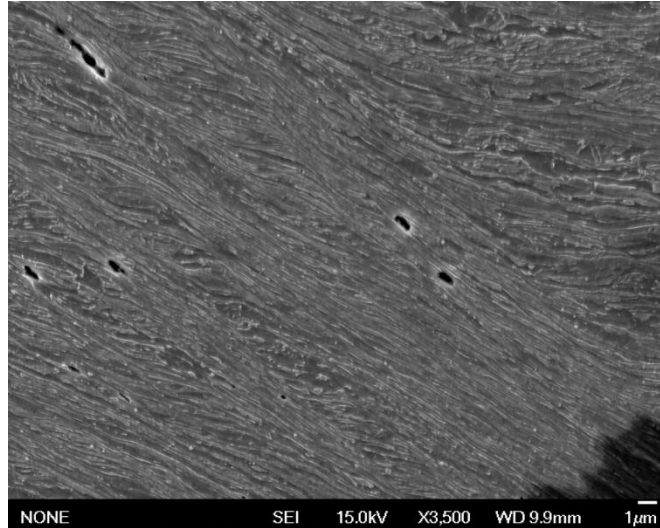
Figure 82: Shear bands and voids.

8.6.8 Sample 0.07C-1.3Mn 815°C bent to an angle of 94°

In this sample stripes of red scale were observed, as seen from Figure 83.

Figure 83: Sample 0.07C-1.3Mn 815°C bent to an angle of 94°.

However, as can be noticed from Figure 83, no visually observable damage appears to occur. This is rather peculiar, since in case of the previously discussed sample, which was bent in a less severe manner, visually observable damage occurred. Even the regions containing red scale appear to be free of damage.

Microstructures of a cross section of a region containing red scale and a region without red scale are separately shown. First the cross sections of the region without red scale are presented. Figure 84a-b present the microstructures of the surface and Figure 84c at the depth of 0.2 mm from upper surface at the bent region.
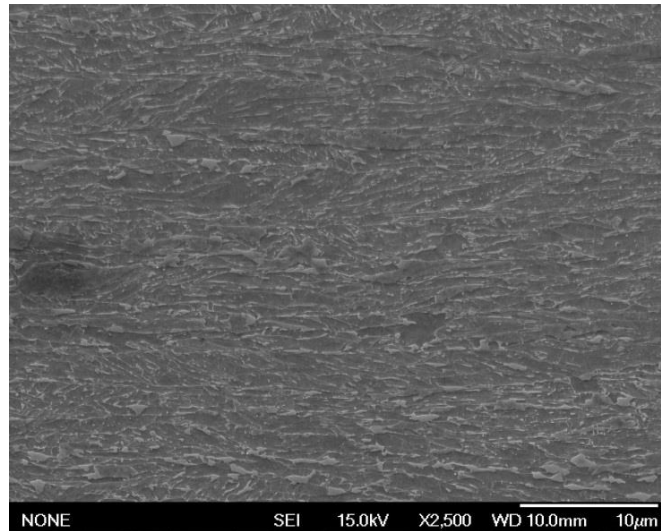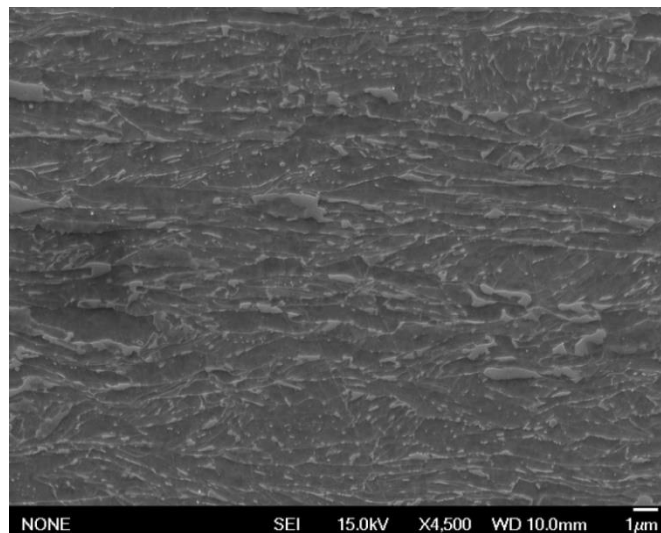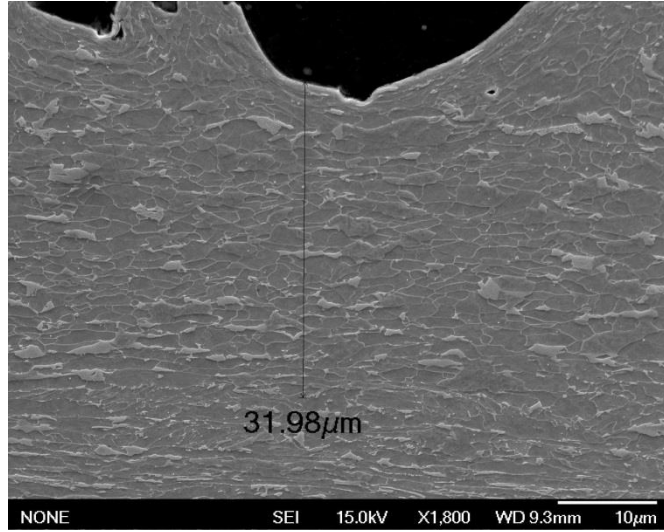
a)
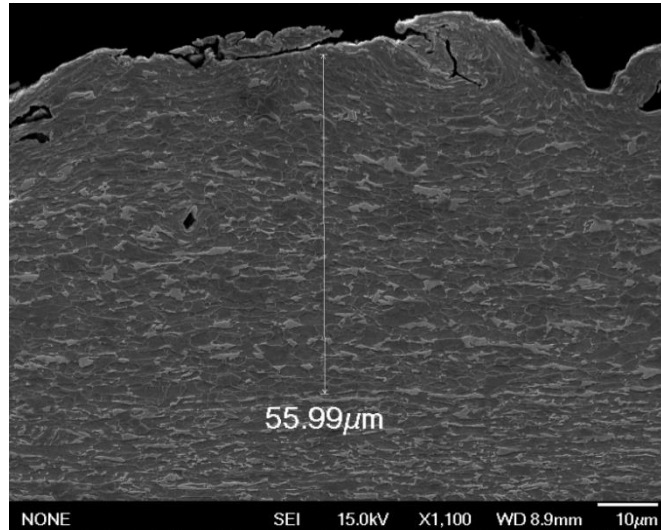
b)
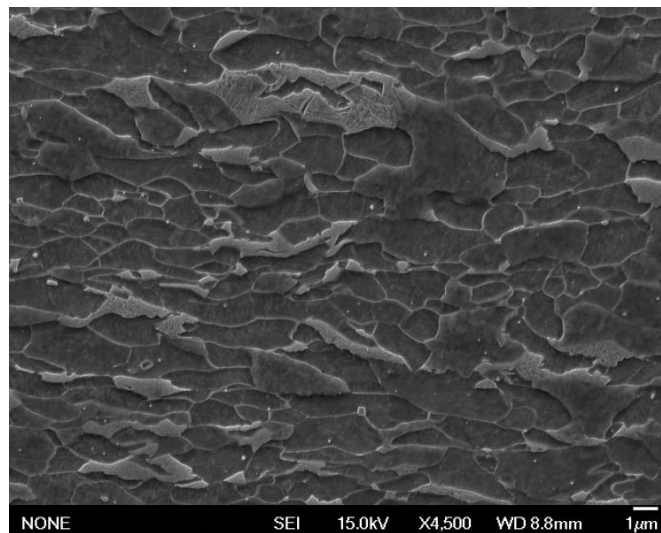
c)
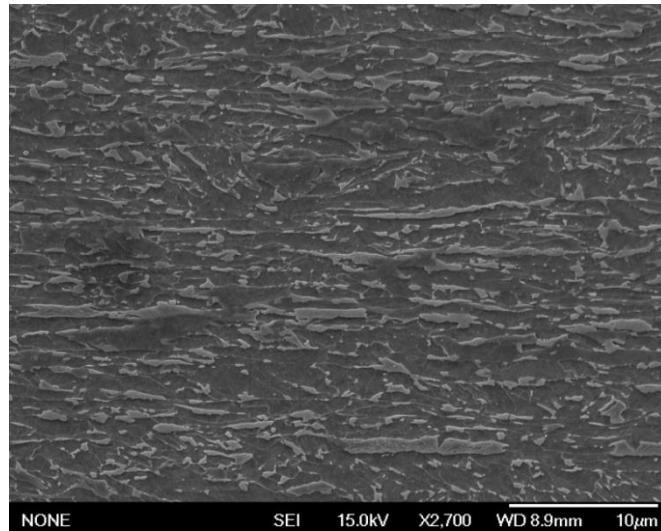
Figure 84: Microstructures of cross section of sample 0.07C-1.3Mn 815°C without red scale bent to an angle of 95°. Figures a) and b) present microstructure of upper surface, and c) microstructure at the depth of 0.2 mm.

It is noteworthy that the soft layer reaches until to the depth of approximately 0.055 mm. At the depth of 0.2 mm the microstructure still consists of M/A constituents of various sizes and morphologies in a bainitic ferritic matrix. No lath-like bainite is observed. The conversion of the microstructure at this given depth, i.e. approximately at 0.06 mm, to more elongated and fine is illustrated more accurately in Figure 85.
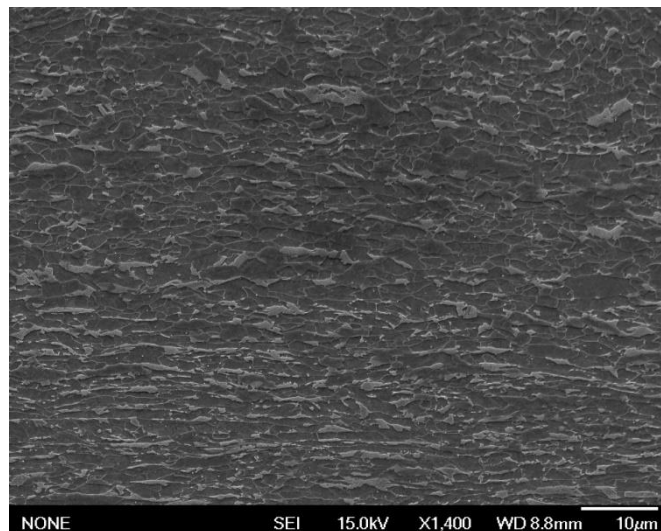
Figure 85: Alteration of microsrtucture to more elongated and fine at the depth of 0.06 mm.

Next, the cross sections of the region containing red scale are presented. Figure 86a-86b present the microstructures of the surface and Figures 86c at the depth of 0.2 mm from the upper surface at the bent region.
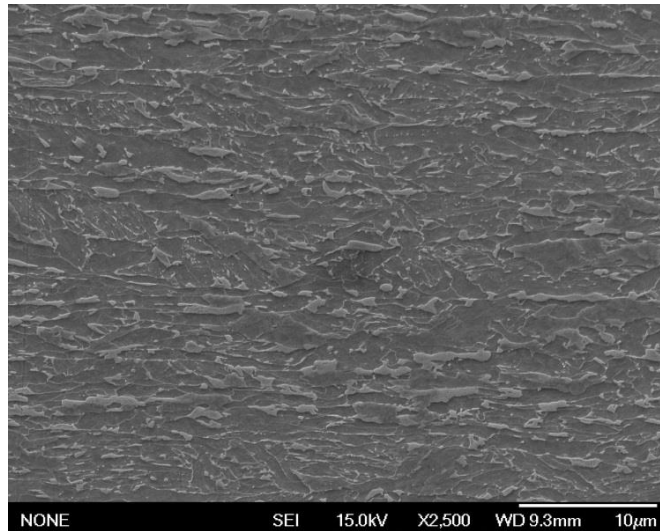
a)
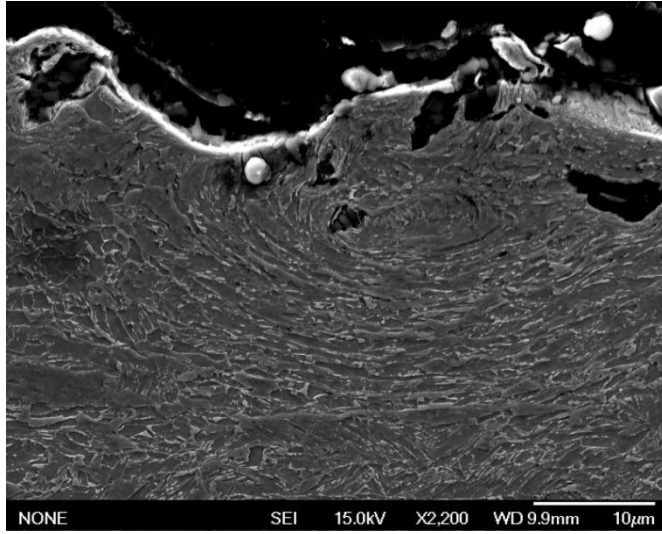
b)
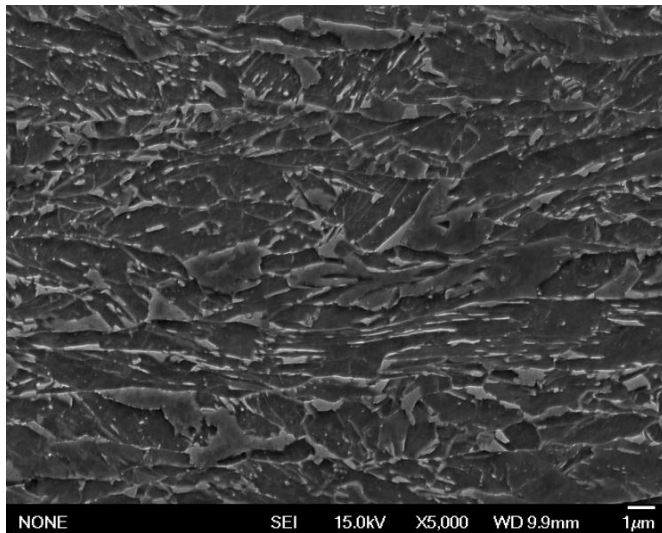
c)
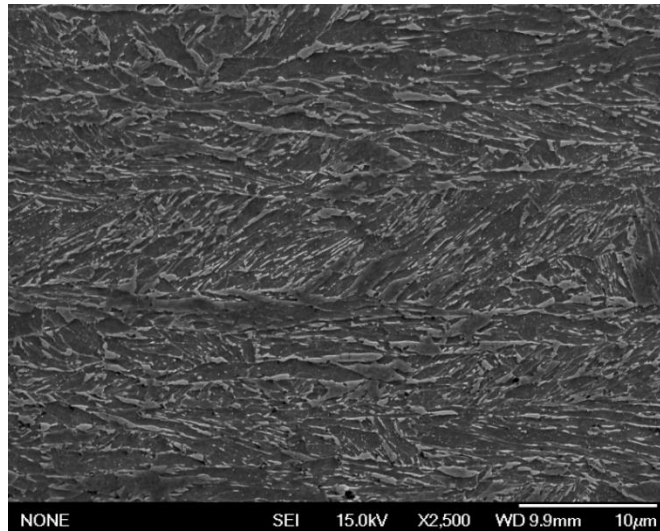
d)
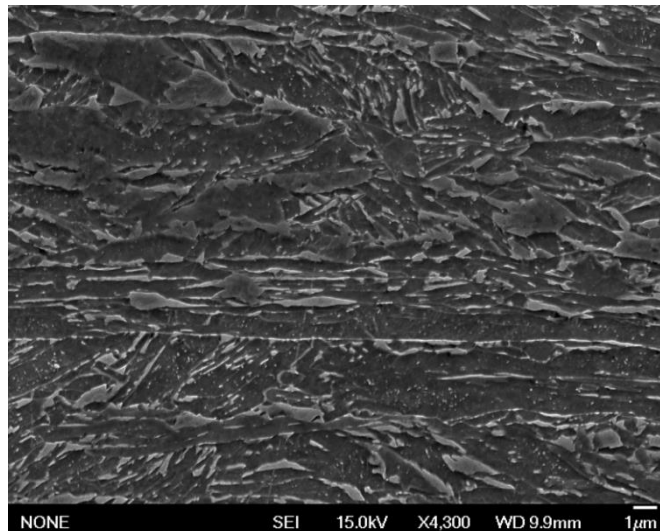
Figure 86: Microstructures of cross section of sample 0.07C-1.3Mn 815°C containing red scale bent to an angle of 95°. Figures a) and b) Microstructure of upper surface, and c) microstructure at the depth of 0.2 mm.

From Figure 86a, it can be seen that the surface at the bent region is highly deformed. As can be noticed from Figure 86a and 86b, basically there is no soft layer present at the surface. Instead, immediately from the surface, the microstructure consists of lath-like bainite and M/A constituents occurring here and there. Additionally the structure is highly fine. At the depth of 0.2 mm, the structure comprises same constituents, yet the volume fraction of lath-like bainite is greater. It is noteworthy, that horizontal carbides are present at the depth of 0.2 mm.

At the surface regions, dark "voids" appeared. These are presented in Figure 87.
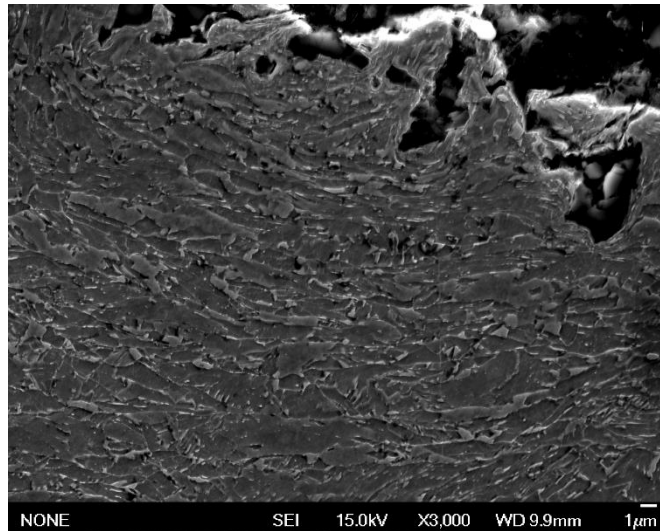
Figure 87: Dark "holes" appearing in the surface of the sample containing red scale.

In case of the sample without red scale, these dark "voids" appeared in a highly smaller volume fraction. In the sample containing red scale, such "voids" appeared most frequently at the surface regions, yet they appeared in smaller volume fractions additionally deeper. Yet, it cannot not be stated without doubt that these present voids in a meaning described in Subchapter 4.3.2. Since it is possible that they are due to preparation of the sample, e.g. due to etching.

9. DISCUSSION

In this chapter the results presented in Chapter 8 are profoundly discussed. First the relationship between microstructure and hardness is studied. In particularly the effects of FRT, and carbon and manganese contents on the developing microstructure and hence hardness are observed. Second, the development of plastic deformation during bending is discussed, i.e. phases of uniform elongation, diffuse necking and strain localization. Third, factors contributing to the extent of uniform elongation are studied. Fourth, factors affecting the extent of diffuse necking, i.e. onset of strain localization are discussed. Fifth, the effects of microstructure homogeneity on bendability are studied, followed by a discussion concerning the effects of red scale. In Subchapter 9.7 bendability of tempered samples are discussed. Finally in Subchapter 9.8, the reliability of the statistical models concerning bendability is observed.

9.1   Relationship between microstructure and hardness

Here the relation between microstructure and hardness is discussed, in particularly in case of the upper surface. It is investigated that how chemical composition and rolling parameters affect the developing microstructure, and hence hardness properties. Especially the effect of carbon and manganese contents, and finish rolling temperature are discussed.

As observed from FESEM images shown in Subchapter 8.1 and microhardness results presented in Subchapter 8.2, commonly a soft layer in various extents is formed at the surface. This layer appears to principally comprise M/A constituents in a bainitic ferrite matrix, i.e. granular bainite or in some cases polygonal ferrite. Below this layer, typically first appears a complex phased structure consisting of various amounts of several constituents, such as lath-like bainite, quasipolygonal ferrite and granular bainite. And as approaching closer to the middle thickness, the structure appears to be increasingly lath-like, consisting of a mixture of lath-like bainite and martensite, and in some cases additionally tempered martensite. The transition from granular to lath-like structure, at a particular depth, can occur either abruptly or gradually.

It is discussed; firstly the effects of FRT on the developing microstructure. Second the effects of carbon and manganese concentrations on the forming microstructure are observed. In both cases in particularly the influences on the surface microstructure are studied. Eventually, in Subchapter 9.1.3, hardness of surface and centre line is statistically modelled in terms of carbon and manganese contents, and FRT.

9.1.1 Effect of finish rolling temperature (FRT)

Here the effect of finish rolling temperature (FRT) on hardness is discussed. FRT affects austenite grain size, which highly determines the grain size in the final product and thus affects mechanical properties. A high FRT leads to complete recrystallization of austenite and by decreasing FRT the size of the recrystallized austenite decreases. As FRT is further decreased, partial recrystallization of austenite occurs. Rolling to still lower temperatures, austenite does not recrystallize and the resulting grain structure is pancaked. [234, p. 277] Thus in cases of higher FRT, the size of austenite grains becomes larger and consequently after cooling the resulting microstructure is coarser [194]. In other words, by decreasing FRT, a finer microstructure and hence greater hardness could be assumed to be obtained. This is generally the case in conventional hot rolled steels [235]. However as noticed from Figures 53-56, this is not accurate in case of the materials studied in this work. Figure 88 illustrates the effect of FRT on hardness in case of Nb-microalloyed steels.
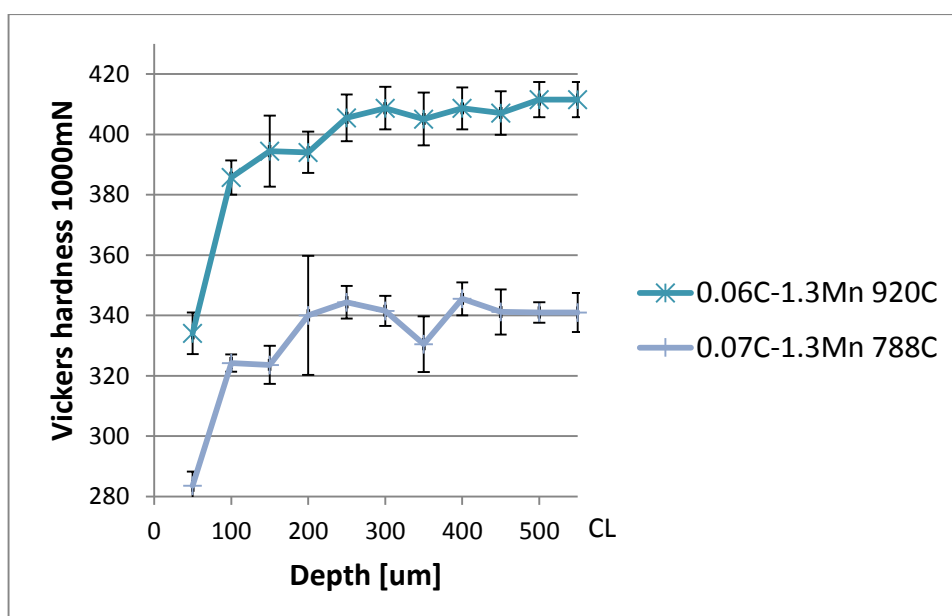
Figure 88: The effect of FRT on hardness.

It can be observed from Figure 88, that throughout the thickness the difference in the hardness values is rather similar. In other words, the shape of the hardness profiles is highly similar. This indicates, that if a soft surface layer is desired to provide, additionally the hardness at the centre line reduces.

As mentioned above, heats presented in Figures 53-54 and 56 are microalloyed with niobium. Niobium highly affects microstructure and mechanical properties of high strength low carbon steels. Niobium can be precipitated as carbonitride or carbide, or instead not precipitate and remain in solid solution. A higher FRT leads to a greater amount of niobium in solid solution. Niobium in solid solution retards the austenite-ferrite transfor-

mation due its large atom size. Additionally due to higher FRT a greater amount of niobium is accessible for the formation of NbC precipitates in ferrite, which increases strength as a result of precipitation hardening. [236, p. 295] Yet, such precipitation occurs via diffusion, which requires time. And the materials used in this work are direct quenched, which signifies that presumably there is not sufficiently time for precipitation to take place. Hence it is proposed that strengthening as a consequence of a higher FRT is not due to increased precipitation hardening.

Niobium highly affects recrystallization behaviour of austenite during hot rolling at a temperature range range of 1040°C to 815°C. A presence of niobium precipitates prevents recrystallization to occur at temperatures as high as 925°C. In addition to Nb, these heats contain vanadium (V). As these two elements are together added recrystallization is even further retarded. [63] Due to the retardation of austenite recrystallization kinetics, pancaked austenite grains can be obtained at relative higher temperatures. In case of materials used in this work, the highest applied FRT is 920 °C, which implies that it can be assumed that austenite in these materials is not recrystallized and the grain structure is pancaked. Furthermore, niobium precipitates restrict the growth of recrystallized austenite, and hence lead to a finer resulting microstructure. [234, p. 277]

The observations from Figures 107-108 imply, that the parent austenite grain size does not affect the hardness is confirmed by studying the relationship between length of austenite grain in different directions (Figure 107) and average grain size of austenite (Figure 108), and Vickers hardness. No correlation between these two factors is found. These results are presented in attachment 6. These findings are in consistent with a proposal by Bhadeshia, who suggests that parent austenite grain size does not affect hardness of bainitic structure. According to Bhadeshia this is because, the size of subgrains is rather independent on the austenite grain size and as discussed previously (Figure 28) the hardness of bainitic structure increases nearly linearly with decreasing average subgrain size. [36, p. 293]

The austenite grain size affects hardenability. A higher FRT leads to an increased hardenability. This is because a greater austenite grain size leads to a reduction in the grain boundary area, which means that there is a fewer amount of nucleation sites for ferrite and pearlite. Consequently these transformations are being retarded and hence hardenability is increased. [237] Additionally increased hardenability due to higher a FRT is attained as consequence of the ability to remain elements in solution, instead that they would form carbides. The carbides promote the formation of ferrite by acting as nucleation sites, and hence decrease hardenability. This explains why samples rolled in higher temperatures, with a given chemical composition, contribute a greater volume fraction of martensite (Figures 46 and 47). This is significant in terms of bendability, since rolling to higher temperatures prevents the formation of the soft layer. This can be observed by

comparing microstructures of surface of sample 0.06C-1.3C 920°C (Figure 46) and 0.06C-1.3C 875°C (Figure 47).

During hot rolling the temperature of the surface highly varies. It can be proposed that in case FRT is low (Figure 50a-b), the surface temperature reduces momentarily below temperatures where nucleation of ferrite and/or granular bainite can occur, or even such phases can develop. This signifies that already during rolling, nucleation and/or development of such phases takes place at the surface layers. Instead, in case of a higher FRT, the temperature does not reduce momentarily below temperatures, where ferrite and/or granular bainite are capable of developing or nucleating. Thus during quenching lath-like microstructure is formed immediately from the surface (Figure 46a-b).

In addition to the surface microstructure, FRT also influences the microstructure through thickness. A lower FRT results in a more pancaked austenite. A pancaked austenite affects phase transformation kinetics, so that on the time-temperature-transformation (TTT) diagram, the bainitic nose, i.e. lower C–curve, is shifted left. This signifies that bainite is formed already at higher temperatures, indicating that coarser bainite is formed compared to the one that would form at lower temperatures. Granular bainite tends to form at higher temperatures and lath-like bainite at lower temperatures. By comparing microstructures of samples 0.06C-1.4Mn 920°C (Figure 46) and 0.06C-1.4Mn 875°C (Figure 47), it can be observed that the one rolled to a higher temperature possesses microstructure that presents obvious orientation. Whereas in case of sample rolled to lower temperature, features of orientation are observable only in small volume fractions.

 As observed from Figure 28, the hardness of bainite is directly proportional to the transformation temperature. This signifies that a lower FRT leads to development of bainite possessing lower hardness level.

It can be concluded that FRT notably affects the microstructure and hence hardness of the material throughout the thickness. A lower FRT results in the development of higher temperature transformation products, i.e. ferrite and granular bainite, on the surface. Additionally as a consequence of a lower FRT, highly pancaked austenite is developed, which affects the phase transformation kinetics. Due to highly pancaked austenite, bainite transformations occur at higher temperatures implying that bainite possessing a coarser microstructure is formed.

9.1.2 Effect of carbon and manganese contents

Here, the effect of chemical composition on microstructure and hence hardness is considered. It can be observed from Figures 57 and 58, that samples with higher contents of carbon and manganese, with a given FRT, possess greater hardness. The main difference between the compositions is in the manganese content; higher manganese content increases hardenability and thus hardness. Due to higher contents of carbon and manganese,

the martensite (M_S) and bainite (B_S) start temperatures are reduced to lower temperatures (Equation (16)). As bainite and martensite are formed at lower temperatures, the forming microstructure is finer, which leads to a greater hardness. However it appears that in these cases, the hardness values do not notably change. This is probably due to the rather small differences in compositions; the difference in carbon content is approximately 0.2wt.% and in case of manganese about 0.5wt.%. Figure 89 illustrates the effect of carbon and manganese contents on hardness.
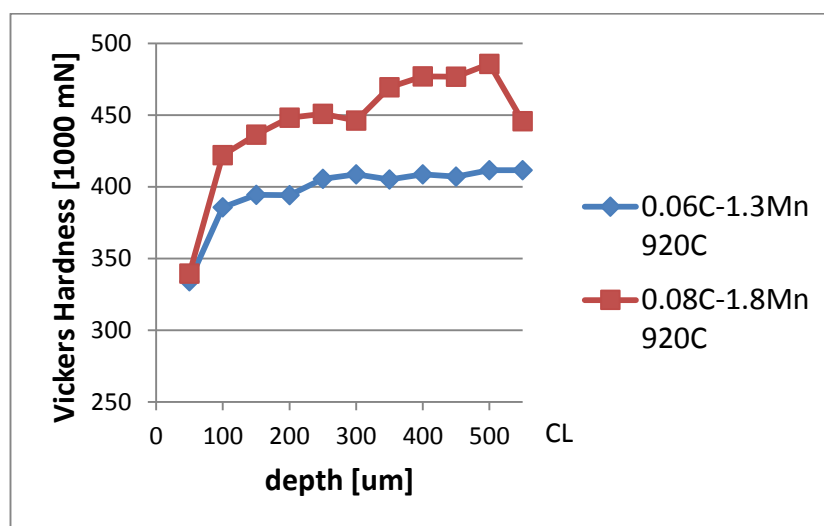
Figure 89: The effect of carbon and manganese contents on hardness.

By observing the microstructures of the samples 0.08C-1.8Mn 920°C (Figure 48) and 0.06C-1,4Mn 920°C (Figure 46) an obvious difference can be identified. By studying the microstructure of sample 0.08C-1.8Mn 920°C (Figure 48a) it can be noticed that a clear layer of M/A islands in a bainitic ferrite does not appear to be present. Granular bainite typically forms at higher temperatures. Due to the higher C- and Mn- contents the B_S temperature is reduced to lower temperatures and consequently the formation of granular bainite is prevented. Instead, lath-like bainite typically forms at lower temperatures, and consequently higher C- and Mn- contents promote its formation by reducing the B_S temperature. This explains, why with a given FRT, materials containing smaller amounts of C and Mn comprise a clearer layer of granular bainite. This can be observed by comparing microstructures of surface of samples 0.08C-1.8Mn 920°C (Figure 48a-b) and 0.06C-1,4Mn 920°C (Figure 46a).

Higher manganese and carbon contents additionally lead to higher hardenability, i.e. higher capability of steel to form martensite on quenching [237]. This explicates why samples 0.08C-1.8Mn 920°C and 0.08C-1.8Mn 870°C (Figures 48 and 49) comprise a greater volume fraction of martensite compared to the ones with lower C- and Mn- contents. This can be noticed by comparing microstructures presented in Figure 48 with Figure 46. Regions of tempered martensite are present nearly immediately from the surface, in case of samples with higher C- and Mn- contents. Whereas in case of materials with

lower C- and Mn- contents, tempered martensite is present in highly small amount approximately not until from the depth of 1 mm.

Furthermore it is proposed, that higher carbon content leads to a greater dislocation density, which consequently increases hardness. Therefore it can be concluded that the microhardness results are in consensus with the suggestions in literature concerning effect of chemical composition on hardness.

9.1.3 Statistical model of hardness of upper surface and middle section in terms of carbon and manganese contents, and finish rolling temperature

As it can be realized from the microhardness results presented in Figures 53-58, the hardness of the surface and middle section are highly dependent on the carbon and manganese contents, and finish rolling temperature. Thus in the present chapter are presented statistical models that can be utilized to evaluate the obtained hardness values at the surface and centre line in terms of carbon and manganese contents, and finish rolling temperature. Statistical modelling was carried out by applying Minitab 16.

The hardness at the depth of 0.5 mm is regarded as the hardness at the centre line, since as can be observed from Figures 53-58, the values at these depths highly similar. Hence the developed statistical models can be utilized to evaluate the hardness at both the surface and centre line. The developed statistical models are valid in case of material comprising properties presented in Table 18.

Table 18: Presentation of properties that must be fulfilled in order to utilize the developed statistical models.

Carbon content [wt.%]	Manganese Content [wt.%]	Niobium Content [wt.%]	FRT [C]
0.06-0.09	1.09-1.84	0.04	815-920

Two different regression analyses for evaluating hardness at a given depth from upper surface are given. These are:

$$Hv = -266 + 0.322 \times FRT + 2486 \times C + 66.3 \times Mn + 44.9 LOGTEN \qquad (18)$$

(σ_{st}=15.9 and $R^2 = 85.5$)

and

$$Hv = -2748 + 1.48 \times FRT + 37433 \times C + 1151 \times Mn - 21.7 \times FRT \times C \quad (19)$$
$$- 13091 \times C \times Mn + 0.125 \times FRT \times LOGTEN - 0.105$$
$$\times Distance$$

(σ_{st}=11.8 and $R^2 = 92.3$)

where FRT is the finish rolling temperature [C], C and Mn are percentage by weight of such elements, Distance is the distance from the upper surface [μm], σ_{st} is standard deviation and R^2 is R-squared value. Both of these regression analyses are highly valid, as can be observed from the R-squared values.

9.2 Development of plastic deformation in bending

In order to understand the factors governing bendability it is essential to recognize the behaviour of steel sheets when subjected to bending. At the first stages of bending, once the yield strength is exceeded, occurs uniform plastic deformation. This takes place as far as hardening is predominant. Yet, once the point in which plastic strengthening cannot accommodate with the stress increase, uniform plastic deformation turns into non-uniform plastic deformation. This point stands for diffuse necking. This corresponds for a higher strain rate on a particular section length, while outside the section takes place only moderate increase in strains. [8] It is suggested that the surface presented in Figure 42b, i.e. nut-shape, is characteristic for a surface developing once diffuse necking occurs. Therefore, as stated by e.g. Hosford and Jeschkea et al., it can be proposed that diffuse necking is not a limitation in forming [238, p. 397, 84]. As deformation is further carried on, the deformation increasingly localizes into a narrow band, termed as shear band. This refers to localized necking, which takes place inside the region of diffuse necking (Figure 81). [8] Once localized necking initiates, the deformation rate, i.e. strain rate, in the localized zone increases rapidly, while outside this zone all deformation terminates [84]. It is proposed that a surface presented in Figure 42c, i.e. surface waviness, develops once localized necking has initiated. Therefore the formation of shear bands is regarded as a limitation in bending.

Yet, the phenomenon of diffuse necking in bending is not entirely unambiguous. It is suggested e.g. by Lopez and Boogaard, and Jeschke et al. that in case of bending the phase of diffuse necking generally cannot occur and hence strain localization occurs immediately once bifurcation of uniform deformation begins [238, 239]. In bending, as discussed above, the upper fibre is subjected to tensile stresses, but immediately below the strain is smaller. Hence even though the necking conditions are satisfied at the upper fibre, the lower fibres, in which necking condition are not satisfied, support the upper fibre in thickness direction and hence diffuse necking is prevented. Figure 90 illustrates schematically a fictitious case where the lower fibres are not supporting the upper fibre and hence necking is enabled.
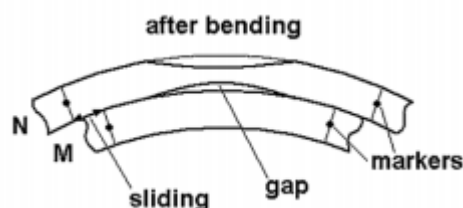
Figure 90: Schematic fictitious illustration of separation of fibers in bending and consequently occurrence of diffuse necking [84, p. 2048].

Yet, in truth, the fibres are connected to each other and the formation of gaps between them is impossible [84]. Therefore it can be concluded that similar diffuse necking to the one occurring in tensile testing, is not possible to occur in bending. On the other hand, it is proposed by Centeno et al. that in case the entire sheet thickness becomes plastically unstable, necking is enabled [240]. Furthermore, according to Joutsenvaara, diffuse necking occurs in bending procedures, since the deformation occurring in bending relates to stretching [9].

However, in bending the thickness reduces at the bent region, i.e. occurs thinning, which indicates that necking takes place. In other words, material "streams" i.e. is removed from the area where necking occurs. Hence, it can be proposed that in bending, diffuse necking does not occur throughout the thickness, but instead so called local diffuse necking occurs. Local diffuse necking occurs at surface regions, where due to the greater strains the phase of uniform plastic deformation is exceeded. Once local diffuse necking occurs, a phenomenon termed as flattening appears. Flattening signifies for a phenomenon, in which the upper surface from the bent region flattens, i.e. curvature is no more present. Therefore it can be concluded that diffuse necking occurs additionally in bending, yet, merely in the surface layers.

During diffuse necking the deformation that occurs within the necking region is not homogeneous. This is illustrated in Figure 91, where a true stress strain curve of an UHSS (YS~700 MPa) and strain values in various regions of a tensile test specimen are presented.
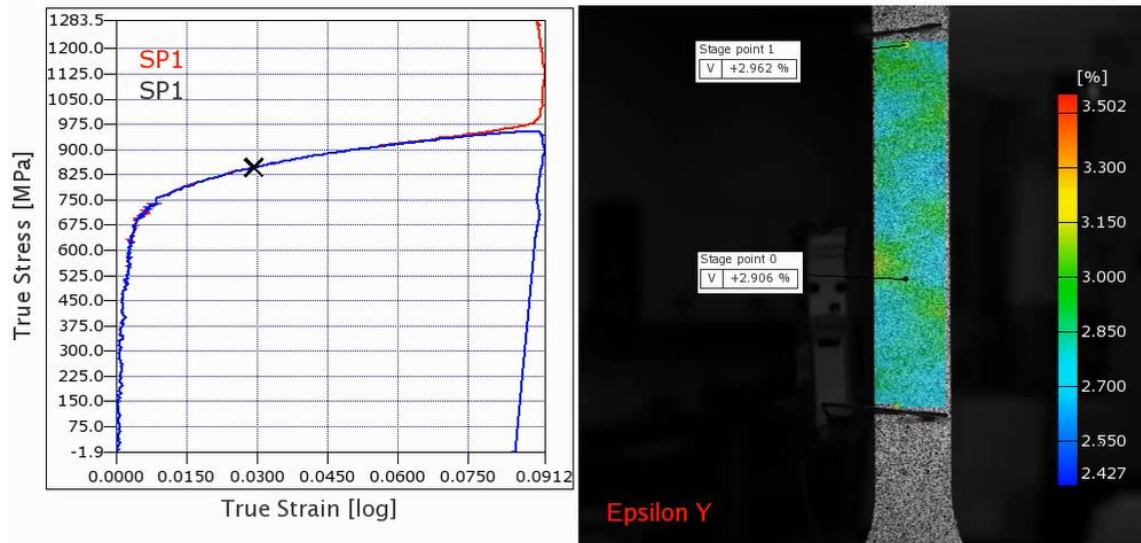
Figure 91: Illustration of distribution of strain values during diffuse necking in tensile testing [241].

It can be seen from Figure 91, that during diffuse necking the amount of strain varies with in the specimen. Hence it can be stated that during diffuse necking the deformation is not homogeneous in slip plane level. During diffuse necking strain basically tries to localize, i.e. find a "weak spot". Consequently, as strains continue to increase such "weak spot" is found and strain localizes. In Figure 92, strain localization, i.e. formation of shear band, is presented.
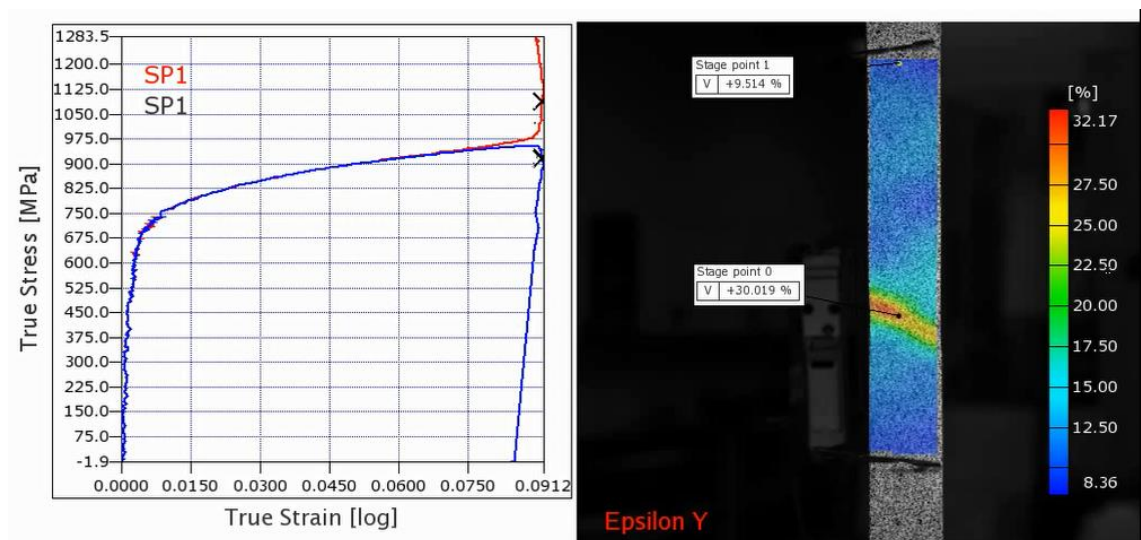
Figure 92: Presentation of formation of a shear band in tensile testing [241].

It can be seen from Figure 92, that once strain localizes, the straining taking place outside the shear band is notably smaller. Furthermore it can be observer from Figure 92, that the shear band is oriented at about 45° with respect to the loading direction, which is consistent with a finding by e.g. Ghadbeigi et al., and Steninger and Melander [145, 158]. Eventually fracture occurs within the region of strain localization.

Therefore, bending process can be basically divided into three stages in terms of plastic deformation; i.e. uniform plastic deformation, diffuse necking and localized necking. Yet, concerning bending capability, once localized necking has initiated, the bending limit is exceeded. Therefore in order to enhance bendability, the phases of uniform plastic deformation and diffuse necking need to be expanded.

9.2.1 Appearance of shear bands

The results (Figure 78) suggests that the formation of shear bands is precursor for damage in bending. This is consistent with several investigations, e.g. Xu et al., and Mitsutoshi and Tvergaard [3, 11]. It is noteworthy to recognize that no voids appear to be present prior to the formation of shear bands. It is found that voids form in shear bands; this can be observed e.g. from Figure 82. It is proposed that fracture occurs hence by typical ductile fracture, i.e. nucleation, growth and coalescence of voids, which takes place within the shear band. The fact that shear bands form prior to voids can be proved by the observing that shear bands without voids are present, however no voids without shear bands are present. According to Kaupper and Merklein this is characteristic for complex phase structures that are rather homogeneous, instead of a typical dual-phase structures [170]. Hence this indicates that the hardness differences between the constituents, i.e. matrix and second phase particles, are not that significant, in order that the interfaces would be critical as far as nucleation of voids is concerned.

Yet, in sample 0.07C-1.3Mn 815°C bent to an angle of 56° voids were present while shear bands did not appear to exist (Figure 75). However the amount of voids was highly small; only a couple was present. Additionally, as can be seen from Figure 75, the microstructure is basically not at all deformed at the region were the void is, indicating that the void was present already before deformation had initiated. Lievers et al. suggest that in such case of early nucleation, voids do not promote strain localization. Due to the notably small density of voids, it can be concluded that their presence does not govern the formation of shear bands and these few voids are only exceptional cases, which do not affect strain localization. [136] Furthermore, as discussed above, it cannot be stated with certainty that these are actually voids equivalent to the ones described in Subchapter 6.3.2. Hence, it can be still concluded that shear bands develop prior to voids.

Figure 78b presents a fracture followed by the formation of shear bands. It can be observed that shear bands are present on both sides of the fracture. Shear bands and, hence fracture, appear to occur below the upper surface, approximately from the depth of 0.1 mm to 0.5 mm. All of the shear bands and the fracture are parallel and additionally they are orientated at about 45° with respect to the surface. This signifies that shear bands grow along maximum shear stresses (Figure 20). The inclination of the shear bands is consistent

with the findings by Steninger and Melander [158]. The size of the shear bands is approximately 0.3 mm and it is observable that shear bands propagate across several grains (Figure 78b).

It is stated that the formation of shear bands initiates by a single slip, but once initiated it does not obey rules of crystallographic, which is noticeable in Figure 78b. It can be proposed that the formation and growth of shear bands is highly abrupt. Since, although in case of sample bent to an angle of 85° a large amount of shear bands are present, yet in case of the same sample 0.07C-1.3Mn 815°C bent to an angle of 56° (Figure 73) no such bands are present. Furthermore, in sample 0.08C-1.8Mn 870°C bent to an angle of 96° (Figure 71) no shear bands appear to be present, although it can be assumed that such bending is notably close to maximum bendability. Furthermore it is peculiar that shear bands and damage did not occur in samples bent to angles greater than 90° degrees, since the applied radius was smaller than the minimum bending radius in bending to 90° degrees. This signifies that the material properties controlling the formation of shear bands are not homogeneous within a sample.

It can be concluded; that in order to improve bendability, it is essential to delay the formation of shear bands, i.e. localized necking. As discussed above, localized necking is an implication of diffuse necking, which in turn is a consequential of uniform plastic deformation. Therefore it can be proposed that concerning bendability, it is desirable to extend both the phases of uniform plastic deformation and diffuse necking. However, it is proposed that total elongation, i.e. sum of uniform and non-uniform, does not affect bendability. It is proposed that complex phase bainitic steels that exhibit poor uniform elongation exhibit good post-uniform elongation. [242, p. 235] This implies that basically there is a trade-off situation concerning these elongation types, and hence both of these elongation types cannot not be increased simultaneously. Therefore it can be suggested that factors governing each elongation type differ. However, it needs to be recognized that concerning bendability merely the surface properties affect, while total elongation attained from tensile testing accounts for throughout thickness properties.

9.3   Extent of uniform plastic deformation in bending

Uniform plastic deformation occurs until the ultimate tensile strength is achieved and plastic instability initiates. It is proposed by Nagataki that the extent of uniform elongation obtained by tensile testing cannot be utilized in evaluating bendability in case of UHSS [6]. Furthermore this proposal is supported by e.g. Chen et al., who claim that in case of formability, which is governed by local ductility, steels with a tensile strength greater than 700 MPa, tensile strength does not notably affect forming capability [174]. This can be suggested to be due to the finding that hardness of surface only correlates with bendability (Tables 13 and 14), whereas hardness at centre line does not appear to

affect Figure (106). And tensile testing accounts for tensile properties throughout the thickness although only the surface properties seem to affect.

A criterion for plastic instability termed as Considere Criterion defines the initiation point for diffusion necking. According to Considere Criterion diffuse necking initiates once strain hardening exponent equals to true strain, i.e.: [243]

$$\varepsilon_t = n \tag{20}$$

where ε_t is true strain and n is work-hardening exponent.

Yet, Considere Criterion is applicable only in case Holloman equation (3) can be applied to describe stress-strain behaviour of material. In addition, it is expected that the material is strain rate insensitive, i.e. m=0. Figure 93 demonstrates the onset point of diffusion necking.
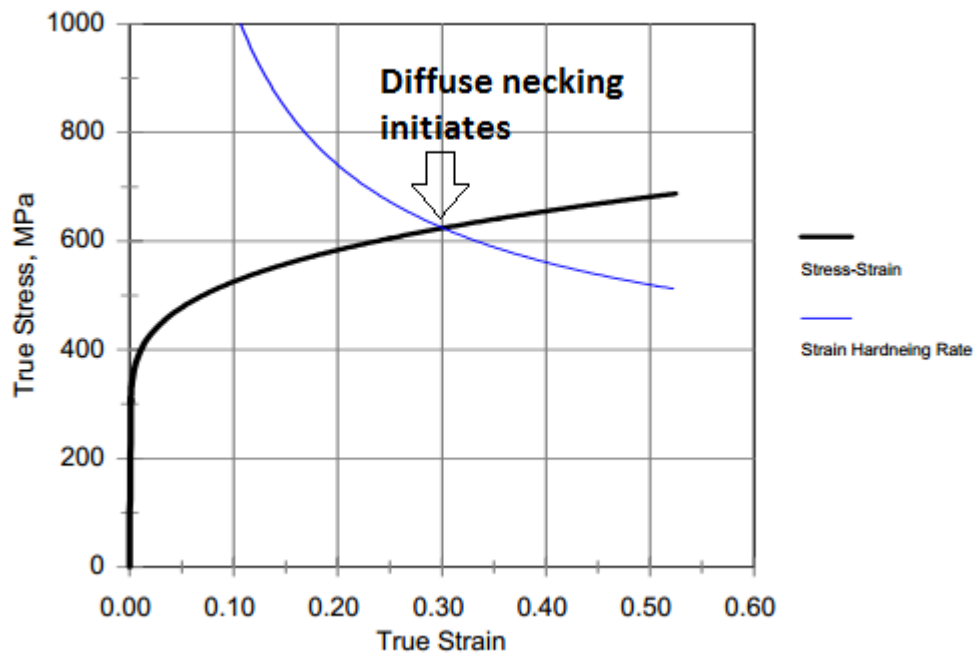
Figure 93: A stress-strain curve presenting the initiation point of diffuse necking [244].

Hence, it can be concluded that the extent of uniform elongation is highly dependent on work-hardening capability. The significant role of work-hardening parameter on the amount of uniform plastic deformation has been generally accepted, e.g. by Marciniak et al., Yu and Balliger and Gladman [4, 109, 245]. However, the effect of work-hardening capability on delaying the onset of diffuse necking has been principally studied in case of dual phase steels, which behave differently compared to the materials used in this work. Dual-phase steels possess high work-hardening capability due to the significant hardness differences between the matrix and the second phase. But instead such steels possess poor

post-uniform elongation due to the incompatibility of deformation between the softer and the harder constituents.

Hart have proposed a criterion for plastic instability that considers in addition to work-hardening exponent, also strain rate sensitivity. According to Hart criterion for plastic stability in uniaxial tension can be expressed:

$$d\sigma_f/d\varepsilon_t + d\ln\sigma_f/d\dot{\varepsilon}_t \geq 1 \tag{21}$$

where σ_f is flow stress, ε_t is true strain, $\dot{\varepsilon}_t$ is true strain rate. In other words, according to equation (21), the sum of work-hardening rate and strain rate sensitivity is required to be equal to or greater than 1 in order to assure stability of plastic flow. [246]

Yet, concerning the effect of strain-rate sensitivity on the extent of uniform deformation, there is no consensus in literature. It is proposed in several investigations, e.g. by Wang and Ayres that high strain rate sensitivity increases resistance to necking and additionally increases post-uniform elongation [247, 248, 249] Additionally, it has been suggested by several models, e.g. Consider, that the amount of uniform deformation highly depends on the strain hardening parameter and/or strain rate sensitivity [243]. Instead, it is suggested by e.g. Marciniak et al. and Shi that strain-rate sensitivity does not affect uniform elongation, instead it only influences post-uniform elongation [4, 250]. In addition several other studies, by e.g. Davis, Miles, Ghosh, and Pearce and propose that the effect of strain rate sensitivity is notably emphasized during post-uniform necking [248, 251, 252]. The insignificant effect of strain rate sensitivity on the onset of diffuse necking is explained to be due to the notably small strain gradient prior to diffuse necking. Instead, as diffuse necking initiates, the strain gradient is increased and hence the effect of strain rate sensitivity is assumed to become significant. [248]

Hence it can be implied, that the main factor controlling the extent of uniform elongation is work-hardening capability, but strain-rate sensitivity additionally affects but not as notably. A higher hardness basically leads to a decrease in both of these parameters. Therefore hardness notably affects the extent of uniform elongation.

9.3.1 Work-hardening capability

Hardness highly relates to work-hardening capability. Work-hardening capability affects the amount of uniform plastic deformation; a higher work-hardening capability delays the onset of bifurcation of uniform deformation. This is because it defines material's ability to distribute strain to adjacent regions and hence delay localization. Increased work-hardening capability is typically related to enhanced ductility and hence increased deformation capability. Work-hardening occurs on condition that the material is capable of producing new dislocations. In case the dislocation density is notably high, the amount of

new generating dislocations, i.e. magnitude of work-hardening, is decreased. This is because the capacity for new dislocations is in such case smaller. Dislocation density depends on the transformation temperature. In case of lower phase transformation temperatures, strains following the transformation are larger and thus the dislocation density is increased. [52] Additionally a relationship between carbon content and dislocation density has been found; a higher carbon content results in a greater dislocation density. [199] Therefore it can be proposed that the high- temperature transformation products possess better work-hardening capability due their greater capacity to generate new dislocations. Work-hardening capability is also affected by the phase structure, to be precise, by the hardness differences between adjacent phases. A greater hardness difference leads to an increased need of dislocations in order to assure the compatible deformation of constituents with various hardness levels. This indicates that work-hardening capability is related to the hardness of microstructural constituents.

As discussed above, the upper layers of the material are subjected to the greatest strains. Therefore it can be concluded that a sufficiently soft layer at the surface contributes to enhanced bendability by ensuring the required deformation capabilities at given depths. Yet, the term "soft layer" is rather misleading, since the required softness only decreases as approaching from the upper surface towards the neutral axis. Meaning that additionally the regions subjected to smaller strains, i.e. regions closer to the neutral axis, require sufficient deformation capability, i.e. softness, in order to prevent strain localization to occur at that particular depth.

It can be observed from Figures 53-58 that the hardness of the materials basically increases as approaching from the surface to the depth of 0.35 mm. From the depth of 0.35 mm the hardness level essentially stabilizes equalling to the hardness of the centre line. As discussed above, work-hardening capability, which is dependent on the hardness, highly affects the capability to deform uniformly. Therefore it can be proposed that the stress-strain curves for the surface region and below this region differ. To be precise, especially the magnitude of uniform deformation is greater at the softer surface region compared to harder region below. This signifies that the softer surface layers endure larger magnitudes of strain before necking initiates. This is desirable, since when bending, the greatest strains occur at the outer surface, continuously decreasing as approaching the neutral axis (Equation 6). Yet, in principle, the hardness level is significantly lower only at the depth of 0.05 mm, although the strain level below this is still nearly as high as immediately at the surface, i.e. 0.05 mm. This indicates that the capability to deform uniformly is notably increased only immediately at the surface (0.05 mm), even though such capability is nearly equally highly needed also below this depth. Hence it can be proposed that diffuse necking occurs approximately at the depth range of 0.1-0.5 mm due to the combination of large strains and high hardness values.

According to Table 13, the correlation between hardness and bendability is most significant at the depth range of 0.1-0.35 mm in case of 8 mm sheets. In addition it can be noticed from Figure 78b that shear bands are present at the depth range of 0.1-0.5 mm. This also confirms that, as stated above, diffuse necking occurs first at this depth range. Thus it can be proposed the hardness level increases more rapidly than the strain level decreases at the depth range of 0.1-0.5 mm. In other words, at this depth range a detrimental combination of locally high strains and lower local deformation capability is present. It can be noticed from the microstructure images represented in Subchapter 8.1, that in most cases the microstructure abruptly changes from granular bainite to a mixture of lath-like bainite and martensite at a given depth. This typically takes place at the range of 0.1-0-4 mm in case of materials used in this work. And as discussed, the hardness of lath-like bainite and martensite is higher compared to granular bainite, and consequently a mixture of lath-like bainite and martensite possess lower work-hardening capability.

As a conclusion it can stated that a lower surface hardness contributes to increased uniform elongation due to the desired work-hardening capability. This indicates that a microstructure comprising granular bainite and/or ferrite is beneficial in order that the onset of diffuse necking is postponed to greater strains. Concerning only the extent of uniform elongation, a dual-phase type of microstructure can be assumed to be desirable in order to attain a high amount of geometrically necessary dislocations. Yet, such microstructure is extremely detrimental concerning the extent of uniform elongation, due to the high hardness differences. Therefore, it can be proposed that a homogeneous microstructure, i.e. small hardness differences between adjacent phases, providing a low hardness level is most desirable.

9.4 Post uniform elongation in bending

At the point where deformation is no more capable of carrying on in a uniform manner diffuse necking initiates to occur. As discussed above, this takes place only at the surface layers, where the ultimate tensile strength is exceeded. At some given point, inside the diffuse necking region, localized necking initiates, i.e. shear bands form. Therefore it is highly significant to comprehend that which factors govern the extent of "pure" diffuse necking. In other words, that which factors cause the strain to localize in an extremely small region. The onset of strain localization is affected by various factors. These include work-hardening rate, strain-rate sensitivity, grain size, texture, hard particles, the hardness difference between adjacent phases and the size and dispersion of the hard phases in complex phase steels. [242, p. 235]

9.4.1 Condition for instability

Dillamore et al. have developed a condition for instability, which determines the onset of the formation of shear bands. This equation implies that shear bands form as local softening occurs, indicating that locally increasing deformations can be provided by decreasing stresses. [253] This is confirmed by several other studies, e.g. Ramesh, Burkhanov and Lopes et al. [85, 90, 95]. Dillamore et al. propose that the condition for the formation of shear bands can be expressed as: [253]

$$\frac{1}{\sigma}\frac{d\sigma}{d\varepsilon} = \frac{n}{\varepsilon} + \frac{m}{\dot{\varepsilon}}\frac{d\dot{\varepsilon}}{d\varepsilon} + \frac{1+n+m}{d\varepsilon}\frac{dM}{d\varepsilon} - \frac{m}{N}\frac{dN}{d\varepsilon} \leq 0 \tag{22}$$

where n in work-hardening exponent, m is strain rate sensitivity, N is the density of mobile dislocations, M is Taylor factor, σ is stress, ε is strain and $\dot{\varepsilon}$ is the normal strain rate. $\dot{\varepsilon}$ can be expressed as $\dot{\gamma}/M$, where $\dot{\gamma}$ is shear strain rate. Shear strain rate can in turn be written by Orowan relation $\dot{\gamma} = N\boldsymbol{b}v$, where $\boldsymbol{b}$ is the magnitude of Burgers vector and v is dislocation velocity. [253]

In order to prevent strain localization, the left-side of equation (22) is required to be equal to zero or greater than zero. According to equation (22) it can be stated that factors affecting the formation of shear bands are work-hardening exponent, strain rate sensitivity, density of mobile dislocations and Taylor factor. Strain and the instantaneous value of strain are below the dividing line. In equation (22), ε is expected to be always positive, although in principle it is possible that work-softening occurs for example due to dynamic recovery or a variation in the deformation mode. This implies that the other factors determine whether given components of the equation (22) are positive or negative.

Due to the aim to bend with extremely small radius, the strain is expected to be large and therefore it is required that the condition for instability must be prevented with large values of strains. Thus it is needed to comprehend how these factors behave as strain increases and how they relate with each other. In equation (22), constant values of N, n and m are considered, although their magnitude changes as deformation is carried on, and hence it would be intelligible to use instantaneous values instead. It is assumed that n and m decrease as deformation is carried on. Furthermore it is not described that in what manner values of n and m where defined.

In case of steel, strain rate sensitivity can be negative due to dynamic strain aging, i.e. DSA. DSA is due to the interactions with dislocations and solute interstitial atoms of carbon and nitrogen. As a result of DSA, many dislocations are immobilized by solute atoms. This indicates that in this case $\frac{dN}{d\varepsilon}$ is expected to be negative. Yet, dynamic strain aging occurs in steel at such high temperature ranges. The temperature range within DSA occurs is proposed to be in the range of 140-340 °C in case of low alloy steels [254, pp.

123-129]. Therefore it can be expected that during bending this phenomenon does not occur, i.e. $m > 0$.

Furthermore, it is proposed that as deformation is carried on the total amount of dislocations increase, while simultaneously the fraction of mobile dislocations decreases. This is demonstrated schematically in Figures 94a and 94b.
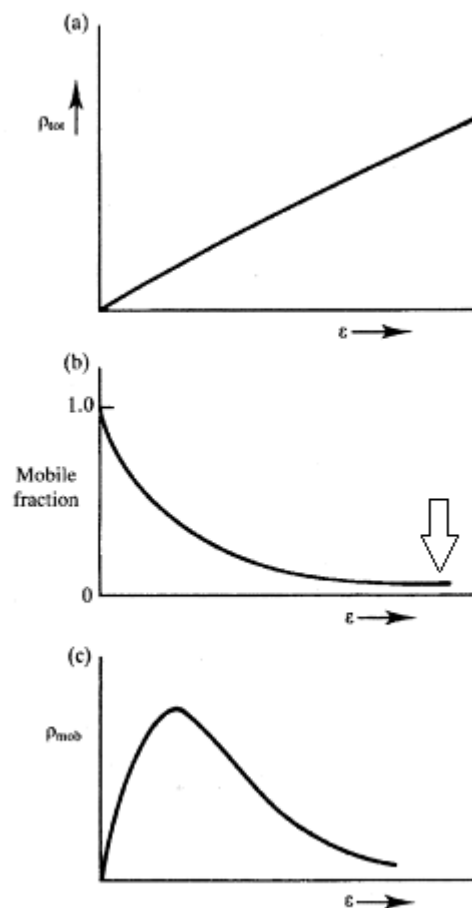
Figure 94: Presentation of the dependence of a) total dislocation density, b) fraction of mobile dislocations and c) density of mobile dislocations, as a function of plastic strain [255, p. 134].

Figure 94c illustrates that first as strain increases the density of mobile dislocations increase, but as deformation is carried on the density eventually decreases. It can be suggested that this is because immobile dislocations act as obstacles to the generating mobile dislocations. In case the mobile dislocation density increases more rapidly than the dislocation mobility decreases because of the developing forest density, strain softening is suggested to occur. This occurs at high strain levels, as the amount of mobile dislocations is notably small and their volume fraction remains nearly similar although the total amount of dislocations increases. This is indicated by an arrow in Figure 94b. Local Softening is related to the formation of shear bands. This implies that at the point where

volume fraction of mobile dislocations is constant, while simultaneously the total dislocation density increases, strain localization is proposed to initiate.

It is suggested that in case the initial dislocation density is notably high or/and coefficient of dislocation multiplication is low, the density of mobile dislocations decreases continuously with strain from the initiation point of plastic deformation. This signifies that in case of low temperature transformation products, i.e. martensite and bainite, the component $\frac{dN}{d\varepsilon}$ is constantly negative. Whereas in case of high temperature transformation products, the component $\frac{dN}{d\varepsilon}$ is first positive, but as strain increases it turns to negative. This additionally implies that higher strains are required until the point of strain softening occurs in case of high temperature transformation products that possess a lower initial dislocation density. Therefore it can be proposed that concerning the delay of strain softening, it is beneficial that the initial dislocation density is low, i.e. hardness value is low. Furthermore, as a conclusion it can be stated, that concerning large values of strain, it can be expected that the density of mobile dislocations decrease, indicating that $\frac{dN}{d\varepsilon}$ is negative. Referring to equation (22), it is desired that magnitude of component $\frac{dN}{d\varepsilon}$ is as large as possible.

Additionally constant value of mobile dislocation density N is concerned in equation (22). According to equation (22) it is desirable that the value N is as small as possible, in case the component $\frac{dN}{d\varepsilon}$ is negative. It can be assumed that value N relates to hardness properties. Again, similarly as in case of component $\frac{dN}{d\varepsilon}$, the curves presented in Figure 94 differ between low and high temperature transformation products due their different initial dislocation densities. Concerning low temperature transformation products, the initial total dislocation density is high, which signifies that the density of mobile dislocations is low. However, additionally in case of notably low total dislocation density, the amount of mobile dislocations is low. Therefore there can be expected to be an optimum hardness value, where the amount of mobile dislocations is the greatest. It is noteworthy to recognize that in equation (22), only the constant value of N is concerned, instead of instantaneous value. This means that basically, the density of mobile dislocations can be similar in case of phases with notably high and low hardness values. However, as discussed above, a high initial dislocation density leads rapidly to a situation where strain softening occurs and thus high hardness values are undesirable. As a conclusion it can be suggested, that concerning component $\frac{m}{N}\frac{dN}{d\varepsilon}$ it is desirable that the hardness value is low in order to minimize the value of N and additionally delay strain softening.

In equation (22), constant values of strain hardening exponent and strain rate sensitivity are included. According to equation (22), it the magnitude of these values is desired to be

a large as possible. The significance of strain rate sensitivity and work-hardening capability on preventing strain localization are understandable due their effects on the capability of distributing strain to adjacent regions during deformation. During deformation, hardening is principally due to strain hardening and strain rate hardening. A simplified expression of hardening as a consequence of these two factors can be expressed as: [248]

$$\sigma = K\varepsilon^n\dot{\varepsilon}^m \tag{23}$$

where σ is stress, K is constant, $\dot{\varepsilon}$ is strain rate, n is work-hardening exponent and m is strain rate sensitivity. Due to strain-hardening the regions where deformation concentrates strain-hardens and becomes resistant to further deformation, and consequently deformation is shifted to adjacent regions that are less deformed. Similarly, as strain rate at the region where deformation is concentrated increases, as a result of strain hardening of these concentrated regions, the deformation is shifted to regions that experience retardation in the rate of deformation. [248] These both factors are highly related to hardness. The relationships between hardness and work-hardening capability, and hardness and dislocation density, were profoundly discussed above. As a short revision from above; as dislocation density increases hardness increases, but instead work-hardening capability decreases since the capacity to form new dislocation decreases. Additionally strain-rate sensitivity is related to hardness. Factors contributing to strain rate sensitivity are further discussed here.

Strain rate sensitivity decreases as the strength level increases, and in case of UHSS it is proposed that it is stabilised at a low level. It is stated that an increase in the grain size results in an increasing strain rate sensitivity [256, p. 234]. In case of multiphase steels, the hardness of the ferrite phase can be utilized as an indicator of strain rate sensitivity; a softer ferrite phase leads to higher strain rate sensitivity [257, p. 113]. Additionally it is proposed that as the volume fraction of bainite or martensite constituents in the ferrite matrix increase, the strain rate sensitivity decreases [256, p. 234]. Strain rate sensitivity is also dependent on the crystal structure, since it determines the nature of dislocations and has an effect on the barrier structure [105, pp. 6-7]. Therefore it can be concluded that in order to attain desirable strain-sensitivity and work-hardening properties, the hardness level is required to be sufficiently small. The requirement concerning the hardness level depends on the desired bending radius; the smaller the hardness level is, the more the onset of diffuse necking is postponed. For example, in order that a minimum bending radius $3t$ is attained, the hardness of the surface layer is needed not to be above 400 HV.

It is proposed by several studies, e.g. Ghosh and Pearce, that the significance of strain rate sensitivity becomes particularly emphasized once diffuse necking has initiated [248, 252]. Since, as strain-rate sensitivity increases both total and local elongation after the initiation of necking increase. Figure 95 demonstrates the effect of strain-rate sensitivity on the extent of post-uniform elongation.
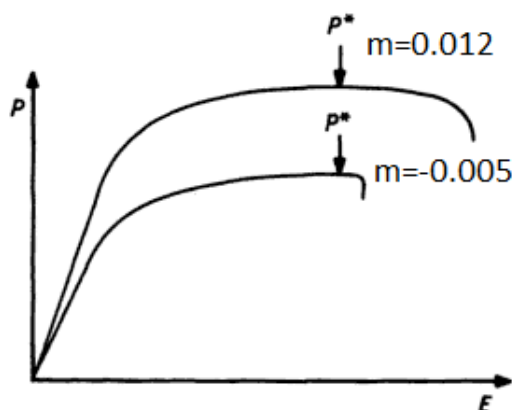
Figure 95: The effect of strain-rate sensitivity on post uniform elongation [252, p. 19].

Once necking has initiated, the region subjected to necking can become hardened compared to the regions outside the neck, as a result of work hardening. Additionally due to the greater strains in the necking region, strain rate hardening can also take place. Consequently due to these two phenomenona the deformation can be shifted to regions outside the generating neck and hence the phase of diffuse necking is prolonged. [258]

A higher work-hardening capability is related to higher local deformation capability, higher local strength as a consequence of strain hardening and higher diffusion of the deformation at the neck than outside the neck [259, p. 2161]. Hence it is peculiar, that in literature there is consensus concerning the effect of work hardening capability on bendability, even though it is generally accepted that a higher *n*-value delays strain localization [2, 185, 186]. This can result from the findings by e.g. Ghosh, that the effect of strain hardening capability is emphasized in preventing the onset of diffuse necking instead of notably affecting strain localization [248]. Moreover, work-hardening exponent is attained from a conventional tensile test, which indicates that work-hardening capability throughout the thickness is considered instead of determining the work-hardening capacity of the surface layers, i.e. the critical regions in bending. Hence it can be suggested that the work-hardening exponent of the surface layers, i.e. to the depth of approximately 0.4 mm, is connected to bendability. However, it is technically challenging to be able to define work-hardening exponent of such thin region. Therefore it can be concluded, that high values of strain rate sensitivity and work-hardening capability are desired in order to prevent strain localization.

Taylor factor M is always positive, however, $\frac{dM}{d\varepsilon}$ can be either positive or negative, since it changes with grain orientation. Taylor factor is dictated by crystal orientation, which in turn changes during deformation. During deformation a softer texture can generate, which results in flow softening and consequently localization of deformation. [260] In case strain rate sensitivity is positive, as can be expected to be the case typically in this work,

the factor $\frac{dM}{d\varepsilon}$ is preferred to be positive. This understandable, since it is stated that a decrease in Taylor factor refers to textural softening, while an increase in Taylor factor relates to textural hardening. [261] And as discussed above, local softening leads to strain localization, and hence it can be suggested that a decrease during deformation in Taylor factor promotes strain localization.

As a conclusion it can be stated that concerning instability condition and hence initiation of shear bands, it is highly beneficial that the hardness level is low. Since low hardness values contribute to desired constant values of *m, n, M* and *N,* which are factors in equation (22). Furthermore low hardness values leads to need of higher strains in order that strain softening is capable of occurring. As discussed, diffuse necking occurs only at the surface layers, i.e. 0.1-05 mm in case of materials used in present work, since due to the combination of greater strains and high hardness; the ultimate tensile strength is first exceeded at this depth range. Thus, eventually strain localization will additionally occur at this depth range, which signifies that a microstructure contributing to a delay of instability condition is highly needed here. Furthermore, by studying the effect of surface hardness on bendability in case of sample 0.08C-1.4Mn 815°C (Figure 60), the detrimental effect of high surface hardness can be confirmed. It can be observed from Table 15 and Figure 60, that in case of region where no damage occurred, the hardness values are highly smaller to the depth of 0.2 mm. This is consistent with the results presented in Table 13, where it is indicated that the most significant correlation in case between surface hardness and bendability is at this particular depth.

It is found by observing hardness profiles (Figures 53-58) that a lower surface hardness leads to lower centre line hardness, and instead a higher surface hardness leads to higher centre line hardness. This indicates that there is a specific limit that how low the hardness can at this depth range, i.e. 0.1-0.5 mm, be in order to attain required hardness at the centre line. This implies that there is a limit concerning magnitude of condition for stability achieved by lower hardness level.

9.5   Effect of microstructural homogeneity on bendability

As stated above, the deformation during diffuse necking is not homogeneous and basically the degree of inhomogeneity continuously increase as bending is carried on. Hence it is proposed that the homogeneity of the microstructure is now highly significant, in order to avoid the presence of a "weak length", where strain is able to highly localize. It is proposed that localization occurs once local softening begins, which signifies that the material at that region reaches the peak stress while elsewhere in the material the peak stress is not yet reached. It can be stated that in case of an inhomogeneous microstructure the condition for instability, i.e. Equation (22), is reached locally, while outside this given region this condition is not yet satisfied. The level of inhomogeneity governs that at which

point the condition for instability is met additionally at other regions. Hence, a more inhomogeneous microstructure leads to more intense strain localization.

As can be observed from images (Figures 46-52) presenting microstructures of materials used in this work, the microstructure consists of mixture of various volume fractions of different constituents representing divergent morphologies and sizes. Therefore microstructural factors affecting the formation of shear bands basically differ throughout the microstructure. This signifies that the factors presented in Equation (22), are different throughout the microstructure. In other words work-hardening capability, strain rate sensitivity and mobile dislocation density which are related to hardness vary throughout the microstructure. Furthermore local M factors vary. Hence it can be concluded due to the inhomogeneous microstructure condition for instability is achieved locally first at some regions, and thus shear bands can be expected to initiate at such regions.

According to the results a correlation between microstructure homogeneity, i.e. homogeneity index, and bendability exists basically only at the very surface, i.e. at the depth of 0.05 mm. As discussed, this is the region where the material is subjected to the greatest strains. In this work the deviation of hardness measurements was applied as an indicator of homogeneity. Even though, microhardness measurements were conducted, as can be noticed from Figure 61 each measurement encompasses a various amount of several phases. Additionally the effects of texture and defects cannot be accurately determined. As discussed above, each measurement defines an average hardness resulting from e.g. the constituents, defects, texture and local composition. Therefore e.g. the hardness differences between adjacent phases cannot to be defined, which is stated to highly affect strain localization, as discussed in Subchapter 4.3.3.

It is rather curious that according to the results the effect of homogeneity is significant only immediately at the surface, i.e. depth of 0.05 mm. Since, the magnitude of the strains is not significantly greater at this depth compared to the depth of 0.1 mm, where the effect of homogeneity appears to be nearly negligible. It is noteworthy, that no shear bands appear to be present at the depth of 0.05 mm, as can be as can be observed from Figure 78. Therefore it cannot be stated in certain that inhomogeneity of surface, i.e. depth of 0.05 mm, leads to poor bendability. Instead it can be proposed that the inhomogeneity at the surface is a result from another factor, which in turn is related to poor bendability. Yet, no significant correlation ($R^2 = 0.39$) between hardness at the depth of 0.2 mm and homogeneity index at the depth of 0.05 mm exists. Furthermore it is worthwhile to recognize, that at this given depth, i.e. 0.05 mm, the hardness level was basically in all cases significantly lower compared to the greater depths. And additionally, the hardness at this depth did not correlate with bendability. It can be proposed that the surface homogeneity does not govern the initiation of shear bands, but instead it can facilitate its growth through the upper surface. Since in case of a highly inhomogeneous microstructure, the strain can be proposed to easily "find" a way to propagate. Yet this cannot be confirmed

by the results attained from this study, since the developed shear bands in this work did not reach to the upper surface.

9.5.1 Homogeneity of phase structure

It has been stated in several studies, e.g. by Bergström and Yamazaki et al. that in an inhomogeneous microstructure consisting of phases with various hardness levels, strain localizes at the softest phase [144, 2]. It has been discovered that in case the hard difference between adjacent phases is significantly great, the harder phase does not deform plastically, and thus it can be proposed that the softer phase is the so called weak length where shear bands initiate at. Hardness difference between neighboring phases leads to an inhomogeneous instability conditions, since hardness relates to values *n, m* and *N,* which are factors in Equation (22). Strain, in a manner of speaking, tries to localize into a softer phase, which possesses both increased work-hardening capability and strain rate sensitivity. Therefore, it can be assumed that in case of a significant hardness difference and hence notable incompatibility of deformation characteristics, the softer phase continues to work harden until a certain limit. Eventually a maximum limit concerning hardening due to work-hardening capability and strain rate sensitivity is met and thus shear bands initiate at this given grain. Moreover, it can be assumed that in such case, the harder phase does not undergo any plastic deformation, indicating that all strain is concentrated into the softer phase. In such case, it can be assumed the extent of uniform elongation is high, but instead the extent of post-uniform elongation is nearly negligible.

However, it can be observed from Figures 77a-b that in case of materials used in this work, additionally the harder M /A constituents deform plastically. This indicates that the hardness difference between the matrix and the M/A islands at the surface is not significant. It has been found that a higher cooling rate leads to a smaller hardness difference [198]. The hardness of M/A islands is highly dependent on carbon content, i.e. higher carbon content results in higher hardness. It is suggested that a high dislocation density in bainitic laths can trap carbon, consequently resulting in reduced carbon content in M/A islands. This additionally confirms that the matrix at the surface is not pure ferrite, but instead ferritic bainite.

Due to the plastic deformation of both the matrix and the harder second phase constituents, the deformation capability of the second phase particles are additionally matter of interest. It is proposed that especially string-like M/A islands are detrimental concerning ductility and therefore bendability [198].

9.5.2 Local orientation

It is stated that the initiation of a shear band occurs with a crystallographic slip within a single grain. This is highly affected by the crystallographic orientation, since it affects the

ease of dislocations to move. The slip planes wherein dislocations movement is facilitated represent texture which possesses enhanced capability to deform. In other words, the slip planes that are favorably oriented for slip, i.e. deformation, possess enhanced plastic deformation capability. Whereas, slip planes that are un-favorable oriented for slip, can initiate cracks during deformation due to the poor deformation capability. Slipping occurs first at slip planes where the movement of dislocations is the easiest, i.e. in slip planes that possess enhanced deformation capability. Homogeneity, concerning texture, is determined by the Taylor factors and the orientations of individual grains.

Taylor theory of plastic deformation suggests that crystallographic orientation, the activated slip systems and the strain mode define the behavior of each grain [262]. Taylor factor M is determined by the imposed strain and orientation of the grains. It connects the deformation behavior of single grain with grain orientation. [123, p. 689] Due to the differences in the local Taylor factors, the amount of deformation occurring within each grain varies. This leads to incompatibility of deformation. It can be suggested, that grains with a lower Taylor factor are susceptible to strain localization due the lower slip resistance that such grain present. Yet, grains with lower Taylor factor additionally possess lower dislocation density, and hence increased work-hardening capability. Thus in case the difference in Taylor factor between neighboring grains is not notable, slipping initiates additionally in the neighboring grains as deformation is carried on. In case, the difference in Taylor Factor is significantly high, it can be suggested that slipping is prevented to occur at the grains with higher Taylor factor. This consequently leads to the formation of shear band in given crystal.

As discussed above, a reduction in Taylor factor during the deformation is connected to textural softening. This is consistent with a proposal by Khatirkar et al. that orientations with greater Taylor factor are commonly the orientations presenting textural softening [126]. This implies that the peak stress is first achieved in grains with a greater Taylor factor and hence the initiation of shear bands is assumed to initiate at such grains.

9.5.3 Scale of homogeneity

It is unresolved and complex, that whether homogeneity is a nanoscale or microscale matter. Since, in nanoscale, even an entirely martensitic microstructure is inhomogeneous due to the hardness difference between carbides and the matrix. While, in microscale such microstructure is regarded as highly homogeneous.

According to literature, the inhomogeneity is typically related to phase structure or to differences in local orientations. Inhomogeneity arising from orientation dissimilarities between adjacent grains is basically a microscale matter, since the size of the grains is several micrometers. Yet, by applying microhardness measurements it is not possible to define the homogeneity of orientations and Taylor factors, since the indentation is larger

than the grain size. Instead, by applying nanoindentation the hardness differences arising from the differences in orientation and Taylor factor between adjacent grains can be evaluated. The influence of orientation on hardness by nanoindentation has been studied by Miura et al. [263]. Additionally, in principal, it can be claimed that the inhomogeneity arising from phase structure is matter of microscale, since the size of the phases and constituents are at microscale. However, similarly to the case of texture, the size of individual phases is smaller than the size of the indentation. Therefore by applying nanoindentation, the hardness differences between adjacent phases are able to be defined.

Instead, the finding that horizontally elongated carbides relate to poor bendability can imply that nanoscale inhomogeneity matters. It is found that heats containing horizontally elongated carbides (e.g. Figure 46f) possess typically poor bendability, in particularly transverse to rolling direction. Horizontally elongated carbides are typically present at the depth range of 0.1-0.5 mm, i.e. at the same depth range where shear bands form. Figure 80 illustrates that highly elongated horizontal carbides are present near the fracture. The presence of such carbides is generally related to high carbon contents, low finish rolling temperature and highly pancaked austenite. The shape of the carbides is dependent on the coherency of the carbides with the crystal [264, p. 157]. It is proposed that large carbides are incoherent with te matrix. It is suggested that incoherent carbide particles are susceptible to fracture produced by void sheeting mechanism [265]. Therefore it can be suggested that horizontally elongated carbides are incoherent with the matrix, and consequently decrease ductility.

Furthermore, the deteriorative effect can be proposed to be due to the significant hardness difference between the carbides and the matrix. It is stated that the hardness of carbides is in the range of 1000-1500 Vickers, which is notably higher compared to hardness of the matrix. Due to such significant hardness difference, when subjected to bending, the amount of deformation in the matrix and in the carbides notably differs. On the other hand, additionally lath-like bainite comprises a microstructure of cementite particles in a bainitic ferrite matrix. And still such microstructure is not believed to be as detrimental as far as bendability is concerned. This can be suggested to be due to a proposition that the cementite in lath-like bainite is coherent with matrix.

9.6   Effect of red scale on bendability

It is natural to assume that the presence of red scale between the steel and rolls affects material properties, as transfer of thermal and mechanical energy occurs at the interfaces. The formation and prevention of red scale in hot rolling of steel have been extensively studied, e.g. by Fukagawa et al. [203, 228]. It has been approved by several investigations that the presence of red scale reduces friction in the roll bite during hot rolling [203, 228]. It has been found that friction influences the rolling load, roll wear and strip shape. Red scale has been found to act as a lubricant and hence it presence leads to a smaller rolling

load. It worthwhile to study if rolling load affects deformation behavior of the underlying material and thus affects the forming microstructure.

Furthermore it has been found that the presence of red scale affects the thermal field in hot rolling. This is because the thermal conductivity of oxide scale is notably lower compared to that of steel; approximately one tenth of steels, which implies that scale insulates the surface [266, p. 158]. Heat transfer coefficient is a significant parameter in hot rolling, since it notably affects temperature changes in the hot steel. It is noteworthy to recognize that lubrication additionally affects heat transfer coefficient, and as discussed above oxide scale has a lubricating effect. Murata et al. have found that heat transfer coefficient is reduced in lubricated rolling, which indicates that the appearance of red scale leads to a decreased heat transfer coefficient [267]. According to Lenard a decrease with the initial oxide scale thickness results in a greater heat transfer coefficient, in case the initial thickness is between 0.1-0.4 mm [268].

It is apparent that red scale affects bendability, since as can be seen from Figure 76, visually observable damage appears to be present only in regions containing red scale. Furthermore it can be proposed that the appearance of red scale affects the underlying microstructure, yet this influence is confusing. According to the microstructures presented in Figures 66a and 66b, the effect of red scale on the microstructure of the surface is obvious. It can be noticed that in case red scale is present at the surface (Figure 66a) the microstructure consists immediately at the surface of a mixture of lath-like bainite and martensite. Instead, in case red scale is not present (Figure 66b) an obvious layer of granular bainite and polygonal ferrite is present at the surface. On the other hand, in case of microstructures presented in Figures 67a and 67b, no obvious difference in microstructures due to red scale is observable.

Due to the insulating effect of red scale, heat is prevented to diffuse from the steel surface to the roll and consequently the temperature of the surface remains high [266, p. 158]. It would be expected that the surface containing red scale, would comprise a microstructure consisting of constituents that form with slower cooling rates, i.e. granular bainite instead of lath-like bainite or martensite. However as discussed above, this is not the case here.

Due to the fact that red scale acts as an insulator at the surface, it can be assumed that the true temperature of the microstructure below the red scale is higher compared to neighboring microstructure, where red scale does not exist. This is because due to the insulating red scale heat cannot be transferred away from the material as rapidly compared to the situation without red scale. This signifies that the true FRT in case of microstructures below red scale is higher than expected. And as found in this work, a higher FRT results in greater hardenability immediately from the upper surface. Surface hardness, i.e. depth of 0.05 mm, as function of FRT is presented in Figure 96.
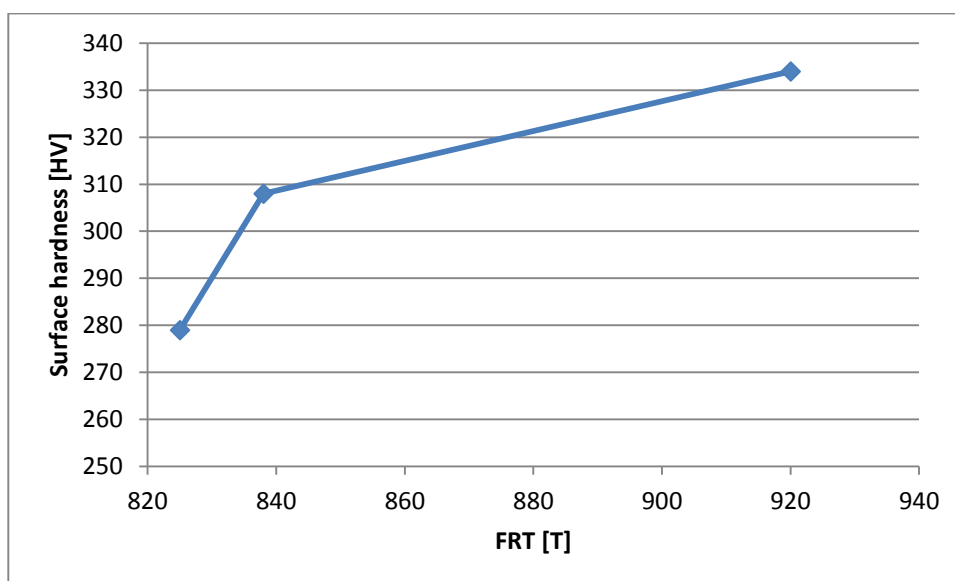
Figure 96: Surface hardness of heats with an equal composition as a function of FRT.

This is in consistent with a proposal by Lenard, who states that a decrease in friction coefficient leads to an increase in the predicted finish rolling temperature [268]. This implies that the regions below red scale are subjected to higher FRT compared to the regions not including red scale.

The effect of red scale on the actual FRT also explains why the effect of red scale is not unambiguous, meaning that the effect is not always similar. In case of a low FRT, it can be proposed that even when red scale is present; the actual FRT is sufficiently low that a layer of granular bainite and/or ferrite is formed at the surface. Furthermore, in case of a notably high FRT, the formation of the soft surface layer is prevented even in regions where red scale is not present, and hence the effect of red scale on underlying microstructure is not clearly observable. This indicates that with a given chemical composition, there is a given temperature range where the presence of red scale leads to a lath-like microstructure, even though the neighboring regions consist of granular bainite and/or ferrite. Although, the effect of red scale on the surface microstructure is not equally easy to observe by SEM inspection, for example in case of lower FRT, it can be assumed to always have an influence. As a conclusion, due the presence of red scale the underlying microstructure is consists of transformation products formed at lower temperatures compared to one without red scale.

A proposal for the influence of red scale on the underlying microstructure is that it prevents decarburization to occur at the final stages of hot rolling at regions below the layer of red scale. Therefore hardenability is greater at microstructures below surface that does not contain red scale. And hence, the formation of lath-like bainite and martensite are more efficiently form, compared to the microstructure under the layer of red scale. It was above discussed, that the hardness of lath-like martensite and bainite is higher compared

to granular bainite or polygonal ferrite. Moreover the significance of surface hardness on bendability is above more profound discussed, but as a short revision; a higher surface hardness leads to a decrease in bendability.

Additionally, the presence of red scale is generally related to surface roughness, which in turn has been found to promote the formation of shear bands [150, p. 815]. It has been widely acknowledged that the lower point of surface can act as nucleation sites for shear bands and in case of notably high surface roughness it replaces the localization bands driven by grain orientation [12]. However, as observed from Figure 78a, in spite of the appearance of red scale, shear bands obviously do not initiate immediately from the surface. Hence it can be suggested that the role of surface roughness is not significant in this case.

The local silicon concentrations can vary. In case of locally higher silicon content, the descaling of FeO is hindered and hence formation of red scale is promoted. Furthermore, is can be suggested that in case of a locally high silicon concentration, silicon combines with oxygen, and thus the formation of MnO is prevented. Therefore a greater amount of manganese remains in solid solution, which contributes to enhanced hardenability.

It can be concluded that the presence of red scale on the surface is detrimental concerning bendability. This is due to the influence of red scale on the underlying microstructure. Due to the red scale, the actual FRT is higher than expected, which leads to a formation of lower temperature transformation products and hence higher hardness level. And as discussed above, higher surface hardness results in a decrease in bendability.

9.7   Tempered samples

Sample 0.07C-1.3Mn 788°C was tempered at two different temperatures. The tempering temperatures of the sample were 350°C and 550°C. Furthermore this same sample was studied as untempered in order to comprehend the effects of tempering on bendability.

The hardness of the tempered samples both at the surface and at the centre line were greater compared to the same sample, which was not tempered (Figure 53). Yet the bendability of the tempered samples were better compared to the untampered sample (Table 12), although the surface hardness of the untampered sample was lower. The sample tempered at higher temperature possessed a slightly better bendability compared to the one tempered at 350°C. However the difference in hardness throughout the upper surface between these two samples is rather small. There appears to be a notable difference only at the depth of 0.05 mm. Yet, as seen from Table 13, hardness at this depth appears to be sufficiently small in case of both samples in order to prevent this depth to be crucial con-

cerning the formation of shear bands. Additionally, the sample tempered at 350°C possesses a smaller homogeneity index at the depth of 0.05 mm. This is inconsistent with the results obtained in this work, see Table 16.

The bendability results obtained in this works are consistent with a study by Nagataki et al. They found that the bendability first deteriorates as the tempering temperature increases; in case of their study this temperature is approximately 200°C. Yet, at a particular tempering temperature the degradation stops; at this tempering temperature the worst bendability is achieved. In case of the investigation by Nagataki et al., the turning point was approximately at the tempering temperature of 350°C. Then, as the tempering temperature continues to increase, the bendability respectively improves. However, with higher tempering temperatures as small bending radius as in lower tempering temperatures, cannot be obtained. [6]

Tempering temperature affect the morphology of carbide precipitates. It has been found that cementite precipitation plays a significant role in bendability. In case of a bcc material, cementites precipitate on the slip planes and grow along the slip directions. It is suggested by Nagataki et al. that tempering at temperature lower than 240°C fine (< a few 10 nm) carbides, i.e. transition carbides, precipitate and when tempering at temperatures above 300 °C coarse (> 100 nm) cementite precipitated. Furthermore at higher tempering temperatures it was found that the carbides inside martensite laths coarsen, and carbides precipitated along the grain boundaries. Hence it is suggested, the in terms of bendability, the material should be tempered at sufficiently low temperatures, in order to suppress the formation of cementite precipitation. [6]

9.8 Evaluation of the reliability of the regression models

The reliability of the regression models presented in Figures 97-99 is evaluated. This is done by determining that how does a test material fit in each of these models. The test material is presented in Table 19.

Table 19: Presentation of the test material used for evaluating the reliability of the models.

Heat	Thickness	Yield Strength	Hardness at the depth of 200 μm	HI at the depth of 50 μm	Standard deviation at the depth of 50 μm	Minimum bending radius $\left(R/t\right)$, (TD)
0.09C-1.1Mn 790°C	8 mm	904 MPa	412.5 HV	2.6	9.0	8

First the regression model presented in Figure 97 concerning the effect of surface hardness at the depth of 200 μm on bendability is evaluated.
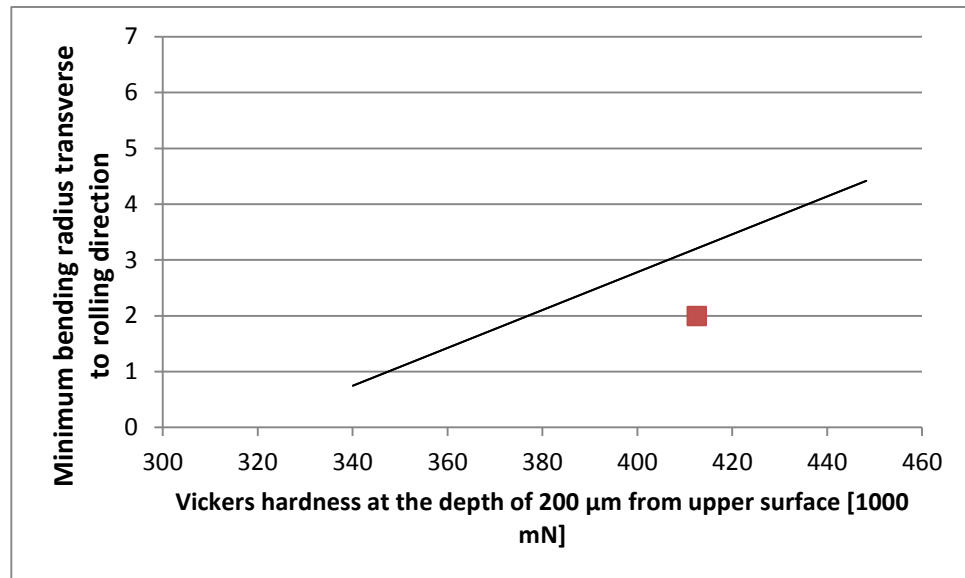
Figure 97: Evaluation of the reliability of the regression model concerning the effect average hardness at the depth of 200 μm on bendability.

According to Figure 97, the reliability of the regression model concerning the effect average hardness at the depth of 200 μm on bendability is mediocre.

Next the regression model presented in Figure 98 concerning the effect of standard deviation of hardness measurements at the depth of 50 μm on bendability is evaluated.
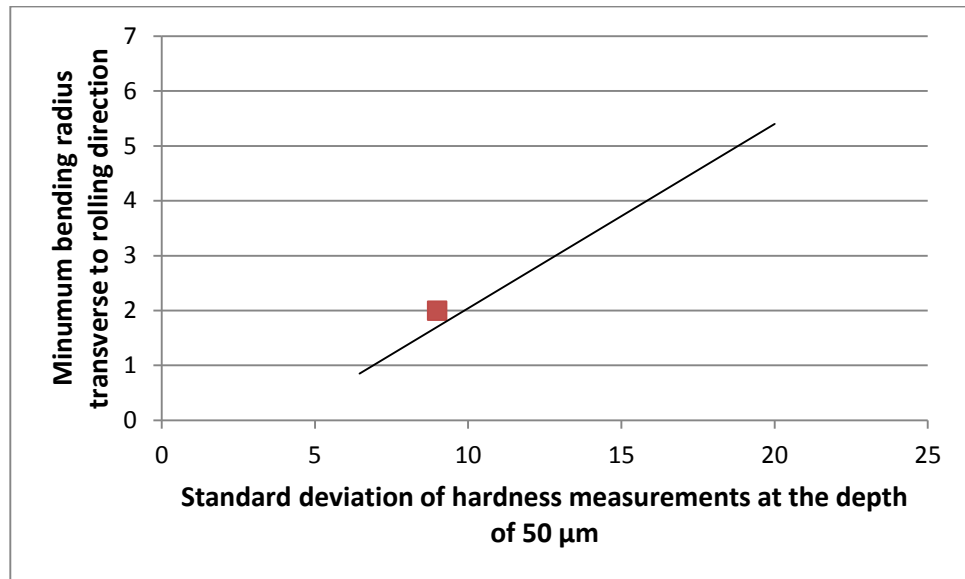
Figure 98: Evaluation of the reliability of the regression model concerning the effect of standard deviation of hardness measurements at the depth of 50 µm on bendability.

According to Figure 98, the test point fits the regression model notably well.

The regression model presented in Figure 99 concerning the effect of homogeneity index at the depth of 50 µm on bendability is evaluated.
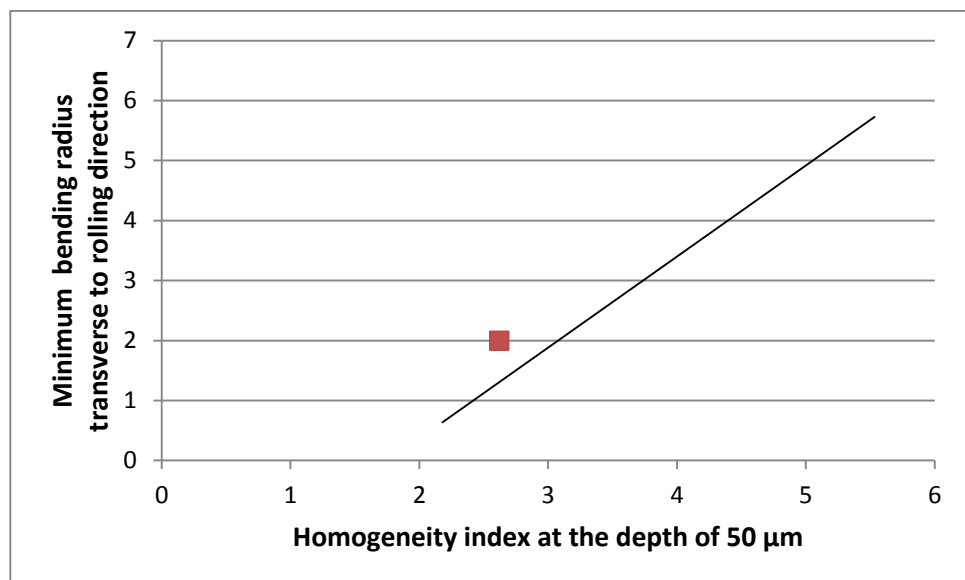
Figure 99: Evaluation of the reliability of the regression model concerning the effect of homogeneity index at the depth of 50 µm on bendability.

According to Figure 99, the test point fits the regression model highly well. Hence, it can be concluded on the grounds of Figures 98 and 99, that the regression model concerning homogeneity of surface is highly reliable.

10. CONCLUSIONS

In the present work the microstructural effects on bendability of complex phased UHSS were studied. The results suggest that the microstructure of the surface, which is subjected to tension, i.e. upper surface, governs bendability. Therefore factors contributing to a desired surface microstructure were additionally studied.

According to the results it can be stated that in case of UHSS microalloyed with niobium, the forming microstructure and hence hardness, are highly related to FRT, and carbon and manganese contents. The relationship between these factors and hardness was able to be defined by a regression analysis that is extremely valid ($R^2 = 92$). The microstructures of the materials used in this work comprise principally a mixture of lath-like bainite and martensite, and additionally a softer surface layer consisting of granular bainite and polygonal ferrite. The presence and extent of such layer are dependent on the material.

The hardness throughout the thickness is found to increase with both FRT, and carbon and manganese contents. A combination of high FRT with high Mn and C contents leads to an absence of the layer of granular bainite and ferrite, indicating that hardening occurs immediately from the surface. A low FRT results in the formation of higher transformation temperature products, i.e. ferrite and granular bainite, on the surface, due to the nucleation or even development of such product during hot rolling. Secondly, it leads to a highly pancaked austenite, which affects the phase transformation kinetics, so that the formation of higher temperature transformation products are promoted. Due to higher carbon and manganese contents, martensite (M_S) and bainite (B_S) start temperatures are reduced to lower temperatures. As a consequence of lower transformation temperatures, the forming microstructure is finer, which contributes to greater hardness. Furthermore, microstructures formed at lower temperatures possess greater dislocation density, due to the larger strains accompanying transformations occurring at low temperatures. Additionally, these elements contribute to enhanced hardenability.

The developing microstructure of surface is found to be affected by the presence of red scale. It is found that microstructure below a stripe of red scale immediately consists of a fine microstructure comprising lath-like bainite and martensite, i.e. lower temperature transformation products. Whereas, microstructure that is below a surface free of red scale, consists of granular bainite and polygonal ferrite, i.e. higher temperature transformation products. The effects of red scale on the underlying microstructure is proposed to be due its influence on thermal field by acting as an insulator. As a consequence of its insulating effect, the true FRT does not correspond to the nominal FRT. This signifies that in case of red scale the true FRT is greater than the nominal one, which leads to the formation of lower temperature transformation products than expected.

Deformation occurring during bending differs from the one taking place during tensile testing, which accounts for that mechanical properties attained by tensile testing are not valid for evaluating bendability. During bending yield strength is first exceeded at the upper layers. Therefore, as strains increase diffuse necking and eventually strain localization within the diffuse necking region occur merely at given upper layers. It is confirmed by the study that the formation of shear bands is a precursor for damage in bending complex phase UHSS. Shear bands are observed to develop prior to voids, which subsequently form with in shear bands. Shear bands appear not to form at the absolute surface. Instead they form at the depth range of 0.1-0.5 mm from upper surface at the bend region, which corresponds 1.25-6.25 % relative to the total sheet thickness. Furthermore, shear bands are found to orient at about 45° with respect to the surface, which signifies that shear bands grow along maximum shear stresses. Thus it can be proposed that microstructure of the upper layers govern bendability, to be precise properties affecting the extents of uniform elongation and diffuse necking in bending.

It is found that hardness of surface is the principal factor affecting bendability of UHSS due its relation with several other properties, which in turn govern the extents of both uniform and post-uniform elongations. A sufficiently soft layer, reaching to approximately 2.3-4.4 % relative to the total sheet thickness, is found to result in increased bendability. In order to guarantee a minimum bending radius of $3t$, microhardness to the depth of 0.35 mm is needed to be less than 400 Vickers. This can be achieved for example by a combination of carbon content of 0.06% and manganese content of 1.4% by weigth, and a FRT of 875°C.

The governing effect of hardness is accountable firstly due to its contribution to the extent of uniform elongation. It is suggested that the onset of diffuse necking is principally dependent on work-hardening capability (n), i.e. Considere Criterion. Yet in addition strain rate-sensitivity (m) is proposed to influence. The effect of both of these factors is explicable in terms of their governing role concerning hardening during deformation. Both of these factors are highly related to hardness; a lower hardness indicates increased values of m and n, and hence a delay concerning the onset of diffuse necking. In addition to the onset of diffuse necking, hardness determines also the initiation of strain localization. Strain localization is proposed to onset once local softening initiates, which signifies that locally increasing deformations can be provided by decreasing stresses. According to a criterion by Dillamore et al., formation of shear bands is prevented by high magnitudes of m and n, low magnitudes of initial dislocation density (N) and Taylor factor (M) and an increase in the gradient of M and N with increasing strain (ε). All of these factors are highly related to hardness; a lower hardness level contributes to desired magnitudes of these influencing factors. This signifies that lower hardness of surface is desirable concerning bendability, since it results in a requirement of larger strains in order that condition for strain localization is attained.

It is found that homogeneity of microstructure, i.e. deviation of hardness, affects merely at the depth of 0.05 mm from upper surface. The detrimental effect of an inhomogeneous microstructure is due to the local variations concerning resistance to dislocation movement. Local resistance to dislocation movement is related to hardness, and thus to factors discussed above. A lower local resistance is attained by a small local Taylor factor and a low initial dislocation density. This implies that grains possessing softer orientations and phases possessing lower hardness values are susceptible to high strain concentrations when bending. Due to the local increase in strains, the condition for instability is attained more rapidly compared to adjacent regions, where in the magnitude of strains is not equally high or even negligible in case of significant hardness differences. Yet, it is found that concerning materials studied in this work, both the harder and the softer constituents deform plastically. This indicates that the hardness difference is not notable and thus deformation is compatible between various phases. Yet, inhomogeneity arises from differences in orientations, and hence local Taylor factors. It is proposed that grains possessing high values of Taylor factor are susceptible to rotate to softer orientations and thus represent textural softening. Therefore it can be concluded that the detrimental effect of inhomogeneity concerning materials used in this work, is due to the difference in local orientations.

11. FUTURE WORK

Future work propositions applying to the development of plastic deformation during bending:

- Instantaneous measurements of strain during bending in order to achieve a comprehensive understanding concerning the development of strain during bending. In particularly, it is required to comprehend the depth range where the greatest strains occur and how the magnitude of strains decrease as approaching the centre line. By comprehending the strain development throughout the thickness enables to understand the requirements concerning the development of hardness, i.e. to what extent the so called softer layer is needed to reach.

Future work proposals concerning the effect of surface hardness on bendability:

- Study if bendability correlates with work-hardening exponent and strain-rate sensitivity values of the surface layer.

Future work proposals concerning the effect of homogeneity of microstructure on bendability:

- Nanoindentation measurements in order that the hardness differences between adjacent phases is able to be defined. This enables to define, whether differences in hardness values between adjacent phases contributes to a decrease in bendability.
- Instantaneous measurements of strain during bending in order that the magnitudes of strains in harder and softer phases are able to be defined.

Future work proposals concerning bendability:

- Clarify, whether the suggestion concerning the percentage thickness in relation to total sheet thickness in universal, i.e. the model can be applied to various sheet thicknesses.
- Comprehend the effect of tempering on bendability, since even though the surface hardness of the tempered samples was high, they possessed good bendability.

Future work suggestions concerning red scale:

- Clarify that at which point of process red scale forms at the surface of the steel.
- The effect of local concentrations, in particularly silicon, on the microstructure.
- Comprehend the effect of red scale on the microstructure. In particularly why the effect is in some cases notable and some cases it appears not to affect. It is needed

to clarify that does for example the thickness of the scale affect its function as an insulator or/and lubricant.

REFERENCES

[1]   S. Matsuoka, K. Hasega, Y. Tanaka, Newly-Developed Ultra-High Tensile Strength Steels with Excellent Formability and Weldability, JFE Steel Corporation, No. 10, 2007, p. 13.

[2]   K. Yamazaki, M. Oka, H. Yasuda, Y. Mizuyama, H. Tsuchiya, Recent Advances in Ultrahigh-Strength Sheet Steels for Automotive Structural Use, Nippon Steel Technical Report, No. 64, 1995, pp. 37-44.

[3]   Y.B. Xu, Y.L. Bai, Q. Xue, L.T. Shen, Formation, microstructure and development of the localized shear deformation in low-carbon steels, Acta Materialia, Vol. 44, Iss. 5, 1996, pp. 1917–1926.

[4]   Z. Marciniak, J.L Duncan, S.J. Hu, Mechanics of Sheet Metal Forming, Second Editon, Elsevier Ltd., 2002, pp. 1-13.

[5]   E. Tempelman, H. Shercliff, B. N. van Eyben, Manufacturing and Design: Understanding the Principles of How Things Are Made, Butterworth Heinemann, 2014, p. 47.

[6]   Y. Nagataki, S. Tsuyama, Y. Hosoya, Effect of Tempering Temperature on the Bendability of Martensitic Steels, JFE Steel Corporation, Steel Research Laboratory, Vol. 99, No. 3, 2013, pp. 245-253.

[7]   D. Reche, T. Sturel, A.F. Gourgues-Lorenzon, J. Besson, Damage Mechanisms of ultrahigh strength steels in bending application to a trip steel, European Conference of Fracture 18, Dresden, 2010, p. 7.

[8]   L. Xue, Localization conditions and diffused necking for damage plastic solids, Engineering Fracture Mechanics, Vol. 77, Iss. 8, 2010, pp. 1275–1297.

[9]   J. Joutsenvaara, Investigation of strain localization of high strength steel with the help of digital image correlation, Kemi-Tornio University of Applied Sciences, Technology RDI Department, Proceedings of the METNET Seminar 2012 in Izmir, 2012, pp. 19-29.

[10]   K. Hashiguchi, Localization and deformation, Elastoplasticity Theory, Springer-Verlag Berlin Heidelberg, Vol. 69, 2014, pp. 333-341.

[11]   M. Kuroda, V. Tvergaard Shear band development in anisotropic bent specimens, European Journal of Mechanics A-solids, Vol. 23, No. 5, 2004, pp. 811-821.

[12]   M. Lie, M. Dao, A micromechanics study on strain-localization fracture initiation in bending using crystal plasticity models, Philosophical Magazine A, Vol. 81, No. 8, 2000, pp. 1997-2020.

[13]   J. R. Rice, The Localization of Plastic Deformation, Theoretical and Applied Mechanics, Proceedings of the 14th International Congress on Theoretical and Applied Mechanics, North-Holland Publishing Company Delft, Vol. 1, 1976, p. 6.

[14]   K. Kawamura, K. Seto, Ultra High Strength Cold Rolled Steel Sheet having Excellent Bendability, Pat. US 20130048151, 16.02.2011 (28.02.2013).

[15]   T.V. Philip and T.J. McCaffrey, Ultrahigh-Strength Steels, Properties and Selection: Irons, Steels, and High-Performance Alloys, ASM Handbook, ASM International, Vol. 1, 1990, pp. 430–448.

[16]   M. Naderi, Hot Stamping of Ultra High Strength Steels, Rheinisch-Westfälischen Technischen Hochschule Aachen, 2007, pp. 7-20.

[17]   A. M. Hall, Introduction to Today's Ultrahigh Strength Structural Steels, ASTM special technical publication, American Society for Testing and Materials, Vol 498, p. 1.

[18]   World Auto Steel: Automotive Steel Definitions. Available (accessed on 20.11.2014): http://www.worldautosteel.org/steel-basics/automotive-steel-definitions/

[19]   S. P. Bhat, Advances in High Strength Steels for Automotive Applications, ArcelorMittal, Great Designs in Steel Seminar, p. 15. Available (accessed on 20.11.2014): http://www.autosteel.org/~/media/Files/Autosteel/Great%20Designs%20in%20Steel/GDIS%202008/12%20-%20Advances%20in%20AHSS%20for%20Automotive%20Applications.pdf

[20]   S. Tanga, Z.Y. Liua, G.D. Wanga, R.D.K. Misra, Microstructural evolution and mechanical properties of high strength microalloyed steels: Ultra Fast Cooling (UFC) versus Accelerated Cooling (ACC), Materials Science and Engineering: A, Vol 580, Iss. 15, 2013, pp. 257–265.

[21]   N. Shikanai, S. Mitao, S. Endo, Recent Development in Microstructural Control Technologies through the Thermo-Mechanical Control Process (TMCP) with JFE Steel's High-Performance Plates, JFE Technical Report, No. 11, 2008, 6 p.

[22]   D. Porter, New Hot-Rolled, High-Strength Structural Steels, High Technology Finland. Available (accessed on 01.02.2015): http://hightechfinland.com/direct.aspx?area=htf&prm1=577&prm2=article

[23]   V. Kesti, A. Kaijalainen, A. Väisänen, A. Järvenpää, A. Määttä, A.M. Arola, K. Mäntyjärvi, R. Ruoppa, Bendability and Microstructure of Direct Quenched Optim® 960QC, Materials Science Forum, Vols. 783-786, p. 1.

[24]   Ruukissa kehitetty suorasammutusteknologia palkittiin Suomalaisella Insinööri-työpalkinnolla, Rautaruukki Oyj, Uutisarkisto, 2012. Available (accessed on 10.11.2014) : http://www.ruukki.fi/Uutiset-ja-tapahtumat/Uutisar-kisto/2012/Ruukissa-kehitetty-suorasammutusteknologia-palkittiin-Suomalai-sella-Insinoorityopalkinnolla

[25]   J. Ehmer, High-strength and ultrahigh-strength TM steels, Cut sheet from hot-rolled steel strip and heavy plate, voestalpine Steel Division, 2014, pp. 1-6.

[26]   D. Reche, Relations between microstructure and bendability on TRIP-aided steels for automotive products, Engineering Sciences, Paris Institute of Technology, 2014, 205 p.

[27]   J. Galán, L. Samek, P. Verleysen, K. Verbeken, Y. Houbaert, Advanced high strength steels for automotive industry, Revista De Metallurgia, Vol. 48, pp. 120-121.

[28]   C. D. Horvath, The Future Revolution in Automotive High Strength Steel Usage, Materials and Appearance Center General Motors Corporation, ArcelorMittal, Great Designs in Steel Seminar, p. 9.

[29]   Introduction to Structures in Metals, Metallography and Microstructures, Vol 9, ASM Handbook, ASM International, 2004, pp. 23–30.

[30]   P.J.J. Kok, F.N.M. Korver, Modelling of Complex Microstructures in Multi Phase Steels, International Conference on Computational Plasticity, Complas X, 2009, 4 p.

[31]   Dual Phase (DP) Steels, Steel Types, World Auto Steel, Available (accessed on 20.11.2014): http://www.worldautosteel.org/steel-basics/steel-types/dual-phase-dp-steels/

[32]   Transformation-Induced Plasticity (TRIP) Steel, Steel Types, World Auto Steel, Available (accessed on 20.11.2014): http://www.worldautosteel.org/steel-ba-sics/steel-types/transformation-induced-plasticity-trip-steel/

[33] High-Strength Structural and High-Strength Low-Alloy Steels, Properties and Selection: Irons, Steels, and High-Performance Alloys, Vol 1, ASM Handbook, ASM International, 1990, pp. 389–420.

[34] G. Krauss, Steels: Processing, Structure, and Performance, ASM International, USA, 2005, 593 p.

[35] W. C. Chiou Jr., E. A. Carter, Structure and stability of Fe3C-cementite surfaces from first principles, Surface Science, Vol. 530, Iss. 1-2, 2003, p. 88.

[36] H.K.D.H. Bhadeshia, Bainite in Steels, The Institute of Materials, Second Edition, England, 2011, 460 p.

[37] B. L. Bramfitt, A.O. Benscote, Metallographer's Guide: Practice and Procedures for Irons and Steels, ASM International, 2002, pp. 33-34.

[38] H.M. Miekk-oja, Metallioppi, Teknillisten tieteiden akatemia, Third Edition, Helsiki, 1965, 671 p.

[39] J. D. Verhoeven, Steel Metallurgy for the Non-Metallurgist, ASM International, 2007, p. 37.

[40] H. K. D. H. Bhadeshia, Martensite in Steels, Materials Science & Metallurgy, 2002, 12 p. Available (accessed on 02.12.2014): http://www.msm.cam.ac.uk/phase-trans/2002/martensite.html

[41] E. Pereloma, D.V. Edmonds, Phase Transformations in Steels, Diffusionless Transformations, High Strength Steels, Modelling and Advanced Analytical Techniques, Vol. 2, Woodhead Publishing Series in Metals and Surface Engineering, 2012, pp. 36-39.

[42] H. R. Jafarian, E. Borhani, Effect of austenite grain morphology on variant selection of martensite transformed from ultra-fine grained austenite, Iranian Journal of Materials Science & Engineering, Vol. 10, No. 2, 2013, pp. 21-28.

[43] S. Morito, Y. Adachi ja T. Ohba, Morphology and Crystallography of Sub-Blocks in Ultra-Low Carbon Lath Martensite Steel, Materials Transactions, Vol. 50, No. 8, The Japan Institute of Metals, Japani, 2009, pp. 1919-1923.

[44] A. Shibata, T. Nagoshi, M. Sone, S. Morito ja Y. Higo, Evaluation of the block boundary and sub-block boundary strengths of ferrous lath martensite using a micro-bending test, Materials Science and Engineering A-structural Materials Properties Microstructure and Processing, Materials Science and Engineering A, Vol. 527, 2010, pp. 7538-7544.

[45] J. Chen, R. Cao, Micromechanism of Cleavage Fracture of Metals: A Comprehensive Microphysical Model for Cleavage Cracking in Metals, Butterworth-Heinemann, 2014, p. 102.

[46] H. K. D. H. Bhadeshia, Bainite in Steels, Graduate Institute of Ferrous Technology, POSTECH, Korea, 8 p., Availabe (accessed on 26.11.2014): http://cml.postech.ac.kr/a/lecture6.pdf

[47] L. Fielding, The Bainite Controversy, Department of Materials Science and Metallurgy University of Cambridge, Materials Science and Technology, Vol 29, Number 4, 2013, pp. 383-399.

[48] Lower Bainite, Department of Materials Science & Metallurgy, University of Cambridge, Available (Accessed on 01.11.2014): http://www.msm.cam.ac.uk/phase-trans/bainitec.html

[49] S. Zajac, J. Komenda, P. Morris, P. Dierickx, S. Matera, F. Penalba, Diaz, Technical Steel Research, Report EUR 21245EN, Luxembourg, 2005, p. 10.

[50] P. Clayton, K.J. Sawley, P.J. Bolton ja G.M. Pell, Wear Behaviour of Bainitic Steels, Wear, Elsevier, Vol. 120, 1987, pp. 199-220.

[51] J.Y.Koo, M.J.Luton , N.V.Bangaru, R. A. Petkovic, D.P.Fairchild, C.W.Petersen, H.Asahi, T.Hara, Y.Terada, M.Sugiyama, H.Tamehiro, Y. Komizo, S. Okaguchi, M. Hamada, A. Yamamoto, I. Takeuchi, Metallurgical Design of Ultra-High Strength Steels for Gas Pipelines, Proceedings of The Thirteenth International Offshore and Polar Engineering Conference Honolulu, Hawaii, USA, 2003, 18 p.

[52] S. Cobo, M. Gomez, P. Karjalainen, G. Kalla, Austenite strengthening and accumulated stress for optimum microstructures in modern bainitic microalloyed steels (Actress), Research Fund for Coal and Steel, European Commission, 2011, 132 p.

[53] Upper bainite, University of Cambridge, Materials Science & Metallurgy: Upper Bainite, Available (accessed on 25.10.2014): http://www.msm.cam.ac.uk/phase-trans/bainiteb.html

[54] P. Suikkanen, Development and Processing of Low Carbon Bainitic Steels, University of Oulu, Teknillinen tiedekunta, Konetekniikan laitos, Oulu, 2009, 486 p.

[55] H. Roelofs, S. Hasler, M. Lembke ja F.G. Caballero, Impact toughness of continuously cooled bainitic steels, Swiss Steel, 2nd International Conference of Super-High Strength Steels, Spain, 20 p.

[56]   S. V. Kailas, Mechanical Properties of Metals, Material Science, Department of Mechanical Engineering, Indian Institute of Science, 21 p.

[57]   W. F. Hosford, R. M. Caddell, Metal Forming: Mechanics and Metallurgy, Cambridge University Press, Edition 4, 2011, 327 p.

[58]   R.K. Bansal, A Text Book of Strength of Materials, Laxmi Publications, 2010, 1106 p.

[59]   M. Tisza, Physical Metallurgy for Engineers, ASM International, 2001, 401 p.

[60]   A. M. Hussein, S. I. Rao, M. D. Uchic, D. M. Dimidukd, A. El-Awady, Microstructurally based cross-slip mechanisms and their effects on dislocation microstructure evolution in fcc crystals, Acta Materialia, Vol. 85, 2015, p. 180.

[61]   A. S. Wadhwa, E. H. S. Dhaliwal, A Textbook of Engineering Material and Metallurgy, Firewall Media, 2008, 465 p.

[62]   X. Cai, Dislocation in Crystals, pp. 6-7. Available (accessed on 02.11.2014): http://www.usu.edu/nanolab/6530/presentation/Defects%20in%20Crystals.pdf

[63]   F.C. Campbell, Elements of metallurgy and engineering alloys, ASM International, 2008, 672 p.

[64]   A. S. Khan, Continuum Theory of Plasticity, John Wiley & Sons, 1995, p. 343.

[65]   R. K. Rajput, Engineering Materials & Metallurgy, S. Chand, 2006, p. 245.

[66]   R.E. Stoller, S.J. Zinkle, On the relationship between uniaxial yield strength and resolved shear stress in polycrystalline materials, Journal of Nuclear Materials, Elsevier, Vols. 283-287, 2000 pp .349-352.

[67]   W. Soboyejo, Mechanical Properties of Engineered Materials, Mechanical engineering, CRC Press, Vol. 152, 2002, p. 195.

[68]   D.P. Field, Textured Structures, Metallography and Microstructures, Vol 9, ASM Handbook, ASM International, 2004, pp. 215–226.

[69]   H. Hu, Texture of Metals, United States Steel Corporation, Research Laboratory, Gordon and Breach Science Publishers Ltd, 1974.

[70]   M. N. Shetty, Dislocations and Mechanical Behaviour of Materials, PHI Learning Pvt. Ltd, 2013, 1000 p.

[71]   The Unit Cell, UC Davis ChemWiki, Available (accessed on 10.11.2014): http://chemwiki.ucdavis.edu/Wikitexts/UC_Davis/UCD_Chem_124A%3A_Kauzlarich/ChemWiki_Module_Topics/The_Unit_Cell

[72]   K.W. Nealea; K. Inala, P.D. Wub,, Effects of texture gradients and strain paths on localization phenomena in polycrystals, International Journal of Mechanical Sciences, Vol. 45, Iss. 10, 2003, pp. 1672-1673.

[73]   R. Srinivasan, Engg Materials And Mettalurgy, Tata McGraw-Hill Education, Second edition, p. 248.

[74]   J.W.L. Pang, W. Liu, J.D. Budai, G.E. Ice, Inhomogeneous deformation behavior in intercrystalline regions in polycrystalline Ni, Acta Materialia, Vol. 65, 2014, pp. 393–399.

[75]   W. Abuzaida, H.Sehitoglua, J. Lambrosb, Plastic strain localization and fatigue micro-crack formation in Hastelloy X, Materials Science and Engineering: A, Vol. 561, 2013, pp. 507–519.

[76]   R. W. Cahn, P.Haasen, Physical Metallurgy, Edition 3, North-Holland, 1983, 1973 p.

[77]   J. C.-M. Li, Microstructure and Properties of Materials, World Scientific, Vol. 2, 2000, p. 206.

[78]   R. Hutanua, L. Claphama, R.B. Roggeb, Intergranular strain and texture in steel Luders bands, Acta Materialia, Vol. 53, Iss. 12, 2005, pp. 3517–3524.

[79]   Y.T. Zhang, Prediction of the Luders band in fine grained steel strips under uniaxial tension, Computational Materials Science, Vol. 41, Iss. 4, 2008, pp. 547–55.

[80]   J. A. Shaw, S. Kyriakides, Initiation and propagation of localized deformation in elasto-plastic strips under uniaxial tension, International Journal of Plasticity, Vol. 13, Iss. 10, 1997, pp. 837–871.

[81]   D.W. Beardsmore, J. Quinta da Fonsecab, J. Romerob, C.A. Englishc, S.R. Ortnerc, J. Sharplesa, A.H. Sherryb, M.A. Wilkes, Study of Lüders phenomena in reactor pressure vessel steels, Materials Science and Engineering: A, Vol. 588, 2013, pp. 151–166.

[82]   J. F. Hallai, S. Kyriakides, On the effect of Lüders bands on the bending of steel tubes. Part I: Experiments, International Journal of Solids and Structures, Vol. 48, Iss. 24, 2011, pp. 3275-3283.

[83]   B.K. Sokolov, V.V. Gubernatorov, I.V. Gervasyeva, A.K. Sbitnev, L.R,. Vladi-
        mirov, The Deformation and Shear Bands in the Fe-3%Si Alloy, Textures and
        Microstructures, Gordon and Breach Science, Vol. 32, 1997, pp. 21-39.

[84]   J. Jeschke, D. Ostermann, R. Krieg, Critical strains and necking phenomena for
        different steel sheet specimens under uniaxial loading, Nuclear Engineering and
        Design, Vol. 241, Iss. 6, 2011, pp. 2045–2052.

[85]   K.T. Ramesh, Nanomaterials: Mechanics and Mechanisms, Springer Science &
        Business Media, 2009, 316 p.

[86]   S. D. Antolovich, R. W. Armstrong, Plastic strain localization in metals: origins
        and consequences, Progress in Materials Science, Vol. 59, 2014, 1-160 p.

[87]   Y. Li, D. G. Karr, Prediction of ductile fracture in tension by bifurcation, locali-
        zation, and imperfection analyses, International Journal of Plasticity, Vol. 25,
        Iss. 6, 2009, pp. 1128–1153.

[88]   X. Sun, K.S. Choi, W.N. Liu, M.A. Khaleel, Predicting failure modes and ductil-
        ity of dual phase steels using plastic strain localization, International Journal of
        Plasticity, Vol 25, Iss 10, 2008, pp. 1888–1909.

[89]   X. Hu, M. Gaspérini, P. Van Houtte, Strain localization observed during shearing
        of some aluminium alloys and texture softening predicted by FC Taylor and
        Adavanced Lamel Model, Trans Tech Publications, Solid State Phenomena Vol
        105, 2005, pp. 363-370.

[90]   G. S. Burkhanov, V. S. Yusupov, A. E. Shelest, E. N. Sheftel, G. Yu. Lazarenko,
        Plastic deformation nonuniformity and localization during metal forming, Rus-
        sian Metallurgy (Metally), Vol. 2012, Iss. 7, 2012, pp. 592-598.

[91]   University of Cambridge: Slip in HCP metals 3: calculation of forces, Availabe
        (accessed on 01.11.2014):
        http://www.doitpoms.ac.uk/tlplib/slip/slip_in_hcp3.php

[92]   N. Jia, P. Eisenlohr, F. Roters, D. Raabe, X. Zhao, Orientation dependence of
        shear banding in face-centered-cubic single crystals, Elsevier, Acta Materialia,
        Vol. 60, 2012, pp. 3415–3434.

[93]   J. E. Bird, J. M. Carlson, Shear Band Formation During Sheet Forming,
        Springer-Verlag, Vol. 38, Iss. 11, 1986, pp. 47-54.

[94]   A.B. Lopes, E.F. Rauch, J.J. Gracio, Textural vs structural plastic instabilities in
        sheet metal forming, Acta Materialia, Vol. 47, Iss. 3, 1999, pp. 859–866.

[95]   H. E. Theis, Handbook of Metalforming Processes, CRC Press, 1999, 672 p.

[96]   X. Zuoa, Y. Chen, M. Wang, Study on microstructures and work hardening be-havior of ferrite-martensite dual-phase steels with high-content martensite, Mate-rials Research, Vol. 15, No. 6, 2012.

[97]   D. R. Askeland, P. P. Fulay, W. J. Wright, The Science and Engineering of Ma-terials, Cengage Learning, Vol. 6, 2010, 896 p.

[98]   M. F. Ashby, The deformation of plastically non-homogeneous materials, Philo-sophical Magazine, Vol. 21, Iss. 170, 1970, pp. 399-424.

[99]   T. Xu,Y. Feng, Z.Jin, S. Song, D. Wang, Determination of the maximum strain–hardening exponent, Materials Science and Engineering: A, Vol. 550, 2012, pp. 80–86.

[100] P. A. Eikrem, Z. L. Zhang, E. Østby, B. Nyhus, Plastic Strain Hardening Effect on Ductile Fracture Resistance, Gruppo Frattura, 8 p.

[101] R. Sedláček, W. Blum, J. Kratochvíl, S. Forest, Subgrain Formation during De-formation: Physical Origin and, Consequences, Metallurgical and Materials Transactions A, ASM International, Vol. 33, Iss. 2, 2002, pp. 319-327.

[102] R. Gedney, Sheet Metal Formability, Advanced Materials and Processes, Admet Inc, 2002, pp. 33-36.

[103] M. R. Akbarpour , A. Ekrami, Effect of ferrite volume fraction on work harden-ing behavior of high bainite dual phase (DP) steels, Materials Science and Engi-neering: A, Vol. 477, Iss. 1–2, 2008, pp. 306–310.

[104] D. T. Llewellyn, Steels: Metallurgy and Applications, Elsevier, 2013, 314 p.

[105] M. Hokka, Effect of Strain rate and temperature on the mechanical behavior of advanced high strength steels, Tampere University of Technology, 2008.

[106] G. Li, C. Zhu, Formation of shear bands in plane sheet, International Journal of Plasticity, Vol. 11, Iss. 5, 1995, pp. 605–622.

[107] S. Ganguly, S. Datta, N. Chakraborti, Genetic algorithm based search on the role of variables in the work hardening process of multiphase steels, Computational Materials Science, Vol. 45, Iss. 1, 2009, pp. 158–166.

[108] H. Ghassemi-Armaki, H. Ghassemi-Armakia, R. Maaß, S.P. Bhat, S. Sriram, J.R. Greerb, K.S. Kumar, Deformation response of ferrite and martensite in a dual-phase steel, Acta Materialia, Vol. 62, 2014, pp. 197–211.

[109] N. K.Balliger, T. Gladman, Work hardening of dual-phase steels, Materials Science and Technology, Vol. 15, Iss. 3, 1981, pp. 95-108.

[110] M. Calcagnotto, D. Ponge, Y. Adachi, D. Raabe, Effect of Grain Refinement on Strength and Ductility in Dual-Phase Steels, Proceedings of the 2nd International Symposium on Steel Science, The Iron and Steel Institute of Japan, 2009, 4 p.

[111] M.D. Taylor, K.S. Choi, X. Sun, D.K. Matlock, C.E. Packard, L. Xu, F. Barla, Correlations between nanoindentation hardness and macroscopic mechanical properties in DP980 steels, Materials Science and Engineering: A, Vol. 597, 2014, pp. 431–439.

[112] M. Gaspérinia, C. Pinnaa, W. Swiatnickib, Microstructure evolution and strain localization during shear deformation of an aluminium alloy, Acta Materialia, Vol. 44, Iss. 10, 1996, pp. 4195–4208.

[113] X. Hu, D. S. Wilkinson, M. Jain, R. K. Mishra, Modeling the influence of grain-level matrix inhomogeneity on strain localization in the presence of hard particles, Modelling and Simulation in Materials Science and Engineering, Vol. 15, No. 8, 2007, p. 908.

[114] M. Kuroda, V. Tvergaard, Effects of texture on shear band formation in plane strain tension/compression and bending, International Journal of Plasticity, Vol. 23, Iss. 2, 2007, pp. 244–272.

[115] S. Suwas, N. P. Gurao, Crystallographic texture in Materials, Journal of the Indian Institute of Science, Vol. 88, 2008, pp. 151-177.

[116] U. F. Kocks, N. Tomé, R. Wenk, Texture and Anisotropy, Preferred Orientations in Polycrystals and their Effect on Materials Properties, Cambridge University Press, 2000, 632 p.

[117] V. Randle, O. Engler, Introduction to Texture Analysis: Macrotexture, Microtexture and Orientation Mapping, CRC Press, 2000, 388 p.

[118] J.I. Verdeja, J. Asensio, J.A. Pero-Sanzb, Texture, formability, lamellar tearing and HIC susceptibility of ferritic and low-carbon HSLA steels, Materials Characterization, Vol. 50, Iss. 1, 2003, pp. 81–86.

[119] R. D. K. Misra, H. Nathani, F. Siciliano, T. Carneiro, Effect of texture and microstructure on resistance to cracking of high-strength hot-rolled Nb-Ti microalloyed steels, Metallurgical and Materials Transactions A, Vol. 35, Iss. 9, 2004, pp. 3024-3029.

[120] L. Xie, E. Nakamachi, Investigations of the formability of BCC steel sheets by using crystalline plasticity finite element analysis, Materials & Design, Vol. 23, Iss. 1, 2002, pp. 59–68.

[121] H. Mecking, U.F. Kocks, C. Hartig, Taylor factors in materials with many deformation modes, Scripta Materialia, Vol. 35, No. 4, 1996, pp. 465-471.

[122] A.J. Wilkinson, D.J. Dingley, Quantitative deformation studies using electron back scatter patterns. Acta Metallurgica et Materialia, Vol. 39, Iss. 12, 1991, pp. 3047-3055.

[123] Y. Liu, C. Wang, Q. Jiang, T. He, L. Zuo, Individual Grain Orientation and Heterogeneous Deformation in Cold-deformed Inter-stitial-Free Sheet Steel, Journal of Material Science and Technology, Vol. 23, No. 5, 2007, pp. 689-692.

[124] Yang, Q. Xie, L. Meng,a H. Dingb, Z. Tang, Dependence of deformation twinning on grain orientation in a high manganese steel, Scripta Materialia, Vol. 56, Iss. 11, 2007, pp. 931–934.

[125] M.R. Stoudt, J.B. Hubbard, M.A Iadicola, S.W. Banowic, A Study of the Fundamental Relationships between Deformation-Induced Surface Roughness and Strain Localization in AA5754, The Minerals, Metals & Materials Society and ASM International 2009, 11 p.

[126] A.D. Rollett, R. Khatirkar, L.A.I. Kestens, R. Petrov, I. Samajda, Strain localization in ultra low carbon steel, Materials Processing and Texture, 23. Relative Preference for Strain Localizations in Ultra Low Carbon Steel, 2008, p. 783.

[127] S.C. Chang, Q.D. Jiang, J.R. Hu and F.R. Chen, The texture and formation of shear bands in a hot rolled 7050 aluminum alloy, Scripta Materialia, Vol. 39, 1998, p. 583.

[128] J. W. Morris, Jr, Materials Science, A Survey of Materials Science I. Structure, Department of Materials Science and Engineering, pp. 106-107.

[129] P. Karjalainen, Myötymän paikallistumiseen vaikuttavista tekijöistä, University of Oulu, 2010, pp. 7-8.

[130] A. Glema, T. Lodygowski, The consequences of imperfections, Introduction to the analysis of plastic strain localization in solids, European Congress on Computational Methods in Applied Sciences and Engineering ECCOMAS 2004, Finland, 2004, 10 p.

[131] S.K Paul, A Ray, Influence of inclusion characteristics on the formability and toughness properties of a hot-rolled deep-drawing quality steel, Journal of Materials Engineering and Performance, Vol. 6, Iss. 1, 1997, pp. 27-34.

[132] A. Grajcar, M. Rozanski, M. Kaminska, B. Grzegorzyk, Study on Non-Metallic Inclusions in Laser-Welded Trip-Aided Nb-Microalloyed Steel, Archives of Metallurgy and Material, Vol. 59, Iss. 3, 2014, pp. 1163-1169.

[133] M. S. Joo, D.-W. Suh, H. K. D. H. Bhadeshia, Mechanical Anisotropy in Steels for Pipelines, ISIJ International, Vol. 53, 2013, pp. 1305-1314.

[134] C.C. Tasan, J.P.M. Hoefnagels, C.H.L.J. ten Horn, M.G.D. Geers, Experimental analysis of strain path dependent ductile damage mechanics and forming limits, Elsevier, Mechanics of Materials, Vol. 41, Iss. 11, 2009, pp. 1264–1276.

[135] J. Sarkar, T.R.G. Kutty, D.S. Wilkinson, J.D. Embury, D.J. Lloyd, Tensile properties and bendability of T4 treated AA6111 aluminum alloys, Materials Science and Engineering: A, Vol. 369, Iss. 1–2, 2004, pp. 258–266.

[136] W.B. Lievers, A.K. Pilkey, M.J. Worswick, The co-operative role of voids and shear bands in strain localization during bending, Mechanics of Materials, Elsevier, Vol. 35, pp. 661-674.

[137] V. Tvergaard, Ductile shear fracture at the surface of a bent specimen, Mechanics of Materials, Vol. 6, Iss. 1, Elsevier, 1987, pp. 53–69.

[138] M. A. Greenfielfd, H. Margolin, The Mechanism of Void Formation, Void Growth, and Tensile Fracture in an A1loy Consisting of Two Ductile Phase, Metallurgical and Materials Transactions A, Vol. 2, 1971, pp. 1841-1847.

[139] A. Gysler, F.-J. Grau, G. Luetjering, Influence of Microstructural Induced Crack Front Geometry Variations on Fatigue Crack Growth of High-Strength Al-Alloys, Fatigue 93, Proceedings of 5th International Conference on Titanium, Vol. 3, 1984.

[140] R.N. Gardner, T.C. Pollock, H.G.F. Wilsdorf, Crack initiation at dislocation cell boundaries in the ductile fracture of metals, Materials Science and Engineering, Vol. 77, 1977.

[141] G. Avramovic-Cingara, A.R. Saleh, M.K. Jain, D.S. Wilkinson, Void nucleation and growth in dual-phase steel 600 during uniaxial tensile testing, Metallurgical and Materials Transactions A, 2009, Vol. 40, Iss. 13, pp. 3117-3127.

[142] D. Hull, D. J. Bacon, Introduction to Dislocations, Materials science and technology, Elsevier, Vol. 37, 2011, p. 203.

[143] M. Oka, H. Takechi, The effect of metallurgical factors on the formability of steel sheets, Formability and Metallurgical Structure, 1986, pp. 83-99.

[144] Y. Bergström, Y. Granbom, D. Sterkenburg, A Dislocation-Based Theory for the Deformation Hardening Behavior of DP Steels: Impact of Martensite Content and Ferrite Grain Size, Journal of Metallurgy, Vol. 2010, 2010, p. 1.

[145] H. Ghadbeigi, C. Pinna, S. Celotto, J.R. Yates, Local plastic strain evolution in a high strength dual-phase steel, Materials Science and Engineering: A, Vol. 527, Iss. 18–19, 2010, pp. 5026–5032.

[146] L. Ryde, O. Lyytinen, P. Peura, M. Titova, Y. Vilander Granbom, T. Hebesberger, Cold-rolled complex-phase (CP) steel grades with optimised bendability, stretch-flangeability and anisotropy (CP-Steels), European Commission Research Fund for Coal and Steel, Directorate-General for Research and Innovation, 2010, p. 10.

[147] N. Hoon Goo, C. Kang, Analysis of the surface-roughening phenomenon in P-added bake-hardened steel sheets, Integrating Materials and Manufacturing Innovation, Vol. 3, Iss. 23, 2014, p. 2.

[148] Y. Guilhem, S. Basseville, H.Proudhon, G. Cailletaud, Effects of surface roughness on plastic strain localization in polycrystalline aggregate, MATEC Web of Conferences 12, EDP Sciences, 2014, p. 1.

[149] T. Abe, Surface roughening and formability in sheet metal forming of polycrystalline metalbased on r-value of grains, International Journal of Mechanical Sciences, Vol. 86, 2014, pp. 2–6.

[150] L. Mattei, D. Daniel, G. Guiglionda, H. Klöcker, J. Drivera, Strain localization and damage mechanisms during bending of AA6016 sheet, Materials Science and Engineering: A, Vol. 559, Elsevier, 2013, pp. 812–821.

[151] B. N. Legarth, A. B. Richelsen, Surface instabilities during straining of anisotropic materials, International Journal of Mechanical Sciences, Vol. 48, Iss. 5, 2006, pp. 517–525.

[152] Z.Q. Wang, I.J. Beyerlein, R. LeSar, Slip band formation and mobile dislocation density generation in high rate deformation of single fcc crystals, Philosophical Magazine, Taylor & Francis, 2008, pp. 1321-1333.

[153] A. Davidkova, M.K. Jainb, R.H. Petrova, D.S. Wilkinsond, R.K. Mishra, Strain localization and damage development during bending of Al–Mg alloy sheets, Materials Science and Engineering: A, Elsevier, Vol. 550, 2012, pp. 395–407.

[154] R. Becker, Effect of strain localization on surface roughening during sheet forming, Acta Materialia, U.S.A., Vol. 46, Iss. 4, 1998, pp. 1385–1401

[155] B. Kinsey, X. Wu, Tailor Welded Blanks for Advanced Manufacturing, Woodhead Publishing, USA, 2011, p. 191.

[156] T. Piiroinen, Teräsrakenteiden suunnitteluohjeita parempaan valmistettavuuteen: Onnistuneen suunnittelun periaatteita - DFMA, Savonia-ammattikorkeakoulu, HitNet, 2013, p. 25.

[157] Press Brakes, Metalworking: Sheet Forming, ASM Handbook, Vol. 14B, ASM International, 2006, pp. 212 – 220.

[158] J. Steninger, A. Melander, The relationship between bendability, tensile properties and particle structure of low carbon steel, Scandinavian Journal of Metallurgy, Vol. 11, 1982, pp. 55-71.

[159] Bending of Sheet Metal, Metalworking: Sheet Forming, Vol 14B, ASM Handbook, ASM International, 2006, pp. 295–306.

[160] A. Karppinen, Ohutlevyjen taivutus, MET, Tekninen tiedotus 23, 1986, p. 12.

[161] T. Erkkilä, Takaisinjousto särmäyksessä, Metalliteollisuuden keskusliitto, Tekninen tiedotus 27, Finland, 1985, pp. 4-5.

[162] T. Altan, A. E. Tekkaya, Sheet Metal Forming: Processes and Applications, ASM International, 2012, pp. 20-22.

[163] Zhang, Z.T., Hu, S.J., Stress and residual stress distributions in plane strain bending, International Journal of Mechanical Sciences, Vol. 40, 1998, pp. 533-543.

[164] Wu, J., Zhou, D., Zhang, L., Zhou, Y.J., Du, C.Q., Shi, M.F., A failure criterion for stretch bendability of advanced high strength steels, SAE Technical Paper, No. 2006-01-034, 2006.

[165] M. K. Choi, H. Huh, Effect of Punch Speed on Amount of Springback in U-bending Process of Auto-body Steel Sheets, Procedia Engineering, 11th International Conference on Technology of Plasticity, Vol. 81, Japan, 2014, pp. 963-968.

[166] T. Vuoristo, Effect of strain rate on the deformation behavior of dual phase steels and particle rein-forced polymer composites, Tampere University of Technology, 2004, pp. 8-222.

[167] D-K. Leu, A simplified approach for evaluating bendability and springback in plastic bending of anisotropic sheet metals, Journal of Materials Processing Technology, Vol. 66, Iss. 1–3, 1997, pp. 9–17.

[168] D. Rèche,T. Sturel, O. Bouaziz, A. Col, A.F. Gourgues-Lorenzon, Damage development in low alloy TRIP-aided steels during air-bending, Materials Science and Engineering: A, Vol. 528, Iss.15, pp. 5241–5250.

[169] K. Mattiasson, J. Jergéus, P. DuBois, On the prediction of failure in metal sheets with special reference to strain path dependence, International Journal of Mechanical Sciences, Vol. 88, 2014, pp. 175-191.

[170] M. Kaupper, M. Merklein, Bendability of advanced high strength steels—A new evaluation procedure, CIRP Annals - Manufacturing Technology, Vol. 62, Iss. 1, 2013, pp. 247-250.

[171] Y. Nagataki, S. Tsuyama, Y. Hosoya, Effect of microstructure on bendability and delayed fracture resistance of ultra-high-strength steel sheet,   29th International Symposium on Automotive Technology and Automation. Vol. 1, 1996, pp. 87-94.

[172] R. Denninger, M. Liewald, C. Hel, M. Sindel, Investigations on Bendability of Lightweight Materials for Various Load Paths, The 14th International ESAFORM Conference on Material Forming: ESAFORM 2011. AIP Conference Proceedings, Vol. 1353, Iss. 1, p. 1601.

[173] A.R. Ragab, Ch. A. Saleh, Evaluation of bendability of sheet metals using void coalescence models, Materials Science and Engineering: A, Vol. 395, Iss. 1–2, 2005, pp. 102–109.

[174] X. Chena, H. Jianga, Z. Cuia, C. Liana, C. Lua, Hole expansion characteristics of ultra high strength steels, Procedia Engineering, 11th International Conference on Technology of Plasticity, ICTP 2014, Vol. 81, Japan, 2014, pp. 718-723.

[175] I. Tsoupis, S. Hildering, M. Merklein, Bending of high-strength low-alloyed steel with respect to edge crack sensitivity caused by shearing operations, Procedia Engineering, 11th International Conference on Technology of Plasticity, ICTP 2014, Vol. 81, Japan, 2014, pp. 712-717.

[176] P. Castany, F. Diologent, A. Rossoll, J.-F. Despois, C. Bezencon, Influence of quench rate and microstructure on bendability of AA6016 aluminum alloys, Materials Science and Engineering: A, Vol. 559, 2013, pp. 558–565.

[177] J. Lämsä, A. Väisänen, J. Heikkala, A. Järvenpää, Correlation of Tensile Test Parameters and Bendability of High-Strength Steels, Key Engineering Materials, Vol. 554-557, 2013, pp. 12-20.

[178] T. Nonaka, K. Goto, H. Taniguchi, K. Yamazaki, Development of Ultra-High-Strength Cold-Rolled Steel Sheets for Automotive Use, Nippon Steel Technical Report, No. 88, 2003, pp. 13-15.

[179] G. D. Motovilina, V. V. Ryabov, E. I. Khlusova, Effect of structure on the amount of uniform elongation for strip steel, Metallurgist, Springer US, Vol. 55, Iss. 9-10, 2012, pp. 678-684.

[180] F. G Caballero, C García-Mateo, j Cornide, S Allain, J Puerta, M Crouvizier, T Mastrorillo, L Jantzen, E Vuorinen, L. E Lindgren, K Eriksson, G Berglund, A Hirvi, V Lang, T. T Nyo, P Suikkanen, A. J Ristola, New Advanced Ultra High Strength Bainitic Steels: Ductility and Formability (DUCTAFORM), Euroopan komissio, Tutkimuksen ja innovoinnin pääosasto, 2013, pp. 50-51.

[181] B.P.J. Sandvik, H.P. Nevalainen, Structure-Property Relationship in Commercial Low-Alloy Baintic-Austenitic Steel with High Strength, Ductility and Toughness, Metal Technology, 1981, pp. 213-220.

[182] D.J. Lloyd, Ductility and Bendability in 6000 Series Automotive Alloys 211, Proceedings of Symposium: Automotive Alloys, TMS, San Diego, 2000, pp. 211–221.

[183] S. Kalpakjian, Mechanical Testing for Metalworking Processes, Mechanical Testing and Evaluation, ASM Handbook, ASM International, Vol 8, 2000, pp. 70–78.

[184] R. K. Rajput, A Textbook of Manufacturing Technology: Manufacturing Processes, Firewall Media, 2007, pp. 195-200.

[185] A. Hudgins, The susceptibility to shear fracture in bending advanced high strength sheet steels, Proceedings from the Materials Science & Technology Conference, 2007, p. 145.

[186] M. Ben Bettaieb, X. Lemoine, L. Duchene, A. Habraken, Study of bendability of steel sheets, Steel Research International, Verlag Stahleisen GmbH, Iss. 79, 2008, pp. 225-232.

[187] G. Revankar, Introduction to Hardness Testing, Mechanical Testing and Evaluation, ASM Handbook, ASM International, Vol. 8 2000, pp. 197–202

[188] K. Herrmann, Hardness Testing: Principles and Applications, ASM International, 2011, p. 4.

[189] G. Zamfirova, V. Lorenzo, R. Benavente, J. M. Pereña, On the Relationship Between Modulus of Elasticity and Microhardness, Journal of Applied Polymer Science, Vol. 88, Iss. 7, 2003, pp. 1794–1798.

[190] M. O. Lai, K. B. Lim, On the prediction of tensile properties from hardness tests, Journal of Materials Science, Vol. 26, Iss. 8, 1991, pp. 2031-2036.

[191] D. Poweleit, Steel Castings Properties, Casting, ASM Handbook, ASM International, Vol. 15, 2008, p 949–974.

[192] Cutting rules for automated processing, Sandvik Dieflex™ Auto, Sandvik, DATASHEET S-5619, 2004, pp. 1-3.

[193] H. Kawata, H. Kawata, N. Maruyam, A. Murasato, A. Minami, Akinobu, T. Yasui, T. Kuwayama, S. Yonemura, High-Strength Galvanized Steel sheet Excellent in Bendability and Manufacturing Method thereof, Pat. US 20140212684, 31.07.2014.

[194] S. Hayato, N. Katsumi, F. Yoshimasa, M. Noriaki, M.Takayuki, High Strength Hot Rolled Steel Sheet Having Excellent Bendability and Method for Manufacturing the Same, Pat. 20130167985, 15.09.2011 (11.07.2013).

[195] S. Takagi, K. Hasegawa, High-strength molten-zinc-plated steel sheet having excellent bendability and weldability, and process for production thereof, Pat. US 20130071687, 30.05.2010 (10.04.2013)

[196] J. H. Lee, Y. R. Cho, S. D. Choo, Tensile properties and bendability of B-bearing martensitic steels, Metal 2014, pp. 1-5.

[197] M. J. Peet, Transformation and tempering of low–temperature bainite, University of Cambridge, Department of Materials Science and Metallurgy, England, 2010.

[198] H. Aydin, Relationship Between a Bainitic Structure and the Hardness in the Weld Zone of the Friction-stir Welded X80 API-grade Pipe-line Steel, Uludag University, Faculty of Engineering and Architecture, Department of Mechanical Engineering, Turkey, 2014, 8 p.

[199] C. Garcia-Mateo, F.G. Caballero, H.K.D.H Bhadeshia, Mechanical properties of low-temperature bainite, Materials Science Forum, Vols. 500-501, 2005, pp. 492-502.

[200] A. Hattiangadi, J. Cai, L. Chuzhoy, M. L. Johnson, Prediction of residual stress and damage distribution using explicit microstructure level simulation of martensitic transformation, ASM Heat treating society, ASM International, 2005, 378 p.

[201] C. Kami, K. Yamazaki, High-strength hot rolled steel sheet with excellent bendability and low-temperature toughness, and method for manufacturing the same, Pat. US 20140251513 A1, 31.10.2012 (11.09.2014).

[202] S.-Y. Lee, H.-C. Lee, Y.-J. Kwon, Ultra-high-strength steel bar and method for manufacturing same, Pat. US20130098513 A1, 18.04.2011 (25.04.2013).

[203] H. Okada, T. Fukagawa, Y. Maehara, Mechanism of red scale defect formation in silicon-added hot-rolled steel sheets, The Iron and Steel Institute of Japan (ISIJ) International, Vol. 34, 1994, pp. 906-911.

[204] R.D.K. Misraa, H. Nathania, J.E. Hartmannc, F. Sicilianod, Microstructural evolution in a new 770 MPa hot rolled Nb–Ti microalloyed steel, Materials Science and Engineering: A, Vol. 394, Iss. 1–2, 2005, pp. 339-352.

[205] J. Talonen, Development of next generation high strength steels, Outokumpu Oyj, FIMECC, 2013, 10 p.

[206] A. Kaijalinen, MSc. (Tech), Reasearcher, University of Oulu, Interview, 2015.

[207] C. Soyarslan, M. Malekipour Gharbi, A.E. Tekkaya, A combined experimental–numerical investigation of ductile fracture in bending of a class of ferritic–martensitic steels, International Journal of Solids and Structures, Vol. 49, Iss. 13, 2012, pp. 1608–1626.

[208] M. Mohrbacher, Microstructural Optimization for Multiphase Steels with Improved Formability and Damage Resistance, NiobelCon, pp. 1-4.

[209] A. Masashi, S. Noriyuki, M. Naoki, M. Akinobu, S. Koji, High strength steel sheet excellent in ductility and bendability and having maximum tensile strength of ≥900 MPa, method for producing high strength cold rolled steel, and method for producing high strength galvanized steel sheet, Pat. JP2009000272069, 30.11.2009 (09.07.2011).

[210] K. Wu, Z. Li, A. M. Guo, X. He, L. Zhang, A. Fang ja L. Cheng, Microstructure Evo-lution in a Low Carbon Nb–Ti Microalloyed Steel, ISIJ International, Vol. 46 No. 1, 2006, pp. 161-165.

[211] X.L. Wan, R. Wei, K.M. Wu, Effect of acicular ferrite formation on grain refinement in the coarse-grained region of heat-affected zone, Materials Characterization, Vol. 61, Iss. 7, 2010, pp. 726–731.

[212] H. F. Lan, L. Xiu Du, X. H. Liu, Microstructure and Mechanical Properties of a Low Carbon Bainitic Steel, Steel Research International, Vol. 84, Iss. 4, 2013, pp. 352–361.

[213] G. Krauss, Martensite in steel: strength and structure, Materials Science and Engineering A273–275, USA, 1999, pp. 40–57.

[214] A. Ghosh, Secondary Steelmaking: Principles and Applications, CRC Press, 2000, p. 256.

[215] F. B. Pickering, Some effects of non-metallic inclusions on the properties of steels, Chicago: Iron and Steel Society, 1989.

[216] Cold rolled steel sheet, T. Murakami, A. Ibano, Pat. US 8343288, 06.06.2009 (01.01.2013).

[217] T. B. Cox, J. R. Low, An investigation of the plastic fracture of high strength steels, Research Grant NGR 39-087-003, NASA Technical Report No. 3, Carnegie-Mellon University, 1972, 40 p.

[218] C. H. Huang, C. F. Huang, Y. K. Juang, C. T. Chen, Improvement in edge bendability of hot rolled high tensile strength steel sheet, China Steel Technical Report, No. 6, 1992, pp. 149-155.

[219] D. Askeland & W. Wright, Essentials of Materials Science & Engineering, Third Edition, Cengage Learning, 2013, 624 p.

[220] T. V. Rajan, C. P. Sharma, A. Sharma, Heat Treatment: Principles and Techniques, Prentice-Hall of India, 1994, p. 101.

[221] A. J. Kaijalainen, P. Suikkanen, L. P. Karjalainen, J. J. Jonas Effect of Austenite Pancaking on the Microstructure, Texture, and Bendability of an Ultrahigh-Strength Strip Steel, Metallurgical and Materials Transactions A, Vol. 45, Iss. 3, 2013, p. 1.

[222] R. D. K. Misra, K. K. Tenneti, G. C. Weatherly, G. Tither, Microstructure and Texture of Hot-Rolled Cb-Ti and V-Cb Microalloyed Steels with Differences in Formability and Toughness, Metallurgical and Materials Transactions A, Vol. 34, Iss. 10, 2003, p. 2348.

[223] C.L. Xie, E. Nakamachi, The effect of crystallographic textures on the formability of high-strength steel sheets, Journal of Materials Processing Technology, Vol. 122, Iss. 1, 2002, pp. 104–111.

[224] K. Ohashi, H. Utsunomiya, R. Matsumoto, Evaluation of r-value of steels using Vickers hardness test, Journal of Physics: Conference Series 379, 2012, p. 1.

[225] K. Tomita, T. Shiozaki, T. Urabe, A. Yoshitake, Development of 780MPa Grade High Strength Hot Rolled Steel Sheet, Seoul 2000 FISITA World Automotive Congress, Korea, 2000, 7 p.

[226] J. J. Haapamäki, S. M. Tamminen, J. J. Röning, Data mining methods in hot steel rolling for scale defect prediction, Neurogroup / ISG, University of Oulu, Department of Electrical and Information Engineering, Computer Engineering Laboratory, 5 p.

[227] Hot rolled descaled steel sheets – TDM, Todoaceros, Available (accessed on 08.02.2015): http://www.todoaceros.com/eng/products/products/tdm-sheets.html.

[228] H. Okada, T. Fukagawa, H. Ishihara, A. Okamoto, M. Azuma, Y. Matsuda, Prevention of Red Scale Formation during Hot Rolling of Steels, The Iron and Steel Institute of Japan (ISIJ) International, Vol. 35, No. 7, 1995, pp. 886-891.

[229] M.Okita, A. Nagai, Sinagawaand, K. Horinouchi, Current Advances in Materials and Processes - The Iron and Steel Institute of Japan (CAMP-ISIJ),

[230] S. Taniguchi, Y. Hanamoto, J. Nakata, Influence of cooling rate and steel composition on the scale failure characteristics during cooling of Si-containing low carbon steels, Material Science Forum, Vol. 522-523, 2006, pp. 505-512.

[231] ASTM E290 – 14, Standard Test Methods for Bend Testing of Material for Ductility, ASTM International, West Conshohocken, PA, 2014.

[232] J.A. Heikkala, A.J. Väisänen, Usability testing of ultra-high-strength steels, Proc. 11th Biennal Conference on Engineering Systems Design and Analysis, Nantes, France, ASME, 2012, pp. 163-173.

[233] K. Ohashi, H. Utsunomiya ja R. Matsumoto, Evaluation of r-value of steels using Vickers hardness test, Division of Materials and Manufacturing Science, Graduate School of Engineering, Osaka University, 2-1 Yamadaoka, Suita, Osaka 565-0871, Japan, 7 p.

[234] R. C. Sharma, Principles of heat treatment of steels, New Age International, 2003, 340 p.

[235] S. A. Balogun, G. I. Lawal, O. I. Sekunowo, S. O. Adeosun, Influence of finishing temperature on the mechanical properties of conventional hot rolled steel bar, Journal of Engineering and Technology Research Vol. 3, Iss. 11, 2011, pp. 307-313.

[236] R. Denys, Pipeline Technology: Proceedings of the 3rd International Pipeline Technology Conference, Gulf Professional Publishing, Belgium, 2000, p. 295.

[237] R. Abbaschian, R. Reed-Hill, Physical metallurgy principles, Cengage Learning, 2008, pp. 603-651.

[238] W. F. Hosford, Mechanical Behavior of Materials, Cambridge University Press, 2005, 425 p.

[239] A. Martinez Lopez, A.H. van den Boogaard, Formability Limit Curves under Stretch-Bending, Research Program of the Materials innovation institute M2i, p 1-2.

[240] G. Centeno, , A.J. Martínez-Donaire, C. Vallellano, L.H. Martínez-Palmeth, D. Morales, C. Suntaxi, F.J. García-Lomas, Experimental Study on the Evaluation of Necking and Fracture Strains in Sheet Metal Forming Processes, Procedia Engineering, Vol. 63, 2013, pp. 650–658

[241] Aramis Tensile Test for a complex phase steel with a yield strength of 700 MPa, Internal article, SSAB Europe Oy, 2014.

[242] Y. Weng, H. Dong, Y. Gan, Advanced Steels: The Recent Scenario in Steel Science and Technology, Springer-Verlag Berlin Heidelberg, 2011, 511 p.

[243] A. Consider, Annales des Ponts et Chaussées 9, chapter L'emploi du fer et de l'acier dans les constructions, 1885, pp. 574-775.

[244] Plastic instability and the onset of tensile instability, p. 5. Available (accessed on): http://www.kstreetstudio.com/science/experiments/files/TensileInstability.pdf

[245] H. Y. Yu, Strain-hardening behaviors of TRIP-assisted steels during plastic deformation, Materials Science and Engineering: A, Vol. 479, Iss. 1–2, 2008, pp. 333–338.

[246] E.W. Hart, Acta Metallurgica, Vol. 15, 1967, pp. 351–355.

[247] R. H. Wagoner, N. M. Wang, Operant strain-rate sensitivity during tensile necking, Metallurgical and Materials Transactions A, Vol. 14A, 1983, pp. 2395-2406.

[248] A. K. Ghosh, The influence of strain hardening and strain rate sensitivity on sheet metal forming, Journal of Engineering Materials and Technology, Vol. 99, Iss. 3, 1977, pp. 264-274.

[249] R. A. Ayres, Thermal gradients, strain rate and ductility in sheet steel tensile specimens, Metallurgical and Materials Transactions A, Vol. 14A, 1985, pp. 37-43.

[250] M. F. Shi, D. J. Meuleman, On certain aspects of strain rate sensitivity of sheet metals, Mechanics of Sheet Metal Forming, Journal of Materials Engineering and Performance, Vol. 4, Iss. 3, 1995, pp. 321-333.

[251] J. R. Davis, Tensile Testing, 2nd Edition, ASM International, 2004, p. 102.

[252] R. Pearce, Sheet Metal Forming, Springer Science & Business Media, 1991, p. 19.

[253] I.L. Dillamore, J.G. Roberts, A.C. Bush, Occurrence of shear bands in heavily rolled cubic metals, Materials Science and Technology, Vol. 13, Iss. 2, 1979, pp. 73–77.

[254] I. S. Kim, S. S. Kang, Dynamic strain aging in SA508-class 3 pressure vessel steel, International Journal of Pressure Vessels & Piping, Vol. 62, Iss. 2. 1995, pp. 123-129.

[255] T. H. Courtney Mechanical Behavior of Materials: Second Edition, Waveland Press, 2005, p. 134.

[256] P. Larour, Strain rate sensitivity of automotive sheet steels: influence of plastic strain, strain rate, temperature, microstructure, bake hardening and pre-strain, Rheinisch -Westfälischen Technischen Hochschule Aachen, 2010, p. 234. Availabe (accessed on 01.01.2015): http://darwin.bth.rwth-aachen.de/opus3/volltexte/2010/3271/pdf/3271.pdf

[257] A. Uenishi, H. Yoshida, S. Yonemura, S. Hiwatashi, S. Hirose, N. Suzuki, High strain rate properties of high strength steel sheets, International Journal of Automotive Engineering, Vol. 2, 2011, p. 113.

[258] B. A. Niemeier, J. R. Newby, Formability Topics - Metallic Materials, ASTM special technical publication, ASTM International, 1978, p. 13.

[259] K. Hyoung Seop, K. Sung Ho, R. Woo-Seog, Finite Element Analysis of the Onset of Necking and the Post-Necking Behaviour during Uniaxial Tensile Testing, Materials Transactions, Vol. 46, No. 10, 2005, pp. 2159-2163.

[260] G.E. Dieter, Evaluation of Workability for Bulk Forming Processes, Metalworking: Bulk Forming, ASM Handbook, ASM International, Vol. 14A, 2005, pp. 587–610.

[261] S. Kalluri, P. J. Bonacuse. Multiaxial Fatigue and Deformation Testing Techniques, ASTM special technical publication, 1996.

[262] S. Hashmi, Comprehensive Materials Processing, Newnes, 2014, p. 476.

[263] T. Miura, K. Fujii, K. Fukuya, K. Takashima, Influence of crystal orientation on hardness and nanoindentation deformation in ion-irradiated stainless steels, Journal of Nuclear Materials, Vol. 417, Iss. 1, 2011, pp. 984-987.

[264] D. A. Porter, K. E. Easterling, M. Sherif, Phase Transformations in Metals and Alloys, Third Edition, CRC Press, 2009, p. 157.

[265] D. Antolovich, Alloy Design for Fatigue and Fracture, Fatigue and Fracture, ASM Handbook, ASM International, Vol. 19, 1996, pp. 27–41.

[266] LV. Samarasekerat, E.B. Hawboltt, Overview of modelling the microstructural state of steel strip during hot rolling, The Joumal of The South African Institute of Mining and Metallurgy, 1995, p. 158.

[267] K. Murata, H. Morise, M. Mitsutsuka, H. Naito, T. Komatsu, S. Shide, Transactions of the Iron and Steel Institute of Japan, Vol. 24, 1984, B-309.

[268] J. G. Lenard, L. Barbulovic-Nad, The Coefficient of Friction During Hot Rolling of Low Carbon Steel Strips, Journal of Tribology, Vol. 124, Iss. 4, 2002, p. 840.

## ATTACHMENT 1: MECHANICAL PROPERTIES OF TEST MATERIALS OF PRESENT PROJECT

Table 20: Mechanical properties of test materials

Heat	Rp 0.2	TS	A %
0,06C-1,4Mn 920°C	992	1081	11.4
0,06C-1,4Mn 875°C	1042	1077	11.6
0,06C-1,4Mn 838°C	904	984	11.0
0,06C-1,4Mn 825°C	941	1017	11.2
0,08C-1,8Mn 920°C	1141	1195	11.2
0,08C-1,8Mn 870°C	1140	1208	11.2
0,08C-1,8Mn 815°C	1024	1207	10.6
0.09C-1.1Mn 835°C	1010	1079	10.8
0.09C-1.1Mn 790°C	904	1014	13
0.07C-1.3Mn 815°C	844	973	11.6
0.07C-1.3Mn 788°C	856	934	11.5

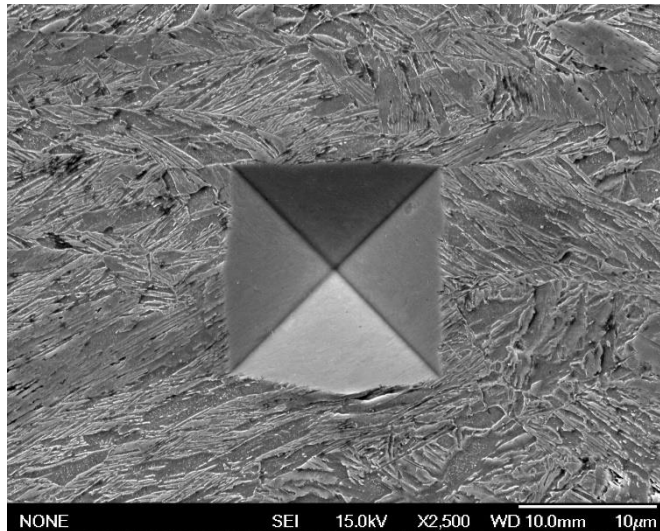# ATTACHMENT 2: FESEM IMAGES OF MICROSTRUCTURES AT THE MIDDLE SECTIONS OF SELECTED MATERIALS
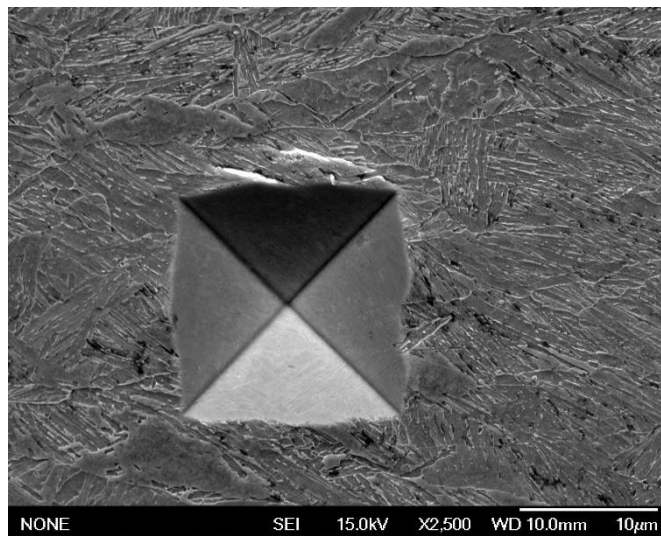
Figure 100: Microstructure of sample 0.06C-1.3Mn 920°C at the middle section.
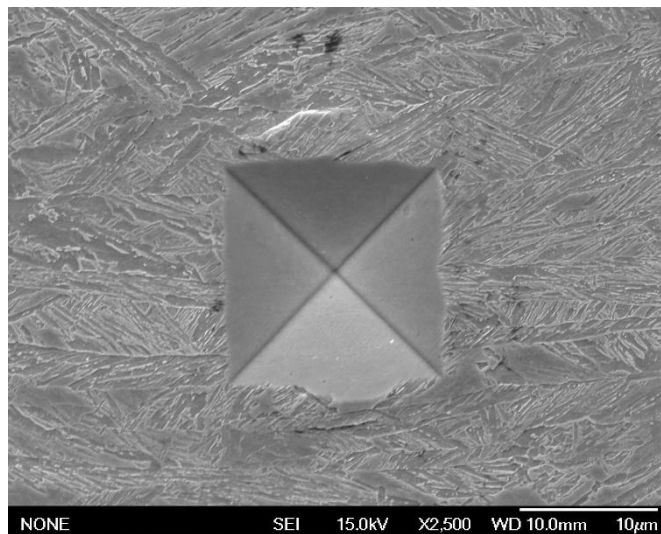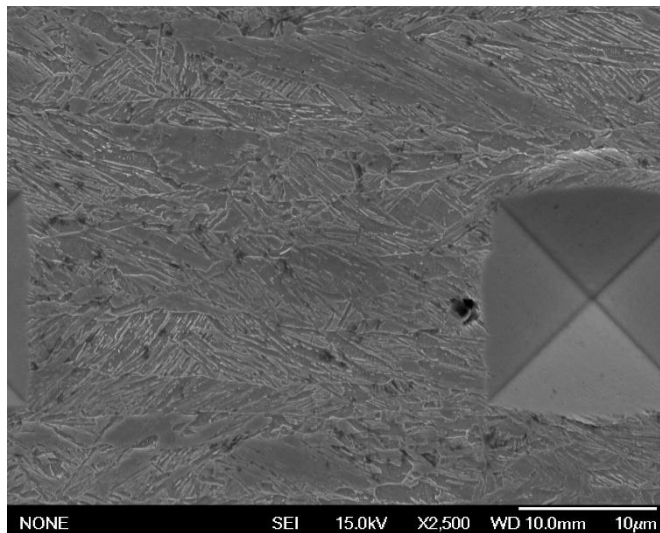

Figure 101: Microstructure of the middle section of sample 0.06C- 1.3Mn 875°C.

Figure 102: Microstructure of the middle section of sample 0.08C-1.8Mn 920°C.

Figure 103: Microstructure of sample 0.08C-1.8Mn 870°C at the middle section.
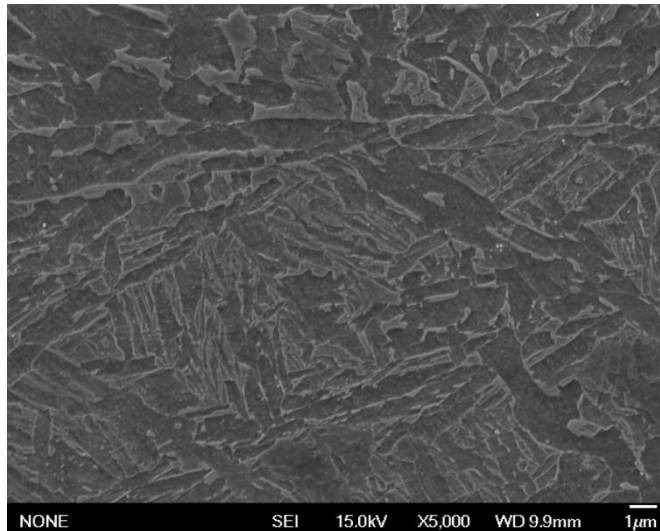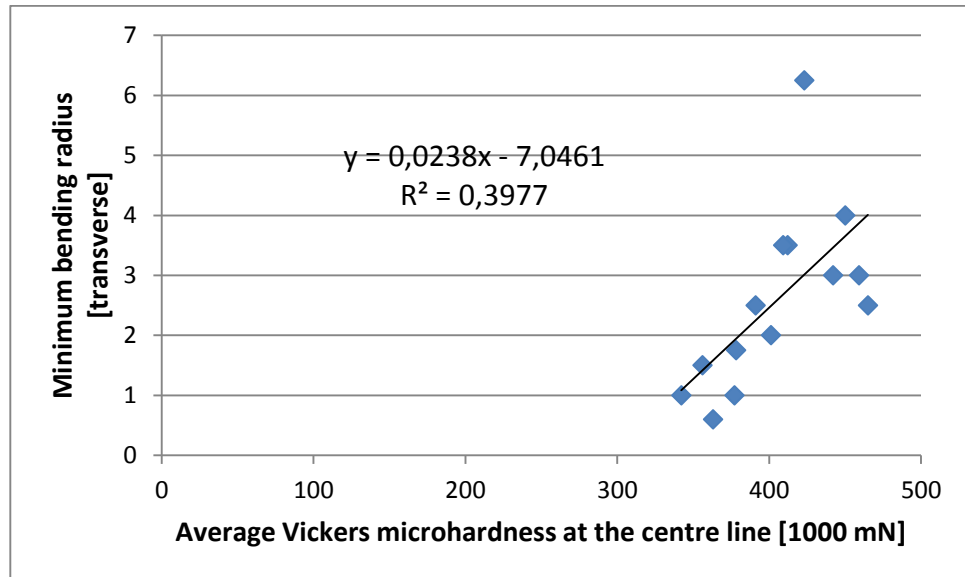
Figure 104: Microstructure at the middle section of material 0.07C-1.3Mn 788°C.
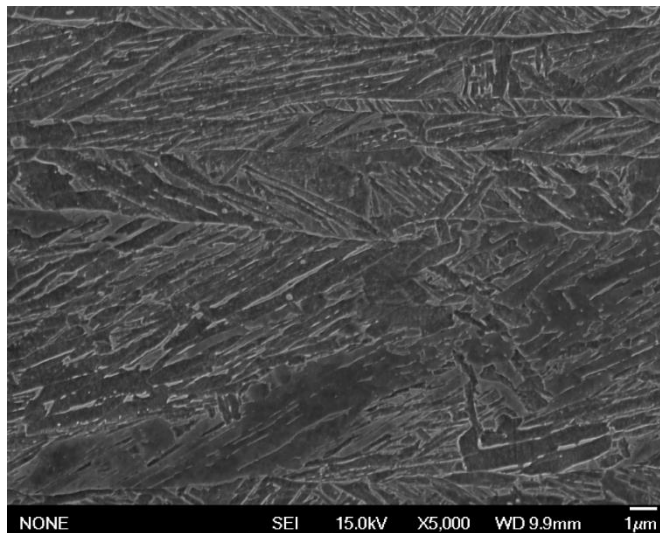
Figure 105: Microstructure at the middle section of material 0.07C-1.3Mn 815°C.

ATTACHMENT 3: CORRELATION BETWEEN HARDNESS AT THE CENTRE LINE AND MINIMUM BENDING RADIUS TRANSVERSE TO ROLLING DIRECTION

Figure 106: Correlation between average centre line hardness and minimum bending radius.

ATTACHMENT 4: HOMOGENEITY INDEX OF EACH HEAT AT GIVEN DEPTHS

Table 21: Homogeneity index of each sample at given depths from upper surface.

Heat	50 um	100 um	150 um	200 um	250 um	300 um	350 um	400 um	450 um	500 um
0.1C-1.1Mn 893°C	4.06	6.10	3.66	2.44	2.69	3.49	1.93	4.57	2.59	2.77
0.1C-1.1Mn 880°C	4.14	1.43	15.55	2.38	2.27	3.47	3.74	3.29	2.89	4.48
0.1C-1.1Mn 855°C	3.23	1.81	4.43	3.57	3.36	3.60	3.65	2.35	3.17	5.92
0,06C-1,4Mn 920°C	3.32	2.37	4.83	2.79	3.10	2.78	3.49	2.75	2.86	2.30
0,08C-1,8Mn 920°C	3.85	3.20	3.37	2.53	4.84	2.22	1.74	2.95	2.29	3.01
0,06C-1,4Mn 880°C	3.77	2.07	14.83	1.86	2.57	2.28	3.12	2.17	3.55	2.57
0,08C-1,8Mn 880°C	5.53	5.12	3.95	2.96	5.77	3.90	3.51	3.26	2.90	4.96
0.08C-1.9Mn 905°C	2.93	2.09	4.93	2.72	2.36	3.65	5.60	3.69	2.75	5.84
0.07C-1.9M 825°C	2.60	2.73	4.82	3.87	3.52	3.54	2.67	4.87	2.77	3.50
0.1C-1.1Mn 898°C	2.95	2.27	3.83	1.87	2.26	1.95	2.85	3.16	3.11	2.51
0.08C-1.8Mn 920°C	3.11	3.92	2.94	4.57	5.39	2.02	3.28	1.98	2.33	3.55
0.12C-1.2Mn 880°C	3.99	3.92	4.79	2.30	3.43	3.61	3.07	3.03	4.80	2.71
0.07C-1.3Mn 815°C	2.18	2.67	2.28	3.00	3.78	2.67	4.32	1.72	3.30	3.64
0.6C-1.3Mn 825°C	3.39	4.18	3.49	2.80	2.75	3.11	2.67	15.46	4.65	5.20
0.6C-1.3Mn 838°C	3.24	4.84	4.22	3.86	2.57	2.49	3.77	4.33	4.62	2.78
0.07C-1.3Mn 788°C	2.71	1.41	3.17	9.37	2.53	2.36	4.51	2.53	3.53	1.60
0.06C-2Mn 820°C	2.51	3.06	1.09	2.05	2.63	2.14	-	-	-	-
0.07C-1.3Mn 788°C, T350°C	3.83	3.94	2.13	2.21	4.42	2.56	1.51	3.38	3.82	3.66
0.07C-1.3Mn 788°C, T550°C	4.46	1.93	2.99	2.25	3.09	2.82	1.63	2.37	2.06	2.10

0.09C-1.1Mn 790°C	2.62	1.66	2.16	2.42	1.50	2.54	-	-	-	-
0.8C-1.8Mn 815C (a)	3.11	3.92	2.94	4.57	5.40	2.02	3.28	1.99	2.33	3.55
0.8C-1.8Mn 815C (b)	8.23	3.91	6.63	2.65	3.68	2.75	1.47	4.11	3.68	3.23

ATTACHMENT 5: STANDARD DEVIATIONS OF HARDNESS MEASUREMENTS AT EVERY GIVEN DEPTH

Table 22: Standard deviations of hardness measurements at every given depth.

Heat	50 um	100 um	150 um	200 um	250 um	300 um	350 um	400 um	450 um	500 um
0.1C-1.1Mn 893°C	15.87	23.97	15.28	10.17	11.18	14.67	7.94	19.80	11.39	12.07
0.1C-1.1Mn 880°C	15.19	6.08	70.47	10.40	9.78	14.93	16.86	15.40	13.07	20.72
0.1C-1.1Mn 855°C	12.54	8.04	19.23	16.24	15.11	16.19	15.48	10.55	13.56	27.69
0,06C-1,4Mn 920°C	11.08	9.14	19.06	10.99	12.56	11.38	14.14	11.22	11.63	9.47
0,08C-1,8Mn 920°C	13.07	13.51	14.70	11.36	21.80	9.92	8.19	14.08	10.93	14.60
0,06C-1,4Mn 880°C	10.23	7.20	52.56	7.08	9.63	8.94	11.98	8.29	13.69	10.04
0,08C-1,84Mn 880°C	20.00	21.73	17.16	13.17	24.66	17.16	15.63	14.64	12.99	22.36
0.08C-1.9Mn 905°C	9.98	7.26	17.32	9.74	8.37	12.82	19.50	12.97	9.78	20.20
0.07C-1.9Mn 825°C	7.44	8.07	14.94	12.26	11.60	11.84	8.73	15.96	9.22	12.20
0.06C-2Mn 820°C	6.50	8.00	6.30	3.30	7.90	6.20	-	-	-	-
0.1C-1.1Mn 898C	11.85	9.74	16.49	8.22	9.87	8.41	12.45	13.90	13.55	11.90
0.8C-1.8Mn 815C (a)	9.05	13.91	11.46	19.05	23.92	8.92	14.78	8.93	10.55	15.90
0.8C-1.8Mn 815C (b)	32.27	17.49	29.16	12.26	16.84	12.40	6.62	18.73	16.39	14.76
0.12C-1.2Mn 880°C	15.07	16.52	20.21	9.72	14.91	15.83	13.29	13.22	20.89	11.84
0.07C-1.3Mn 815°C	6.46	8.85	7.88	10.82	14.33	10.04	16.07	6.86	13.00	14.03
0.6C-1.3Mn 825°C	9.47	13.88	11.91	10.41	10.09	11.56	9.98	60.80	17.07	18.50
0.6C-1.3Mn 838°C	9.98	17.48	15.33	14.65	9.99	9.67	14.41	15.98	17.13	10.51
0.07C-1.3Mn 788°C	7.69	4.59	10.25	31.87	8.71	8.05	14.91	8.76	12.03	5.47
0.07C-1.3Mn 788°C, T350°C	12.20	13.95	7.42	7.78	16.05	9.03	5.46	12.33	13.94	13.38
0.07C-1.3Mn 788°C, T550°C	12.79	6.25	10.11	7.86	11.23	10.31	5.64	8.79	7.70	7.63

| 0.09C-1.1Mn 790°C | 9.26 | 6.41 | 8.72 | 9.99 | 6.24 | 10.55 | - | - | - | - |

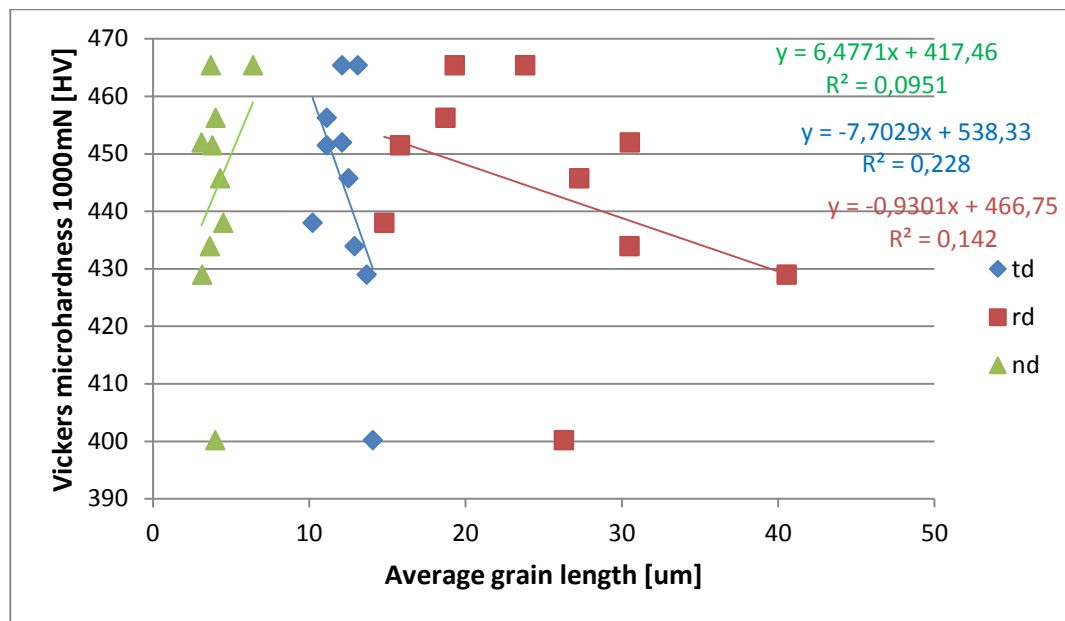## ATTACHMENT 6: THE EFFECT OF AUSTENITE GRAIN SIZE ON HARNDESS

Figure 107: The effect of average austenite grain length of hardness in different directions (rd=rolling direction, td=transverse to rolling direction and nd=normal to rolling direction).
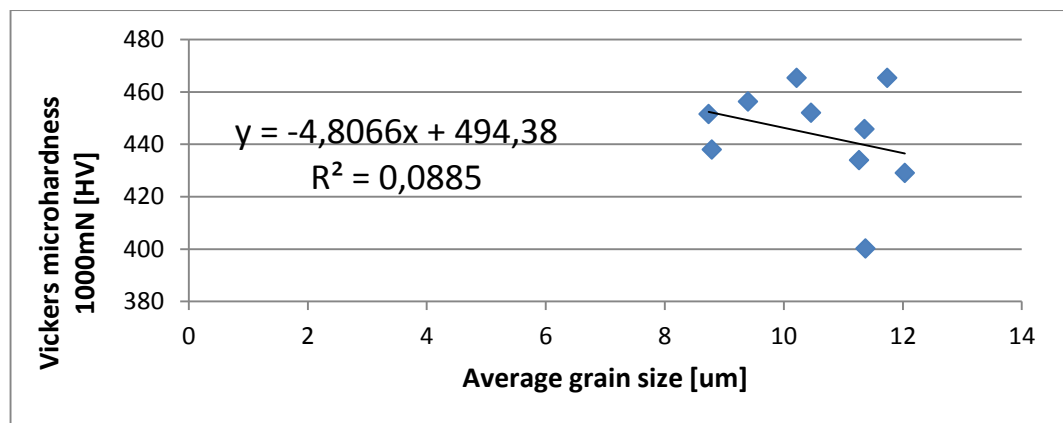

Figure 108: The effect of average austenite grain size on hardness, assuming that the morphology of the grain is round.